THE UNIVERSITY OF READING

Numerical Techniques for Morphodynamic Modelling

by

Justin Hudson

Department of Mathematics,
University of Reading,
Whiteknights PO Box 220,
Reading RG6 6AX

This thesis is submitted for the degree of Doctor of Philosophy

October 2001

Abstract

In the hydraulics industry, an accurate numerical approximation of the equations governing sediment transport in coastal regions has recently become a major topic of interest. These equations comprise the shallow water equations governing the water flow with the addition of a bed transport equation. It is common practice in industry to simplify the equations governing sediment transport by assuming the water flow is in an equilibrium state and the bed has a negligible effect on the water flow. However, this approach is limited as only steady flow and a slow moving bed can be approximated accurately in this manner. Thus, an unsteady approach is required that is considerably more robust and approximates the full system simultaneously. Until recently, the classic Lax-Wendroff scheme has been widely used in industry to obtain a numerical solution to the equations, but not surprisingly the numerical results obtained suffered from spurious oscillations resulting in the numerical scheme becoming unstable for long time periods. In industry, different measures have been applied to the use of classic Lax-Wendroff scheme to try to eliminate the spurious oscillations such as flux-limiter methods and using a small Courant number. Unfortunately, the spurious oscillations could not be eliminated and overpowered the numerical results for long computational run times. In this thesis, a variety of numerical schemes are discussed including adapted versions of the Lax-Friedrichs scheme, classic Lax-Wendroff scheme, MacCormack scheme and Roe's scheme. High resolution schemes are also derived that satisfy the TVD property so that no spurious oscillations will occur in the numerical results. Five different formulations are then derived, which are based on either a steady or unsteady approach, and are used with the most accurate scheme and compared with the classic Lax-Wendroff scheme to obtain a numerical approximation of the equations. The numerical results are compared to determine which approach and numerical scheme is the most accurate. Sediment transport in both one and two dimensions is considered and dimensional splitting schemes are also discussed in two dimensions.

Acknowledgements

First, I would like to thank my supervisor Dr. Peter Sweby for his continuous guidance and support throughout the past three years. I would also like to thank my industrial supervisor Jesper Damgaard and Tim Chesher from HR Wallingford for many interesting discussions.

I am also grateful to Dr. Matthew Hubbard (University of Leeds) and Prof. Mike Baines (University of Reading) for many useful discussions. In addition, I would like to thank the postgraduate secretary Sue Davis for her help throughout the past three years.

I would like to give a special mention to my girlfriend Louise Collins and my friend Chris Anderson who have given me countless support and have always been there for me throughout the past three years.

I would also like to thank the **E**ngineering and **P**hysical **S**cience **R**esearch **C**ouncil and HR Wallingford for their funding.

Finally, I would like to dedicate this thesis to Dr. Peter Sweby, Prof. Mike Baines and Dr. David Wilton (University of Plymouth) for believing in me and helping me to realize my dream.

Contents

List of Figures

List of Tables

Chapter 1

Introduction

1.1 Motivation

In recent years, sand transport has become a major topic of interest in the hydraulics community. The understanding of how sand interacts in certain environments is crucial for both the environment and businesses. For example, sand transport influences how harbours are constructed since if too much sand enters a harbour, the walls may become severely damaged and the costs of dredging the harbour may become too expensive and impractical. Reservoirs can lose all storage capacity due to sediment build up. Cunge *et al.* [3] stated that by 1973, 33% of the US reservoirs built before 1935 had lost between 25% to 50% of their original capacity due to sediment build up.

In this thesis, we discuss a variety of numerical techniques that can be used to obtain a numerical solution of the equations that govern sediment transport. For a one dimensional channel, these comprise the equation for conservation of mass,

$$\frac{\partial h}{\partial t} + \frac{\partial (uh)}{\partial x} = 0, \tag{1.1}$$

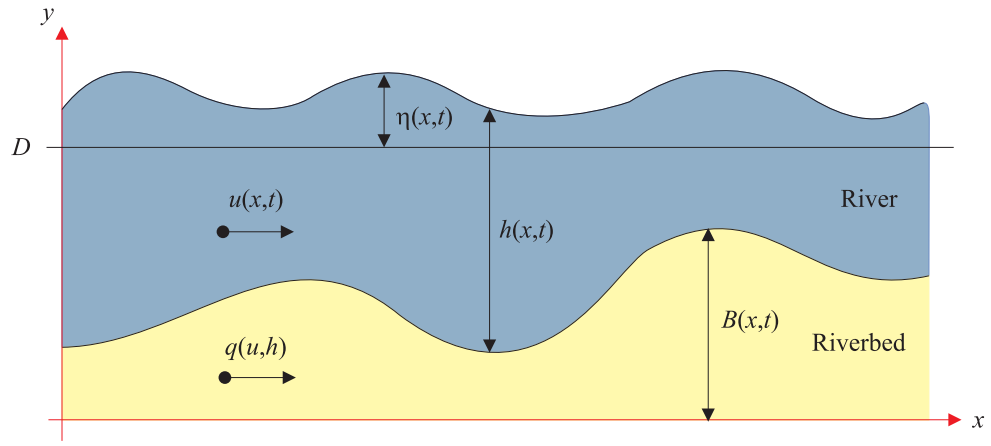

Figure 1.1: The shallow water domain.

the equation for conservation of momentum,

$$\frac{\partial(uh)}{\partial t} + \frac{\partial\left[hu^2 + \frac{1}{2}gh^2\right]}{\partial x} = -ghB_x, \tag{1.2}$$

and the bed-updating equation,

$$\frac{\partial B}{\partial t} + \xi\frac{\partial q}{\partial x} = 0, \tag{1.3}$$

where $\xi = \frac{1}{1-\epsilon}$, ϵ being the porosity of the bed, which is non-dimensional, with $0 \leq \epsilon < 1$. In this thesis, we use a value of 0.4 for the porosity. Here $\eta(x,t)$ represents the surface elevation, $h(x,t)$ is the total height above the bottom of the channel (m), $B(x,t)$ is the height of the riverbed (m), $u(x,t)$ is the velocity in the x direction (m/s) and $q(u,h)$ is the total (suspended and bedload) volumetric sediment transport rate in the x direction (m^2/s), see Figure 1.1. As suggested by the notation, the sediment transport flux $q(u,h)$ is not in general a direct function of B, which can cause difficulties in obtaining an accurate numerical approximation. In some cases, the sediment transport flux cannot be written analytically and is calculated by using a "black box" approach where the flux is deduced from experimental data. Unfortunately, the equation for conservation of momentum (1.2) is not valid when discontinuities appear in the bed thus, a modified version of the equation is derived for this special case in Section 1.3.

Until recently, the system (1.1) to (1.3) has been approximated by using a steady approach, which was pioneered by Cunge *et al.* [3]. The approach assumes that the changes in the bed have a negligible effect on the water flow and decouples the system. The system is decoupled into a water flow approximation, which is iterated to an equilibrium state, followed by a bed update. The approach is used with the classic Lax-Wendroff scheme in industry, but the scheme suffers from dispersion resulting in spurious oscillations occurring in the numerical results. Various techniques, including flux-limiter methods, have been used to try to eliminate the spurious oscillations. Unfortunately, the spurious oscillations could not be eliminated and overpowered the numerical results for long computational run times, see Damgaard [4] and Damgaard & Chesher [5]. Thus, even with the various techniques, the classic Lax-Wendroff scheme could only be used for short computational run times otherwise, spurious oscillations overpowered the numerical results resulting in the scheme becoming unstable. In this thesis, we discuss a variety of numerical techniques for approximating the equations governing sediment transport so that an accurate solution with no numerical oscillations present may be obtained.

In this chapter, we discuss the derivation of the equations governing sediment transport together with two alternative sediment transport flux formulae. In Chapter 2, a variety of numerical schemes including adaptations of the classic Lax-Friedrichs, classic Lax-Wendroff, MacCormack and Roe's scheme are discussed and applied to the shallow water equations without bed movement. To determine which scheme is the most accurate, three test problems are used to compare the numerical results of the different schemes. In Chapter 3, five different formulations of the governing equations are derived, which can be used to obtain a numerical approximation of the equations governing sediment transport. One of the formulations is based on the steady approach and the other four on the unsteady approach, where the water flow and bed update are approximated simultaneously. The flux-limited version of Roe's scheme and the classic Lax-Wendroff scheme are then used to obtain a numerical solution of the different formulations for two test problems. The different formulations and numerical schemes are then compared to see which is the most accurate combination. In Chapter 4 the two dimensional

case is considered and a variety of two dimensional schemes are discussed and applied to the 2D shallow water equations without bed movement. A test problem is used to determine which of the schemes is the most accurate. In Chapter 5, we discuss how to obtain an accurate approximation of the equations governing sediment transport in two dimensions. The different formulations used in one dimension are adapted to two dimensions and are numerically approximated using the classic 2D Lax-Wendroff scheme, a flux-limited 2D version of Roe's scheme and a dimensional splitting scheme. A conical sand dune test problem is used to determine which formulation and numerical scheme produced the most accurate numerical results. In Chapter 6, we discuss the results found in this thesis and propose further work.

1.2 Derivation of the Equations

We first derive the equations that govern fluid flow with sediment transport. By considering a region between x_1 and x_2 in the one dimensional channel illustrated in Figure 1.1, we can derive the equations governing sediment transport.

1.2.1 Conservation of Mass

In the region x_1 to x_2, we can determine that

$$\begin{bmatrix}\text{Net volume of fluid into}\\ \text{the region } x_1 \text{ to } x_2\end{bmatrix} = \begin{bmatrix}\text{Rate of change of total volume}\\ \text{of fluid in the region } x_1 \text{ to } x_2\end{bmatrix}.$$

Now, the total volume of fluid in the region x_1 to x_2 is

$$\int_{x_1}^{x_2}\int_{B}^{h+B} dydx = \int_{x_1}^{x_2} (h+B-B)\ dx = \int_{x_1}^{x_2} h\ dx$$

and by differentiating with respect to t, we obtain

$$\begin{bmatrix}\text{Rate of change of total volume}\\ \text{of fluid in the region } x_1 \text{ to } x_2\end{bmatrix} = \frac{d}{dt}\int_{x_1}^{x_2} h \ dx.$$

Also,

$$\begin{bmatrix}\text{Total volume of}\\ \text{fluid entering at } x_1\end{bmatrix} = (uh)_{x_1} \quad \text{and} \quad \begin{bmatrix}\text{Total volume of}\\ \text{fluid leaving at } x_2\end{bmatrix} = (uh)_{x_2}$$

thus,

$$\begin{bmatrix}\text{Net volume of fluid into}\\ \text{the region } x_1 \text{ to } x_2\end{bmatrix} = (uh)_{x_1} - (uh)_{x_2}.$$

Hence, we obtain the integral form of the equation for conservation of mass

$$\frac{d}{dt}\int_{x_1}^{x_2} h \ dx + [uh]_{x_1}^{x_2} = 0. \tag{1.4}$$

To obtain the differential form, we integrate (1.4) with respect to t over the interval $[t_1,t_2]$, where $t_2 > t_1$,

$$\int_{x_1}^{x_2} h(x,t_2) \ dx - \int_{x_1}^{x_2} h(x,t_1) \ dx + \int_{t_1}^{t_2} [uh]_{x_1}^{x_2} \ dt = 0.$$

Then, by assuming that $h(x,t)$ and $u(x,t)$ are differentiable functions and using

$$h(x,t_2) - h(x,t_1) = \int_{t_1}^{t_2} \frac{\partial h}{\partial t} \ dt \quad \text{and} \quad [uh]_{x_1}^{x_2} = \int_{x_1}^{x_2} \frac{\partial (uh)}{\partial x} \ dx,$$

we obtain

$$\int_{t_1}^{t_2}\int_{x_1}^{x_2} \left\{ \frac{\partial h}{\partial t} + \frac{\partial (uh)}{\partial x} \right\} \ dxdt = 0.$$

Since x_1, x_2 and t_1, t_2 are arbitrary, we obtain the differential form of the equation for conservation of mass,

$$\frac{\partial h}{\partial t} + \frac{\partial (uh)}{\partial x} = 0.$$

Note that the common practice of re-writing this equation as

$$\frac{\partial \eta}{\partial t} + \frac{\partial (u(\eta - B))}{\partial x} = \frac{\partial B}{\partial t}$$

for the case of a fixed bed is not valid for the moving bed case considered here since $B_t \neq 0$.

1.2.2 Conservation of Momentum

In the region x_1 to x_2, we can determine that

$$\begin{bmatrix}\text{Total rate of change of} \\ \text{momentum in } x \text{ direction}\end{bmatrix} = [\text{Force applied in } x \text{ direction}]\,.$$

Now,

$$\begin{aligned}\begin{bmatrix}\text{Total rate of change of} \\ \text{momentum in } x \text{ direction}\end{bmatrix} &= \frac{d}{dt}\int_{x_1}^{x_2}\int_{B}^{h+B} u\ dydx + (hu^2)_{x_2} - (hu^2)_{x_1} \\ &= \frac{d}{dt}\int_{x_1}^{x_2} uh\ dx + (hu^2)_{x_2} - (hu^2)_{x_1}.\end{aligned}$$

Also

$$\begin{aligned}[\text{Pressure force on ends}] &= g\left[\int_{B}^{h+B}(y-(h+B))\ dy\right]_{x_1}^{x_2} \\ &= g\left[\left[\frac{1}{2}y^2-(h+B)y\right]_{B}^{h+B}\right]_{x_1}^{x_2} \\ &= \left[-\frac{1}{2}gh^2\right]_{x_1}^{x_2}\end{aligned}$$

and

$$[\text{Pressure force from riverbed}] = -g\int_{C_{B1,2}} h\ dy,$$

where $C_{B1,2}$ is the path of the line integral and denotes the curve of the riverbed in the region x_1 to x_2. By assuming that no discontinuities are present in the riverbed

$$[\text{Pressure force from riverbed}] = -g\int_{x_1}^{x_2} h\frac{dB}{dx}\ dx,$$

we obtain

$$[\text{Force applied in } x \text{ direction}] = \left[-\frac{1}{2}gh^2\right]_{x_1}^{x_2} - g\int_{x_1}^{x_2} h\frac{dB}{dx}\ dx.$$

Hence,

$$\frac{d}{dt}\int_{x_1}^{x_2} uh\ dx + (hu^2)_{x_2} - (hu^2)_{x_1} = \left[-\frac{1}{2}gh^2\right]_{x_1}^{x_2} - g\int_{x_1}^{x_2} h\frac{dB}{dx}\ dx$$

and by re-arranging, we obtain the integral form of the equation for conservation of momentum,

$$\frac{d}{dt}\int_{x_1}^{x_2} uh\ dx + \left[hu^2 + \frac{1}{2}gh^2\right]_{x_1}^{x_2} = -g\int_{x_1}^{x_2} h\frac{dB}{dx}\ dx. \tag{1.5}$$

To obtain the differential form of the equation for conservation of momentum, we use the same approach as we did for the equation for conservation of mass and assume that $h(x,t)$ and $u(x,t)$ are differentiable functions and obtain

$$\frac{\partial(uh)}{\partial t} + \frac{\partial\left[hu^2 + \frac{1}{2}gh^2\right]}{\partial x} = -ghB_x.$$

1.2.3 Bed-Updating Equation

In the region x_1 to x_2, we can determine that

$$\begin{bmatrix}\text{Net flux of mass into}\\ \text{the region } x_1 \text{ to } x_2\end{bmatrix} = \begin{bmatrix}\text{Rate of change of total mass}\\ \text{in the region } x_1 \text{ to } x_2\end{bmatrix}.$$

Now, the total volume of sediment in the region x_1 to x_2 is

$$\int_{x_1}^{x_2}\int_0^B dydx = \int_{x_1}^{x_2} B\ dx$$

and by differentiating with respect to t, we obtain

$$\begin{bmatrix}\text{Rate of change of total mass}\\ \text{in the region } x_1 \text{ to } x_2\end{bmatrix} = \frac{d}{dt}\int_{x_1}^{x_2} B \; dx.$$

In addition we have

$$\begin{bmatrix}\text{Total volume of}\\ \text{sediment entering at } x_1\end{bmatrix} = \xi q(u,h)_{x_1} \quad \text{and} \quad \begin{bmatrix}\text{Total volume of}\\ \text{sediment leaving at } x_2\end{bmatrix} = \xi q(u,h)_{x_2},$$

where $\xi = \frac{1}{1-\epsilon}$ and ϵ is the porosity of the bed material, see Cunge *et al.* [3]. Thus,

$$\begin{bmatrix}\text{Net flux of mass into}\\ \text{the region } x_1 \text{ to } x_2\end{bmatrix} = \xi \left(q(u,h)_{x_1} - q(u,h)_{x_2}\right).$$

Hence, we obtain the integral form of the bed-updating equation,

$$\frac{d}{dt}\int_{x_1}^{x_2} B \; dx + \xi \left[q(u,h)\right]_{x_1}^{x_2} = 0. \tag{1.6}$$

To obtain the differential form of the bed-updating equation, we use the same approach as we did for the equation for conservation of mass and assume that $h(x,t)$ and $u(x,t)$ are differentiable functions and obtain

$$\frac{\partial B}{\partial t} + \xi \frac{\partial q}{\partial x} = 0.$$

1.3 Modification for a Discontinuity in the Riverbed

When a discontinuity is present in the riverbed, see Figure 1.2, the integral conservation laws (1.4) and (1.6) are valid for non complex discontinuities (Needham & Hey [29] and Zanré & Needham [46]). However, the integral form of the equation for conservation of momentum (1.5) becomes invalid along the face of the discontinuity due to the term on the right side of (1.5) being derived with

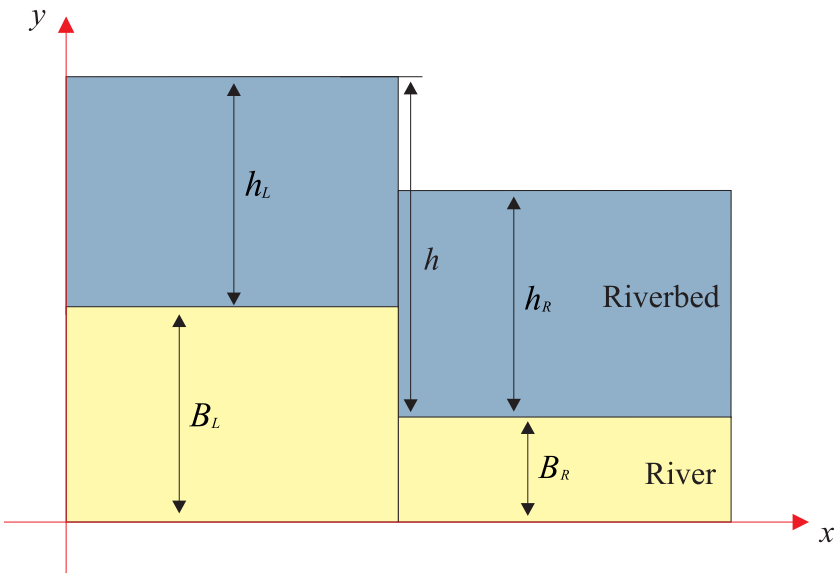

Figure 1.2: A discontinuity present in the riverbed.

the assumption that no discontinuities are present in the riverbed. This term arises from the hydrostatic pressure force from the riverbed

$$-g \int_{C_{B1,2}} h \; dy,$$

where $C_{B1,2}$ is the path of the line integral and denotes the curve of the riverbed in the region x_1 to x_2. Away from the discontinuity, the line integral along $C_{B1,2}$ can be determined

$$-g \int_{C_{B1,2}} h \; dy = -g \int_{x_1}^{x_2} h \frac{dB}{dx} \; dx$$

and equation (1.5) can be used. However, along the face of the discontinuity, we cannot evaluate this integral as $h(x,t)$ is undefined. Zanré & Needham [46] noted that when a discontinuity appears in the riverbed, we can use

$$h = d'(y), \quad \min(B_L, B_R) \leq y \leq \max(B_L, B_R), \tag{1.7}$$

where

$$d'(y) = h_L + \frac{(h_R - h_L)(y - B_L)}{B_R - B_L} \tag{1.8}$$

to determine the value of $h(x,t)$ along the face of the discontinuity. By integrating (1.8), we obtain

$$d(y) = h_L y + \frac{y(h_R - h_L)(y - 2B_L)}{2(B_R - B_L)}. \tag{1.9}$$

Thus, away from the discontinuity, the integral conservation laws (1.4), (1.5) and (1.6) can be used but at the discontinuity, (1.5) must be replaced with

$$\frac{d}{dt}\int_{x_1}^{x_2} uh \ dx + \left[hu^2 + \frac{1}{2}gh^2\right]_{x_1}^{x_2} = -g\int_{C_{B1,2}} h \ dy$$

where (1.7), (1.8) and (1.9) provide a definition of depth along the face of the discontinuity

1.4 Sediment Transport Flux Formulae

The total load sediment transport flux includes suspended and bed-load sediment transport. Bed-load sediment transport includes the effects of grains of sand being transported on the surface of the bed by friction and gravity (for slopes). Suspended sediment transport includes the effects of grains of sand being picked up by the water flow and transported above the bed. For slow water flow, bed-load sediment transport is more dominant as not much sediment is carried by the water flow but as the water flow increases, suspended sediment transport becomes more dominant and sediment can be transported several meters above the bed especially if the grain size is small (see Soulsby [36] for more details).

Numerous analytical sediment transport flux formulae have been derived that include both suspended and bed-load sediment transport and the choice of which to use is usually determined by the situation being modelled. In this thesis, we consider two of the more well known sediment transport flux formulae:

- Grass [14] discussed one of the most basic sediment transport fluxes which

follows a simple power law,

$$q(u) = Au|u|^{m-1}. \tag{1.10}$$

Here, A is a dimensional constant (s^2/m), that encompasses the effects of grain size and kinematic viscosity and is usually determined from experimental data with m being chosen so that $1 \leq m \leq 4$. Unless u is not allowed to change sign, (1.10) cannot be differentiated with respect to u. However, by considering odd integer values of m only, (1.10) can be differentiated and is valid for all values of u. For example, if we let $m = 3$ then

$$q(u) = Au|u^2| = Au^3, \tag{1.11}$$

which can now be differentiated with respect to u and is valid for all values of u.

- Van Rijn [42, 43] derived a more complex sediment transport flux,

$$q(u,h) = \begin{cases} Au\left(|u| - u_{cr}\right)^{2.4} & \text{if } |u| > u_{cr} \\ 0 & \text{otherwise} \end{cases}, \tag{1.12}$$

where u_{cr} is the threshold current speed which is calculated from

$$u_{cr} = \begin{cases} 0.19(d_{50})^{0.1}\log_{10}\left(\dfrac{2h}{d_{50}}\right) & \text{if } 100 \leq d_{50} \leq 500\mu m \\ 8.5(d_{50})^{0.6}\log_{10}\left(\dfrac{2h}{d_{50}}\right) & \text{if } 500 \leq d_{50} \leq 2000\mu m \end{cases},$$

$$A = \frac{d_{50}\left(0.005\left(\frac{d_{50}}{h}\right)^{0.2} + 0.012\mathrm{D}_*^{-0.6}\right)}{\left(gd_{50}(s^* - 1)\right)^{1.2}} \tag{1.13}$$

and the particle diameter is

$$\mathrm{D}_* = d_{50}\left(\frac{g}{\gamma^2}(s^\star - 1)\right)^{1/3}.$$

Here, d_{50} is the median grain diameter in m, $s^\star = \frac{\rho_s}{\rho}$ is the specific gravity, ρ_s

is the mineral density of the sediment in kg/m^3 ($2650kg/m^3$ for quartz), ρ is the density of the water in kg/m^3 and γ is the kinematic viscosity of the water in m^2/s. Values of d_{50}, ρ_s and γ can be obtained from Table 1.1, Table 1.2 and Table 1.3 respectively. When calculating the threshold current speed, d_{50} must be in m and not in μm.

The sediment transport flux (1.12) is a simplified version of the full method of van Rijn [42] and is only valid for $0.5 \leq |u(x,t)| \leq 2.5m/s$ and $1 \leq h(x,t) \leq 20m$. Van Rijn derived (1.12) for fresh water, whose salinity is 0 parts per thousand (ppt), at a temperature of 15^oC but the method can be used with a different salinity (i.e. salt water whose salinity is 35 ppt) and temperature with a minimal loss of accuracy.

Notice that the sediment transport flux of van Rijn is considerably harder to differentiate than the sediment transport flux discussed by Grass. A variety of other sediment transport fomulae can be found in Soulsby [36] and van Rijn [43].

The sediment transport flux of van Rijn can be re-written in the form of (1.10) by assuming that the threshold wave speed is $u_{cr} = 0$ and setting $m = 3.4$. Thus, by assuming that h is constant, we can use (1.13) to obtain a realistic approximation of A for (1.10). For example, if the situation being modelled is for seawater, whose salinity is 35ppt, with a temperature of 10^oC, the following values are obtained

1. $\rho_s = 2650kg/m^3$, which is the mineral density of quartz.
2. $\rho = 1027kg/m^3$, which is the density.
3. $s = \frac{\rho_s}{\rho} = 2.580331061$, which is the specific gravity.
4. $\nu = 1.357 \times 10^{-6} m^2/s$, which is the kinematic viscosity.
5. $d_{50} = 0.2 \times 10^{-4} m$, which is the grain diameter of fine sand.
6. $h \approx 10m$, which is the total height above the bottom of the channel.

Hence, by using the above values, we obtain the realistic value

$$A \approx 0.00680396635637,$$

which can be used with the sediment transport flux discussed by Grass.

Mud / Sand	d_{50} in μm
Fine Clay	0 to 0.9765625
Medium Clay	0.9765625 to 1.953125
Coarse Clay	1.953125 to 3.90625
Very Fine Silt	3.90625 to 7.8125
Fine Silt	7.8125 to 15.625
Medium Silt	15.625 to 31.25
Coarse Silt	31.25 to 62.5
Very Fine Sand	62.5 to 125
Fine Sand	125 to 250
Medium Sand	250 to 500
Coarse Sand	500 to 1000
Very Coarse Sand	1000 to 2000

Table 1.1: The grain size in μm (taken from Soulsby [36]).

1.5 Summary

In this chapter, we have derived the equations governing sediment transport in one dimension. We have also discussed two different sediment transport formulae that can be used. In the next chapter, we discuss a variety of numerical schemes that can be used to numerically approximate the equations governing sediment transport.

	Temperature ^{o}C								
Salinity	0	5	10	15	20	25	30	35	40
0	999.8	1000	999.7	999.1	998.2	997	995.7	994	992.2
5	1003.9	1004	1003.6	1003	1002	1000.8	999.4	997.7	995.9
10	1008	1007.9	1007.5	1006.8	1005.8	1004.6	1003.1	1001.4	999.6
15	1012	1011.9	1011.4	1010.6	1009.6	1008.3	1006.8	1005.1	1003.2
20	1016	1015.8	1015.3	1014.4	1013.4	1012.1	1010.5	1008.8	1006.9
25	1020	1019.8	1019.2	1018.3	1017.2	1015.8	1014.3	1012.5	1010.6
30	1024.1	1023.7	1023.1	1022.1	1021	1019.6	1018	1016.2	1014.3
35	1028.1	1027.7	1027	1026	1024.8	1023.3	1021.7	1019.9	1018
40	1032.2	1031.6	1030.9	1029.8	1028.6	1027.1	1025.5	1023.7	1021.7

Table 1.2: Density of water in kg/m^3 (taken from Ramsing & Gundersen [32]).

	Temperature ^{o}C								
Salinity	0	5	10	15	20	25	30	35	40
0	1790.1	1517.5	1305.2	1140.2	1009.9	901.5	802.2	699.5	580.4
5	1795.2	1524.5	1312.9	1147.8	1016.9	907.7	807.9	705.1	586.9
10	1800.2	1531.4	1320.5	1155.3	1023.8	913.9	813.6	710.8	593.4
15	1805.3	1538.3	1328.1	1162.8	1030.7	920	819.2	716.3	599.8
20	1810.3	1545.2	1335.6	1170.2	1037.5	926.1	824.7	721.9	606.2
25	1820.2	1558.7	1350.5	1184.8	1050.9	938.1	835.7	727.4	612.5
30	1820.2	1558.7	1350.5	1184.8	1050.9	938.1	835.7	732.8	618.8
35	1825.1	1565.4	1357.8	1192	1057.6	944.1	841.1	738.2	625
40	1829.9	1572	1365.1	1199.2	1064.2	949.9	846.5	743.6	631.2

Table 1.3: Kinematic viscosity of water in $\times 10^{-9} m^2/s$ (taken from Ramsing & Gundersen [32]).

Chapter 2

Numerical Schemes for Systems of Conservation Laws in One Dimension

Now that we have derived the equations governing sediment transport, we discuss a variety of numerical schemes that can be used to numerically approximate the equations. We discuss an adapted version of the Lax-Friedrichs (LxF) scheme (see Garcia-Navarro *et al.* [9]), the staggered, non-staggered and central LxF and NT scheme (see Nessyahu & Tadmor [30] and Jiang *et al.* [22]), the Lax-Wendroff scheme (see Lax & Wendroff [24]), an adapted version of the MacCormack approach (see LeVeque & Yee [27], Yee [45] and Hudson [20]) and an adaptation of Roe's Scheme (see Roe [33], Glaister [11] and Hubbard & Garcia-Navarro [18]). Flux limiter methods and slope limiter methods are employed to minimise numerical oscillations.

The equations governing sediment transport can be written as a system of conservation laws with source term, i.e.

$$\frac{\partial \mathbf{w}}{\partial t} + \frac{\partial \mathbf{F}(\mathbf{w})}{\partial x} = \mathbf{R}, \tag{2.1}$$

where $\mathbf{F}(\mathbf{w})$ is the flux-function and $\mathbf{R}$ is the source term. Before considering the full system, we illustrate the numerical techniques for systems of conservation laws using the example of the shallow water equations,

$$\begin{bmatrix} h \\ uh \end{bmatrix}_t + \begin{bmatrix} uh \\ hu^2 + \frac{1}{2}gh^2 \end{bmatrix}_x = \begin{bmatrix} 0 \\ -ghB_x \end{bmatrix}, \tag{2.2}$$

which are a system of conservation laws. Some of the numerical schemes discussed in this chapter require the Jacobian matrix associated with the system (2.1), which for the shallow water equations is

$$\mathbf{A}(\mathbf{w}) = \begin{bmatrix} 0 & 1 \\ gh - u^2 & 2u \end{bmatrix},$$

whose eigenvalues are

$$\lambda_1 = u - \sqrt{gh} \quad \text{and} \quad \lambda_2 = u + \sqrt{gh},$$

with corresponding eigenvectors

$$\mathbf{e}_1 = \begin{bmatrix} 1 \\ u - \sqrt{gh} \end{bmatrix} \quad \text{and} \quad \mathbf{e}_2 = \begin{bmatrix} 1 \\ u + \sqrt{gh} \end{bmatrix}.$$

2.1 Test Problems

We use the following three test problems for the shallow water equations to illustrate the accuracy of the numerical schemes discussed in this chapter. For all three test problems, the riverbed is fixed.

2.1.1 Test Problem A: The Dam Break Problem

For this test problem, the riverbed is of constant depth thus, the source term is no longer present, $\mathbf{R} = 0$. The test problem consists of a 1D channel of length $1m$ with walls at either end. The initial velocity is 0 and a barrier is present at $x = 0.5$, which is removed at $t = 0$. The initial conditions consist of

$$u(x,0) = 0 \quad \text{and} \quad h(x,0) = \begin{cases} h_L & \text{if } 0 \leq x \leq \frac{1}{2} \\ h_R & \text{if } \frac{1}{2} < x \leq 1 \end{cases}$$

and are illustrated in Figure 2.1.

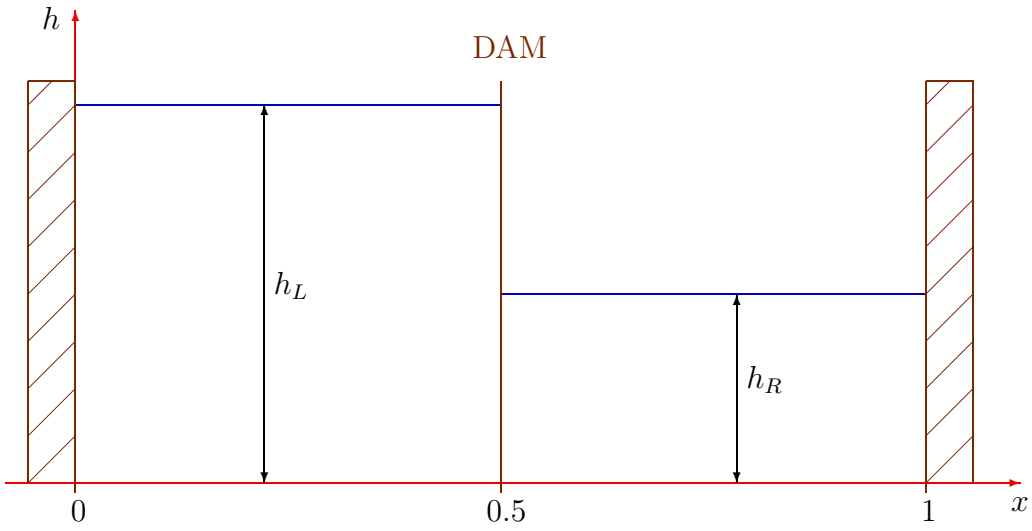

Figure 2.1: Initial conditions of the dam break problem.

Stoker [38] derived an analytical solution of the dam break problem which can be used to illustrate the accuracy of the numerical schemes. The exact solution is

$$u(x,t) = \begin{cases} 0 & \text{if } x < \frac{1}{2} - t\sqrt{gh_L} \\ \frac{1}{3t}\left(2(x + t\sqrt{gh_L}) - 1\right) & \text{if } \frac{1}{2} - t\sqrt{gh_L} \leq x \leq (u_2 - c_2)t + \frac{1}{2} \\ u_2 & \text{if } (u_2 - c_2)t + \frac{1}{2} < x \leq St + \frac{1}{2} \\ 0 & \text{if } x > St + \frac{1}{2} \end{cases}$$

and

$$h(x,t) = \begin{cases} h_L & \text{if } x < \frac{1}{2} - t\sqrt{gh_L} \\ \frac{1}{9g}\left(2\sqrt{gh_L} - \frac{1}{2t}(2x-1)\right)^2 & \text{if } \frac{1}{2} - t\sqrt{gh_L} \le x \le (u_2 - c_2)t + \frac{1}{2} \\ \frac{h_R}{2}\left(\sqrt{1 + \frac{8S^2}{gh_R}} - 1\right) & \text{if } (u_2 - c_2)t + \frac{1}{2} < x \le St + \frac{1}{2} \\ h_R & \text{if } x > St + \frac{1}{2} \end{cases}$$

where

$$u_2 = S - \frac{gh_R}{4S}\left(1 + \sqrt{1 + \frac{8S^2}{gh_R}}\right) \quad \text{and} \quad c_2 = \sqrt{\frac{gh_R}{2}\left(\sqrt{1 + \frac{8S^2}{gh_R}} - 1\right)}.$$

The bore speed, S, is the positive root of

$$u_2 + 2c_2 - 2\sqrt{gh_L} = 0.$$

The exact solution with $h_L = 1m$ and $h_R = 0.5m$ is illustrated in Figure 2.2 and Figure 2.3, where the bore speed is approximately $S = 2.957918120187525$. The exact solution is only valid until either the bore or the rarefraction wave hits the walls. For a more in depth analysis of the exact solution, see Stoker [38] and Glaister [11].

2.1.2 Test Problem B: Wave Propagation Test Problem

LeVeque [26] discussed a wave propagation test problem with a pulse present in the riverbed and a small disturbance in the river. Since the riverbed is not constant, a source term is now present. The initial conditions are

$$u(x,0) = 0, \quad h(x,0) = \begin{cases} 1 + \omega - B(x) & \text{if } 0.1 \le x \le 0.2 \\ 1 - B(x) & \text{otherwise} \end{cases}$$

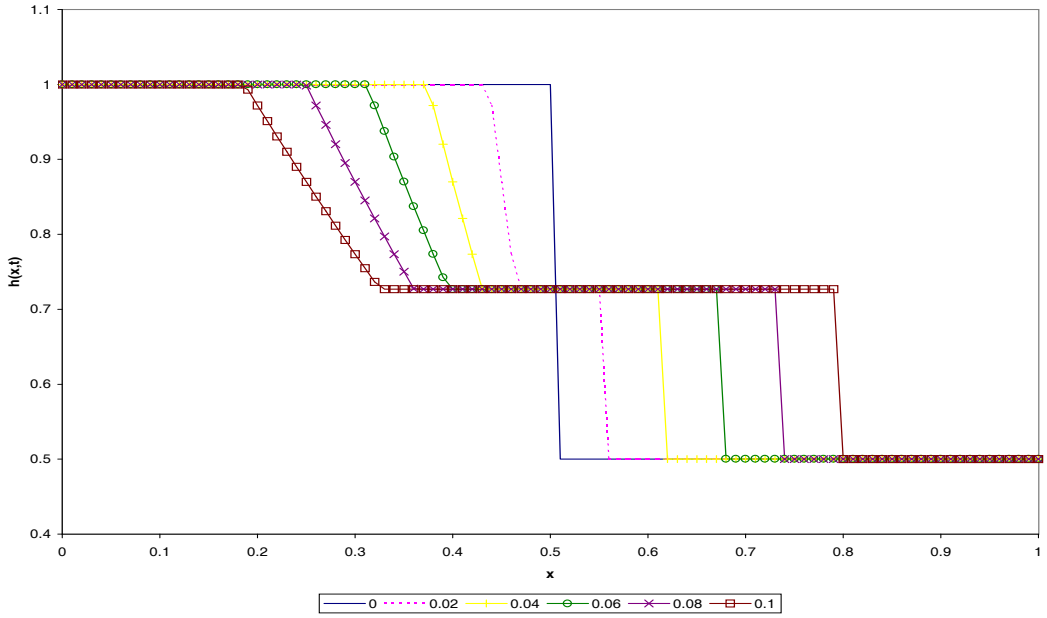

Figure 2.2: Exact solution of the dam break test problem for $t = 0$ to $0.1s$ (h).

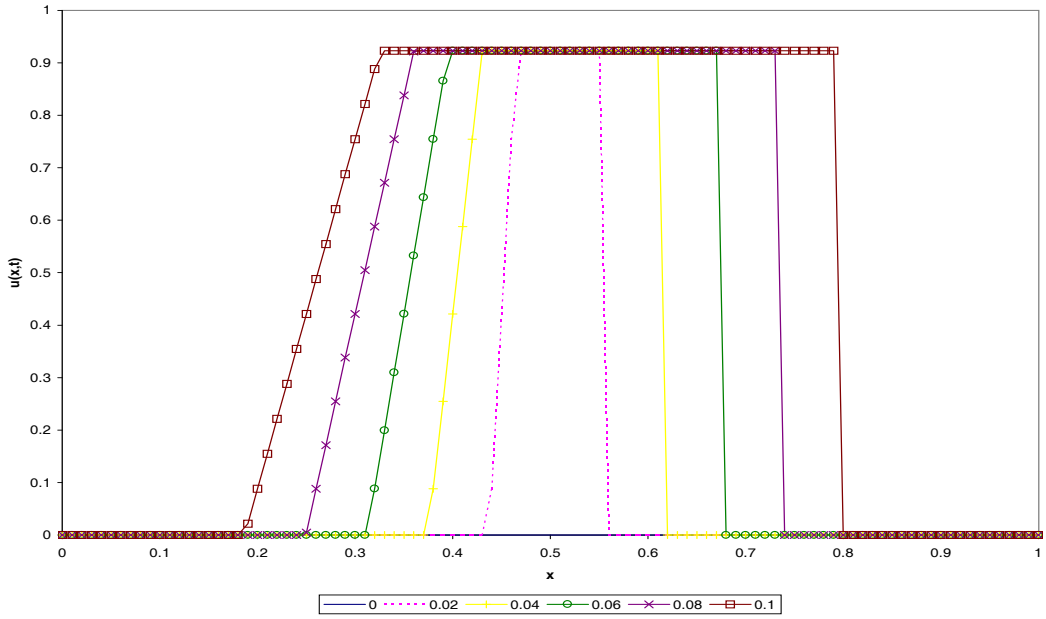

Figure 2.3: Exact solution of the dam break test problem for $t = 0$ to $0.1s$ (u).

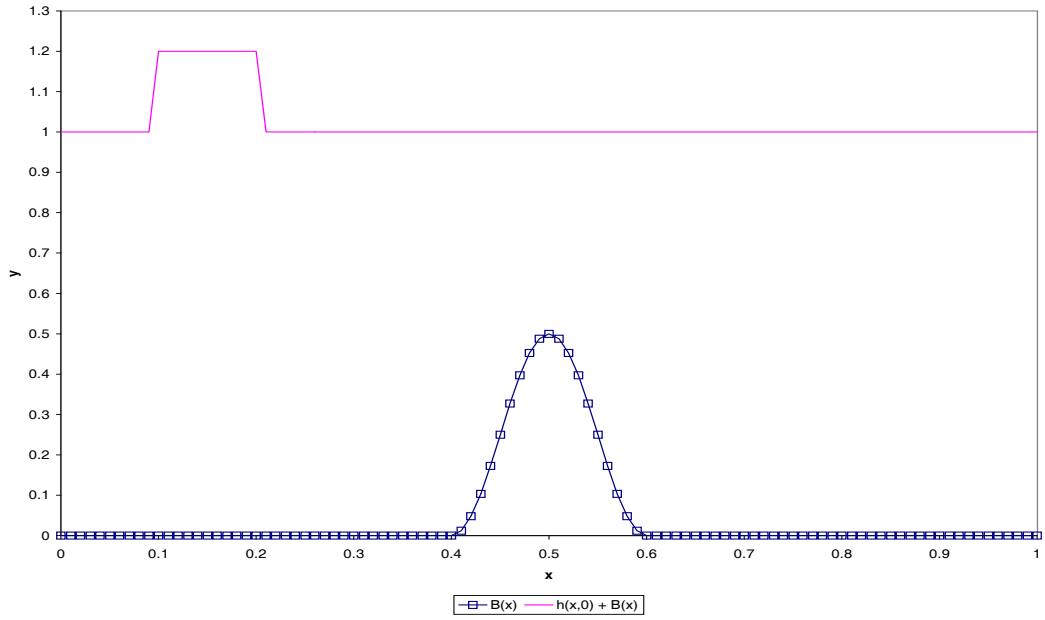

Figure 2.4: Initial conditions of the wave propagation test problem with $\omega = 0.2$ (h & B).

and the bathymetry is

$$B(x) = \begin{cases} \frac{1}{4}\left(\cos\left(10\pi\left(x - \frac{1}{2}\right)\right) + 1\right) & \text{if } |x - \frac{1}{2}| \leq \frac{1}{10} \\ 0 & \text{otherwise} \end{cases},$$

which are illustrated in Figure 2.4 for $\omega = 0.2$. The value of ω is taken as either 0.2 or 0.01 and we follow LeVeque [26] and use a gravitational constant of $g = 1$. The disturbance in the river created by ω splits into two waves propagating in opposite directions and for small ω the characteristic speeds are approximately $\pm\sqrt{gh}$. For small ω, an accurate numerical solution is harder to obtain.

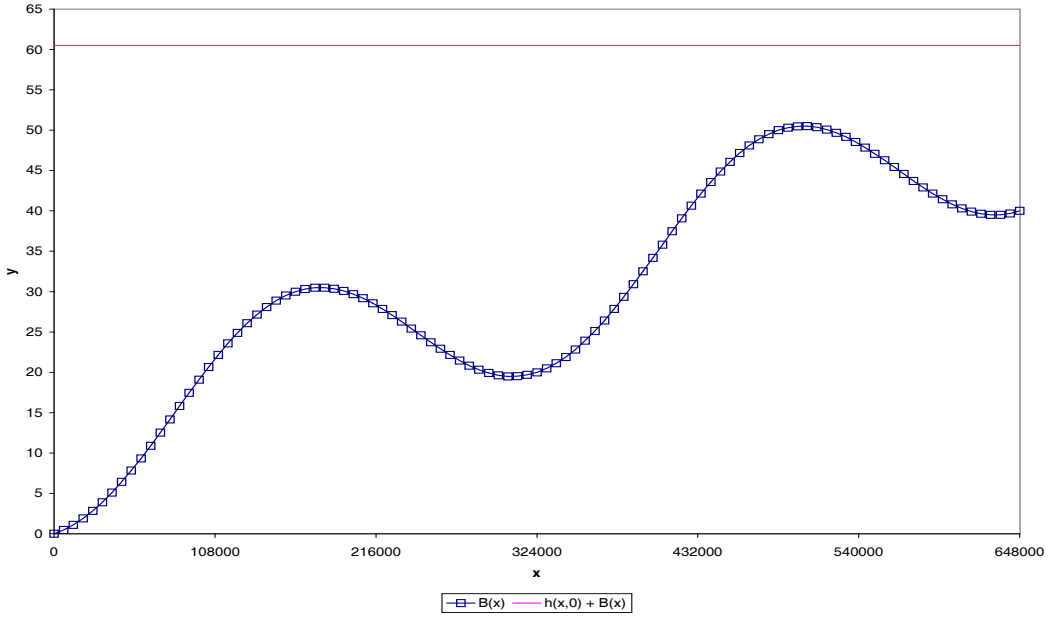

Figure 2.5: Initial conditions of the tidal wave propagation test problem (h & B).

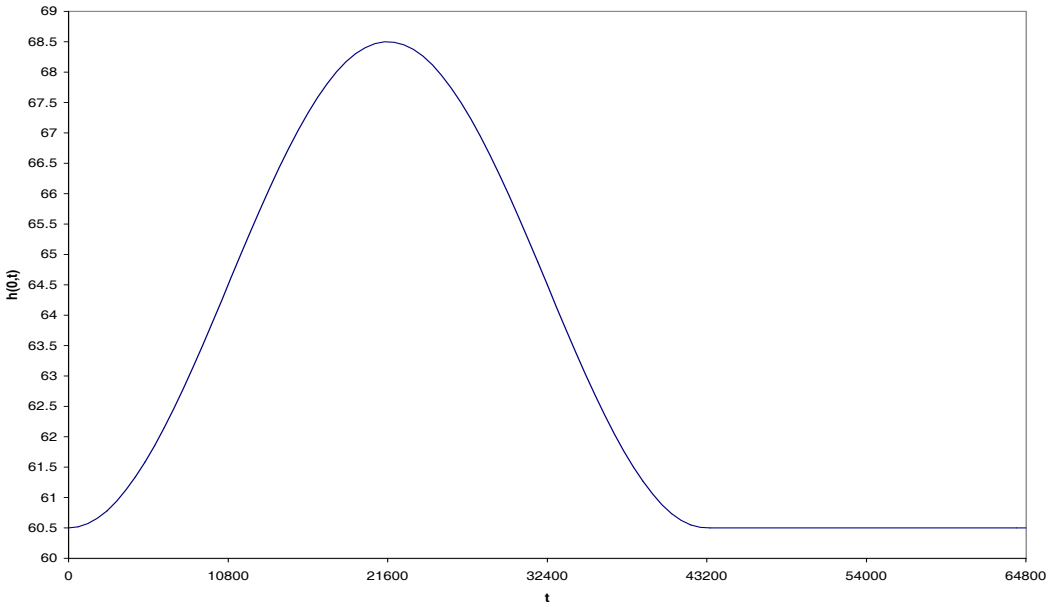

Figure 2.6: Upstream boundary condition of the tidal wave propagation test problem (h).

2.1.3 Test Problem C: Tidal Wave Propagation Test Problem

Bermúdez & Vázquez [1] discussed a tidal wave propagation test problem that consists of the initial conditions

$$u(x,0) = 0, \quad h(x,0) = 60.5 - B(x)$$

and bathymetry

$$B(x) = \frac{40x}{L} + 10\left(1 - \sin\left(\pi\left(\frac{4x}{L} + \frac{1}{2}\right)\right)\right),$$

where L is the length of the channel which is usually taken as $L = 648,000m$. The physical boundary condition,

$$h(0,t) = \begin{cases} 64.5 + 4\sin\left(\frac{\pi}{2}\left(\frac{t}{10800} - 1\right)\right) & \text{if } t \leq 43,200s \\ 60.5 & \text{if } t > 43,200s \end{cases}$$

is used to simulate a tidal wave of $4m$ amplitude entering the region at the upstream boundary, see Figure 2.6. At the downstream boundary, the physical boundary condition $u(L,t) = 0$ is also required. The tidal wave reaches a full height of $8m$ at $t = 21,600s$ and since the wave propagates at approximately $\sqrt{gh}$, at $t = 10,800s$ the tidal wave should have only reached as far as $x \approx 216,000m$ for $L = 648,000m$.

2.2 Conservative Numerical Schemes

We can accurately numerically approximate a system of conservation laws by using a conservative numerical scheme with source term approximation,

$$\mathbf{w}_i^{n+1} = \mathbf{w}_i^n - s(\mathbf{F}^*_{i+\frac{1}{2}} - \mathbf{F}^*_{i-\frac{1}{2}}) + s\mathbf{R}^*_i, \tag{2.3}$$

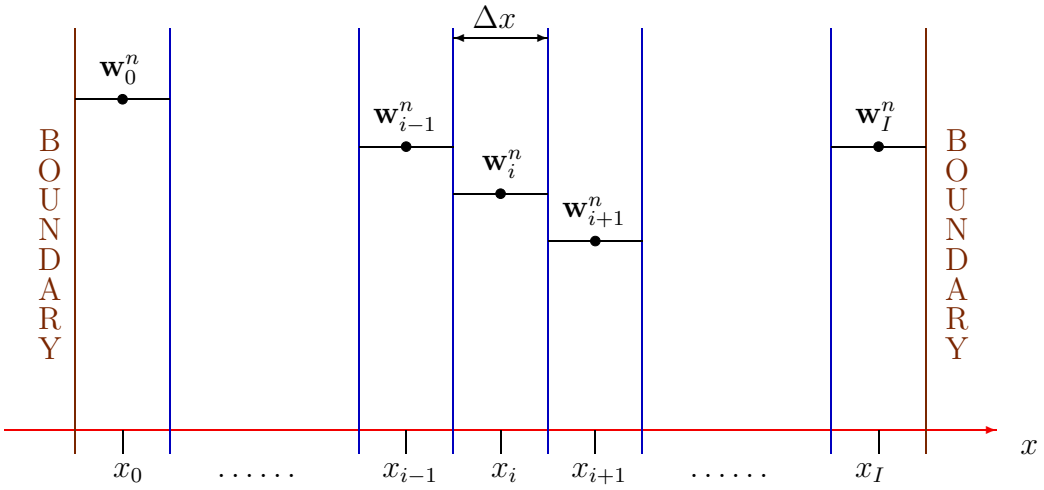

Figure 2.7: The one dimensional mesh.

where $s = \frac{\Delta t}{\Delta x}$, Δx and Δt are the step sizes in space and time respectively, $\mathbf{F}^*_{i+\frac{1}{2}}$ is the numerical flux, $\mathbf{R}^*_i$ is the source term approximation and

$$\mathbf{w}_i^n \approx \frac{1}{\Delta x} \int_{x_{i-\frac{1}{2}}}^{x_{i+\frac{1}{2}}} \mathbf{w}(x, t^n)\ dx$$

is the numerical approximation, see Figure 2.7. Here, the points $x = x_{-\frac{1}{2}}$ and $x = x_{I+\frac{1}{2}}$ are the spatial boundaries and we require numerical boundary conditions at these points. The spatial step size, Δx, is fixed and we use a variable time step,

$$\Delta t = \frac{\nu \Delta x}{\max_i(|\lambda_k|)},$$

where λ_k are the eigenvalues of the Jacobian matrix and ν is the required CFL number (Courant, Friedrichs and Lewey). Unless stated, all schemes discussed in this chapter are stable for $\nu \leq 1$.

To ensure the error of a numerical scheme does not grow, the variables are non-dimensionalised so that the spatial and time step-sizes are less than one, i.e. $\Delta x < 1$ and $\Delta t < 1$. For the shallow water equations, we non-dimensionalise the variables

by using

$$x^* = \frac{x}{L}, \quad t^* = \frac{t}{T}, \quad h^* = \frac{h}{L}, \quad B^* = \frac{B}{L}, \quad g^* = \frac{gT^2}{L} \quad \text{and} \quad u^* = \frac{uT}{L},$$

where

$$L = |x_I - x_0| \quad \text{and} \quad T = \sqrt{\frac{L}{g}}$$

denote the non-dimensional coefficients and L is the length of the domain.

2.2.1 Source Term Approximation

In gas dynamics, source terms can become stiff being extremely difficult to approximate accurately, see LeVeque & Yee [27] for more details. For the shallow water equations, the source term becomes increasingly difficult to approximate as the variation in the riverbed becomes more pronounced, see Hudson [20] for more details. In general, the source term can be approximated in two ways:

- a pointwise approach, where the source term approximation is calculated at the nodal points, i.e.
$$\mathbf{R}_i^* \approx \Delta x \mathbf{R}(\mathbf{w}_i^n).$$
- an upwind characteristic based approach, where the source term is approximated in a more physical way by averaging the source term,
$$\mathbf{R}_i^* \approx \frac{\Delta x}{2}\left(\mathbf{R}_{i+\frac{1}{2}}^n + \mathbf{R}_{i-\frac{1}{2}}^n\right),$$
and obtaining upwind approximations, $\mathbf{R}_{i\pm\frac{1}{2}}^n$, of the source term.

In general, the pointwise approach is considerably less accurate than the upwind approach due to the pointwise approach not satisfying the C-property, which is discussed in the next section.

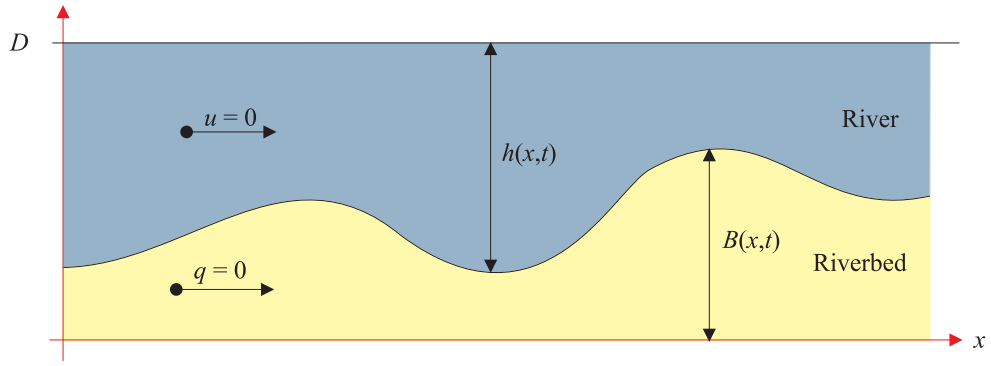

Figure 2.8: The quiescent flow case: $u = 0$ and $h = D - B$.

2.2.2 C-Property

Bermúdez & Vázquez [1] and Vázquez-Cendón [44] discussed an approach for approximating source terms which is designed for quasi-steady and steady flow. Consider the shallow water equations for the quiescent flow case,

$$u(x,t) \equiv 0 \quad \text{and} \quad h(x,t) \equiv D - B(x,t) \quad \forall (x,t),$$

see Figure 2.8. For this stationary case $\mathbf{w}_t = 0$ and thus the flux function and source term balance:

$$\mathbf{F}_x = \mathbf{R}.$$

Therefore, an accurate numerical scheme would also balance the numerical flux with the source term approximation,

$$\mathbf{F}^*_{i+\frac{1}{2}} - \mathbf{F}^*_{i-\frac{1}{2}} = \mathbf{R}^*_i.$$

Hence, we derive numerical schemes that satisfy the C-property (conservation property) when applied to the quiescent flow case. If the source term approximation balances with the numerical fluxes, then the numerical scheme satisfies:

- the approximate C-property, if the numerical scheme is accurate to the order $O(\Delta x^2)$ when applied to the quiescent flow case;

- the exact C-property, if the numerical scheme is exact when applied to the quiescent flow case.

If a numerical scheme does not satisfy the C-property (exact or approximate) then spurious waves may occur in the numerical results.

2.3 High-Resolution Schemes

Unfortunately, second order numerical schemes suffer from dispersion resulting in spurious oscillations appearing in the numerical results, especially around discontinuities. This is due to second order numerical schemes not satisfying the Total Variational Diminishing (TVD) property, which is discussed in the next section. Thus, we construct a numerical scheme that satisfies the TVD property by using a second order accurate numerical scheme on smooth solutions and adding diffusion to the numerical scheme near discontinuities. We call such numerical schemes high-resolution schemes, which are at least second order accurate on smooth solutions and minimise the spurious oscillations present near discontinuities.

2.3.1 Total Variational Diminishing

Consider the scalar conservation law

$$w_t + f_x = 0, \tag{2.4}$$

which can be numerically approximated by using the conservative numerical scheme

$$w_i^{n+1} = w_i^n - s\left(f^*_{i+\frac{1}{2}} - f^*_{i-\frac{1}{2}}\right). \tag{2.5}$$

The exact solution of a scalar conservation law (2.4) has Total Variation,

$$\mathrm{TV}(w) = \int |w_x| \; dx,$$

which does not increase and only decreases across shocks, see Lax [23] for more details. For scalar conservation laws (2.4), this property can be used to eliminate spurious oscillations present in a numerical scheme. Unfortunately, this property does not hold for systems of conservation laws but the design criteria based on this property can still be used to minimise the spurious oscillations present in a numerical scheme when applied to systems. Harten [15] deduced that a numerical scheme should also satisfy the Total Variation Diminishing (TVD) property,

$$\mathrm{TV}(w^{n+1}) \leq \mathrm{TV}(w^n),$$

where the numerical Total Variation is defined by

$$\mathrm{TV}(w^{n+1}) = \sum_i |w_{i+1}^{n+1} - w_i^{n+1}|.$$

For scalar conservation laws, if a numerical scheme satisfies the TVD property, then no spurious oscillations will occur in the numerical results. Harten [15] discussed an approach that determines if a numerical scheme is TVD by re-writing (2.5) as

$$w_i^{n+1} = w_i^n + D_{i+\frac{1}{2}}^n \left(w_{i+1}^n - w_i^n\right) - C_{i-\frac{1}{2}}^n \left(w_i^n - w_{i-1}^n\right).$$

and determining if the inequalities

$$C_{i+\frac{1}{2}}^n \geq 0, \quad D_{i+\frac{1}{2}}^n \geq 0 \quad \text{and} \quad 0 \leq C_{i+\frac{1}{2}}^n + D_{i+\frac{1}{2}}^n \leq 1$$

are satisfied $\forall i$. If the inequalities are satisfied, the numerical scheme satisfies the TVD property.

Flux-limiter	$\Phi(\theta)$
Minmod	$\max(0, \min(1, \theta))$
Roe's Superbee	$\max(0, \min(2\theta, 1), \min(\theta, 2))$
van Leer	$\dfrac{\lvert\theta\rvert + \theta}{1 + \lvert\theta\rvert}$
van Albada	$\dfrac{\theta^2 + \theta}{1 + \theta^2}$

Table 2.1: Some flux-limiters

2.3.2 Flux-Limiter Methods

One approach we can use to construct a high-resolution scheme is to use a flux-limiter method as discussed by Sweby [40] and LeVeque [25]. For the scalar conservation law (2.4), we used the conservative numerical scheme (2.5). Flux-limiter methods construct a numerical flux of the form

$$f^{TVD}_{i+\frac{1}{2}} = f^{FO}_{i+\frac{1}{2}} + \Phi^n_{i+\frac{1}{2}} \left(f^{SO}_{i+\frac{1}{2}} - f^{FO}_{i+\frac{1}{2}} \right), \tag{2.6}$$

where $f^{SO}_{i+\frac{1}{2}}$ is a second order numerical flux, $f^{FO}_{i+\frac{1}{2}}$ is a first order numerical flux and $\Phi^n_{i+\frac{1}{2}}$ is a limiter. The limiter is chosen such that if the data is smooth, then the limiter is 1, which reverts the numerical flux to a second order approximation but if the data is near a discontinuity, the limiter is 0, which reverts the numerical flux to a first order approximation. van Leer [41] and Roe [34] discussed an approach we can use to measure the smoothness of the data by looking at the ratio of consecutive gradients,

$$\theta^n_{i+\frac{1}{2}} = \frac{w^n_{I+1} - w^n_I}{w^n_{i+1} - w^n_i}, \quad \text{where} \quad I = i - \operatorname{sgn}\left(\lambda^n_{i+\frac{1}{2}}\right).$$

Here, λ is the wave speed and if $\theta^n_{i+\frac{1}{2}}$ is close to 1, then the data is smooth, but if $\theta^n_{i+\frac{1}{2}}$ is near 0, then a kink is present in the data. Thus, we take $\Phi^n_{i+\frac{1}{2}}$ to be a

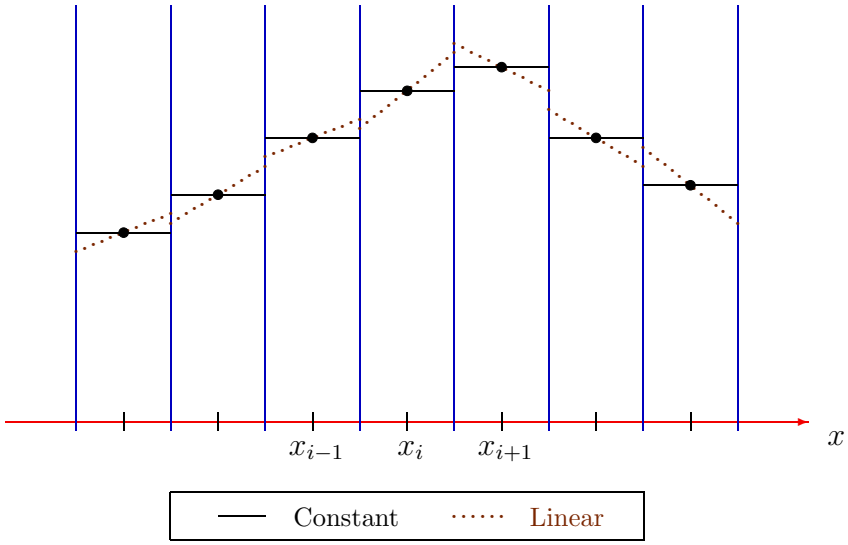

Figure 2.9: A piecewise constant and linear representation.

function of $\theta^n_{i+\frac{1}{2}}$, i.e.

$$\Phi^n_{i+\frac{1}{2}} = \Phi\left(\theta^n_{i+\frac{1}{2}}\right),$$

where Φ is a given function. Sweby [40] discussed a variety of limiters that guarantee second order accuracy whilst still satisfying the TVD property, which are listed in Table 2.1.

2.3.3 Slope-Limiter Methods

We can also use a geometric approach to obtain a high-resolution scheme. LeVeque [25] discussed slope-limiter methods in detail and noted that to obtain a slope-limiter method, we must construct a numerical scheme as follows:

1. We use the numerical data w^n_i and construct a piecewise linear function

$$\tilde{w}^n(x, t^n) = w^n_i + \sigma^n_i(x - x_i) \quad \text{where} \quad x_{i-\frac{1}{2}} < x < x_{i+\frac{1}{2}}$$

and $\sigma^n_i = \frac{\Delta_i w}{\Delta x}$ is the slope of the ith cell, see Figure 2.9, which is based on the numerical data.

2. The exact solution of a generalised Riemann problem, $\tilde{w}^n(x, t^{n+1})$, which is related to (2.4) is then obtained using the piecewise linear function.

3. The exact solution is then averaged,

$$w_i^{n+1} = \frac{1}{\Delta x} \int_{x_{i-\frac{1}{2}}}^{x_{i+\frac{1}{2}}} \tilde{w}^n(x, t^{n+1}) dx,$$

to obtain the new data w_i^{n+1} and the process is repeated.

Consider the following example, as discussed by LeVeque [25], for the scalar linear advection equation,

$$w_t + a w_x = 0,$$

whose exact solution is

$$w(x, t) = w(x - at, 0).$$

By constructing the piecewise linear function described in step 1 from the data, we obtain the exact solution

$$\tilde{w}^n(x, t^{n+1}) = \tilde{w}^n(x - a\Delta t, t^n),$$

and by integrating the exact solution (for $a > 0$) as described in step 3, we obtain

$$w_i^{n+1} = w_i^n - \nu(w_i^n - w_{i-1}^n) - \frac{1}{2} a \Delta t (1 - \nu)(\sigma_i^n - \sigma_{i-1}^n). \tag{2.7}$$

Now, we must choose the slopes, σ_i^n, such that the scheme (2.7) is second order accurate and satisfies the TVD property. If we choose $\sigma_i^n = 0$, we obtain the first order upwind scheme and by choosing $\sigma_i^n = \frac{1}{\Delta x}(w_{i+1}^n - w_i^n)$, we obtain the classic Lax-Wendroff scheme. If the upwind slopes are used, the scheme is not second order accurate and if the Lax-Wendroff slopes are used, then overshoots may occur in the piecewise linear representation, see Figure 2.9, which results in an increase in Total Variation. Thus, we can view these as being a poor choice of slopes. A better choice of slopes, which makes the scheme second order accurate and satisfy the TVD

property, is to use the minmod limiter,

$$\sigma_i^n = \frac{1}{\Delta x}\text{minmod}(w_{i+1}^n - w_i^n, w_i^n - w_{i-1}^n),$$

where

$$\text{minmod}(a, b) = \frac{1}{2}(\text{sgn}(a) + \text{sgn}(b))\min(|a|, |b|).$$

It is also interesting to note that by setting

$$\sigma_i^n = \frac{1}{\Delta x}(w_{i+1}^n - w_i^n)\Phi_{i+\frac{1}{2}}^n,$$

the scheme reverts back to a flux-limited scheme, where $\Phi_{i+\frac{1}{2}}^n$ is a flux-limiter, which was discussed in the previous section. Thus, the minmod limiter can also be used as a slope-limiter.

2.4 Boundary Conditions

Boundary conditions are required at the upstream and downstream boundaries. For:

- Test Problem A, walls are present at the upstream and downstream boundaries and thus we need to reflect the velocity

  $$u_{-i}^n = -u_{i-1}^n \quad \text{and} \quad u_{I+i}^n = -u_{I-i-1}^n$$

  and for the water depth, we use the simple boundary conditions

  $$h_{-i}^n = h_0^n \quad \text{and} \quad h_{I+i}^n = h_I^n,$$

  where $i = 1, 2$.

- Test Problem B, we require transmissive boundary conditions due to the disturbance in the river splitting into two waves travelling in opposite directions, which we discuss next.

- Test Problem C, we use the physical boundary conditions

$$h^n_{-i} = h(0, t^n) \quad \text{and} \quad u^n_{I+i} = 0,$$

where $i = 0, 1, 2$ and the numerical boundary conditions

$$h^n_{I+i} = h^0_I \quad \text{and} \quad u^n_{-i} = u^n_0,$$

where $i = 1, 2$.

2.4.1 Transmissive Boundary Conditions

In some test problems, waves pass through the boundaries and, if the incorrect boundary conditions are chosen, then the wave may be reflected back into the domain resulting in an inaccurate numerical solution. Transmissive boundary conditions allow waves to leave the region without being reflected back into the domain. One type of transmissive boundary conditions can be obtained by using the k-Riemann invariants (see Godlewski & Raviart [13]), which are obtained by solving

$$\frac{\partial r_k}{\partial \mathbf{w}} \cdot \mathbf{e}_k = 0,$$

where $\mathbf{e}_k$ are the eigenvectors, r denotes the k-Riemann invariants and k is the k^{th} component of the system. For the shallow water equations we have

$$\frac{\partial r_1}{\partial h} + \left(u - \sqrt{gh}\right) \frac{\partial r_1}{\partial (uh)} = 0$$

and

$$\frac{\partial r_2}{\partial h} + \left(u + \sqrt{gh}\right) \frac{\partial r_2}{\partial (uh)} = 0$$

and by solving the two equations, we obtain

$$r_1 = u - 2\sqrt{gh} \quad \text{and} \quad r_2 = u + 2\sqrt{gh}.$$

Hence, by using the k-Riemann invariants, we obtain the following approximations of u and h,

$$u = \frac{1}{2}(r_1 + r_2) \quad \text{and} \quad h = \frac{1}{16g}(r_2 - r_1)^2.$$

We can use these approximations of u and h at the boundaries to allow waves to pass through without being reflected back into the domain. For subcritical flow, i.e. $\sqrt{gh} > |u|$, r_1 and r_2 represent the left and right moving waves respectively. Thus, at the upstream boundary, we want to eliminate all the right moving waves but let the left moving waves pass through the boundary, which may be obtained by setting

$$r_1 = u_1^n - 2\sqrt{gh_1^n} \quad \text{and} \quad r_2 = u_0^* + 2\sqrt{gh_0^*},$$

where u_0^* and h_0^* denote the initial values of the velocity and height of the river at the upstream boundary respectively. Similarly, at the downstream boundary, we want to eliminate all the left moving waves but let the right moving waves pass through the boundary, which may be obtained by setting

$$r_1 = u_I^* - 2\sqrt{gh_I^*} \quad \text{and} \quad r_2 = u_{I-1}^n + 2\sqrt{gh_{I-1}^n},$$

where u_I^* and h_I^* denote the initial values of the velocity and height of the water above the bottom of the channel at the downstream boundary respectively.

2.5 LxF and NT Scheme

2.5.1 Adapted LxF Scheme

One of the most basic numerical schemes we can use to approximate (2.1) is the Lax-Friedrichs (LxF) scheme as discussed by Garcia-Navarro *et al.* [9],

$$\mathbf{w}_i^{n+1} = \theta \mathbf{w}_i^n + \frac{1-\theta}{2}(\mathbf{w}_{i+1}^n + \mathbf{w}_{i-1}^n) - \frac{s}{2}(\mathbf{F}_{i+1}^n - \mathbf{F}_{i-1}^n) + s\mathbf{R}_i^*, \tag{2.8}$$

where $0 \leq \theta \leq 1$. The scheme is unstable for a value of $\theta = 1$ and as $\theta \longrightarrow 0$, the scheme becomes more stable but unfortunately more diffusive. The value of $\theta = 0.1$ is most commonly used and $\theta = 0$ is the classic Lax-Friedrichs scheme. Unfortunately, the Lax-Friedrichs scheme suffers badly from diffusion and a "staircase" effect, where kinks are present in the numerical results, can sometimes occur in the numerical results, especially for $\theta = 0$. However a numerical approximation of the Jacobian is not required.

We use a centralised pointwise approach to approximate the source term, $\mathbf{R}_i^n$, and for the shallow water equations this takes the form

$$\mathbf{R}_i^* = \begin{bmatrix} 0 \\ -\dfrac{g}{4}(h_{i+1}^n + h_{i-1}^n)(B_{i+1}^n - B_{i-1}^n) \end{bmatrix}.$$

Unfortunately, we cannot derive a source term approximation that makes the Lax-Friedrichs scheme satisfy the C-property. For the quiescent flow case,

$$h_i^{n+1} = \theta h_i^n + \frac{1-\theta}{2}\left(h_{i+1}^n + h_{i-1}^n\right)$$

and since $h \approx D - B$ and $h_i^{n+1} = h_i^n$, we obtain

$$(\theta - 1)\left(B_{i+1} - 2B_i + B_{i-1}\right) = 0,$$

which can only be satisfied if either $\theta = 1$ or the riverbed is linear. Taking $\theta = 1$ renders the numerical scheme unstable and the source term is zero when the bed is linear.

2.5.2 Staggered and Non-Staggered LxF Scheme

Nessyahu & Tadmor [30] and Jiang *et al.* [22] discussed a first order central scheme called the staggered LxF scheme,

$$\mathbf{w}_{i+\frac{1}{2}}^{n+1} = \frac{1}{2}(\mathbf{w}_{i+1}^n + \mathbf{w}_i^n) - s(\mathbf{F}_{i+1}^n - \mathbf{F}_i^n) + s\mathbf{R}_{i+\frac{1}{2}}^n, \tag{2.9}$$

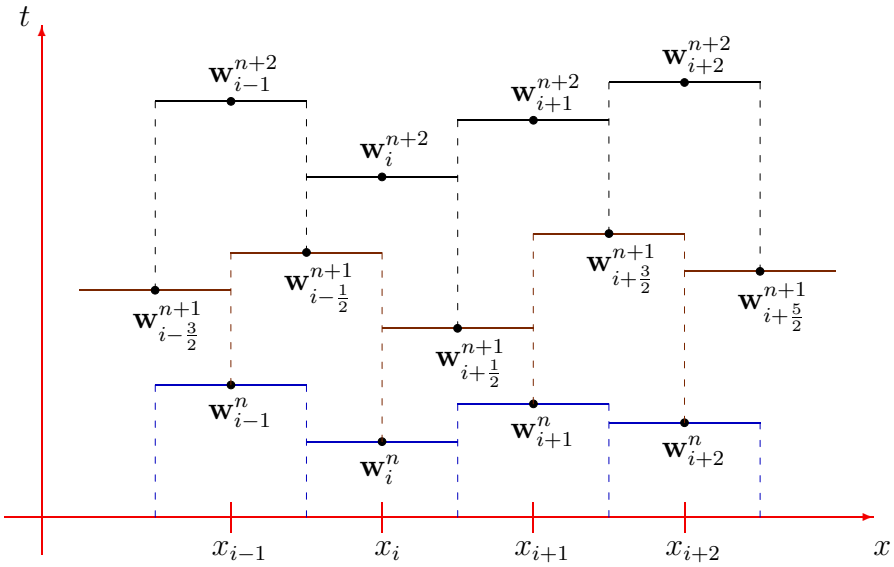

Figure 2.10: Staggered grid.

which is a modified version of the classic Lax-Friedrichs scheme (LxF) and is derived on a staggered grid, see Figure 2.10. The scheme has been adapted to include a pointwise source term approximation, which for the shallow water equations takes the form

$$\mathbf{R}^*_{i+\frac{1}{2}} = \begin{bmatrix} 0 \\ -\dfrac{g}{2}(h^n_{i+1} + h^n_i)(B^n_{i+1} - B^n_i) \end{bmatrix}.$$

We can obtain a non-staggered version of this scheme by averaging the two neighbouring staggered cells,

$$\begin{aligned} \mathbf{w}_i^{n+1} &= \frac{1}{2}\left(\mathbf{w}^{n+1}_{i+\frac{1}{2}} + \mathbf{w}^{n+1}_{i-\frac{1}{2}}\right) \\ &= \frac{1}{4}\left(\mathbf{w}^n_{i+1} + 2\mathbf{w}^n_i + \mathbf{w}^n_{i-1}\right) - \frac{s}{2}\left(\mathbf{F}^n_{i+1} - \mathbf{F}^n_{i-1}\right) + \frac{s}{2}\left(\mathbf{R}^n_{i+\frac{1}{2}} + \mathbf{R}^n_{i-\frac{1}{2}}\right). \end{aligned} \quad (2.10)$$

By averaging the staggered version of the scheme, we slightly reduce the accuracy but obtain numerical results at the desired points. As with the adapted LxF scheme, both the staggered and non-staggered version of the LxF scheme do not satisfy the C-property and are stable for $\nu \leq 0.5$. Notice that by using the staggered or non-staggered LxF scheme, the Courant number has halved compared to the adapted LxF scheme.

2.5.3 Central, Staggered and Non-Staggered NT Scheme

Nessyahu & Tadmor [30] extended the staggered LxF scheme to second order and derived a high-resolution non-oscillatory central difference scheme called the staggered NT scheme,

$$\mathbf{w}_{i+\frac{1}{2}}^{n+1} = \frac{1}{2}\left(\mathbf{w}_{i+1}^{n} + \mathbf{w}_{i}^{n}\right) - \frac{1}{8}\left((\mathbf{w}_x)_{i+1}^{n} - (\mathbf{w}_x)_{i}^{n}\right) - s\left(\mathbf{F}_{i+1}^{n+\frac{1}{2}} - \mathbf{F}_{i}^{n+\frac{1}{2}}\right) + s\mathbf{R}_{i+\frac{1}{2}}^{n+\frac{1}{2}}, \quad (2.11)$$

where

$$\mathbf{w}_{i}^{n+\frac{1}{2}} = \mathbf{w}_{i}^{n} + \frac{s}{2}\left(\mathbf{R}_{i}^{n} - (\mathbf{F}_x)_{i}^{n}\right).$$

The staggered NT scheme (2.11) has been adapted to approximate a system of conservation laws with source term present (2.1). To ensure that the staggered NT scheme is non-oscillatory, we use either the limiter

$$(\mathbf{w}_x)_{i}^{n} = \mathrm{MM}\left(\alpha\Delta\mathbf{w}_{i+\frac{1}{2}}, \frac{1}{2}\left(\Delta\mathbf{w}_{i+\frac{1}{2}} + \Delta\mathbf{w}_{i-\frac{1}{2}}\right), \alpha\Delta\mathbf{w}_{i-\frac{1}{2}}\right), \quad (2.12)$$

where $0 \leq \alpha < 4$, or the UNO limiter [16]

$$(\mathbf{w}_x)_{i}^{n} = \mathrm{MM}\left(\Delta\mathbf{w}_{i+\frac{1}{2}} - \frac{1}{2}\mathrm{MM}\left(\Delta^2\mathbf{w}_{i+1}, \Delta^2\mathbf{w}_{i}\right), \Delta\mathbf{w}_{i-\frac{1}{2}} + \frac{1}{2}\mathrm{MM}\left(\Delta^2\mathbf{w}_{i}, \Delta^2\mathbf{w}_{i-1}\right)\right), \quad (2.13)$$

where $\Delta\mathbf{w}_{i+\frac{1}{2}} = \mathbf{w}_{i+1}^{n} - \mathbf{w}_{i}^{n}$, $\Delta^2\mathbf{w}_{i} = \mathbf{w}_{i+1}^{n} - 2\mathbf{w}_{i}^{n} + \mathbf{w}_{i-1}^{n}$. Here, MM denotes the minmod limiter

$$\mathrm{minmod}(a,b,c) = \begin{cases} d\min(|a|,|b|,|c|) & \text{if } d = \mathrm{sgn}(a) = \mathrm{sgn}(b) = \mathrm{sgn}(c), \\ 0 & \text{otherwise.} \end{cases}$$

The value of $(\mathbf{F}_x)_{i}^{n}$ can be determined from either the UNO limiter, (2.12) or from $(\mathbf{F}_x)_{i}^{n} = \mathbf{A}_{i}^{n}(\mathbf{w}_x)_{i}^{n}$. Notice that setting the numerical approximations $(\mathbf{w}_x)_{i}^{n} = (\mathbf{F}_x)_{i}^{n} = 0$ reverts the scheme to the first order LxF scheme.

We use a centralised pointwise approach to approximate the source term, $\mathbf{R}_{i}^{n}$,

and for the shallow water equations this takes the form

$$\mathbf{R}_i^n = \begin{bmatrix} 0 \\ -gh_i^n(B_x)_i^n \end{bmatrix} \quad \text{and} \quad \mathbf{R}_{i+\frac{1}{2}}^{n+\frac{1}{2}} = \begin{bmatrix} 0 \\ -\frac{g}{2}(h_{i+1}^{n+\frac{1}{2}} + h_i^{n+\frac{1}{2}})(B_{i+1}^{n+\frac{1}{2}} - B_i^{n+\frac{1}{2}}) \end{bmatrix}.$$

A non-staggered version of the NT scheme can be obtained with a slight loss of accuracy by averaging the neighbouring staggered cells with a piecewise-linear interpolant to obtain

$$\mathbf{w}_i^{n+1} = \frac{1}{2}\left(\mathbf{w}_{i+\frac{1}{2}}^{n+1} + \mathbf{w}_{i-\frac{1}{2}}^{n+1}\right) - \frac{1}{8}\left((\mathbf{w}_x)_{i+\frac{1}{2}}^n - (\mathbf{w}_x)_{i-\frac{1}{2}}^n\right),$$

where

$$(\mathbf{w}_x)_{i+\frac{1}{2}}^n = \mathrm{MM}\left(\Delta\mathbf{w}_{i+1}^{n+1}, \Delta\mathbf{w}_i^{n+1}\right) \quad \text{and} \quad \Delta\mathbf{w}_i^{n+1} = \mathbf{w}_{i+\frac{1}{2}}^{n+1} - \mathbf{w}_{i-\frac{1}{2}}^{n+1}.$$

Hence,

$$\mathbf{w}_i^{n+1} = \frac{1}{4}\left(\mathbf{w}_{i+1}^n + 2\mathbf{w}_i^n + \mathbf{w}_{i-1}^n\right) - \frac{1}{16}\left((\mathbf{w}_x)_{i+1}^n - (\mathbf{w}_x)_{i-1}^n\right) - \frac{1}{8}\left((\mathbf{w}_x)_{i+\frac{1}{2}}^n - (\mathbf{w}_x)_{i-\frac{1}{2}}^n\right) - \frac{s}{2}\left(\mathbf{F}_{i+1}^{n+\frac{1}{2}} - \mathbf{F}_{i-1}^{n+\frac{1}{2}}\right) + \frac{s}{2}\left(\mathbf{R}_{i+\frac{1}{2}}^{n+\frac{1}{2}} + \mathbf{R}_{i-\frac{1}{2}}^{n+\frac{1}{2}}\right), \quad (2.14)$$

which is the non-staggered NT scheme. Both the staggered and non-staggered version of the NT scheme are stable for $\nu \leq 0.5$ and as with the first order LxF schemes, neither satisfy the C-property.

Nessyahu & Tadmor [30] also extended the classic central Lax-Friedrichs scheme, (2.8) with $\theta = 0$, to second order. The high-resolution central NT scheme is

$$\mathbf{w}_i^{n+1} = \frac{1}{2}\left(\mathbf{w}_{i+1}^n + \mathbf{w}_{i-1}^n\right) - \frac{1}{4}\left((\mathbf{w}_x)_{i+1}^n - (\mathbf{w}_x)_{i-1}^n\right) - \frac{s}{2}\left(\mathbf{F}_{i+1}^{n+\frac{1}{2}} - \mathbf{F}_{i-1}^{n+\frac{1}{2}}\right) + s\mathbf{R}_i^{n+\frac{1}{2}}, \quad (2.15)$$

where

$$\mathbf{w}_i^{n+\frac{1}{2}} = \mathbf{w}_i^n + \frac{s}{2}\left(\mathbf{R}_i^n - (\mathbf{F}_x)_i^n\right)$$

and for the shallow water equations the source term approximations are

$$\mathbf{R}_i^n = \begin{bmatrix} 0 \\ -gh_i^n(B_x)_i^n \end{bmatrix} \quad \text{and} \quad \mathbf{R}_i^{n+\frac{1}{2}} = \begin{bmatrix} 0 \\ -\frac{g}{4}(h_{i+1}^{n+\frac{1}{2}} + h_{i-1}^{n+\frac{1}{2}})(B_{i+1}^{n+\frac{1}{2}} - B_{i-1}^{n+\frac{1}{2}}) \end{bmatrix}.$$

The high-resolution central NT scheme is stable for $\nu \leq 1$ and does not satisfy the C-property. If we set the numerical approximations $(\mathbf{w}_x)_i^n = (\mathbf{F}_x)_i^n = 0$, then the central NT scheme reverts back to the classic Lax-Friedrichs scheme.

2.5.4 Numerical Results of the First Order LxF Schemes

To compare the different versions of the LxF schemes, we use Test Problem A, which is the dam break test problem. The dam break test problem is used with $h_L = 1m$ and $h_R = 0.5m$. The central and adapted LxF schemes are used with $\nu = 0.8$ and the staggered and non-staggered LxF schemes are used with $\nu = 0.4$. By using the different first order LxF schemes with $\Delta x = 0.01m$, we obtain the numerical results in Figure 2.11 and Figure 2.12. The dam break test problem also has an exact solution which is illustrated to show the accuracy of the different LxF schemes. Here, we can see that the staggered LxF scheme produced the most accurate numerical results but the scheme was still very dissipative. The non-staggered LxF scheme produced similar numerical results to the staggered LxF scheme but they were less accurate due to the scheme being more diffusive. The adapted LxF scheme with $\theta = 0.1$ was more diffusive than both the staggered and non-staggered LxF schemes. The central LxF scheme, which is the classic Lax-Friedrichs scheme, produced completely inaccurate numerical results due to the "staircase" effect.

Test Problem A does not have a source term present thus, we use Test Problem B, which is the wave propagation test problem to determine which first order LxF scheme is the most accurate when a source term is present. For this test problem, we use $\omega = 0.2$ and $\Delta x = 0.01$. The central and adapted LxF schemes are used with $\nu = 0.8$ and the staggered and non-staggered LxF schemes are used with $\nu = 0.4$. A flux-limited second order version of Roe's scheme, which is discussed in Section 2.7,

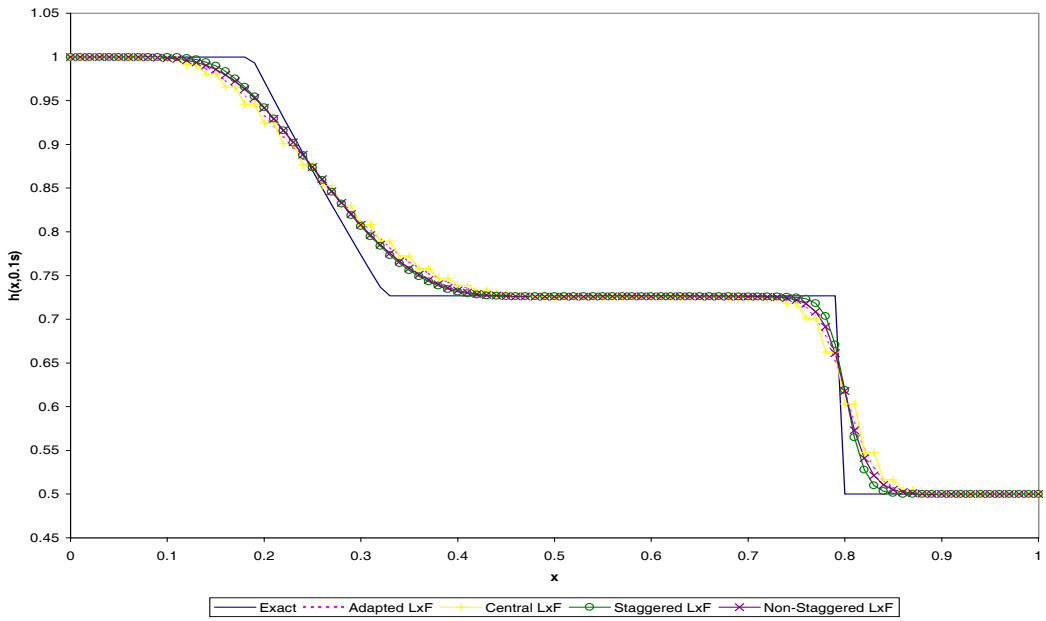

Figure 2.11: Numerical results of the different first order LxF schemes for Test Problem A at $t = 0.1s$ (h).

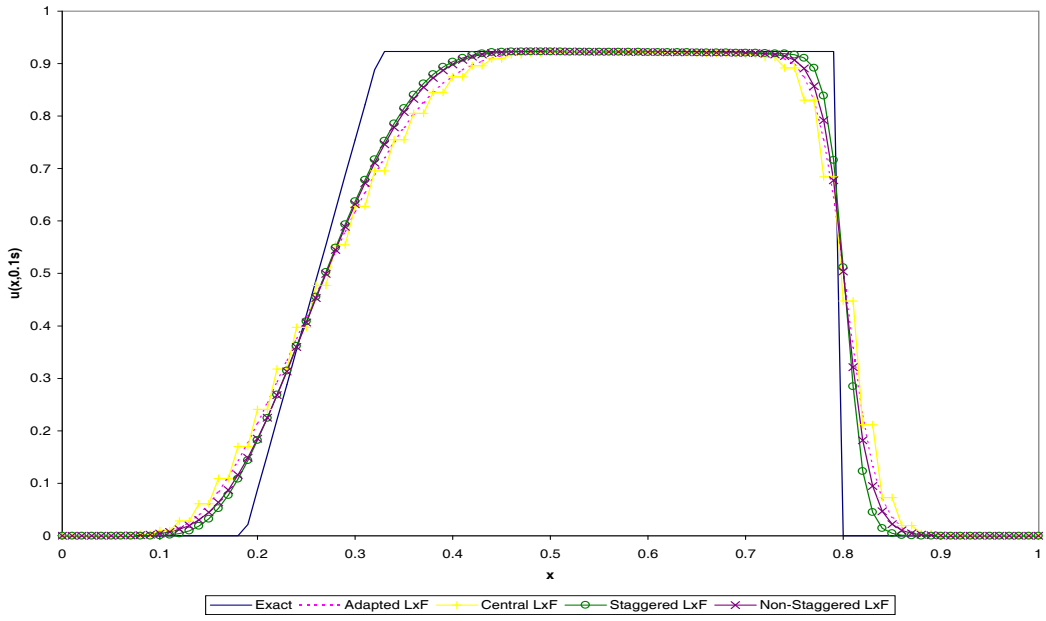

Figure 2.12: Numerical results of the different first order LxF schemes for Test Problem A at $t = 0.1s$ (u).

on a fine mesh, $\Delta x = 0.0001$, is also used as a reference solution. From Figure 2.13 and Figure 2.14, we can see that none of the different first order LxF schemes have produced accurate results compared to the fine mesh numerical results. All of the numerical schemes suffered badly from diffusion and have produced oscillations over the pulse in the riverbed. This is due to none of the numerical schemes satisfying the C-property and thus oscillations have occurred in the numerical results.

2.5.5 Numerical Results of the High-Resolution NT Schemes

To compare the different versions of the high-resolution NT schemes, we use Test Problem B, which is the wave propagation test problem. For this test problem, we use $\omega = 0.2$ and $\Delta x = 0.01$. The central and adapted NT schemes are used with $\nu = 0.8$ and the staggered and non-staggered NT schemes are used with $\nu = 0.4$. A flux-limited second order version of Roe's scheme, which is discussed in Section 2.7, on a fine mesh, $\Delta x = 0.0001$, is also used as a reference solution. From Figure 2.15 and Figure 2.16, we can see that as with the first order LxF schemes, none of the different high-resolution NT schemes have produced accurate results compared to the fine mesh numerical results. All of the numerical schemes suffered badly from oscillations and the central NT scheme has again produced the "staircase" effect. This is due to none of the numerical schemes satisfying the C-property and thus, oscillations have occurred in the numerical results.

Hence, when a source term is present, the LxF and NT schemes produce inaccurate numerical results due to spurious oscillations being present. These spurious oscillations can be reduced by making the LxF and NT schemes satisfy the C-property but unfortunately, no source term approximation can be derived that makes the schemes satisfy the C-property.

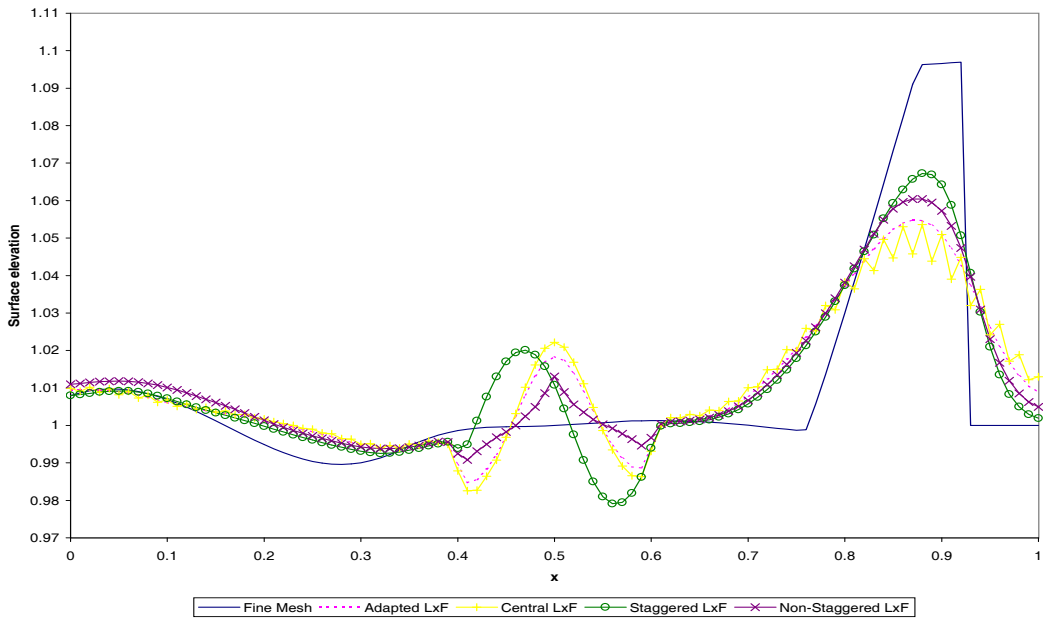

Figure 2.13: Numerical results of the different first order LxF schemes for Test Problem B with $\omega = 0.2$ at $t = 0.7$ $(h + B)$.

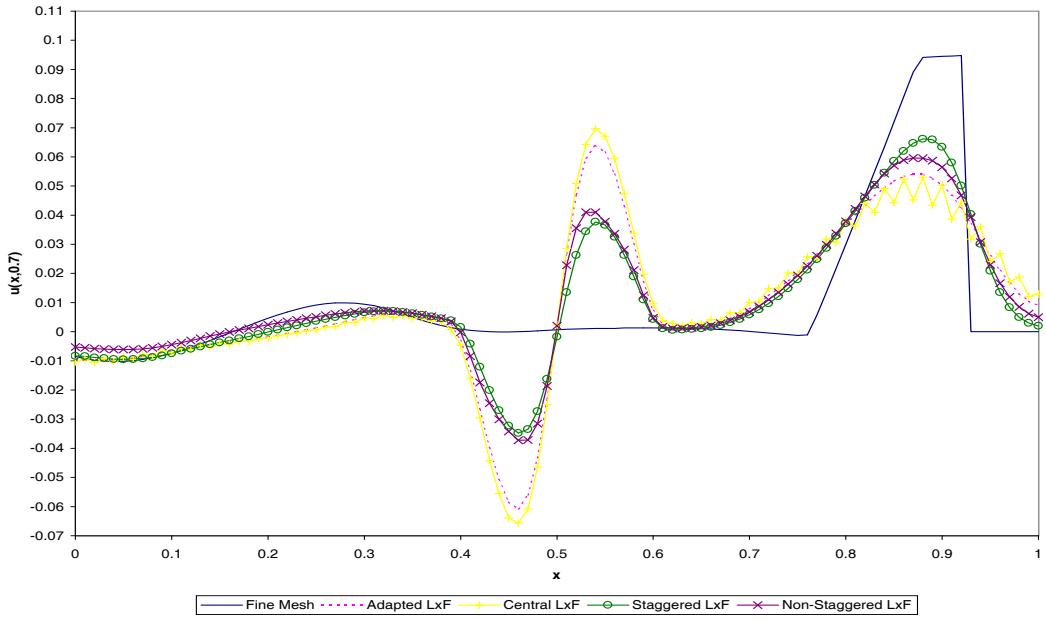

Figure 2.14: Numerical results of the different first order LxF schemes for Test Problem B with $\omega = 0.2$ at $t = 0.7$ (u).

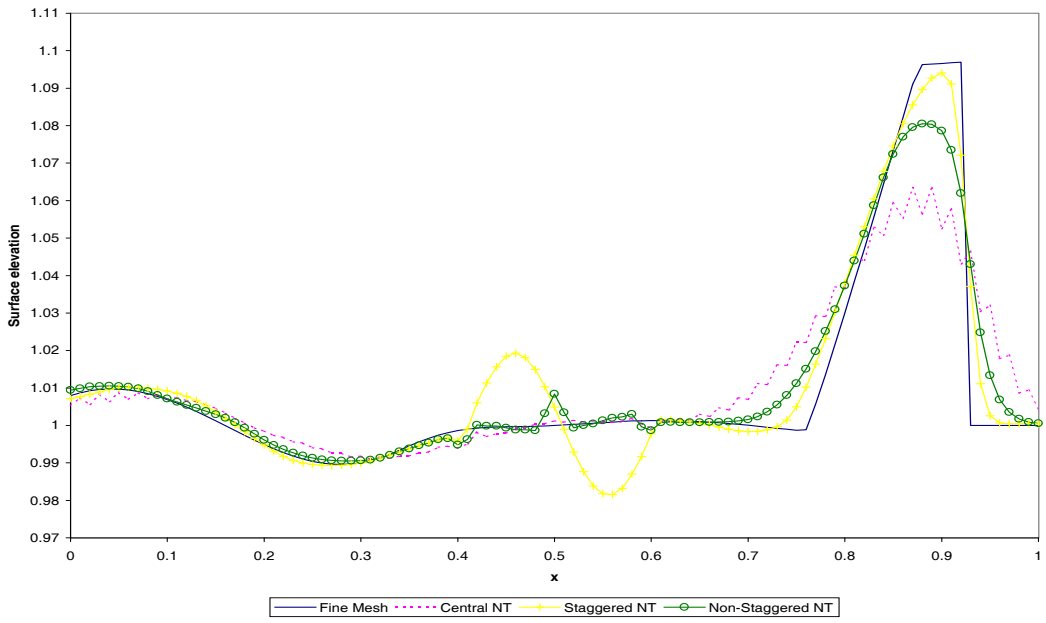

Figure 2.15: Numerical results of the different high-resolution NT schemes for Test Problem B with $\omega = 0.2$ at $t = 0.7$ (h+B).

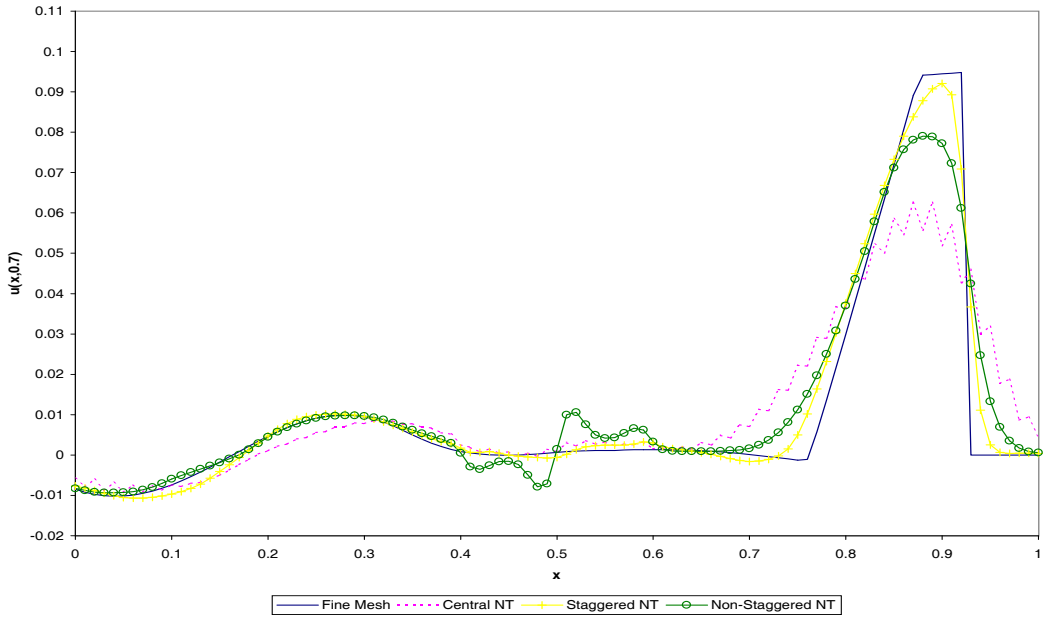

Figure 2.16: Numerical results of the different high-resolution NT schemes for Test Problem B with $\omega = 0.2$ at $t = 0.7$ (u).

2.6 Lax-Wendroff & MacCormack Scheme

2.6.1 Lax-Wendroff Scheme

The Lax-Wendroff scheme [24] is derived from a Taylor's series expansion,

$$\mathbf{w}_i^{n+1} \approx \mathbf{w}_i^n + \Delta t(\mathbf{w}_t)_i^n + \frac{\Delta t^2}{2}(\mathbf{w}_{tt})_i^n + O(\Delta t^3),$$

where the partial differential equation is used to replace the time derivatives with spatial derivatives and leads to the Lax-Wendroff numerical flux-function

$$\mathbf{F}^*_{i+\frac{1}{2}} = \frac{1}{2}\left(\mathbf{F}^n_{i+1} + \mathbf{F}^n_i\right) - \frac{s}{2}\mathbf{A}^n_{i+\frac{1}{2}}\left(\mathbf{F}^n_{i+1} - \mathbf{F}^n_i\right). \tag{2.16}$$

The Lax-Wendroff scheme requires a numerical approximation of the Jacobian matrix, which can be approximated by averaging the neighbouring cells,

$$\mathbf{A}_{i+\frac{1}{2}} = \mathbf{A}\left(\frac{\mathbf{w}^n_{i+1} + \mathbf{w}^n_i}{2}\right). \tag{2.17}$$

For the shallow water equations, we can use a pointwise approach,

$$\mathbf{R}^*_i = \begin{bmatrix} 0 \\ -\dfrac{g}{4}(h^n_{i+1} + h^n_{i-1})(B^n_{i+1} - B^n_{i-1}) \end{bmatrix}, \tag{2.18}$$

to approximate the source term but this is a crude approximation as it does not satisfy the C-property and reduces the accuracy of the numerical scheme as the scheme is no longer strictly second order accurate. Another more accurate approach, which maintains second order accuracy is to include the source term in the Taylor series expansion to obtain

$$\mathbf{R}^* = \Delta t\mathbf{R} + \frac{\Delta t^2}{2}\left(\mathbf{R}_t - (\mathbf{AR})_x\right).$$

Thus, we obtain

$$\begin{aligned}\mathbf{R}_i^* &= \frac{1}{2}\left(\mathbf{R}^n_{i+\frac{1}{2}} + \mathbf{R}^n_{i-\frac{1}{2}}\right) - \frac{s}{2}\left(\mathbf{A}^n_{i+\frac{1}{2}}\mathbf{R}^n_{i+\frac{1}{2}} - \mathbf{A}^n_{i-\frac{1}{2}}\mathbf{R}^n_{i-\frac{1}{2}}\right) \\ &= \frac{1}{2}\left(\left(\mathbf{I} - s\mathbf{A}^n_{i+\frac{1}{2}}\right)\mathbf{R}^n_{i+\frac{1}{2}} + \left(\mathbf{I} + s\mathbf{A}^n_{i-\frac{1}{2}}\right)\mathbf{R}^n_{i-\frac{1}{2}}\right) \end{aligned} \tag{2.19}$$

where for the shallow water equations,

$$\mathbf{R}^n_{i+\frac{1}{2}} = \begin{bmatrix} 0 \\ -\dfrac{g}{2}(h^n_{i+1} + h^n_i)(B^n_{i+1} - B^n_i) \end{bmatrix}.$$

Here, the $\mathbf{R}_t$ term has been omitted resulting in a slight loss of accuracy but the Lax-Wendroff scheme with (2.19) satisfies the C-property. Alternatively, we can approximate this term by using the chain rule $\mathbf{R}_t = \mathbf{R}_\mathbf{w}\mathbf{w}_t$. Thus, we obtain a semi-implicit version of the Lax-Wendroff scheme

$$\mathbf{w}_i^{n+1} = \mathbf{w}_i^n - s\left[\mathbf{I} - \frac{s}{2}(\mathbf{R}_\mathbf{w})^n_i\right]^{-1}\left(\mathbf{F}^*_{i+\frac{1}{2}} - \mathbf{F}^*_{i-\frac{1}{2}} - \mathbf{R}^*_i\right) \tag{2.20}$$

where for the shallow water equations

$$(\mathbf{R}_\mathbf{w})^n_i = \begin{bmatrix} 0 & 0 \\ -\frac{g}{2}(B^n_{i+1} - B^n_{i-1}) & 0 \end{bmatrix}.$$

Unfortunately, the semi-implicit approach cannot be used for all systems of conservation laws as the derivative of $\mathbf{R}$ with respect to $\mathbf{w}$ can sometimes be difficult to obtain.

2.6.2 Flux-Limited Lax-Wendroff Scheme

The Lax-Wendroff scheme suffers from dispersion resulting in spurious oscillations occurring in the numerical results. However, we can minimise these spurious oscillations by constructing a high-resolution scheme as discussed in Section 2.3, which also satisfies the TVD property. We use flux-limiter methods to adapt the Lax-Wendroff scheme for a system of conservation laws to a high-resolution scheme

by constructing a numerical flux-function of the form

$$\mathbf{F}^{TVD}_{i+\frac{1}{2}} = \mathbf{F}^{FO}_{i+\frac{1}{2}} + \mathbf{\Phi}\left(\mathbf{F}^{SO}_{i+\frac{1}{2}} - \mathbf{F}^{FO}_{i+\frac{1}{2}}\right), \tag{2.21}$$

where $\mathbf{F}^{SO}_{i+\frac{1}{2}}$ is a second order numerical flux, $\mathbf{F}^{FO}_{i+\frac{1}{2}}$ is a first order numerical flux, $\mathbf{\Phi} = \text{diag}(\Phi_k)$ where Φ_k is a flux-limiter, which can be any of the flux-limiters listed in Table 2.1, and k is the k^{th} component of the system. For the second order numerical flux, we use the Lax-Wendroff numerical flux (2.16) and re-write it by using

$$\mathbf{A} = \mathbf{X}\mathbf{\Lambda}\mathbf{X}^{-1},$$

where $\mathbf{X}$ is a matrix containing the right eigenvectors, $\mathbf{e}_k$, of $\mathbf{A}$ and $\mathbf{\Lambda} = \text{diag}(\lambda_k)$ is the diagonal matrix of eigenvalues, λ_k of $\mathbf{A}$. Hence, we obtain

$$\begin{aligned}
\mathbf{F}^{LW}_{i+\frac{1}{2}} &= \frac{1}{2}\left(\mathbf{F}^{n}_{i+1} + \mathbf{F}^{n}_{i}\right) - \frac{s}{2}\left(\mathbf{X}\mathbf{\Lambda}\mathbf{X}^{-1}\right)^{n}_{i+\frac{1}{2}}\left(\mathbf{F}^{n}_{i+1} - \mathbf{F}^{n}_{i}\right) \\
&= \frac{1}{2}\left(\mathbf{F}^{n}_{i+1} + \mathbf{F}^{n}_{i}\right) - \frac{s}{2}(\mathbf{X}\mathbf{\Lambda}^2\mathbf{X}^{-1})^{n}_{i+\frac{1}{2}}\left(\mathbf{w}^{n}_{i+1} - \mathbf{w}^{n}_{i}\right).
\end{aligned}$$

For the first order approximation, we use the upwind numerical flux

$$\begin{aligned}
\mathbf{F}^{UP}_{i+\frac{1}{2}} &= \frac{1}{2}\left(\mathbf{F}^{n}_{i+1} + \mathbf{F}^{n}_{i}\right) - \frac{1}{2}|\mathbf{A}|^{n}_{i+\frac{1}{2}}\left(\mathbf{w}^{n}_{i+1} - \mathbf{w}^{n}_{i}\right) \\
&= \frac{1}{2}\left(\mathbf{F}^{n}_{i+1} + \mathbf{F}^{n}_{i}\right) - \frac{1}{2}(\mathbf{X}|\mathbf{\Lambda}|\mathbf{X}^{-1})^{n}_{i+\frac{1}{2}}\left(\mathbf{w}^{n}_{i+1} - \mathbf{w}^{n}_{i}\right).
\end{aligned} \tag{2.22}$$

Thus,

$$\mathbf{F}^{LW}_{i+\frac{1}{2}} - \mathbf{F}^{UP}_{i+\frac{1}{2}} = \frac{1}{2}\left(\mathbf{X}|\mathbf{\Lambda}|\left(\mathbf{I} - s|\mathbf{\Lambda}|\right)\mathbf{X}^{-1}\right)^{n}_{i+\frac{1}{2}}\left(\mathbf{w}^{n}_{i+1} - \mathbf{w}^{n}_{i}\right)$$

and by using (2.6), we obtain the flux-limited Lax-Wendroff numerical flux

$$\mathbf{F}^{*}_{i+\frac{1}{2}} = \frac{1}{2}\left(\mathbf{F}^{n}_{i+1} + \mathbf{F}^{n}_{i}\right) - \frac{1}{2}\left(\mathbf{X}|\mathbf{\Lambda}|\mathbf{L}\mathbf{X}^{-1}\right)^{n}_{i+\frac{1}{2}}\left(\mathbf{w}^{n}_{i+1} - \mathbf{w}^{n}_{i}\right), \tag{2.23}$$

where

$$\mathbf{L} = \text{diag}\left(1 - \Phi(\theta_k)(1 - s|\lambda_k|)\right).$$

A more convenient way of writing (2.23) is in a decomposed form,

$$\mathbf{F}^*_{i+\frac{1}{2}} = \frac{1}{2}\left(\mathbf{F}^n_{i+1} + \mathbf{F}^n_i\right) - \frac{1}{2}\sum_{k=1}^{p}\left[\alpha_k|\lambda_k|(1-\Phi(\theta_k)(1-|\nu_k|))\mathbf{e}_k\right]^n_{i+\frac{1}{2}}, \tag{2.24}$$

where

$$\theta_k = \frac{(\alpha_k)^n_{I+\frac{1}{2}}}{(\alpha_k)^n_{i+\frac{1}{2}}}, \quad I = i - \mathrm{sgn}(\nu_k)^n_{i+\frac{1}{2}}, \quad \nu_k = s\lambda_k.$$

Here, p is the number of components of the system, $k = 1, 2, \ldots, p$ represents the k^{th} component of the system and α_k are the wave strengths, i.e. $\mathbf{X}^{-1}\Delta\mathbf{w}$, associated with each component of the decomposition onto the eigenvectors $\mathbf{e}_k$. We can determine the values of α_k by using

$$\Delta\mathbf{w}^n_{i+\frac{1}{2}} = \sum_{k=1}^{p}(\alpha_k\mathbf{e}_k)^n_{i+\frac{1}{2}} \quad \text{where} \quad \Delta\mathbf{w}_{i+\frac{1}{2}} = \mathbf{w}_{i+1} - \mathbf{w}_i$$

and for the shallow water equations, we obtain

$$(\alpha_{1,2})^n_{i+\frac{1}{2}} = \frac{1}{2}\left[\Delta h \mp \frac{1}{\sqrt{gh}}\left(\Delta(uh) - u\Delta h\right)\right]^n_{i+\frac{1}{2}}.$$

We require a source term approximation for the numerical scheme and adopt an approach discussed by Hubbard & Garcia-Navarro [18, 19], which is based on the approach of Roe [35] and Glaister [11]. The approach derives an upwind source term approximation that balances with the flux functions thus, making the numerical scheme satisfy the C-property. The source term approximation is constructed in a similar way to the numerical flux,

$$\mathbf{R}^*_i = \mathbf{R}^{TVD}_{i+\frac{1}{2}} + \mathbf{R}^{TVD}_{i-\frac{1}{2}}, \tag{2.25}$$

where

$$\mathbf{R}^{TVD}_{i+\frac{1}{2}} = \mathbf{R}^{FO}_{i+\frac{1}{2}} + \mathbf{\Phi}\left(\mathbf{R}^{SO}_{i+\frac{1}{2}} - \mathbf{R}^{FO}_{i+\frac{1}{2}}\right).$$

For the first order approximation, we used the upwind flux (2.22) and adopt the approach of Bermúdez & Vázquez [1] where

$$\begin{aligned}\mathbf{R}^{FO}_{i\pm\frac{1}{2}} &= \frac{1}{2}\left(\left(\mathbf{I}\mp|\mathbf{A}|\mathbf{A}^{-1}\right)\mathbf{R}\right)_{i\pm\frac{1}{2}} \\ &= \frac{1}{2}\left(\mathbf{X}\left(\mathbf{I}\mp\mathbf{\Lambda}^{-1}|\mathbf{\Lambda}|\right)\mathbf{X}^{-1}\mathbf{R}\right)_{i\pm\frac{1}{2}},\end{aligned}$$

which satisfies the C-property. Now, for the second order approximation, we used the Lax-Wendroff numerical flux. For the Lax-Wendroff flux, we deduced that a more accurate approximation of the source term was to use the second order accurate approximation (2.19), which satisfies the C-property. Thus, we use this second order approximation to balance the Lax-Wendroff numerical flux. Now,

$$\begin{aligned}\mathbf{R}^{LW}_{i\pm\frac{1}{2}} &= \frac{1}{2}\left(\left(\mathbf{I}\mp s\mathbf{A}\right)\mathbf{R}\right)_{i\pm\frac{1}{2}} \\ &= \frac{1}{2}\left(\mathbf{X}\left(\mathbf{I}\mp s\mathbf{\Lambda}^{-1}\mathbf{\Lambda}^{2}\right)\mathbf{X}^{-1}\mathbf{R}\right)_{i\pm\frac{1}{2}}.\end{aligned}$$

Therefore

$$\mathbf{R}^{LW}_{i\pm\frac{1}{2}} - \mathbf{R}^{UP}_{i\pm\frac{1}{2}} = \mp\frac{1}{2}\left(\mathbf{X}\mathbf{\Lambda}^{-1}|\mathbf{\Lambda}|\left(s|\mathbf{\Lambda}|-\mathbf{I}\right)\mathbf{X}^{-1}\mathbf{R}\right)_{i\pm\frac{1}{2}}$$

and by using (2.25) we obtain a flux-limited second order approximation of the source term

$$\mathbf{R}^{*}_{i} = \mathbf{R}^{-}_{i+\frac{1}{2}} + \mathbf{R}^{+}_{i-\frac{1}{2}}, \tag{2.26}$$

where

$$\mathbf{R}^{\pm}_{i+\frac{1}{2}} = \frac{1}{2}\left(\mathbf{X}\left(\mathbf{I}\pm\mathbf{\Lambda}^{-1}|\mathbf{\Lambda}|\mathbf{L}\right)\mathbf{X}^{-1}\mathbf{R}\right)_{i+\frac{1}{2}}$$

and for the shallow water equations,

$$\mathbf{R}^{n}_{i+\frac{1}{2}} = \begin{bmatrix} 0 \\ -\dfrac{g}{2}(h^{n}_{i+1}+h^{n}_{i})(B^{n}_{i+1}-B^{n}_{i}) \end{bmatrix}.$$

Alternatively, we can re-write (2.26) in decomposed form,

$$\mathbf{R}^{\pm}_{i+\frac{1}{2}} = \frac{1}{2}\sum_{k=1}^{p}\left[\beta_k\mathbf{e}_k(1\pm\mathrm{sgn}(\lambda_k)(1-\Phi(\theta_k)(1-|\nu_k|)))\right]^{n}_{i+\frac{1}{2}}$$

where the values of β_k are the components of $\mathbf{X}^{-1}\mathbf{R}$ and can be determined from

$$\sum_{k=1}^{p} [\beta_k \mathbf{e}_k]^n_{i+\frac{1}{2}} = \mathbf{R}^n_{i+\frac{1}{2}}.$$

For the shallow water equations, we obtain

$$(\beta_{1,2})^n_{i+\frac{1}{2}} = \pm\frac{1}{2}\left(\sqrt{gh}\Delta B\right)^n_{i+\frac{1}{2}} \quad \text{where} \quad \Delta B^n_{i+\frac{1}{2}} = B^n_{i+1} - B^n_i$$

and to satisfy the C-property, we must take $\mathbf{w}^n_{i+\frac{1}{2}} = \frac{1}{2}\left(\mathbf{w}^n_{i+1} + \mathbf{w}^n_i\right)$.

It should be noted at this point that by applying flux-limiters to the source term approximation as well as the flux-function, spurious oscillations can still occur in the numerical results, especially if the source term is significant. For the shallow water equations, the source term becomes more significant as the variation of the riverbed becomes more pronounced. To minimise the chances of spurious oscillations occurring in the numerical results, we must choose the flux-limiter carefully. For example, the superbee flux-limiter reduces the CFL limit of the scheme more than the minmod flux-limiter and thus, the superbee flux-limiter has more of a chance of producing spurious oscillations than the minmod flux-limiter. Hudson [20] illustrated the importance of choosing the correct limiter and deduced that, in general, the minmod limiter was the most accurate limiter. In some cases, even with the minmod limiter, the scheme can still produce spurious oscillations but this is very rare and can usually be resolved by using a smaller Courant number.

2.6.3 MacCormack Approach

LeVeque & Yee [27] and Yee [45] adapted the MacCormack approach [28] to approximate systems of conservation laws with a source term present,

$$\mathbf{w}^{n+1}_i = \frac{1}{2}(\mathbf{w}^n_i + \mathbf{w}^{(1)}_i) - \frac{s}{2}(\mathbf{F}^{(1)}_i - \mathbf{F}^{(1)}_{i-1}) + \frac{s}{2}\mathbf{R}^{(1)}_{i-\frac{1}{2}}, \tag{2.27}$$

where

$$\mathbf{w}_i^{(1)} = \mathbf{w}_i^n - s(\mathbf{F}_{i+1}^n - \mathbf{F}_i^n) + s\mathbf{R}_{i+\frac{1}{2}}^n.$$

The MacCormack scheme is a predictor-corrector scheme and reverts back to the classic Lax-Wendroff scheme for the constant coefficient case. The advantage of using (2.27) is that we do not need to approximate the eigenvalues and eigenvectors of the Jacobian matrix. However, the numerical scheme does not satisfy the TVD property, thus spurious oscillations may occur in the numerical solution. LeVeque & Yee [27] adapted (2.27) so that the numerical scheme satisfies the TVD property by using slope limiters

$$\mathbf{w}_i^{n+1} = \mathbf{w}_i^{(2)} + \mathbf{D}_{i+\frac{1}{2}}^n - \mathbf{D}_{i-\frac{1}{2}}^n \tag{2.28}$$

where $\mathbf{w}_i^{(2)}$ is the numerical approximation derived from (2.27),

$$\mathbf{D}_{i+\frac{1}{2}}^n = \frac{1}{2}\sum_{k=1}^{p} \left[|\nu_k|(1-|\nu_k|)(\alpha_k - Q_k)\mathbf{e}_k\right]_{i+\frac{1}{2}}^n,$$

and α_k are the wave strengths associated with each component of the decomposition, i.e. $\mathbf{X}^{-1}\Delta\mathbf{w}$, and can be determined by using

$$\Delta\mathbf{w}_{i+\frac{1}{2}}^n = \sum_{k=1}^{p} (\alpha_k \mathbf{e}_k)_{i+\frac{1}{2}}^n \quad \text{where} \quad \Delta\mathbf{w}_{i+\frac{1}{2}} = \mathbf{w}_{i+1} - \mathbf{w}_i.$$

The slope-limiter, $(Q_k)_{i+\frac{1}{2}}^n = Q_{i+\frac{1}{2}}^k$, can be any of the following (see Yee [45])

$$Q_{i+\frac{1}{2}}^k = \text{minmod}(\alpha_{i-\frac{1}{2}}^k, \alpha_{i+\frac{1}{2}}^k, \alpha_{i+\frac{3}{2}}^k) \tag{2.29a}$$

$$Q_{i+\frac{1}{2}}^k = \text{minmod}(\alpha_{i-\frac{1}{2}}^k, \alpha_{i+\frac{1}{2}}^k) + \text{minmod}(\alpha_{i+\frac{1}{2}}^k, \alpha_{i+\frac{3}{2}}^k) - \alpha_{i+\frac{1}{2}}^k \tag{2.29b}$$

$$Q_{i+\frac{1}{2}}^k = \text{minmod}(2\alpha_{i-\frac{1}{2}}^k, 2\alpha_{i+\frac{1}{2}}^k, 2\alpha_{i+\frac{3}{2}}^k, \frac{1}{2}(\alpha_{i-\frac{1}{2}}^k + \alpha_{i+\frac{3}{2}}^k)) \tag{2.29c}$$

where

$$\text{minmod}(a,b,c) = \begin{cases} d\ \min(|a|,|b|,|c|) & \text{if } d = \text{sgn}(a) = \text{sgn}(b) = \text{sgn}(c), \\ 0 & \text{otherwise.} \end{cases}$$

For the shallow water equations, the source term approximation is

$$\mathbf{R}^n_{i+\frac{1}{2}} = \begin{bmatrix} 0 \\ -\dfrac{g}{2}(h^n_{i+1} + h^n_i)(B^n_{i+1} - B^n_i) \end{bmatrix},$$

which makes the MacCormack scheme satisfy the C-property for the second order scheme (2.27).

Unfortunately, the slope-limited version of the MacCormack scheme (2.28) does not satisfy the C-property, for consider the shallow water equations with the quiescent flow case, $u = 0$ and $h = D - B$. Here, the second term on the right hand side of (2.28) is

$$\mathbf{D}^n_{i+\frac{1}{2}} = \begin{bmatrix} d_1 + d_2 \\ \sqrt{gh}(d_2 - d_1) \end{bmatrix}_{i+\frac{1}{2}} \quad \text{where} \quad d_k = \frac{s}{2}\sqrt{gh}(1 - s\sqrt{gh})(\alpha_k - Q_k).$$

Now, for the shallow water equations,

$$\alpha_{1,2} = \frac{1}{2}\left[\Delta h \mp \frac{1}{\sqrt{gh}}\left(\Delta(uh) - u\Delta h\right)\right],$$

thus, for the quiescent flow case $\alpha_k = \frac{1}{2}\Delta h$ and so, $Q_1 = Q_2$. Therefore,

$$d_1 = d_2 = \frac{s}{2}\sqrt{gh}(1 - s\sqrt{gh})(\frac{1}{2}\Delta h - Q)$$

and we obtain

$$\mathbf{D}^n_{i+\frac{1}{2}} = \begin{bmatrix} s\sqrt{gh}(1 - s\sqrt{gh})(\frac{1}{2}\Delta h - Q) \\ 0 \end{bmatrix}_{i+\frac{1}{2}} \neq 0.$$

Hence, (2.28) does not satisfy the C-property unless $Q = \frac{1}{2}\Delta h$, which reverts the scheme to the second order MacCormack approach. Unfortunately, the MacCormack scheme cannot satisfy the C-property by using slope-limiters but the scheme can if

we use flux-limiters instead. Hence, the flux-limited MacCormack approach is

$$\mathbf{w}_i^{n+1} = \mathbf{w}_i^{(2)} + \mathbf{D}_{i+\frac{1}{2}}^n - \mathbf{D}_{i-\frac{1}{2}}^n \tag{2.30}$$

where $\mathbf{w}_i^{(2)}$ is the numerical approximation derived from (2.27),

$$\mathbf{D}_{i+\frac{1}{2}}^n = \frac{s}{2}\sum_{k=1}^{p}\left[(\alpha_k|\lambda_k| - \beta_k \text{sgn}(\lambda_k))\left(1-|\nu_k|\right)(1-\Phi(\theta_k))\mathbf{e}_k\right]_{i+\frac{1}{2}}^n$$

and Φ is now a flux-limiter, which can be any of the limiters listed in Table 2.1. As in the previous section, the values of β_k are the components of $\mathbf{X}^{-1}\mathbf{R}$ and can be determined from

$$\sum_{k=1}^{p}\left[\beta_k\mathbf{e}_k\right]_{i+\frac{1}{2}}^n = \mathbf{R}_{i+\frac{1}{2}}^n.$$

The source term approximation $\mathbf{R}_{i+\frac{1}{2}}^n$ must first be carefully chosen so that (2.27) satisfies the C-property.

2.6.4 Numerical Results of the Different Lax-Wendroff Schemes

To illustrate the accuracy of the Lax-Wendroff scheme and the flux-limited Lax-Wendroff scheme (2.23), we use Test Problem B, which is the wave propagation test problem, with $\omega = 0.01$. The Lax-Wendroff scheme (LxW) is used with both the pointwise (PW) source term approximation (2.18) and the second order accurate source term approximation (2.19), which satisfies the C-property (CP). The flux-limited (FxL) Lax-Wendroff scheme (2.23) is also used with the pointwise (PW) source term approximation (2.18) and the flux-limited source term approximation (2.26), which makes the scheme satisfy the C-property (CP). For both numerical schemes, we use $\nu = 0.8$, $\Delta x = 0.01$ and the minmod flux-limiter. A flux-limited second order version of Roe's scheme, which is discussed in Section 2.7, on a fine mesh, $\Delta x = 0.0001$, is also used as a reference solution. The semi-implicit version of the schemes are not illustrated as the numerical results produced were practically

identical to the explicit schemes. From Figure 2.17 and Figure 2.18, we can see that both schemes with the pointwise source term approximation have produced poor numerical results due to spurious oscillations being present. The Lax-Wendroff scheme with the second order accurate source term approximation has produced considerably more accurate numerical results due to the numerical scheme satisfying the C-property but spurious oscillations are still present near the disturbance. The flux-limited scheme with the flux-limited source term approximation produced the most accurate numerical results due to the numerical scheme satisfying the C-property.

2.6.5 Numerical Results of the Different MacCormack Approaches

To illustrate the accuracy of the different MacCormack schemes, we use Test Problem C, which is the tidal wave propagation test problem. We use the second order (2.27), slope-limited (2.28) and flux-limited (2.30) versions of the MacCormack scheme. For all numerical schemes, we use $\nu = 0.8$, a spacial step-size of $\Delta x = 6,480m$ and a final time of $t = 10,800s$. For the slope-limited version of the MacCormack scheme, we use the limiter (2.29a) and for the flux-limited version of the MacCormack scheme, we use the minmod limiter. For this test problem, at $t = 10,800s$ no movement should occur past $x \approx 216,000m$ as the tidal wave has not propagated past this point. However, from Figure 2.19 and Figure 2.20 we can see that the slope-limited version of the MacCormack scheme has produced spurious waves past this point whereas the second order and flux-limited versions have not produced any movement past this point. This is due to the slope-limited version not satisfying the C-property whereas the other two versions satisfy this property. Hence, the slope-limited version is considerably less accurate than the second order and flux-limited versions of the MacCormack scheme. It should be noted that even though the second order version has produced very similar results to the flux-limited version, when a discontinuity is present the second order scheme will produce spurious oscillations due to the numerical scheme not satisfying the TVD property.

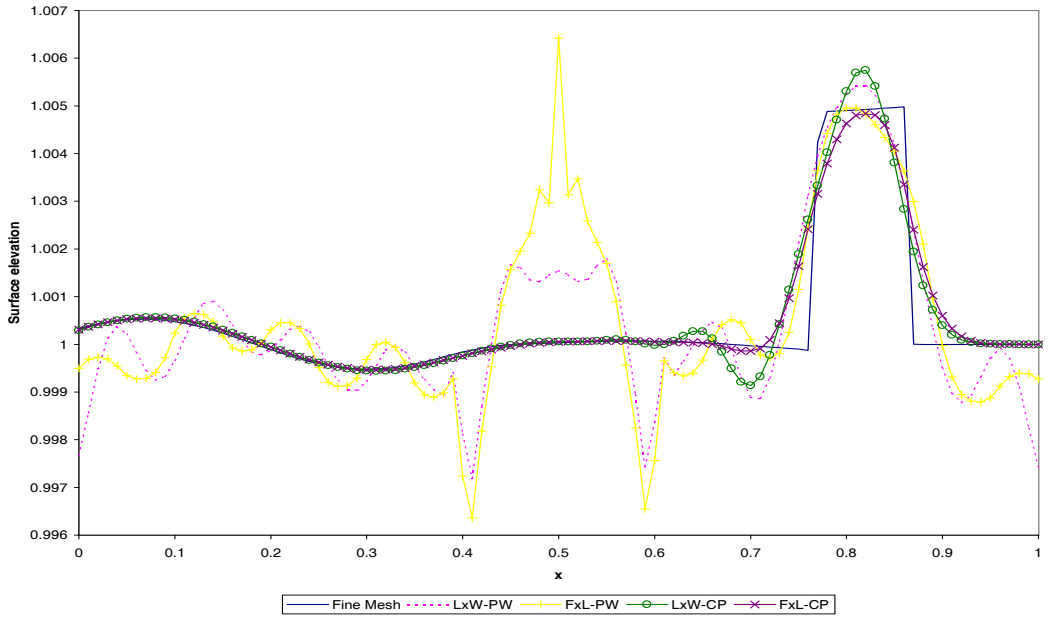

Figure 2.17: Numerical results of the different Lax-Wendroff schemes for Test Problem B with $\omega = 0.01$ at $t = 0.7$ $(h + B)$.

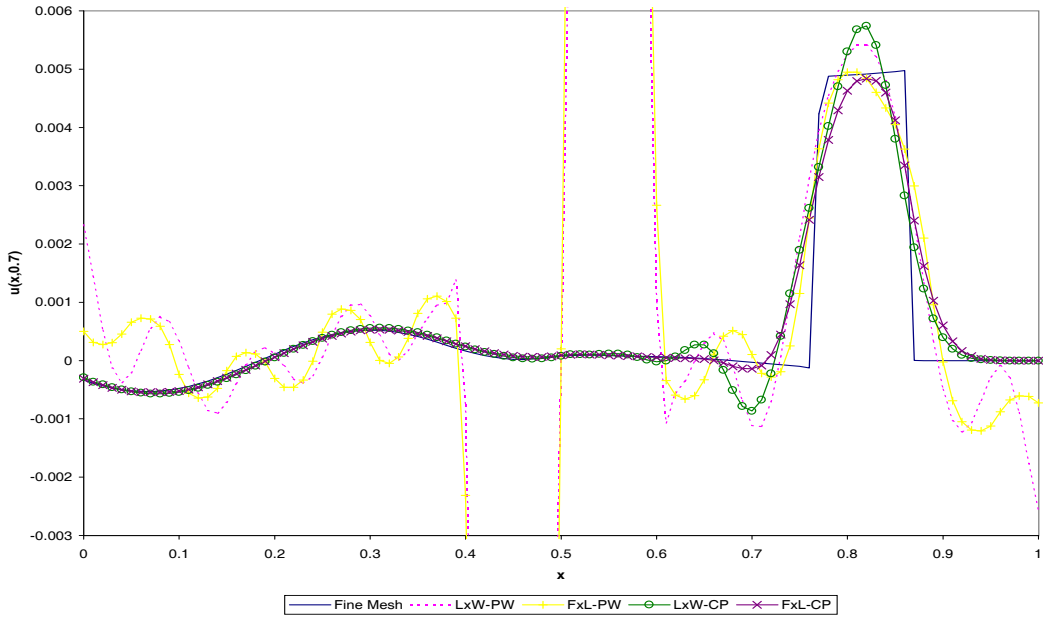

Figure 2.18: Numerical results of the different Lax-Wendroff schemes for Test Problem B with $\omega = 0.01$ at $t = 0.7$ (u).

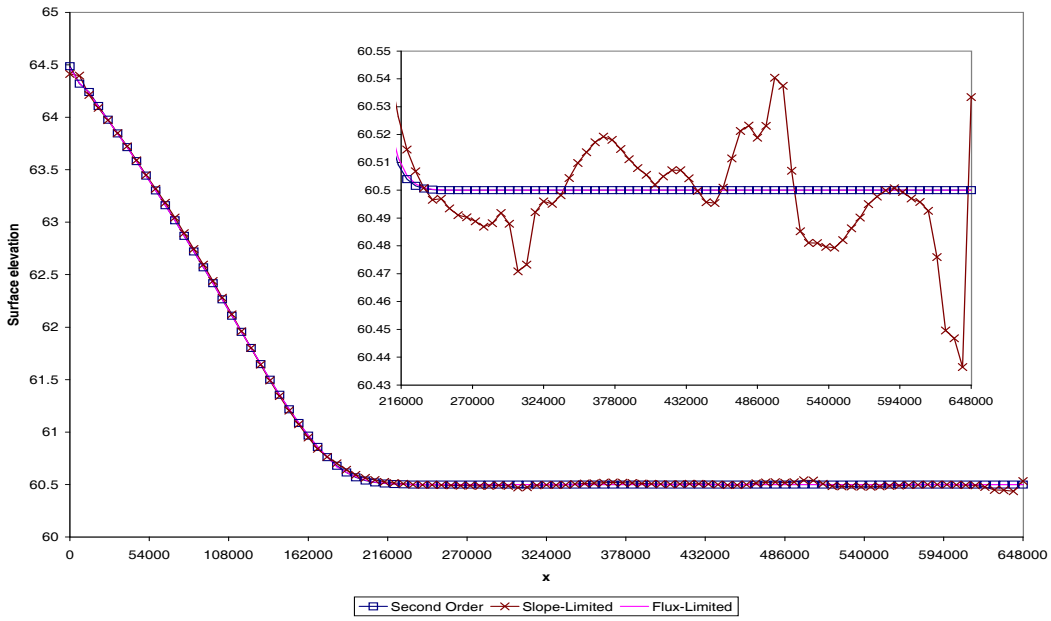

Figure 2.19: Numerical results of the different MacCormack schemes for Test Problem C at $t = 10,800\ s$ $(h + B)$.

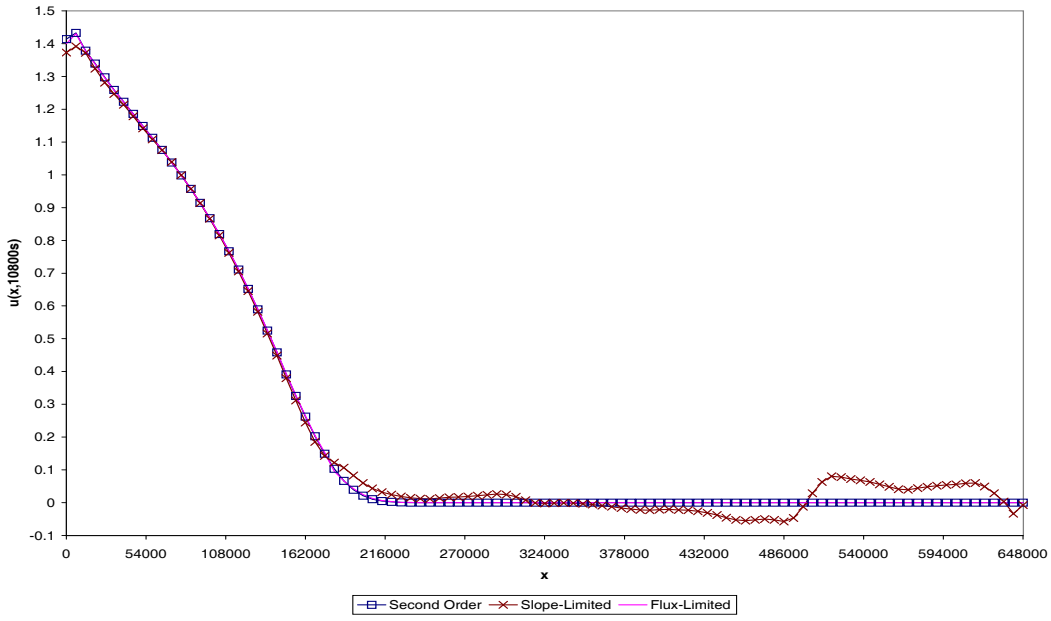

Figure 2.20: Numerical results of the different MacCormack schemes for Test Problem C at $t = 10,800\ s$ (u).

2.7 Roe's Scheme

Roe [33] derived an approach which approximates systems of conservation laws,

$$\frac{\partial \mathbf{w}}{\partial t} + \frac{\partial \mathbf{F}}{\partial x} = 0, \tag{2.31}$$

by using the numerical data, $\mathbf{w}_i^n$, to construct a piecewise constant function

$$\mathbf{w}\left(x, t^n\right) = \mathbf{w}_i^n, \quad x \in \left[x_{i-\frac{1}{2}}^n, x_{i+\frac{1}{2}}^n\right].$$

Now, for any two adjacent states of the piecewise data, $\mathbf{w}_L$ and $\mathbf{w}_R$, (2.31) can be solved by determining the exact solution of a linearised Riemann problem,

$$\frac{\partial \mathbf{w}}{\partial t} + \tilde{\mathbf{A}}(\mathbf{w}_L, \mathbf{w}_R)\frac{\partial \mathbf{w}}{\partial x} = 0,$$

which is related to (2.31) where $\tilde{\mathbf{A}}(\mathbf{w}_L, \mathbf{w}_R) \approx \frac{\partial \mathbf{F}}{\partial \mathbf{w}}$ is the linearised Jacobian matrix and $\tilde{}$ is called the Roe average. The Roe averaged Jacobian matrix, $\tilde{\mathbf{A}}(\mathbf{w}_L, \mathbf{w}_R)$, must be chosen such that the following properties are satisfied

- $\tilde{\mathbf{A}}(\mathbf{w}_L, \mathbf{w}_R)$ must be diagonalisable with real eigenvalues (hyperbolicity);
- $\tilde{\mathbf{A}}(\mathbf{w}_L, \mathbf{w}_R) \longrightarrow \mathbf{A}(\mathbf{w})$ as $\mathbf{w}_L, \mathbf{w}_R \longrightarrow \mathbf{w}$ (consistency);
- $\Delta\mathbf{F} = \tilde{\mathbf{A}}(\mathbf{w}_L, \mathbf{w}_R)\Delta\mathbf{w}$ (conservation).

The eigenvalues and eigenvectors of $\tilde{\mathbf{A}}$ are $\tilde{\lambda}$ and $\tilde{\mathbf{e}}$ respectively which are determined from the decomposition

$$\Delta\mathbf{F} = \sum_{k=1}^{p} \tilde{\alpha}_k \tilde{\lambda}_k \tilde{\mathbf{e}}_k = \tilde{\mathbf{A}}\Delta\mathbf{w}$$

where $\Delta\mathbf{w} = \mathbf{w}_R - \mathbf{w}_L$, p is the number of components in the system and $\tilde{\alpha}_k$ represents the wave strengths associated with each component of the decomposition,

i.e. $\tilde{\mathbf{X}}^{-1}\Delta\mathbf{w}$, and are determined from

$$\Delta\mathbf{w} = \sum_{k=1}^{p} \tilde{\alpha}_k \tilde{\mathbf{e}}_k.$$

Once the eigenvalues, eigenvectors and wave strengths associated with the linearised Riemann problem have been obtained, we can use any of the numerical schemes discussed in the previous section with the Roe averaged values. For example, the flux-limited version of the Lax-Wendroff scheme can be used,

$$\mathbf{F}^*_{i+\frac{1}{2}} = \frac{1}{2}(\mathbf{F}^n_{i+1} + \mathbf{F}^n_i) - \frac{1}{2}\sum_{k=1}^{p}\left[\tilde{\alpha}_k|\tilde{\lambda}_k|(1-\Phi(\theta_k)(1-|\nu_k|))\tilde{\mathbf{e}}_k\right]_{i+\frac{1}{2}}, \tag{2.32}$$

where

$$\nu_k = s\tilde{\lambda}_k, \quad \theta_k = \frac{(\tilde{\alpha}_k)_{I+\frac{1}{2}}}{(\tilde{\alpha}_k)_{i+\frac{1}{2}}}, \quad I = i - \mathrm{sgn}(\nu_k)_{i+\frac{1}{2}},$$

and Φ_k can be any of the flux-limiters listed in Table 2.1. Since this version of the flux-limited Lax-Wendroff scheme uses the Roe averaged values, we call this a flux-limited version of Roe's Scheme. Glaister [11, 12] determined the following Roe averaged Jacobian matrix for the shallow water equations

$$\tilde{\mathbf{A}} = \begin{bmatrix} 0 & 1 \\ \tilde{c}^2 - \tilde{u}^2 & 2\tilde{u} \end{bmatrix}, \quad \text{where} \quad \tilde{c} = \sqrt{g\tilde{h}},$$

with eigenvalues

$$\tilde{\lambda}_1 = \tilde{u} - \tilde{c} \quad \text{and} \quad \tilde{\lambda}_2 = \tilde{u} + \tilde{c}$$

and corresponding eigenvectors

$$\tilde{\mathbf{e}}_1 = \begin{bmatrix} 1 \\ \tilde{u} - \tilde{c} \end{bmatrix} \quad \text{and} \quad \tilde{\mathbf{e}}_2 = \begin{bmatrix} 1 \\ \tilde{u} + \tilde{c} \end{bmatrix}$$

and wave strengths

$$\tilde{\alpha}_{1,2} = \frac{1}{2}\Delta h \mp \frac{1}{2\tilde{c}}\left(\Delta(uh) - \tilde{u}\Delta h\right),$$

where the Roe averages are

$$\tilde{u} = \frac{\sqrt{h_R}u_R + \sqrt{h_L}u_L}{\sqrt{h_R} + \sqrt{h_L}} \quad \text{and} \quad \tilde{h} = \frac{1}{2}\left(h_R + h_L\right).$$

The Roe averaged values can also be used for the source term approximations. For example, the source term approximation that was derived for the flux-limited Lax-Wendroff scheme (2.26) can be used,

$$\mathbf{R}^{\pm}_{i+\frac{1}{2}} = \frac{1}{2}\sum_{k=1}^{p}\left[\tilde{\beta}_k\tilde{\mathbf{e}}_k(1 \pm \text{sgn}(\tilde{\lambda}_k)(1 - \Phi_k(1 - |\nu_k|)))\right]_{i+\frac{1}{2}} \tag{2.33}$$

where the values of $\tilde{\beta}_k$ are the components of $\tilde{\mathbf{X}}^{-1}\tilde{\mathbf{R}}$ and are determined from

$$\frac{1}{\Delta x}\sum_{k=1}^{p}\tilde{\beta}_k\tilde{\mathbf{e}}_k = \tilde{\mathbf{R}}.$$

Glaister [11, 12] also determined that for the shallow water equations,

$$\tilde{\beta}_1 = \frac{\tilde{c}\Delta B}{2} \quad \text{and} \quad \tilde{\beta}_2 = -\frac{\tilde{c}\Delta B}{2}.$$

2.7.1 Numerical Results of the Flux-Limited Version of Roe's Scheme

To compare the accuracy of the Roe averaged Jacobian matrix with the averaged Jacobian matrix (2.17), we use the flux-limited Lax-Wendroff numerical flux (2.23) with the source term approximation (2.33), which satisfies the C-property. Test Problem C is used with a final time of $t = 21,600s$ and both schemes are run using $\nu = 0.9$, a spatial step-size $\Delta x = 6,480m$ and the minmod flux-limiter. Figure 2.21 illustrates a comparison of the numerical results of the surface elevation for both schemes. Here, we can see that both approximations have produced very similar numerical results. The numerical results are smooth and are free from spurious oscillations. Both schemes have produced similar numerical

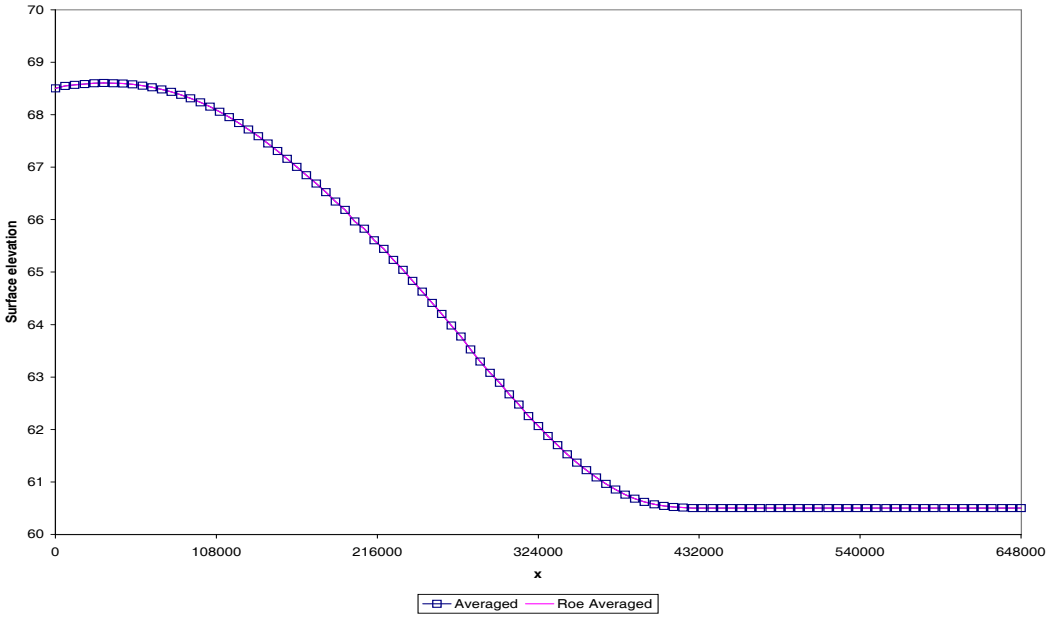

Figure 2.21: Numerical results of the flux-limited scheme with the different Jacobian approximations for Test Problem C at $t = 21,600s$ $(h + B)$.

results due to the approximations of the Jacobian matrices being similar. For the shallow water equations, the only difference between the two approximations of the Jacobian is the approximation of u,

$$\hat{u} = \frac{1}{2}(u_R + u_L) \quad \text{and} \quad \tilde{u} = \frac{\sqrt{h_R}u_R + \sqrt{h_L}u_L}{\sqrt{h_R} + \sqrt{h_L}},$$

as the approximation of h is the same. This results in both approximations of the Jacobian matrices being similar for most test problems. However, the two approximations of the Jacobian matrices will become increasingly different as the system grows due to the complexity of the Jacobian.

2.8 Summary

Throughout this chapter, we have discussed a variety of numerical scheme that can be used to approximate systems of conservation laws with source terms. We have shown that the LxF and NT schemes are accurate when a source term is not present but inaccurate when a source term is present due to the numerical schemes not satisfying the C-property. We have derived a flux-limited version of the Lax-Wendroff scheme, which satisfies the C-property, and is very accurate even when the source term is significant. A flux-limited version of the MacCormack scheme was also derived that is also accurate for all of the test problems discussed in this chapter. Two approximations of the Jacobian matrix, a basic averaged approximation and a Roe averaged approximation, were derived for the flux-limited Lax-Wendroff scheme. For the shallow water equations, both approximations of the Jacobian matrix produced very similar results. However, for larger systems the Jacobian matrix becomes more complex, which may result in the two approximations of the Jacobian matrix producing different results. In the next chapter, we extend the schemes discussed in this chapter to approximate the equations governing sediment transport in one dimension.

Chapter 3

Numerical Formulations for Approximating the Equations Governing Sediment Transport in One Dimension

In the previous chapter we discussed a variety of numerical schemes that can be used to approximate systems of conservation laws in one dimension. We used the shallow water equations to illustrate the derivation and accuracy of the different numerical schemes. In this chapter we adapt the numerical schemes discussed in the previous chapter to numerically approximate the equations governing sediment transport in 1D. The classic Lax-Wendroff scheme and the flux-limited version of Roe's scheme are adapted to approximate the equations. The classic Lax-Wendroff scheme is widely used in industry, but not surprisingly the numerical results obtained suffer from spurious oscillations resulting in the numerical scheme becoming unstable for long time periods. Different measures have been applied to the classic Lax-Wendroff scheme to try to eliminate the spurious oscillations such as a smaller Courant number and the scheme has been adapted to satisfy the TVD property. Unfortunately, the spurious oscillations could not be eliminated and overpowered the numerical results

for long computational run times, see Damgaard [4] and Damgaard & Chesher [5]. These difficulties are mainly due to the source term approximation, i.e. the scheme does not satisfy the C-property. The flux-limited version of Roe's scheme was derived to overcome these difficulties so that we can obtain accurate numerical results with no spurious oscillations present, even for long time periods. Thus, it is useful to illustrate the numerical results obtained from both schemes to highlight the improved accuracy of the flux-limited version of Roe's scheme compared to the classic Lax-Wendroff scheme.

Before we adapt the numerical schemes, we look at five different formulations that can be used with the numerical schemes to approximate the equations.

3.1 Different Formulations

There are numerous approaches that can be used to obtain an approximation of the equations governing sediment transport. In this thesis, we consider following two approaches:

1. the steady approach, where the water flow is assumed to be steady and the changes in the bed update have a negligible effect on the water flow, i.e. the wave speed of the bed-updating equation is considerably smaller in magnitude than the wave speeds of the water flow. By making these assumptions, the system is decoupled into a water flow approximation, which is iterated to an equilibrium state, followed by a bed update.

2. the unsteady approach, where no assumptions are made and the water flow and riverbed are calculated simultaneously. With this approach, the water flow can be either steady or unsteady and the changes in the bed update are considered to be significant, i.e. the wave speed of the bed-updating equation is of a similar magnitude to the wave speeds of the water flow. For this approach, the system is discretised simultaneously.

A considerable amount of research has been carried out on the steady approach, which was pioneered by Cunge *et al.* [3] who discussed both approaches at length. Cunge *et al.* stated that for most physical cases, the bed moves at a considerably slower speed than the water flow. For example, for a 100 km channel, the water flow usually takes one or two days to propagate over the entire channel whereas the bed usually takes many years. Thus, we expect the wave speed of the bed-updating equation to be considerably smaller in magnitude than the wave speeds associated with the water flow. This enables the steady approach to be derived, where the water flow and the bed update is decoupled and discretised separately making the equations considerably easier to numerically approximate. The steady approach of Cunge *et al.* also assumes the water flow is in an equilibrium state which allows equations (1.1) and (1.2) to be re-written as

$$Q_x = 0 \quad \Rightarrow \quad Q(x,t) = Q_c \quad \forall (x,t), \tag{3.1}$$

which results in a constant discharge throughout the domain, and

$$\left[\frac{1}{2}u^2 + g(h+B)\right]_x = 0, \tag{3.2}$$

where the equation has been re-written in nonconservative variable form. Thus, a numerical approximation of (3.2) and (1.3) is now only required. In this thesis, we slightly adapt the approach by iterating the water flow to an equilibrium state, which has the effect of imposing a constant discharge, and then updating the bed. Unfortunately, the steady approach is very limited as the water flow is assumed to be in an equilibrium state, but rarely is. There are also cases, where the wave speed of the bed-updating equation is of a similar magnitude to the wave speeds of the water flow, see Perdreau and Cunge [31], but this case is rare. However, the steady approach cannot be used for these cases as the bed is assumed to have a negligible effect on the water flow.

The unsteady approach approximates the whole system simultaneously on the same time scale. This approach can be used with steady and unsteady water flow and is considerably more robust than the steady approach. Little research has been

carried out on the unsteady approach as until recently, a full numerical solution of the approach was considered to be too complex and expensive to obtain, see Cunge *et al.* [3]. This is mainly due to the complexity of the sediment transport flux, which can range from a basic analytical function, as discussed in Section 1.4, to a system of equations such as the equations derived by Einstein [8]. In some cases, the sediment transport flux cannot be written analytically and is determined by using a "black box" approach where the flux is deduced from empirical data. The steady approach can easily incorporate all of these sediment transport fluxes, but the unsteady approach is considerably harder.

In this thesis, to determine the validity of the steady and unsteady approach, we consider five different formulations that can be used to approximate the equations governing sediment transport. Each formulation will be derived for the sediment transport flux (1.10) for positive values of u,

$$q(u) = Au^m \quad \text{where} \quad u \geq 0. \tag{3.3}$$

Four of the formulations will be based on the unsteady approach and one will be based on the steady approach.

3.1.1 Formulation A

The equations (1.1), (1.2) and (1.3) can be used as written in three different ways:

1. Formulation A-CV: The following method is based on the steady approach and consists of

   - a "fixed-bottom step", where the shallow water equations,

   $$\begin{bmatrix} h \\ uh \end{bmatrix}_t + \begin{bmatrix} uh \\ hu^2 + \frac{1}{2}gh^2 \end{bmatrix}_x = \begin{bmatrix} 0 \\ -ghB_x \end{bmatrix},$$

   are iterated to an equilibrium state whilst keeping the bed fixed.

- a "changing bottom step", where the bed is updated whist keeping all other variables fixed.

Numerically, an equilibrium state has been obtained when

$$|\mathbf{w}_i^{n+1} - \mathbf{w}_i^n| \leq \text{tol} \quad \forall i,$$

where tol is the desired tolerance level. Thus the numerical approximation of the water flow must satisfy the tolerance level before the bed is updated and the process is repeated. The overall time step of this formulation is the morphological time step of the bed-updating equation.

2. Formulation A-NC: Here, the shallow water equations and the bed-updating equation are numerically approximated sequentially using the same time step. This formulation is similar to Formulation A-CV as the water flow is still calculated separately from the bed update. However, the water flow is no longer iterated to an equilibrium or steady state after each bed update.

3. Formulation A-SF: All three equations are re-written in system form,

$$\begin{bmatrix} h \\ uh \\ B \end{bmatrix}_t + \begin{bmatrix} uh \\ hu^2 + \frac{1}{2}gh^2 \\ \xi q \end{bmatrix}_x = \begin{bmatrix} 0 \\ -ghB_x \\ 0 \end{bmatrix} \tag{3.4}$$

and the whole system is numerically approximated simultaneously. This formulation is based on the unsteady approach.

All three formulations have a source term present, which must be treated carefully to avoid difficulties obtaining an accurate numerical approximation. The Jacobian matrix will be required for each variation of Formulation A. For

1. Formulations A-NC and A-CV, the shallow water equations' Jacobian matrix is

$$\mathbf{A} = \begin{bmatrix} 0 & 1 \\ c^2 - u^2 & 2u \end{bmatrix},$$

where $c = \sqrt{gh}$, which has eigenvalues

$$\lambda_1 = u - c \quad \text{and} \quad \lambda_2 = u + c,$$

with corresponding eigenvectors

$$\mathbf{e}_1 = \begin{bmatrix} 1 \\ u - c \end{bmatrix} \quad \text{and} \quad \mathbf{e}_2 = \begin{bmatrix} 1 \\ u + c \end{bmatrix}.$$

Both Formulations A-CV and A-NC require an approximation of the wave speed of the bed-updating equation,

$$\lambda = \xi \left[\frac{\partial q}{\partial B} \right],$$

which can be difficult to obtain as the sediment transport flux is not a direct function of B, see Section 3.4.

2. Formulation A-SF, if the sediment transport flux (3.3) is used then the Jacobian matrix is

$$\mathbf{A} = \begin{bmatrix} 0 & 1 & 0 \\ c^2 - u^2 & 2u & 0 \\ -ud & d & 0 \end{bmatrix},$$

where $c = \sqrt{gh}$ and $d = \frac{\xi}{h} A m u^{m-1}$ for $u \geq 0$. Notice that this Jacobian matrix is singular, which we might expect to create difficulties when implementing a numerical scheme for this formulation. The eigenvalues of the Jacobian matrix are

$$\lambda_1 = u - c, \quad \lambda_2 = 0 \quad \text{and} \quad \lambda_3 = u + c,$$

with corresponding eigenvectors

$$\mathbf{e}_1 = \begin{bmatrix} 1 \\ u - c \\ \dfrac{-cd}{u - c} \end{bmatrix}, \quad \mathbf{e}_2 = \begin{bmatrix} 0 \\ 0 \\ 1 \end{bmatrix} \quad \text{and} \quad \mathbf{e}_3 = \begin{bmatrix} 1 \\ u + c \\ \dfrac{cd}{u + c} \end{bmatrix}.$$

For this formulation, notice that the eigenvalue associated with the bed-

updating equation is zero due to the Jacobian being singular. This implies that movement in the bed is created only by the water flow and thus, implies that the water flow cannot be decoupled from the bed update.

3.1.2 Formulation B

Another approach that can be used is to re-write the equation of conservation of momentum (1.2) as

$$\frac{\partial u}{\partial t} + \frac{\partial \left[\frac{1}{2}u^2 + g(h+B)\right]}{\partial x} = 0, \tag{3.5}$$

by using (1.1) and then combine (1.1), (3.5) and (1.3) into system form to obtain Formulation B,

$$\begin{bmatrix} h \\ u \\ B \end{bmatrix}_t + \begin{bmatrix} uh \\ \frac{1}{2}u^2 + g(h+B) \\ \xi q \end{bmatrix}_x = 0. \tag{3.6}$$

Notice that this formulation does not have a source term present, hence, Formulation B will be easier to approximate numerically. However, Formulation B may not be in conservative variable form, which could results in shocks propagating at incorrect speeds. If the sediment transport flux (3.3) is used then the Jacobian matrix of Formulation B is

$$\mathbf{A} = \begin{bmatrix} u & h & 0 \\ g & u & g \\ 0 & d & 0 \end{bmatrix},$$

where $d = A\xi m u^{m-1}$ for $u \geq 0$. Notice that the Jacobian matrix of Formulation B is not singular. The eigenvalues, λ, of the Jacobian matrix cannot be easily written analytically since they are the roots of the polynomial

$$P(\lambda, \mathbf{w}) = \lambda^3 - 2u\lambda^2 + \left[u^2 - g(h+d)\right]\lambda + gud = 0.$$

However, we can prove that the roots of $P(\lambda, \mathbf{w})$ are always real by using formulae for the roots of a cubic, see Spiegel & Liu [37]. For a cubic equation,

$$P(x) = x^3 + a_1x^2 + a_2x + a_3 = 0,$$

if we let

$$Q = \frac{1}{9}(3a_2 - a_1^2) \quad \text{and} \quad R = \frac{1}{54}(9a_1a_2 - 27a_3 - 2a_1^3),$$

then the *discriminant* is $D = Q^3 + R^2$ and if

1. $D > 0$ then one root is real and two are complex;
2. $D = 0$ then all roots are real and two are equal;
3. $D < 0$ then all roots are real and unequal.

If $D < 0$ then the roots of $P(x)$ are

$$x_1 = 2\sqrt{-Q}\cos(\frac{1}{3}\theta) - \frac{1}{3}a_1, \tag{3.7a}$$

$$x_2 = 2\sqrt{-Q}\cos(\frac{1}{3}(\theta + 2\pi)) - \frac{1}{3}a_1 \tag{3.7b}$$

and

$$x_3 = 2\sqrt{-Q}\cos(\frac{1}{3}(\theta + 4\pi)) - \frac{1}{3}a_1 \tag{3.7c}$$

where $\cos\theta = \dfrac{R}{\sqrt{-Q^3}}$.

Now, by using the above approach, for Formulation B

$$a_1 = -2u, \quad a_2 = u^2 - g(h + d) \quad \text{and} \quad a_3 = gud$$

which implies that

$$Q = -\frac{1}{9}(u^2 + 3g(h + d)) \quad \text{and} \quad R = \frac{u}{54}(9g(2h - d) - 2u^2).$$

Hence,

$$D = \frac{g}{108}[8gu^2h^2 - u^2(4hu^2 + gd(d + 20h)) - 4g^2(h^3 + d^3 + 3hd(h + d))]$$

and for all three roots to be real and unequal,

$$8gu^2h^2 < u^2(4hu^2 + gd(d + 20h)) + 4g^2(h^3 + d^3 + 3hd(h + d)),$$

which is always satisfied since $h(x, t) > 0$ and $u(x, t) \geq 0 \Rightarrow d \geq 0$. Hence, the roots of $P(\lambda, \mathbf{w})$ are always real and unequal. The signs of the roots of the Jacobian can be obtained from the determinant of $\mathbf{A}$

$$|\mathbf{A}| = \lambda_1\lambda_2\lambda_3 = -udg \tag{3.8}$$

and since, the determinant is negative this implies that either all three eigenvalues are negative or two are positive and one is negative. Also, as the parameter $A \to 0$, the eigenvalues of the Jacobian tend to

$$\lambda_1 \to u - c, \quad \lambda_2 \to 0 \quad \text{and} \quad \lambda_3 \to u + c,$$

which are identical to the eigenvalues of Formulation A-SF. Thus, we can determine that one of the roots is negative and two of the roots are positive, i.e.

$$\lambda_1 < 0 < \lambda_2 < \lambda_3.$$

De Vries [7] obtained an approximation of the eigenvalue associated with the bed-updating equation by assuming

$$\lambda_1 = u - c \quad \text{and} \quad \lambda_3 = u + c,$$

and substituting into (3.8) to obtain

$$\lambda_2 = \frac{gud}{c^2 - u^2}.$$

De Vries deduced from this approximation that $\lambda_1 < 0$ and $\lambda_2 > 0$ for subcritical flow, $u < c$, whereas $\lambda_1 > 0$ and $\lambda_2 < 0$ for supercritical flow, $u > c$. Now that we have proved that the roots of $P(\lambda)$ are always real, the eigenvectors,

$$\mathbf{e}_k = \begin{bmatrix} 1 \\ \dfrac{1}{h}(\lambda_k - u) \\ \dfrac{(u-\lambda_k)^2 - gh}{gh} \end{bmatrix},$$

can be obtained where the λ_k are given by (3.7).

3.1.3 Formulation C

In order to obtain a formulation that is written in conservative variable form and whose Jacobian matrix is not singular, we use the product rule, $(hB)_x = hB_x + Bh_x$, to re-write the equation of the conservation of momentum (1.2) as

$$\frac{\partial(uh)}{\partial t} + \frac{\partial\left[hu^2 + \frac{1}{2}gh^2 + ghB\right]}{\partial x} = gBh_x. \tag{3.9}$$

Now, combining equations (1.1), (3.9) and (1.3) into system form, we obtain

$$\begin{bmatrix} h \\ uh \\ B \end{bmatrix}_t + \begin{bmatrix} uh \\ hu^2 + \frac{1}{2}gh^2 + ghB \\ \xi q \end{bmatrix}_x = \begin{bmatrix} 0 \\ gBh_x \\ 0 \end{bmatrix}. \tag{3.10}$$

Unfortunately, Formulation C has a source term present. If the sediment transport flux (3.3) is used then the Jacobian matrix of Formulation C is

$$\mathbf{A} = \begin{bmatrix} 0 & 1 & 0 \\ g(h+B) - u^2 & 2u & gh \\ -ud & d & 0 \end{bmatrix},$$

where $d = \frac{\xi}{h} A m u^{m-1}$ for $u \geq 0$. The eigenvalues, λ, of the Jacobian matrix again cannot be easily written analytically since they are the roots of the polynomial

$$P(\lambda, \mathbf{w}) = \lambda^3 - 2u\lambda^2 + \left[u^2 - g(h + B + hd)\right] \lambda + ghud = 0.$$

However, we can prove that the roots of $P(\lambda, \mathbf{w})$ are always real by using the approach discussed in Section 3.1.2. For Formulation C,

$$a_1 = -2u, \quad a_2 = u^2 - g(h + B + hd) \quad \text{and} \quad a_3 = ghud$$

which implies that

$$Q = -\frac{1}{9}(u^2 + 3g(h + B + hd)) \quad \text{and} \quad R = -\frac{u}{54}(2u^2 - 9g(2h + 2B - hd)).$$

Hence,

$$D = \frac{g}{108}[8u^2 g(h + B)^2 - u^2[4u^2(B + h) + ghd(20(h + B) + hd)] \\ -4g^2(h^3 + B^3 + h^3 d^3 + 3h(d + 1)(h + B)(hd + B))]$$

and for all three roots to be real and unequal,

$$8u^2 g(h + B)^2 < u^2[4u^2(B + h) + ghd(20(h + B) + hd)] \\ +4g^2(h^3 + B^3 + h^3 d^3 + 3h(d + 1)(h + B)(hd + B)),$$

which is satisfied if $h(x, t) + B(x, t) > 0$ since $h(x, t) > 0$, $u(x, t) \geq 0 \Rightarrow d \geq 0$ and $-\infty < B(x, t) < \infty$. Hence, the roots of $P(\lambda, \mathbf{w})$ are always real and unequal if $h(x, t) + B(x, t) > 0$. As with Formulation B, it can also be shown that $P(\lambda, \mathbf{w})$ has one negative root and two positive roots, i.e.

$$\lambda_1 < 0 < \lambda_2 < \lambda_3.$$

Now that we have proved that the roots of $P(\lambda)$ are always real, we need to determine the eigenvectors. The eigenvectors of the Jacobian matrix are

$$\mathbf{e}_k = \begin{bmatrix} 1 \\ \lambda_k \\ \dfrac{u^2 - g(h+B) + (\lambda_k - 2u)\lambda_k}{gh} \end{bmatrix},$$

where again λ_k are given by (3.7).

Throughout this section, we have discussed five different formulations that can be used to numerically approximate the system (1.1), (1.2) and (1.3). In the next section, we discuss how these different formulations can be numerically approximated using the flux-limited version of Roe's scheme, which was discussed in the previous chapter.

3.2 Adaptation of the Classic Lax-Wendroff Scheme

The classic Lax-Wendroff scheme (2.16) can be used to approximate the equations governing sediment transport. Unfortunately, the scheme suffers from spurious oscillations, which can result in an inaccurate numerical solution. For the source term approximation, we adopt the pointwise approach, which is used in industry. The classic Lax-Wendroff scheme does not satisfy the C-property when the pointwise source term approximation is used.

The classic Lax-Wendroff scheme can easily be adapted to approximate the different formulations discussed in the previous section.

3.2.1 Formulation A-CV

For Formulation A-CV, the system is decoupled into a water flow approximation followed by a bed update. The classic Lax-Wendroff scheme can easily be adapted to approximate this formulation. In the previous chapter, the shallow water equations were approximated using the classic Lax-Wendroff scheme, see Section 2.6.1. However, for the bed-updating equation we need to adapt the scheme to numerically approximate the scalar conservation law. For the bed-updating equation, we obtain

$$B_i^{n+1} = B_i^n - \xi s \left(q^*_{i+\frac{1}{2}} - q^*_{i-\frac{1}{2}} \right), \tag{3.11}$$

where the numerical flux-function is

$$q^*_{i+\frac{1}{2}} = \frac{1}{2}\left(q^n_{i+1} + q^n_i\right) - \frac{s}{2}\lambda^n_{i+\frac{1}{2}}\left(q^n_{i+1} - q^n_i\right)$$

and the wave speed approximation is

$$\lambda^n_{i+\frac{1}{2}} = \xi \left[\frac{\partial q}{\partial B}\right]^n_{i+\frac{1}{2}}.$$

Unfortunately, (3.11) requires an accurate approximation of the wave speed, which can be very difficult to obtain since the sediment transport flux is not a direct function of B. A variety of approaches that can be used to obtain an approximation of the wave speed are discussed in Section 3.4 where the advantages and disadvantages of each approach are discussed as well.

3.2.2 Formulation A-NC

Formulation A-NC is practically identical to Formulation A-CV, with the exception that the shallow water equations are no longer iterated to an equilibrium or steady state.

3.2.3 Formulation A-SF

The classic Lax-Wendroff scheme (2.16) can be used to approximate Formulation A-SF as written. The Jacobian matrix is given in Section 3.1 and the source term is approximated using a pointwise approach,

$$\mathbf{R}_i^* = \begin{bmatrix} 0 \\ -\frac{g}{4}(h_{i+1}^n + h_{i-1}^n)(B_{i+1}^n - B_{i-1}^n) \\ 0 \end{bmatrix}.$$

3.2.4 Formulation B

The classic Lax-Wendroff scheme (2.16) can be used to approximate Formulation B. The Jacobian matrix is given in Section 3.1 and no source term is present for Formulation B, thus

$$\mathbf{R}_i^* = 0.$$

3.2.5 Formulation C

The classic Lax-Wendroff scheme (2.16) can be used to approximate Formulation C as written. The Jacobian matrix is given in Section 3.1 and the source term is approximated using a pointwise approach,

$$\mathbf{R}_i^* = \begin{bmatrix} 0 \\ \frac{g}{4}(B_{i+1}^n + B_{i-1}^n)(h_{i+1}^n - h_{i-1}^n) \\ 0 \end{bmatrix}.$$

3.3 Adaptation of the Flux-Limited Version of Roe's Scheme

In the previous chapter, we discussed a variety of numerical schemes that can be used to approximate systems of conservation laws with source term. We used the shallow water equations to illustrate our techniques and to determine which scheme produced the most accurate numerical results. We determined that out of all of the numerical schemes discussed, the flux-limited version of Roe's scheme (2.32) with the source term approximation (2.33) was the most accurate numerical scheme. This was mainly due to the scheme satisfying the C-property. Thus, in this section we adapt the flux-limited version of Roe's scheme to approximate the different formulations discussed in the previous section.

3.3.1 Formulation A-CV

For Formulation A-CV, the system is decoupled into a water flow approximation, the shallow water equations, and a bed update. The flux-limited version of Roe's scheme can easily adapted to approximate this formulation. In the previous chapter, this scheme was discussed based on the shallow water equations. However, for bed-updating equation, we need to adapt the flux-limited version of Roe's scheme to numerically approximate the scalar conservation law. For the bed-updating equation, we obtain

$$B_i^{n+1} = B_i^n - s\left(q^*_{i+\frac{1}{2}} - q^*_{i-\frac{1}{2}}\right), \tag{3.12}$$

where the numerical flux-function is

$$q^*_{i+\frac{1}{2}} = \frac{\xi}{2}\left(q^n_{i+1} + q^n_i\right) - \frac{1}{2}\left|\lambda^n_{i+\frac{1}{2}}\right|\left(1 - \Phi\left(\theta^n_{i+\frac{1}{2}}\right)\left(1 - \left|\nu^n_{i+\frac{1}{2}}\right|\right)\right)\left(B^n_{i+1} - B^n_i\right),$$

$$\nu^n_{i+\frac{1}{2}} = s\lambda^n_{i+\frac{1}{2}}, \quad \theta^n_{i+\frac{1}{2}} = \frac{B^n_{I+1} - B^n_I}{B^n_{i+1} - B^n_i},$$

$$I = i - \text{sgn}\left(\nu^n_{i+\frac{1}{2}}\right), \quad \lambda^n_{i+\frac{1}{2}} = \xi \left[\frac{\partial q}{\partial B}\right]^n_{i+\frac{1}{2}}$$

and Φ can be any of the flux-limiters listed in Table 2.1. In order to be able to use (3.12), we need to be able to obtain an accurate approximation of the wave speed, λ, which can be very difficult to obtain since the sediment transport flux is not a direct function of B. A variety of approaches that can be used to obtain an approximation of the wave speed are discussed in Section 3.4 where the advantages and disadvantages of each approach are discussed as well.

3.3.2 Formulation A-NC

Formulation A-NC is practically identical to Formulation A-CV, with the exception that the shallow water equations are no longer iterated to an equilibrium or steady state.

3.3.3 Formulation A-SF

Formulation A-SF can easily be used with the flux-limited version of Roe's scheme. For the sediment transport flux (3.3), we obtain the Roe averaged Jacobian matrix

$$\tilde{\mathbf{A}} = \begin{bmatrix} 0 & 1 & 0 \\ \tilde{c}^2 - \tilde{u}^2 & 2\tilde{u} & 0 \\ -\tilde{u}\tilde{d} & \tilde{d} & 0 \end{bmatrix},$$

where $\tilde{c} = \sqrt{g\tilde{h}}$. The eigenvalues of the Roe averaged Jacobian matrix are

$$\tilde{\lambda}_1 = \tilde{u} - \tilde{c}, \quad \tilde{\lambda}_2 = 0 \quad \text{and} \quad \tilde{\lambda}_3 = \tilde{u} + \tilde{c},$$

with corresponding eigenvectors

$$\tilde{\mathbf{e}}_1 = \begin{bmatrix} 1 \\ \tilde{u} - \tilde{c} \\ \dfrac{-\tilde{c}\tilde{d}}{\tilde{u} - \tilde{c}} \end{bmatrix}, \quad \tilde{\mathbf{e}}_2 = \begin{bmatrix} 0 \\ 0 \\ 1 \end{bmatrix} \quad \text{and} \quad \tilde{\mathbf{e}}_3 = \begin{bmatrix} 1 \\ \tilde{u} + \tilde{c} \\ \dfrac{\tilde{c}\tilde{d}}{\tilde{u} + \tilde{c}} \end{bmatrix}$$

and the wave strengths are

$$\tilde{\alpha}_1 = \frac{1}{2}\Delta h - \frac{1}{2\tilde{c}}\left(\Delta(uh) - \tilde{u}\Delta h\right)$$

$$\tilde{\alpha}_2 = \Delta B - \frac{\tilde{d}\left(\Delta(uh) - (\tilde{u}^2 + \tilde{c}^2)\Delta h\right)}{(\tilde{u} - \tilde{c})(\tilde{u} + \tilde{c})},$$

and

$$\tilde{\alpha}_3 = \frac{1}{2}\Delta h + \frac{1}{2\tilde{c}}\left(\Delta(uh) - \tilde{u}\Delta h\right).$$

The Roe averaged values are

$$\tilde{u} = \frac{\sqrt{h_R}u_R + \sqrt{h_L}u_L}{\sqrt{h_R} + \sqrt{h_L}}, \quad \tilde{h} = \frac{1}{2}(h_R + h_L)$$

and

$$\tilde{d} = \frac{\xi\Delta(Au^m)}{\Delta(uh) - \tilde{u}\Delta h}.$$

If m is an integer, then $\tilde{d}$ can be re-written as

$$\tilde{d} = \frac{A\xi(\sqrt{h_R} + \sqrt{h_L})}{\sqrt{h_L}h_R + \sqrt{h_R}h_L} \sum_{k=0}^{m-1} (u_R)^k (u_L)^{m-(1+k)}.$$

For the source term approximation,

$$\tilde{\beta}_1 = \frac{\tilde{c}\Delta B}{2}, \quad \tilde{\beta}_2 = \frac{\tilde{d}\tilde{u}\tilde{c}^2\Delta B}{(\tilde{u} - \tilde{c})(\tilde{u} + \tilde{c})} \quad \text{and} \quad \tilde{\beta}_3 = -\frac{\tilde{c}\Delta B}{2}.$$

3.3.4 Formulation B

Formulation B can also be used with the flux-limited version of Roe's scheme. For the sediment transport flux (3.3), we can obtain the following Roe averaged Jacobian matrix

$$\mathbf{A} = \begin{bmatrix} \tilde{u} & \tilde{h} & 0 \\ g & \tilde{u} & g \\ 0 & \tilde{d} & 0 \end{bmatrix}.$$

The eigenvalues, $\tilde{\lambda}$, of the Roe averaged Jacobian are obtained by finding the roots of the polynomial

$$\tilde{P}(\tilde{\lambda}) = \tilde{\lambda}^3 - 2\tilde{u}\tilde{\lambda}^2 + \left[\tilde{u}^2 - g(\tilde{h} + \tilde{d})\right]\lambda + g\tilde{u}\tilde{d} = 0.$$

The roots of $\tilde{P}(\tilde{\lambda})$ are determined by using the approach which was discussed in Section 3.1.2. Once the Roe averaged eigenvalues have been obtained, they are used to determine the values of the corresponding eigenvectors,

$$\tilde{\mathbf{e}}_k = \begin{bmatrix} 1 \\ \dfrac{1}{\tilde{h}}(\tilde{\lambda}_k - \tilde{u}) \\ \dfrac{(\tilde{u} - \tilde{\lambda}_k)^2 - g\tilde{h}}{g\tilde{h}} \end{bmatrix}$$

and the wave strengths

$$\tilde{\alpha}_k = \frac{((\tilde{u} - \tilde{\lambda}_a)(\tilde{u} - \tilde{\lambda}_b) + g\tilde{h})\Delta h + (2\tilde{u} - \tilde{\lambda}_a - \tilde{\lambda}_b)h\Delta u + g\tilde{h}\Delta B}{(\tilde{\lambda}_k - \tilde{\lambda}_a)(\tilde{\lambda}_k - \tilde{\lambda}_b)}$$

where $a \neq k \neq b$. The Roe averaged values are

$$\tilde{u} = \frac{1}{2}(u_R + u_L), \quad \tilde{h} = \frac{1}{2}(h_R + h_L) \quad \text{and} \quad \tilde{d} = \frac{\xi\Delta(Au^m)}{\Delta u}.$$

If m is an integer, then $\tilde{d}$ can be re-written as

$$\tilde{d} = A\xi \sum_{k=0}^{m-1} (u_R)^k (u_L)^{m-(1+k)}.$$

Since Formulation B does not have a source term present,

$$\tilde{\beta}_k = 0.$$

3.3.5 Formulation C

We can also adapt the flux-limited version of Roe's scheme to approximate Formulation C. For the sediment transport flux (3.3), the Jacobian matrix is

$$\mathbf{A} = \begin{bmatrix} 0 & 1 & 0 \\ g(\tilde{h} + \tilde{B}) - \tilde{u}^2 & 2\tilde{u} & g\tilde{h} \\ -\tilde{u}\tilde{d} & \tilde{d} & 0 \end{bmatrix}.$$

The eigenvalues, $\tilde{\lambda}$, of the Roe averaged Jacobian matrix are obtained by finding the roots of the polynomial

$$\tilde{P}(\tilde{\lambda}) = \tilde{\lambda}^3 - 2\tilde{u}\tilde{\lambda}^2 + \left[\tilde{u}^2 - g(\tilde{h} + \tilde{B} + \tilde{h}\tilde{d})\right]\tilde{\lambda} + g\tilde{h}\tilde{u}\tilde{d} = 0.$$

The roots of $\tilde{P}(\tilde{\lambda})$ are determined by using the approach which was discussed in Section 3.1.2. Once the Roe averaged eigenvalues have been obtained, they are used to determine the values of the corresponding eigenvectors,

$$\tilde{\mathbf{e}}_k = \begin{bmatrix} 1 \\ \tilde{\lambda}_k \\ \dfrac{\tilde{u}^2 - g(\tilde{h} + \tilde{B}) + (\tilde{\lambda}_k - 2\tilde{u})\tilde{\lambda}_k}{g\tilde{h}} \end{bmatrix},$$

and wave strengths

$$\tilde{\alpha}_k = \frac{(\tilde{\lambda}_a\tilde{\lambda}_b + g(\tilde{h}+\tilde{B}) - \tilde{u}^2)\Delta h + (2\tilde{u} - \tilde{\lambda}_a - \tilde{\lambda}_b)\Delta(uh) + g\tilde{h}\Delta B}{(\tilde{\lambda}_k - \tilde{\lambda}_a)(\tilde{\lambda}_k - \tilde{\lambda}_b)},$$

where $a \neq k \neq b$. The Roe averages are

$$\tilde{u} = \frac{\sqrt{h_R}u_R + \sqrt{h_L}u_L}{\sqrt{h_R} + \sqrt{h_L}}, \quad \tilde{h} = \frac{1}{2}(h_R + h_L), \quad \tilde{B} = \frac{1}{2}(B_R + B_L)$$

and

$$\tilde{d} = \frac{\xi\Delta(Au^m)}{\Delta(uh) - \tilde{u}\Delta h}.$$

If m is an integer, then $\tilde{d}$ can be re-written as

$$\tilde{d} = \frac{A\xi(\sqrt{h_R} + \sqrt{h_L})}{\sqrt{h_L}h_R + \sqrt{h_R}h_L} \sum_{k=0}^{m-1} (u_R)^k (u_L)^{m-(1+k)}.$$

For the source term approximation, we use

$$\tilde{\beta}_k = \frac{g\tilde{B}(2\tilde{u} - \tilde{\lambda}_a - \tilde{\lambda}_b)\Delta h}{(\tilde{\lambda}_k - \tilde{\lambda}_a)(\tilde{\lambda}_k - \tilde{\lambda}_b)} \quad \text{where} \quad a \neq k \neq b.$$

3.4 Approximating the Wave Speed of the Bed-Updating Equation

Most of the numerical schemes that can be used with Formulations A-NC and A-CV require a numerical approximation of the wave speed of the bed-updating equation,

$$\frac{\partial B}{\partial t} + \xi\frac{\partial q}{\partial x} = 0,$$

whose wave speed is $\lambda = \xi\frac{\partial q}{\partial B}$. Unfortunately, the sediment transport flux, q, is not a direct function of B, which can create difficulties in obtaining an accurate approximation of the wave speed.

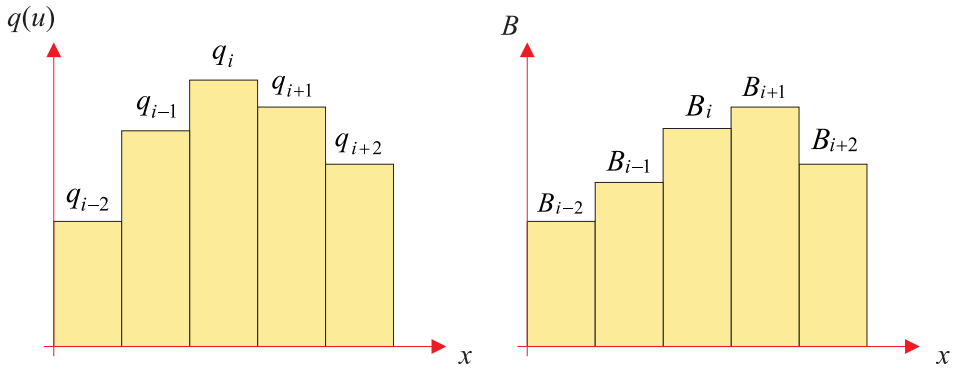

Figure 3.1: The occurrence of a negative wave speed.

One approach that can be used to approximate the wave speed is to use a finite difference approach,

$$\lambda_{i+\frac{1}{2}} = \xi \frac{q_{i+1} - q_i}{B_{i+1} - B_i} \quad \text{if} \quad B_{i+1} - B_i \neq 0. \tag{3.13}$$

Unfortunately, the finite difference approach can only be used when $B_{i+1} - B_i \neq 0$ and can also produce an inaccurate approximation of the wave speed when the gradient of the riverbed changes sign. If the gradient of the riverbed and the velocity do not change sign at the same time, the sign of the wave speed may change. For example, for a small positive velocity, the wave speed of the bed-updating equation is always positive. However, the finite difference approach may produce a negative wave speed, as illustrated in Figure 3.1, where it can be seen that $B_{i+1} - B_i > 0$ but $q_{i+1} - q_i < 0$, which implies that for the illustrated data

$$\lambda_{i+\frac{1}{2}} = -\xi \frac{|q_{i+1} - q_i|}{|B_{i+1} - B_i|}.$$

Hence, the finite difference approach has produced a negative wave speed but the analytic wave speed is positive.

Another approach that can be used is an analytical approach as discussed by Chesher *et al.* [2], but can only be used for problems where the height of the water from the bottom of the channel is considerably larger than the height of the riverbed.

The approach assumes the river is of a constant height, $h + B \approx D$, and $Q = uh$ so that u can be re-written in terms of B,

$$u = Qh^{-1} \approx Q(D - B)^{-1}.$$

As an example, consider the sediment transport flux (3.3), which can be re-written in terms of B as

$$q(u) = Au^m \approx AQ^m(D - B)^{-m}.$$

Thus, the sediment transport flux can now be differentiated with respect to B,

$$\frac{\partial q}{\partial B} \approx AmQ^m(D - B)^{-m-1}.$$

Hence, we obtain an analytical approximation of the wave speed for the bed-updating equation,

$$\lambda \approx \frac{\xi Am}{h} u^m. \tag{3.14}$$

This approximation of the wave speed for the bed-updating equation is very limited as it can only be used for subcritical flow, $u < \sqrt{gh}$. For supercritical flow, the bed should propagate upstream but the analytical approximation of the wave speed results in the bed propagating downstream.

De Vries [7] also derived an analytical approximation of the wave speed associated with the bed-updating equation,

$$\lambda_2 = \frac{gud}{c^2 - u^2} \quad \text{where} \quad d = \xi \left[\frac{\partial q}{\partial u} \right],$$

and was discussed in Section 3.1.2. Unfortunately, the wave speed approximation is only valid for sediment transport fluxes that are know functions of u only, i.e. $q(u)$, and the approximation cannot be used when the flow is near critical. However, the approximation can be used for subcritical and supercritical flow. For the sediment transport flux (3.3), $d = Amu^{m-1}$ thus,

$$\lambda_2 = \frac{A\xi mgu^m}{gh - u^2}. \tag{3.15}$$

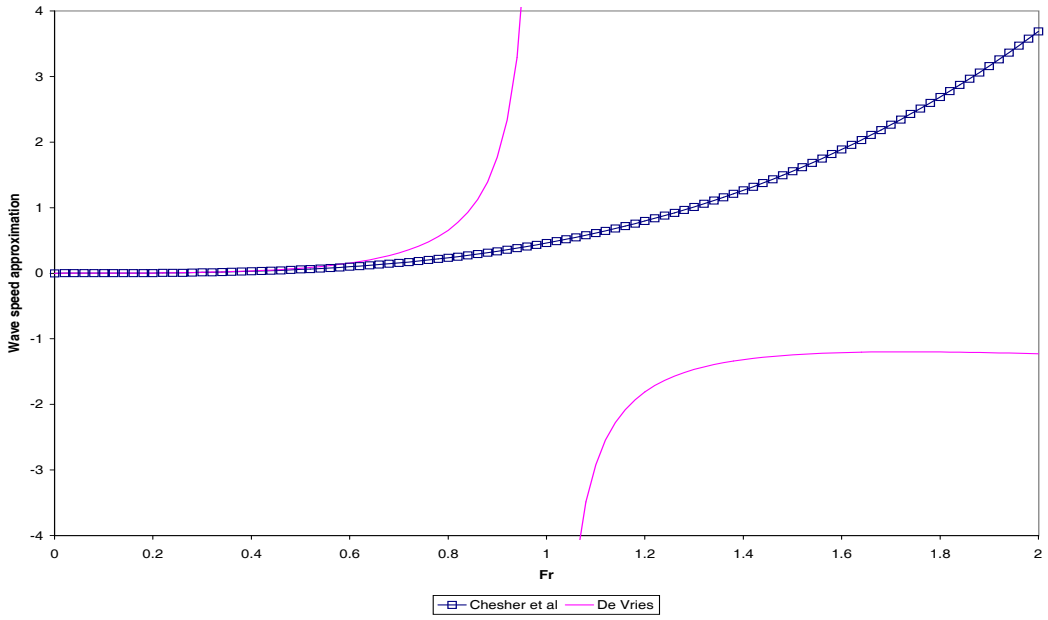

Figure 3.2: Comparison of the analytical wave speed approximations (3.14) and (3.15) with $D = 10$ and $A = 0.001$ for $F_r = 0$ to 2.

From Figure 3.2, we can see that the analytical wave speed approximations of De Vries and Chesher *et al.* produce similar values when the Froude number is small, i.e. $F_r < 0.4$. In this thesis, only small Froude numbers are considered thus, the wave speed approximation derived by Chesher *et al.* (3.14) is used.

3.5 Test Problems

To determine which formulation with the flux-limited version of Roe's scheme produces the most accurate numerical results, we use the following two test problems. Both test problems consist of a channel of length $1000m$ with the following dummy initial conditions

$$h^*(x,0) = 10 - B^*(x,0) \quad \text{and} \quad u^*(x,0) = \frac{Q}{h^*(x,0)}$$

where Q is a constant. The bathymetry for

1. Channel Test Problem A is

$$B(x,0) = \begin{cases} \hat{B}\sin^2\left(\dfrac{\pi(x-300)}{200}\right) & \text{if } 300 \leq x \leq 500 \\ 0 & \text{otherwise} \end{cases},$$

   where $\hat{B}$ is the maximum height of the bed.

2. Channel Test Problem B is

$$B(x,0) = \begin{cases} B_L & \text{if } x \leq 300 \\ B_R & \text{if } x > 300 \end{cases}.$$

To obtain the initial conditions, the water flow is iterated with the dummy initial conditions to an equilibrium state whilst keeping the riverbed fixed, i.e.

$$|\mathbf{w}_i^{n+1} - \mathbf{w}_i^n| \leq \text{tol},$$

where tol is the desired tolerance level. This ensures that the initial conditions of the water flow and bed are consistent and greatly reduces the possibility of an impulsive start occurring for larger values of A. The initial conditions for Channel Test Problem A with $\hat{B} = 1m$ and $Q = 10$ are illustrated in Figure 3.3 and Figure 3.4 and for Channel Test Problem B with $B_L = 1m$, $B_R = 0m$ and $Q = 10$ are illustrated in Figure 3.5 and Figure 3.6.

For both test problems, the sediment transport flux discussed by Grass (1.10) is used with $m = 3$,

$$q(u) = Au^3,$$

which is valid for all values of u. To ensure the error of the numerical schemes do not grow, the variables are non-dimensionalised,

$$x^* = \frac{x}{L}, \quad t^* = \frac{t}{T}, \quad h^* = \frac{h}{L}, \quad B^* = \frac{B}{L}, \quad g^* = \frac{gT^2}{L},$$

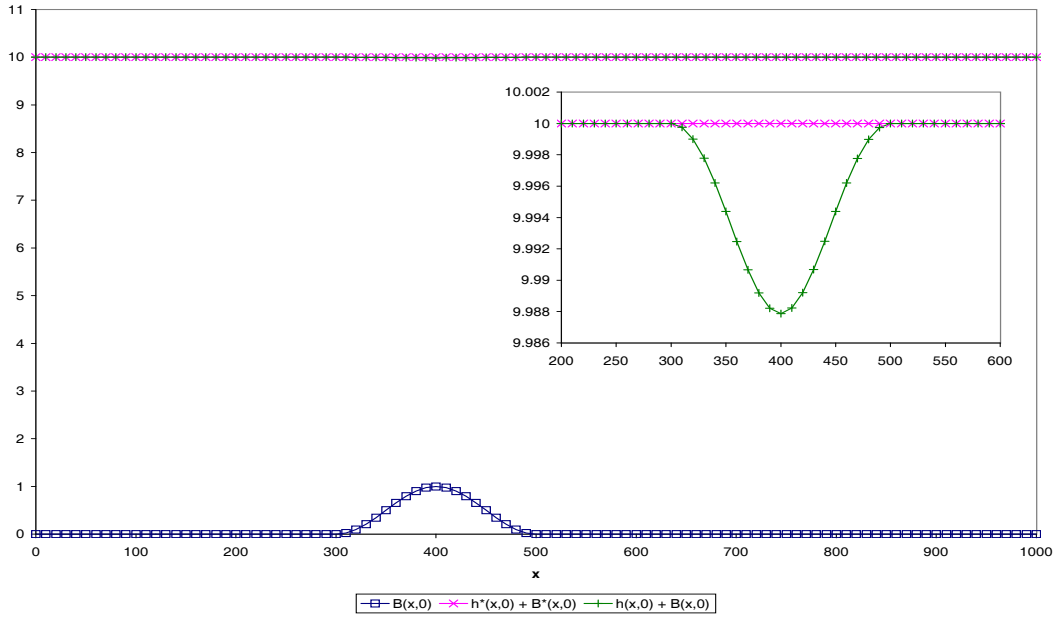

Figure 3.3: Initial conditions for Channel Test Problem A (h & B).

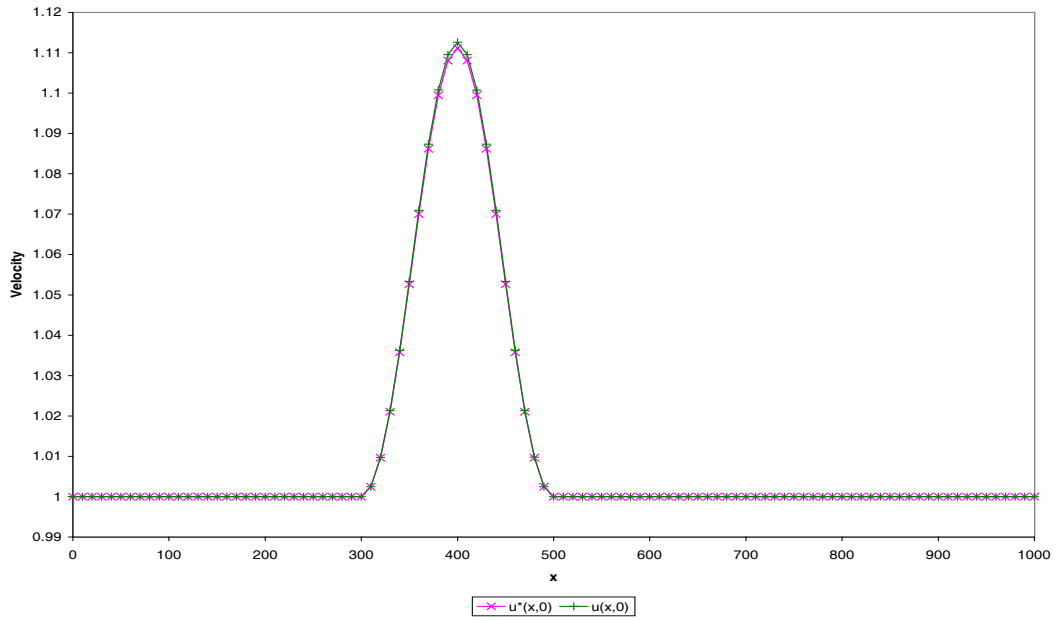

Figure 3.4: Initial conditions for Channel Test Problem A (u).

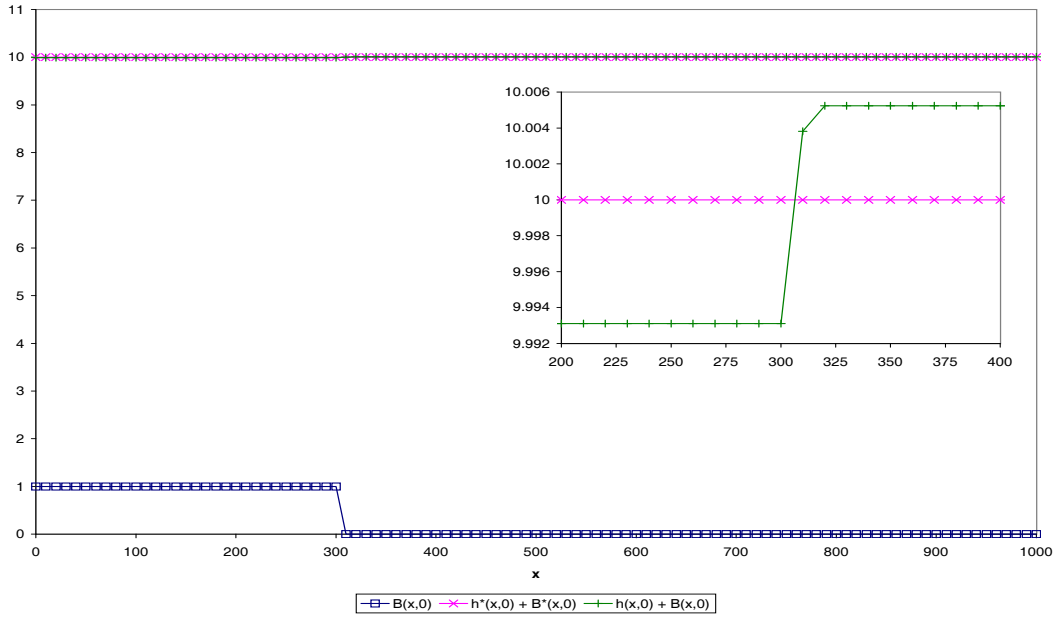

Figure 3.5: Initial conditions for Channel Test Problem B (h & B).

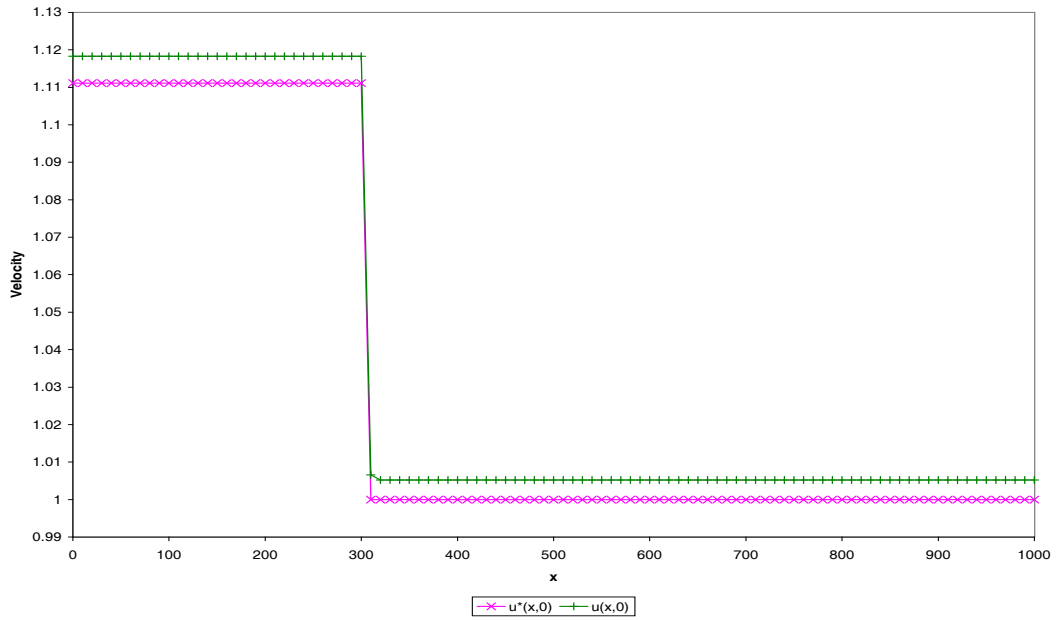

Figure 3.6: Initial conditions for Channel Test Problem B (u).

$$u^* = \frac{uT}{L}, \quad A^* = \frac{AL}{T^2} \quad \text{and} \quad \text{tol}^* = \frac{\text{tol}}{L},$$

where $L = 1000$ and $T = \sqrt{\frac{1000}{g}}$ are the non-dimensional coefficients. Here, L is taken as the length of the channel.

It should be noted that even though in Chapter 1 it was stated that the differential form of equation for conservation of momentum (1.2) becomes invalid when a discontinuity appears in the riverbed, this is only analytically and the equation holds numerically as long as the discontinuity in the riverbed is small. Thus, Channel Test Problem B can be used as long as the discontinuity in the riverbed is small.

3.5.1 Approximate Solution for Channel Test Problem A

We can determine an approximate solution of Channel Test Problem A by assuming that the total height of the river is constant and the discharge is constant throughout the whole domain, i.e.

$$h(x,t) \approx D - B(x,t) \quad \text{and} \quad u(x,t)h(x,t) \approx Q_c \quad \forall (x,t),$$

where Q_c is a constant. These assumptions are only valid when the riverbed is interacting slowly with the water flow, $A < 0.01$, and when the water flow is moving slowly, $Q_c \leq 10$. However, the assumptions enable the velocity to be re-written in terms of the riverbed,

$$u(x,t) \approx \frac{Q_c}{D - B(x,t)}.$$

An approximate solution of $B(x,t)$ is now required. The bed-updating equation (1.3) can be re-written in quasi-linear form as

$$B_t + \lambda B_x = 0,$$

where the wave speed is

$$\lambda = \xi \left[\frac{\partial q}{\partial B} \right].$$

Since the sediment transport flux is not a direct function of B, the wave speed of the bed-updating equation can be difficult to obtain. However in Section 3.4, an analytical approximation was derived which assumes the total height of the river is constant and uses $u \approx Q(D-B)^{-1}$ to re-write the sediment transport flux (3.3) in terms of the riverbed,

$$q(u) = Au^m \approx AQ^m(D-B)^{-m}.$$

The sediment transport flux can now be differentiated with respect to B and we obtain the analytical approximation of the wave speed

$$\lambda \approx A\xi m Q^m (D-B)^{-m-1}.$$

By assuming the discharge is constant, the characteristics are given by

$$\frac{dx}{dt} = A\xi m Q_c^m (D - B(x_0, 0))^{-m-1}$$

and with initial bathymetry

$$B(x,0) = \begin{cases} \hat{B}\sin^2\left(\dfrac{\pi(x-300)}{200}\right) & \text{if } 300 \le x \le 500 \\ 0 & \text{otherwise} \end{cases}$$

thus

$$\frac{dx}{dt} = A\xi m Q_c^m \begin{cases} \left(D - \hat{B}\sin^2\left(\dfrac{\pi(x_0-300)}{200}\right)\right)^{-(m+1)} & \text{if } 300 \le x_0 \le 500, \\ D^{-(m+1)} & \text{otherwise.} \end{cases}$$

Now, by integrating we obtain

$$x = x_0 + A\xi m Q_c^m t \begin{cases} \left(D - \hat{B}\sin^2\left(\frac{\pi(x_0-300)}{200}\right)\right)^{-(m+1)} & \text{if } 300 \le x_0 \le 500, \\ D^{-(m+1)} & \text{otherwise,} \end{cases} \tag{3.16}$$

which unfortunately cannot be re-written in terms of x_0. Hence, the approximate solution of B is

$$B(x,t) = \begin{cases} \hat{B}\sin^2\left(\dfrac{\pi(x_0-300)}{200}\right) & \text{if } 300 \leq x_0 \leq 500, \\ 0 & \text{otherwise,} \end{cases}$$

where the value of x is determined by substituting values of x_0 and t into (3.16). Unfortunately, this approximate solution is only valid until the characteristics cross, which first occurs in the region $300 \leq x_0 \leq 500$. We can determine the time the characteristics first cross by using

$$\frac{dx}{dx_0} = 0$$

and finding the smallest positive value of t. For the current approximate solution, the characteristics first cross in the region $300 \leq x_0 \leq 500$,

$$\frac{dx}{dx_0} = 1 + \frac{m(m+1)A\xi Q_c^m \hat{B}\pi t \sin\left(\frac{2\pi(x_0-300)}{200}\right)}{200\left[D - \hat{B}\sin^2\left(\frac{\pi(x_0-300)}{200}\right)\right]^{m+2}}.$$

Thus, by setting this equal to zero and re-arranging, we obtain

$$t = \frac{-200\left[D - \hat{B}\sin^2\left(\frac{\pi(x_0-300)}{200}\right)\right]^{m+2}}{m(m+1)A\xi Q_c^m \pi \hat{B}\sin\left(\frac{\pi(x_0-300)}{100}\right)}.$$

Hence, we can determine the time the characteristics first cross by finding the minimum positive value of t in the region $300 \leq x_0 \leq 500$. For $m = 3$, $\hat{B} = 1m$, $\epsilon = 0.4$ and $Q_c = 10$, we can determine that the approximate solution is only valid until

$$t = 238079.124A^{-1} \quad \text{seconds} \quad .$$

3.6 Numerical Results

In the next few sections, we use the classic Lax-Wendroff scheme and the flux-limited version of Roe's scheme with the different formulations to obtain a numerical solution of either Channel Test Problem A or B. Both numerical schemes use $\Delta x = 10m$ and $\nu = 0.8$ and the flux-limited version of Roe's scheme uses the minmod flux-limiter. All schemes use the basic free flow boundary conditions,

$$\mathbf{w}_{-i,j}^{n+1} = \mathbf{w}_{0,j}^{n}, \quad \mathbf{w}_{I+i,j}^{n+1} = \mathbf{w}_{I,j}^{n}, \quad \mathbf{w}_{i,-j}^{n+1} = \mathbf{w}_{i,0}^{n} \quad \text{and} \quad \mathbf{w}_{i,J+j}^{n+1} = \mathbf{w}_{i,J}^{n},$$

where $i, j = 1$ to 5. Formulation A-CV used a tolerance level of tol $= 0.000001$ to determine when the shallow water equations have reached an equilibrium state. If a formulation's numerical results are not illustrated for a particular scheme then this is due to the scheme becoming unstable for this formulation.

3.6.1 Channel Test Problem A: Numerical Results for a Small Bed which is Interacting Slowly with the Water Flow

For the first test case, we simulate a small pulse in the riverbed which is interacting slowly with the water flow, where the water flow is moving slowly. To simulate this, we use the values $A = 0.001$, $\hat{B} = 1m$ and $Q = 10$. Thus, by using these values with the two different schemes, we obtain the numerical results of the classic Lax-Wendroff scheme, which are illustrated in Figure 3.7, and the flux-limited version of Roe's scheme, which are illustrated in Figure 3.8.

From Figure 3.7, we can see that the classic Lax-Wendroff scheme has produced poor numerical results for all formulations. The scheme became unstable for Formulations A-CV and A-SF and the numerical results of Formulation A-NC were completely inaccurate due to spurious oscillations occurring initially in the numerical results that were then propagated over the whole domain. This resulted in the

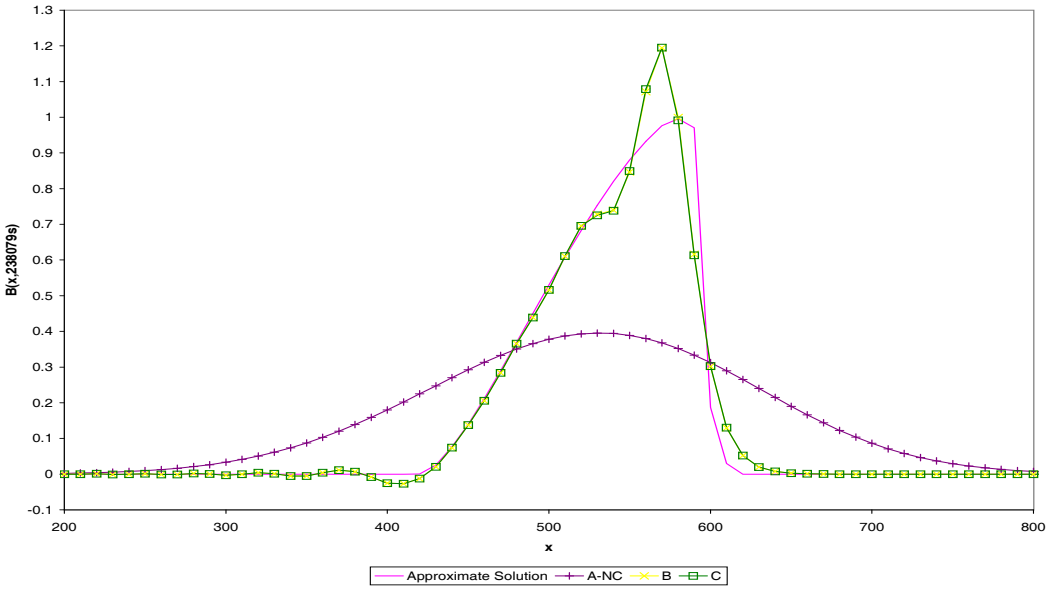

Figure 3.7: Comparison of the different formulations for Channel Test Problem A using the classic Lax-Wendroff scheme with $A = 0.001$ and $Q = 10$ at $t = 238079s$ (B).

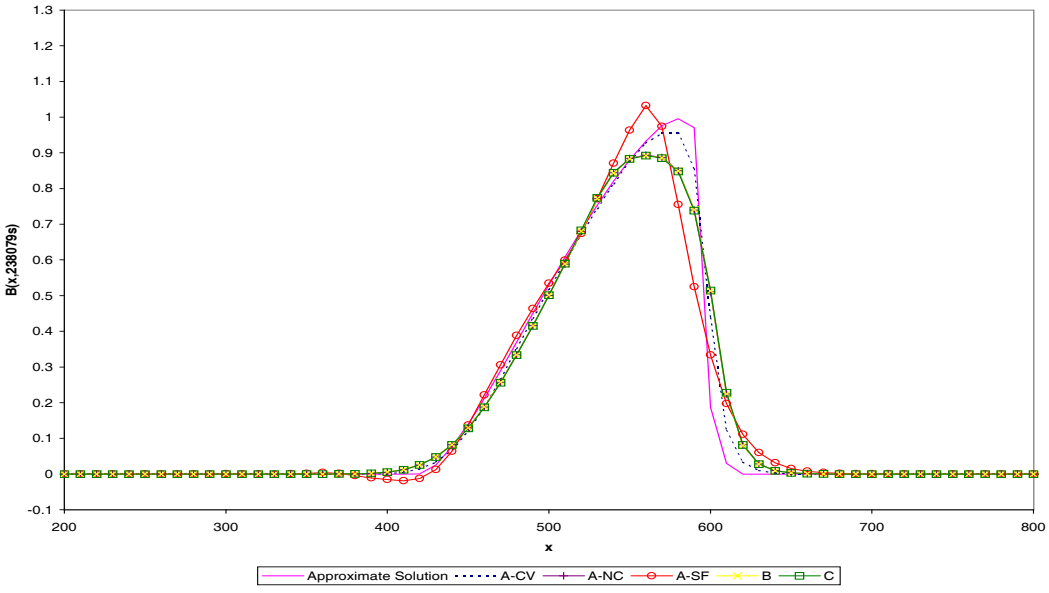

Figure 3.8: Comparison of the different formulations for Channel Test Problem A using the flux-limited version of Roe's scheme with $A = 0.001$ and $Q = 10$ at $t = 238079s$ (B).

total height of the river, the height of the riverbed and the overall velocity being greatly reduced (initially, the overall velocity was approximately $1m/s$, but at $t = 238079s$, the overall velocity was approximately $0.92m/s$). The scheme is considerably more accurate with Formulations B and C, but the numerical results were still poor due to spurious oscillations being present in the numerical results.

From Figure 3.8, we can see that the flux-limited version of Roe's scheme has produced accurate numerical results for all formulations except Formulation A-SF due to spurious oscillations beginning to occur in the numerical results. For Formulation A-CV, the scheme produced numerical results that were very close to the approximate solution (for the bathymetry). The scheme produced practically identical numerical results for Formulations A-NC, B and C with no spurious oscillations present. However, the numerical results of Formulations A-NC, B and C were more diffusive than Formulation A-CV due to Formulation A-CV requiring considerably less time steps to reach the final time than Formulations A-NC, B and C. Formulation A-CV had an overall time step of $\Delta t \approx 2.9$ hours and required approximately 3 minutes to iterate the water flow to an equilibrium state each time the bed was updated whereas Formulations A-NC, B and C had an overall time step of $\Delta t \approx 0.7$ seconds). Also, notice that Formulations A-NC, B and C have produced slightly different numerical results than the approximate solution and Formulation A-CV due to the position of the top of the pulse in the bathymetry. Formulations A-NC, B and C placed the top of the pulse in the bathymetry slightly to the left of Formulation A-CV and the approximate solution.

To determine if the numerical schemes become unstable for longer computational run times, we run the test problem with the same values for longer until $t = 150$ hours (540,000 seconds). Thus, we obtain the numerical results of the classic Lax-Wendroff scheme, which are illustrated in Figure 3.9, and the flux-limited version of Roe's scheme, which are illustrated in Figure 3.10.

From Figure 3.9, we can see that the numerical results of the classic Lax-Wendroff scheme have become considerably worse for a longer computational run time. All variations of Formulation A have now become unstable and Formulations B and C

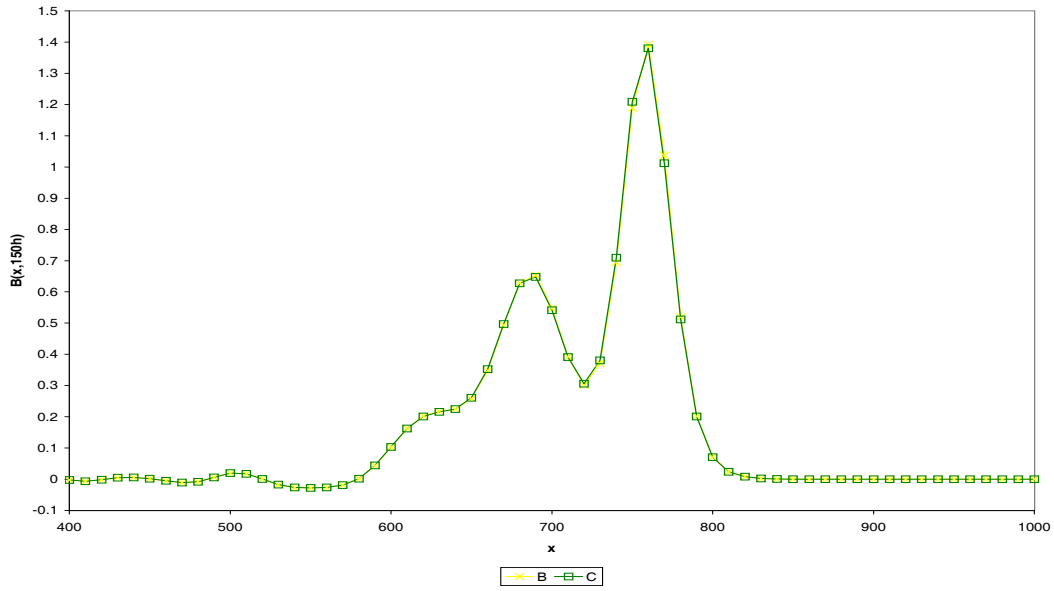

Figure 3.9: Comparison of the different formulations for Channel Test Problem A using the classic Lax-Wendroff scheme with $A = 0.001$ and $Q = 10$ at $t = 150h$ (B).

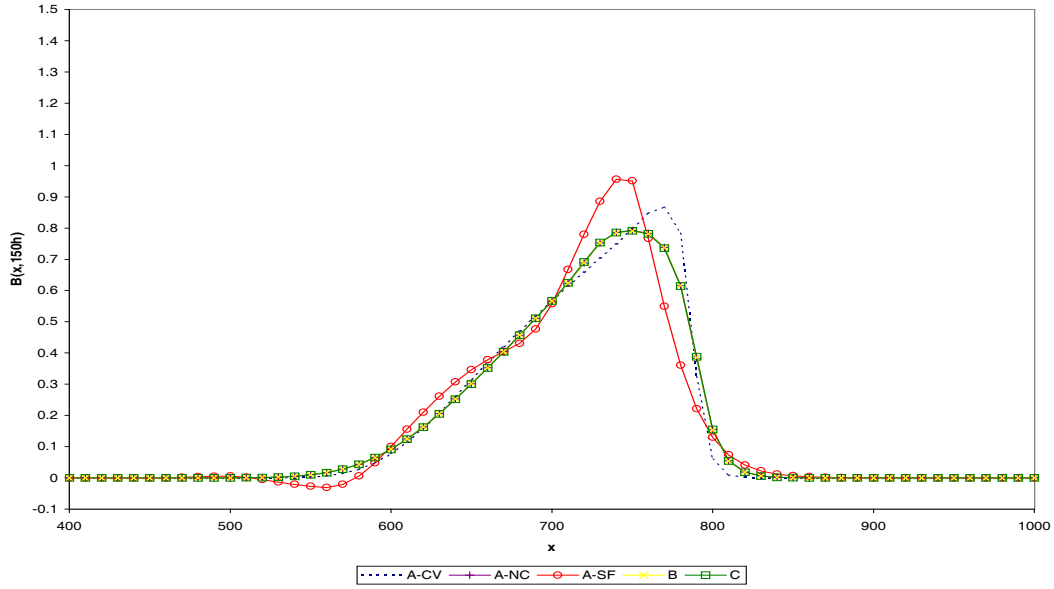

Figure 3.10: Comparison of the different formulations for Channel Test Problem A using the flux-limited version of Roe's scheme with $A = 0.001$ and $Q = 10$ at $t = 150h$ (B).

have both produced very poor numerical results with spurious oscillations present.

From Figure 3.10, we can see that the flux-limited version of Roe's scheme has again produced very accurate numerical results for all formulations, with the exception of Formulation A-SF that suffered badly from spurious oscillations. Notice that the difference of the position of the top of the pulse in the bathymetry between Formulation A-CV and Formulations A-NC, B and C has increased. Formulations A-CV and A-NC are identical apart from Formulation A-CV iterates the water flow to an equilibrium state each time the bed is updated. Thus, the difference is created by Formulation A-CV iterating the water flow to an equlibrium state each time the bed is updated. If the test problem is run for even longer then the difference becomes more significant.

Hence, the flux-limited version of Roe's scheme is considerably more accurate than the classic Lax-Wendroff scheme for all formulations. Formulation A-SF is the least accurate formulation for both schemes and Formulations A-NC and A-CV were accurate with the flux-limited version of Roe's scheme but became unstable with the classic Lax-Wendroff scheme. Formulations B and C worked well for both schemes but the classic Lax-Wendroff scheme produced spurious oscillations in the numerical results.

3.6.2 Channel Test Problem A: Numerical Results for a Small Bed which is Interacting Quickly with the Water Flow

In the previous section we used a value of $A = 0.001$, which simulated a slow moving riverbed. We now use a value of $A = 1$ to simulate a fast moving riverbed, which is now reacting quickly with the water flow. There are a few cases where the bed interacts quickly with the water flow, see Perdreau and Cunge [31], but these cases are rare. However, it is interesting to study the numerical results of the different formulations for this case so that we can determine which formulations can be used

with large values of A. Unfortunately when using large values of A, the initial conditions used produce an impulsive start for all unsteady approaches due to the initial conditions not representing a fast moving riverbed. Formulation A-CV is the only formulation that does not produce an impulsive start with the initial conditions due to the formulation being a steady approach, which assumes the riverbed is interacting slowly with the water flow. At present, obtaining initial conditions for a fast moving riverbed can be very difficult. To obtain such initial conditions, empirical data could be used but physical cases where the riverbed is interacting quickly with the riverbed are very rare. Alternatively, the initial conditions could be obtained by iterating an unsteady approach, which includes bed movement, until the water flow has settled down, see Hudson & Sweby [21].

Now, by using $Q = 10$, $\hat{B} = 1m$ and $A = 1$ with a final time of $t = 238s$, we obtain the numerical results of the classic Lax-Wendroff scheme, which are illustrated in Figure 3.11, and the flux-limited version of Roe's scheme, which are illustrated in Figure 3.12. Notice that the pulse in the riverbed has moved at a considerably quicker wave speed than with the smaller value of A.

From Figure 3.11, we can see that by using the classic Lax-Wendroff scheme, the scheme became unstable for all of the variations of Formulation A. The scheme only remained stable for Formulations B and C, but the numerical results of both schemes suffered from spurious oscillations.

From Figure 3.12, we can see that by using the flux-limited version of Roe's scheme, the scheme became unstable for Formulations A-SF and A-NC. Formulations A-CV, B and C have all produced smooth numerical results free from spurious oscillations. However, as with the classic Lax-Wendroff scheme, the numerical results obtained from Formulation A-CV differed significantly from all the other formulations. The pulse in the riverbed has been moved at a slower speed for Formulations B and C than Formulation A-CV. The difference between Formulations B and C and Formulation A-CV still occurs when the scheme is used with a finer mesh, $\Delta x = 0.5$, see Figure 3.13. The difference also occurred with the small value of A used in the previous section, but the difference was considerably less significant.

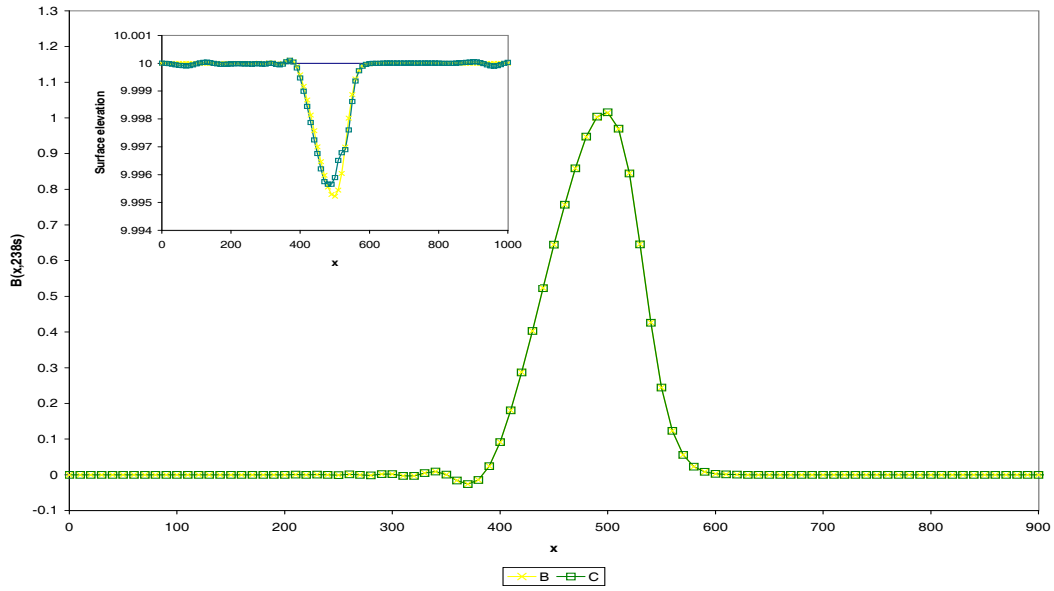

Figure 3.11: Comparison of the different formulations for Channel Test Problem A using the classic Lax-Wendroff scheme with $A = 1$ and $Q = 10$ at $t = 238s$ (h & B).

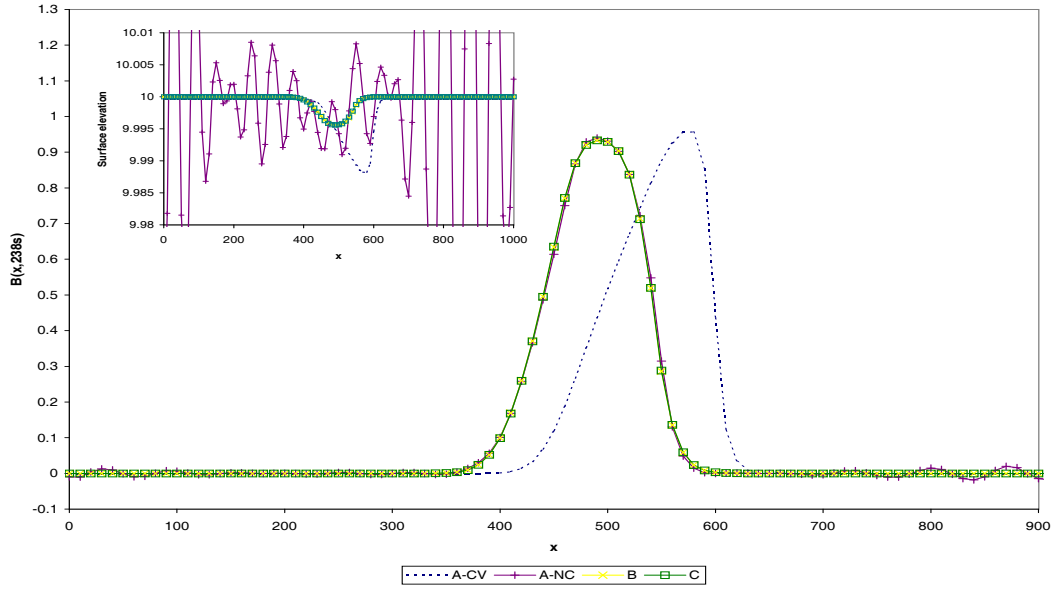

Figure 3.12: Comparison of the different formulations for Channel Test Problem A using the flux-limited version of Roe's scheme with $A = 1$ and $Q = 10$ at $t = 238s$ (h & B).

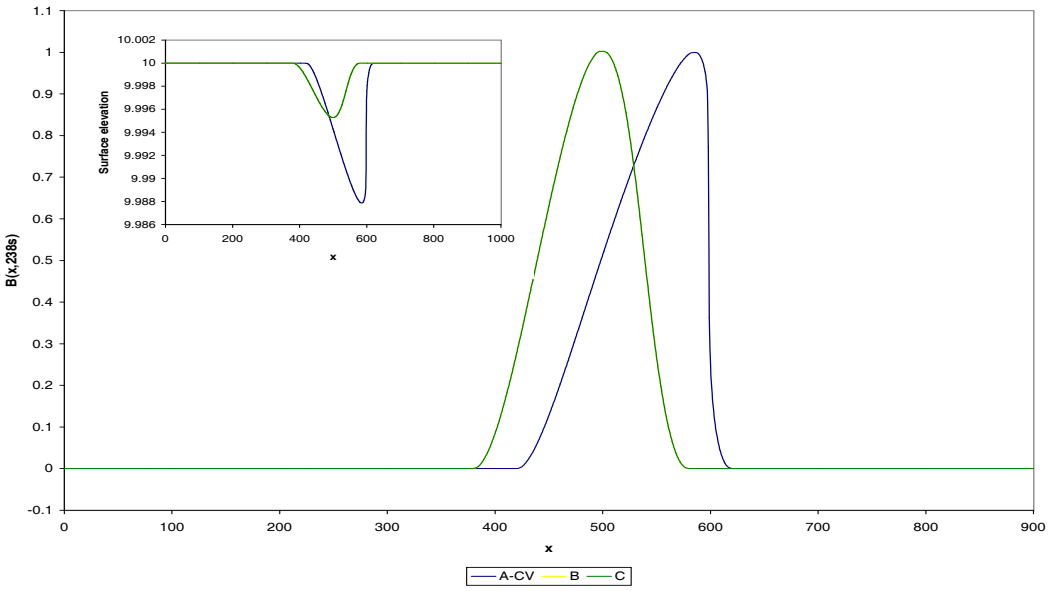

Figure 3.13: Comparison of the different formulations for Channel Test Problem A using the flux-limited version of Roe's scheme on a fine mesh with $A = 1$, and $Q = 10$ at $t = 238s$ (h & B).

The difference is due to the assumptions made when deriving a steady approach. The steady approach assumes that the water flow has a negligible effect on the bed, which results in the system being decoupled into a water flow approximation, that is iterated to an equilibrium state, followed by a bed update. By iterating the water flow to an equilibrium state, the equation for conservation of mass (1.1) becomes

$$Q_x = 0 \quad \Rightarrow \quad Q(x,t) = Q_c \quad \forall (x,t),$$

where Q_c is a constant. Thus, when the water flow has reached an equilibrium state, the discharge is constant over the whole domain. Hence, since Formulation A-CV iterates the water flow to an equilibrium state, this has the effect of imposing a constant discharge.

Figure 3.14 and Figure 3.15 illustrate the discharge, Q, for each formulation compared to the assumed value, $Q_c = 10$, with $A = 0.001$ and $A = 1$ respectively. From Figure 3.14, we can see for $A = 0.001$, the approximate values of the discharge

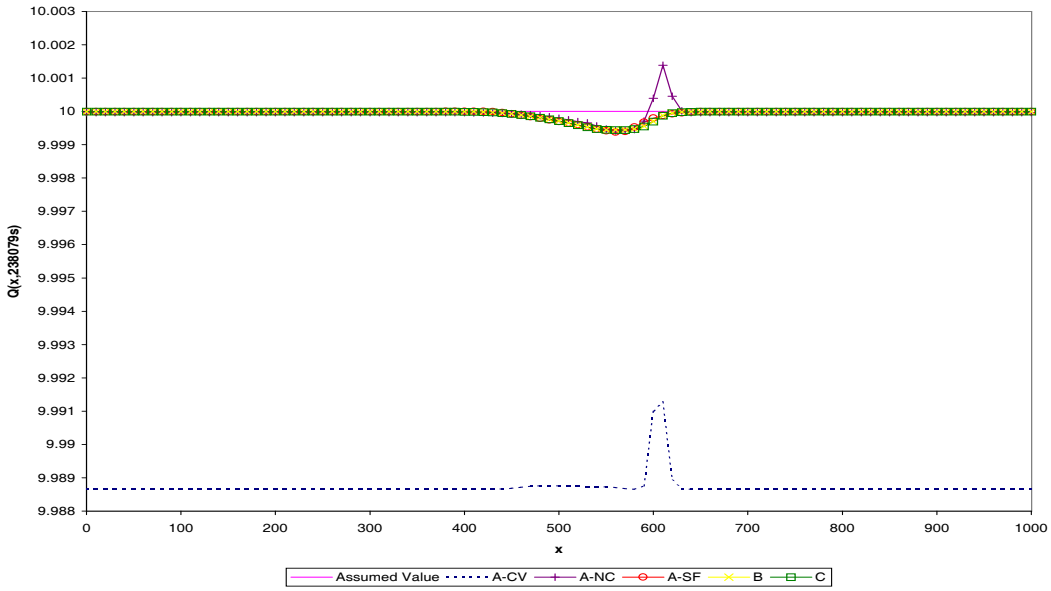

Figure 3.14: Comparison of the discharge for the different formulations with $A = 0.001$ at $t = 238079s$ (Q).

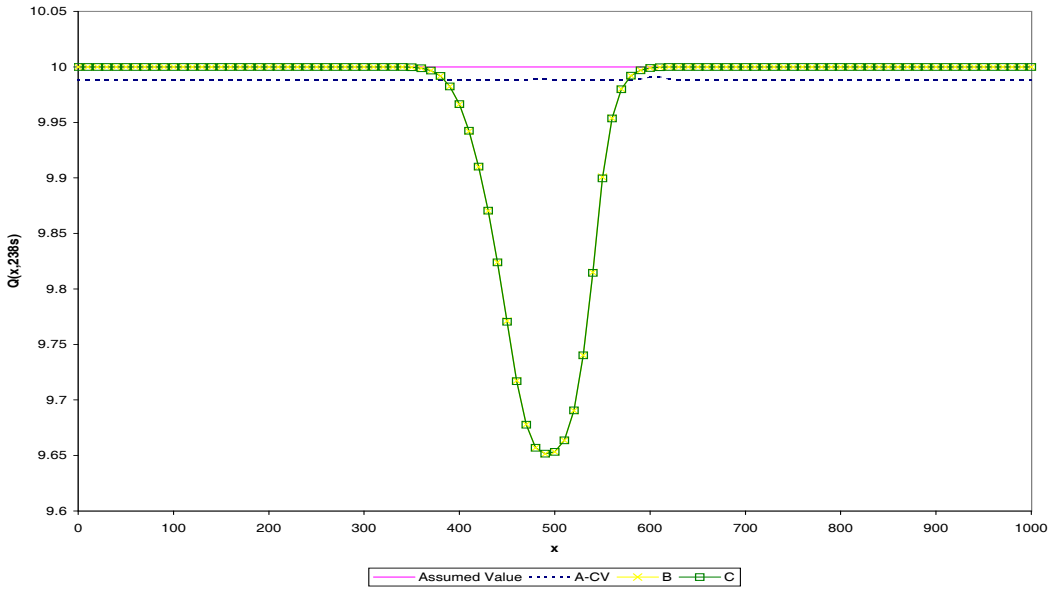

Figure 3.15: Comparison of the discharge for the different formulations with $A = 1$ at $t = 238s$ (Q).

are very close to the assumed values for all formulations. From Figure 3.15 we can see for $A = 1$, the approximate values of the discharge for Formulation A-CV are practically identical to the values obtained with $A = 0.001$ and are close to the assumed values. However, Formulations B and C have produced values that are beginning to differ from the assumed value. Formulation A-CV assumes the water flow is in and equilibrium state, which has the effect of imposing a constant discharge. This implies that Formulation A-CV becomes invalid as $A \to 1$ and can only be used for small values of A whereas Formulations B and C can be used for all values of A. More detailed comparisons of the different formulations with $A = 1$ can be found in Hudson & Sweby [21], where it is also illustrated that the numerical results of Formulations C and A-CV differ.

3.6.3 Channel Test Problem A: Numerical Results for a Large Bed which is Interacting Slowly with the Water Flow

For the third test problem, we increase the height of the pulse in the bed from $\hat{B} = 1m$ to $\hat{B} = 5m$. The riverbed is interacting slowly with the water flow, $A = 0.001$, and the discharge is $Q = 10$. By using these values, we obtain the numerical results of the classic Lax-Wendroff scheme, which are illustrated in Figure 3.16, and the flux-limited version of Roe's scheme, which are illustrated in Figure 3.17. The numerical results are for $t = 5339s$ and are illustrated with the approximate solution, which cannot be calculated beyond this time.

From Figure 3.16, we can see that the classic Lax-Wendroff scheme has again produced spurious oscillations in the numerical results. The scheme has moved the pulse at the same wave speed for all formulations, but Formulation A-SF suffers the most from spurious oscillations. Formulation A-CV produced results with the least spurious oscillations present and the results were similar to the approximate solution.

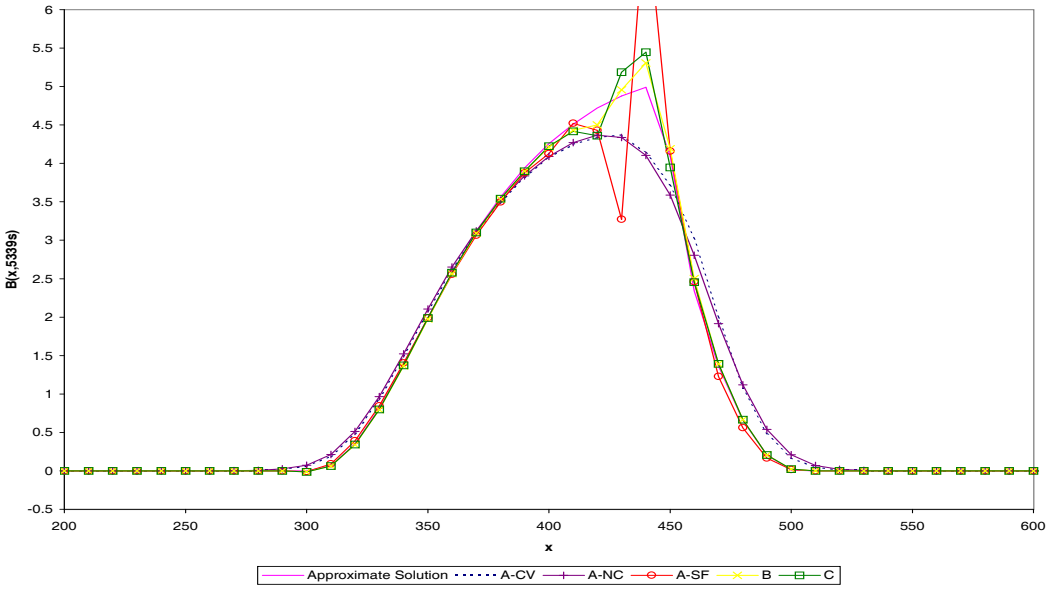

Figure 3.16: Comparison of the different formulations for Channel Test Problem A using the classic Lax-Wendroff scheme with $A = 0.001$, $\hat{B} = 5m$ and $Q = 10$ at $t = 5339s$ (B).

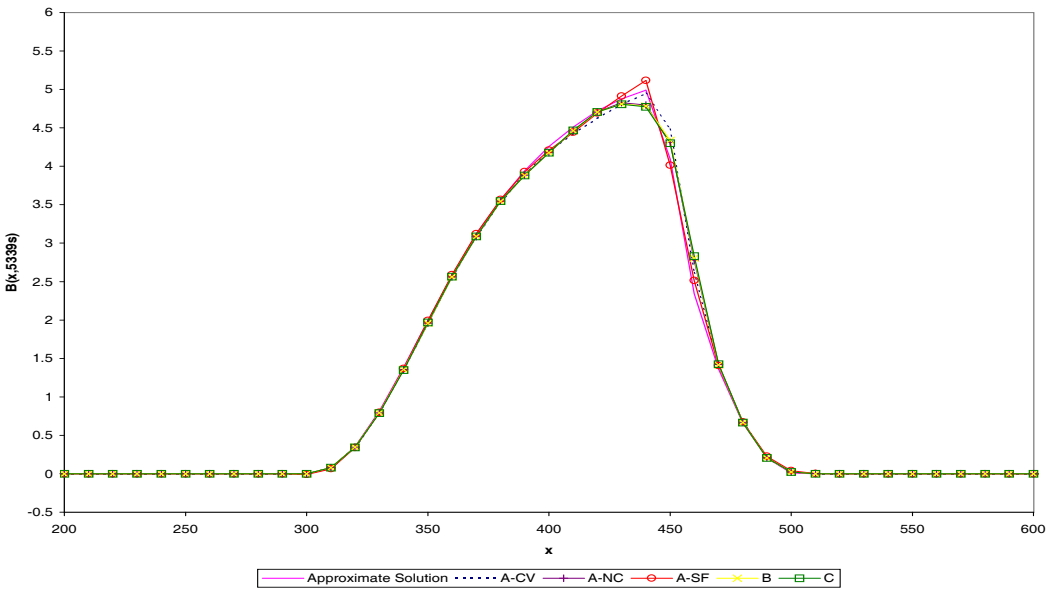

Figure 3.17: Comparison of the different formulations for Channel Test Problem A using the flux-limited version of Roe's scheme with $A = 0.001$, $\hat{B} = 5m$ and $Q = 10$ at $t = 5339s$ (B).

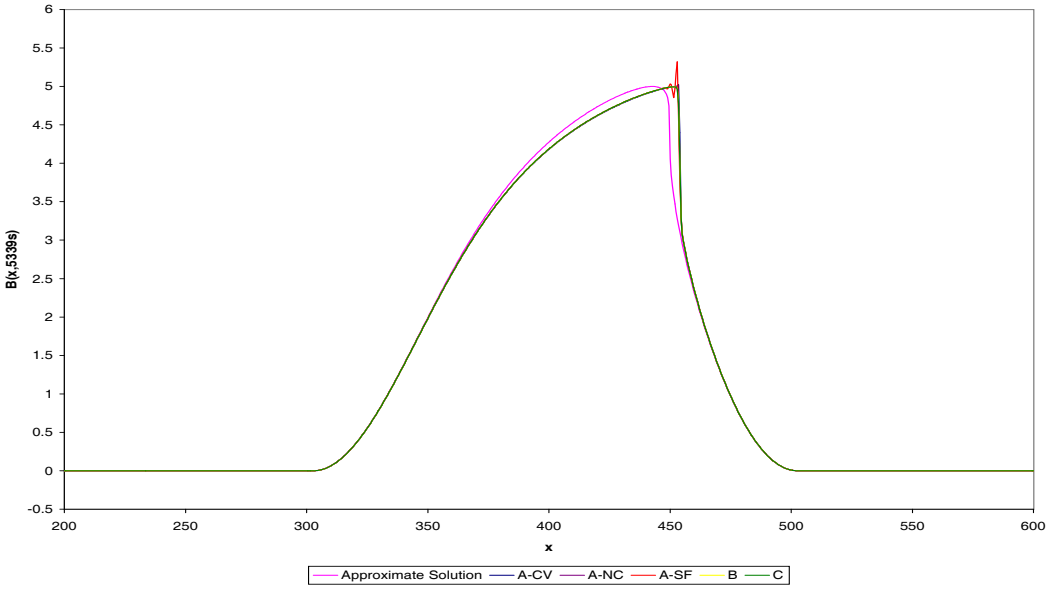

Figure 3.18: Comparison of the different formulations for Channel Test Problem A using the flux-limited version of Roe's scheme on a fine mesh with $A = 0.001$, $Q = 10$ and $\hat{B} = 5m$ at $t = 5339s$ (B).

From Figure 3.17, we can see that the flux-limited version of Roe's scheme produced very accurate results for all formulations, except for Formulation A-SF, where the scheme is starting to produce spurious oscillations. The numerical results for all formulations were very close to the approximate solution. Figure 3.18 illustrates the numerical results obtained using the flux-limited version of Roe's scheme on a finer mesh, $\Delta x = 0.5$, with the different formulations. Here, we can see that all of the different formulations with the scheme have produced practically identical results. Formulation A-SF with the scheme has produced spurious oscillations whereas all of the other formulations produced smooth numerical results. Notice that the top of the pulse in the bed has been moved slightly further with the different formulations than the approximate solution. This implies that the approximate solution has become invalid for $\hat{B} = 5m$.

Hence, the flux-limited version of Roe's scheme was again considerably more accurate than the classic Lax-Wendroff scheme. The numerical results of all formulations with the flux-limited version of Roe's scheme were very similar to the

approximate solution if $\Delta x = 10$ was used, but the results started to differ if a finer mesh was used, i.e. $\Delta x = 0.5$. Formulation A-SF with both schemes produced the least accurate numerical results due to spurious oscillations being present.

3.6.4 Channel Test Problem A: Numerical Results for a Large Velocity with a Small Bed which is Interacting Slowly with the Water Flow

So far, all variations of Channel Test Problem A have been with a small velocity resulting in a small Froude number. However, for this test case, we use $Q = 50$ with $A = 0.001$ and $\hat{B} = 1m$ to simulate a small pulse in a riverbed that is still interacting slowly with the water flow, but the speed of the water flow has been increased. For this test problem, the Froude number is approximately 0.5, and the flow is still subcritical. By using these values, we obtain the numerical results of the classic Lax-Wendroff scheme, which are illustrated in Figure 3.19, and the flux-limited version of Roe's scheme, which are illustrated in Figure 3.20.

From Figure 3.19, we can see that the classic Lax-Wendroff scheme has again produced spurious oscillations in the numerical results. For Formulation A-CV, the scheme has become unstable and the scheme has produced poor numerical results for all formulations, with the exception of Formulation A-NC. Surprisingly, the numerical results of Formulation A-NC do not have any spurious oscillations present even though the classic Lax-Wendroff scheme is used.

From Figure 3.20, we can see that the flux-limited version of Roe's scheme produced very accurate results for Formulations B and C but produced spurious oscillations for Formulation A-SF. The scheme became unstable for Formulation A-CV and with Formulation A-NC, and a small kink has appeared at the top of the pulse in the bed. Formulations A-CV and A-NC require an approximation of the wave speed of the bed-updating equation, see Section 3.4. The wave speed approximation of Chesher *et al.* (3.14) was used for Formulations A-CV and A-NC,

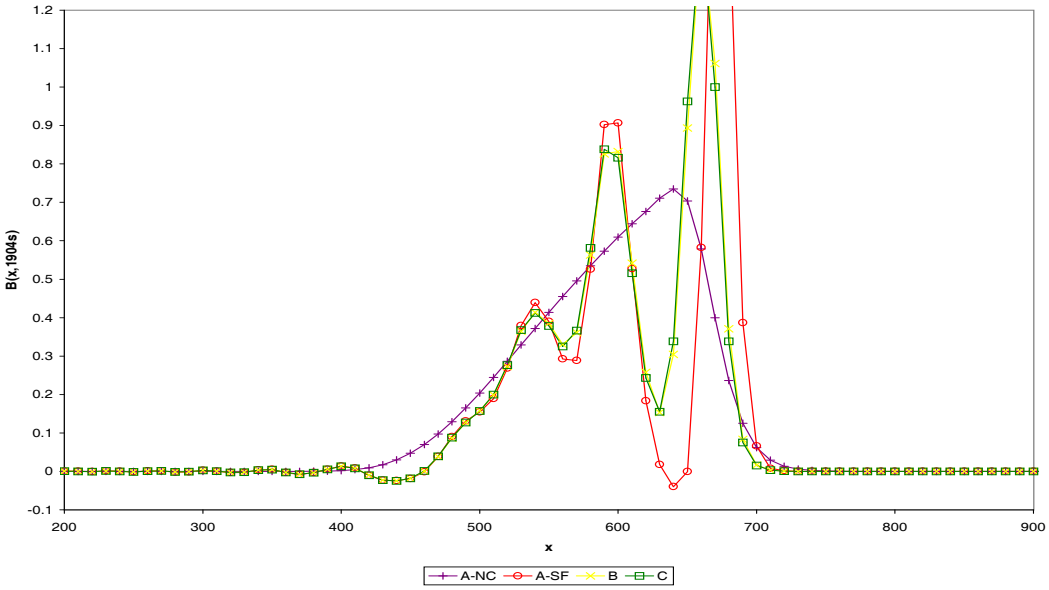

Figure 3.19: Comparison of the different formulations for Channel Test Problem A using the classic Lax-Wendroff scheme with $A = 0.001$ and $Q = 50$ at $t = 1904s$ (B).

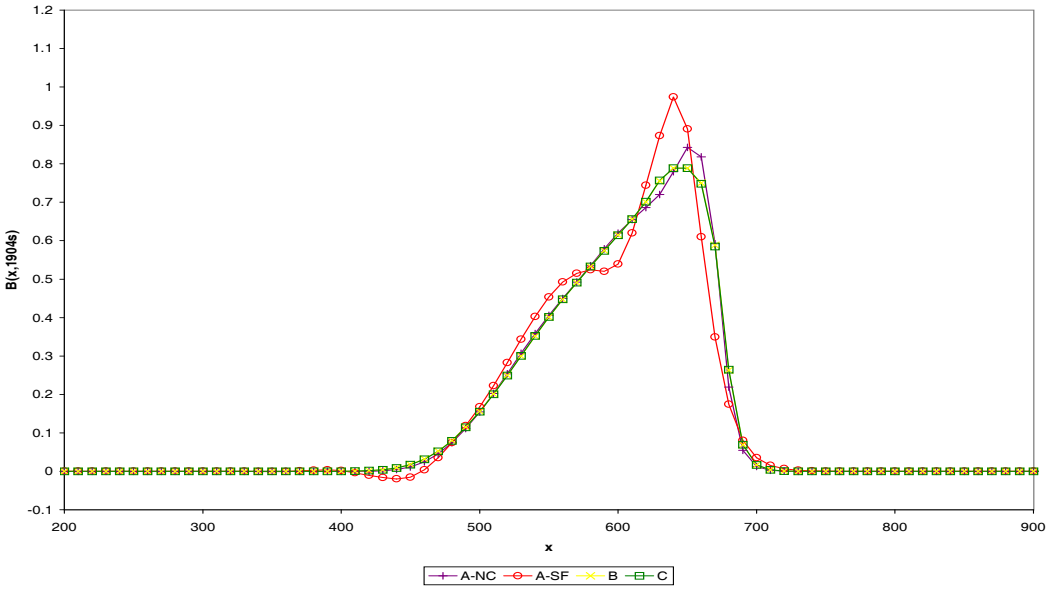

Figure 3.20: Comparison of the different formulations for Channel Test Problem A using the flux-limited version of Roe's scheme with $A = 0.001$ and $Q = 50$ at $t = 1904s$ (B).

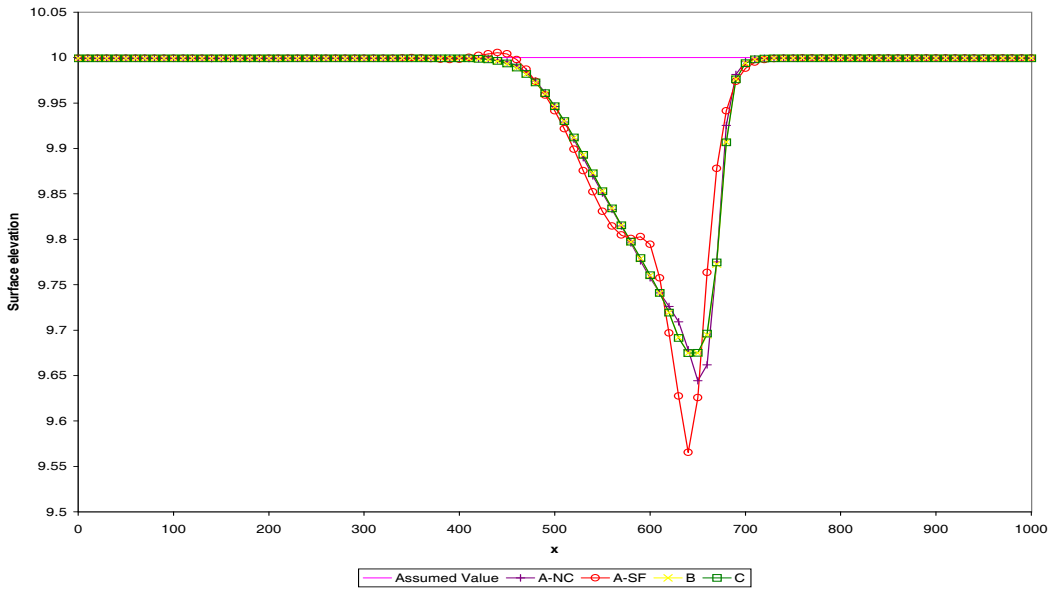

Figure 3.21: Comparison of the different formulations for Channel Test Problem A using the flux-limited version of Roe's scheme with $A = 0.001$ and $Q = 50$ at $t = 1904s$ $(h + B)$.

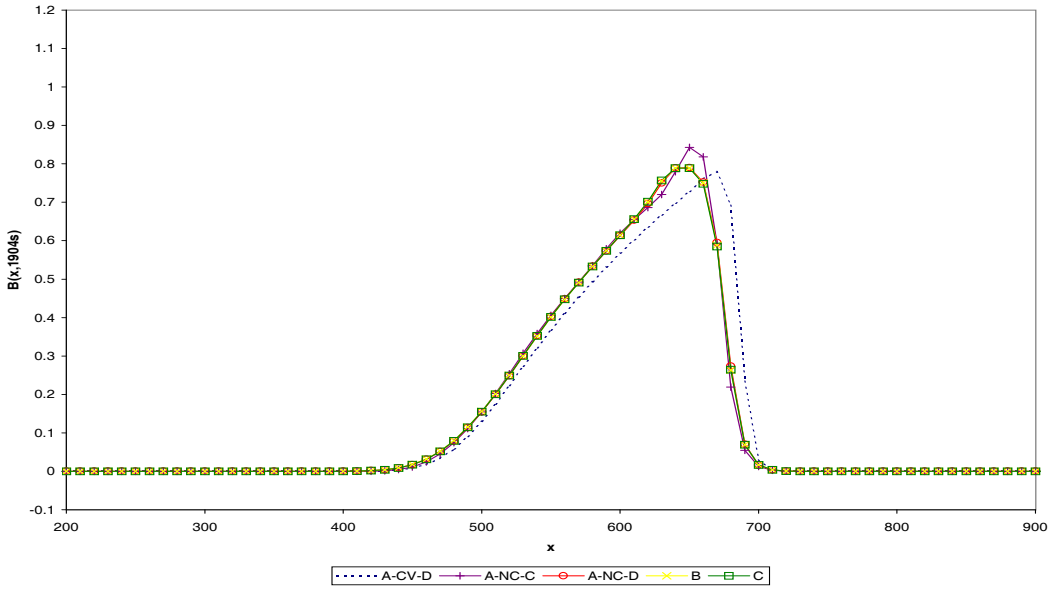

Figure 3.22: Comparison of Formulations A-CV and A-NC for Channel Test Problem A using the flux-limited version of Roe's scheme with $A = 0.001$ and $Q = 50$ at $t = 1904s$ (B).

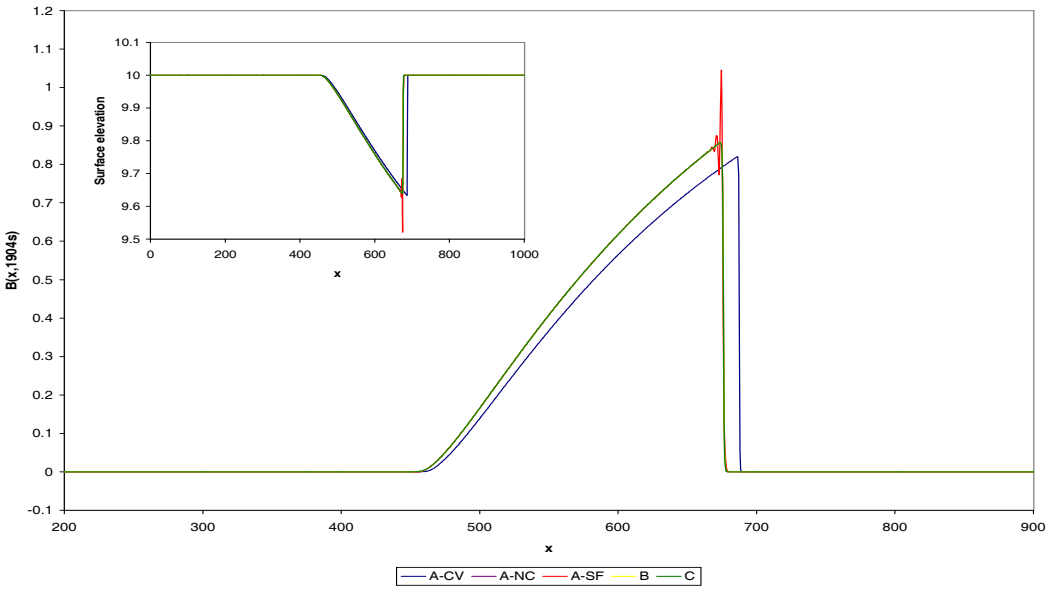

Figure 3.23: Comparison of the different formulations for Channel Test Problem A using the flux-limited version of Roe's scheme on a fine mesh with $A = 0.001$ and $Q = 50$ at $t = 1904s$ (h & B).

but the approximation assumes that the surface elevation is constant, i.e. $h \approx 10 - B$. From Figure 3.21 we can see that the numerical values of the surface elevation for the different formulation are not constant. This implies that for Formulations A-CV and A-NC, the wave speed approximation of Chesher *et al.* has become inaccurate. In Section 3.4, we also discussed the wave speed approximation of De Vries (3.15). Figure 3.22 illustrates the numerical results of the flux-limited version of Roe's scheme with Formulations A-CV and A-NC using either the wave speed approximation of Chesher *et al.* (A-CV/NC-C) or De Vries (A-CV/NC-D). The numerical results of Formulations B and C are also illustrated. From the results, we can see that Formulation A-NC has produced smoother numerical results with the wave speed approximation of De Vries due to the kink at the top of the pulse in the bed no longer being present. The scheme became unstable for Formulation A-CV with the wave speed approximation of Chesher *et al.*, but with the approximation of De Vries, the scheme remained stable and produced smooth numerical results. However, the formulation moved the pulse in the bed at a faster speed than Formulations A-NC, B and C. This difference still occurs when the

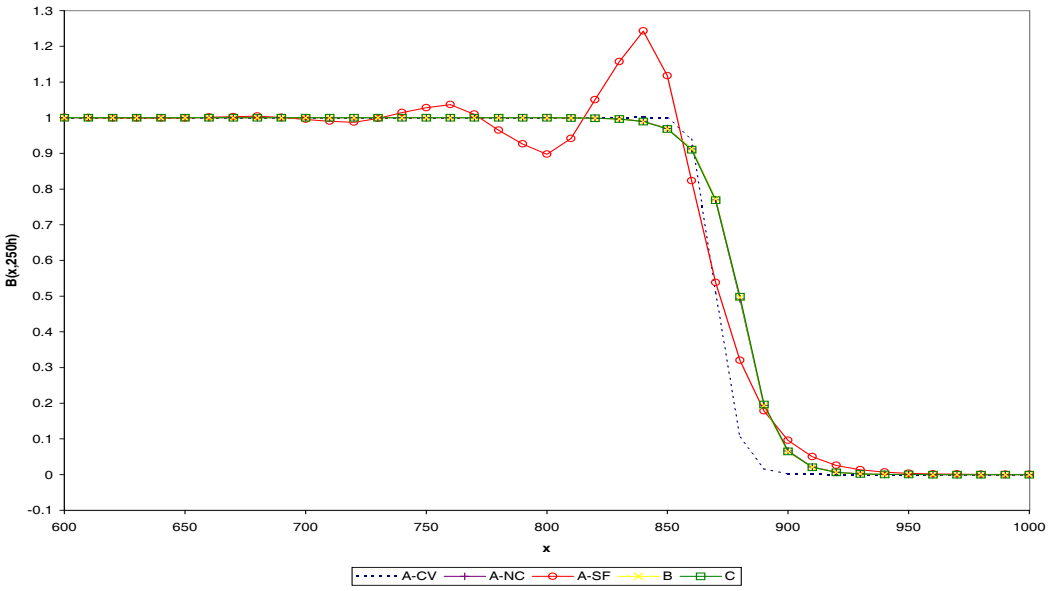

Figure 3.24: Comparison of the different formulations for Channel Test Problem B using the flux-limited version of Roe's scheme with $A = 0.001$ and $Q = 10$ at $t = 250h$ (B).

scheme is used with a finer mesh, $\Delta x = 0.5$, see Figure 3.23.

Hence, overall the flux-limited version of Roe's scheme was again considerably more accurate than the classic Lax-Wendroff scheme. Formulations B and C with the flux-limited version of Roe's scheme produced accurate numerical results with no spurious oscillations present. Formulation A-NC produced accurate numerical results for both schemes and the wave speed approximation of De Vries was the most accurate. Formulation A-CV became unstable with the classic Lax-Wendroff scheme, and only remained stable with the flux-limited version of Roe's scheme if the wave speed approximation of De Vries was used. Formulation A-SF produced completely inaccurate numerical results for both schemes.

3.6.5 Channel Test Problem B: Numerical Results for a Small Discontinuity in the Bed

So far, we have only numerically approximated variations of Channel Test Problem A. We now use Channel Test Problem B with $A = 0.001$, $Q = 10$, $B_L = 1m$ and $B_R = 0m$ to simulate a small sediment bore propagating in a river. By using these values, we obtain the numerical results of the the flux-limited version of Roe's scheme, which are illustrated in Figure 3.24, at $t = 250h$. The numerical results obtained with the classic Lax-Wendroff scheme are not illustrated due to the scheme becoming unstable for all formulations.

From Figure 3.24, we can see that the flux-limited version of Roe's scheme produced spurious oscillations in the numerical results for Formulation A-SF. The scheme did not produce any spurious oscillations for any of the other formulations. Formulations A-NC, B and C produced practically identical numerical results but moved the sediment bore slightly further than Formulation A-CV. This is due to Formulation A-CV assuming the discharge and surface elevation are constant, which is clearly not the case when a discontinuity is present in the riverbed. Notice that Formulation B has moved the sediment bore at the same speed as Formulation C even for this long computational run time. This implies that Formulation B may be written in conservative variable form, but more investigation is required to verify this.

3.7 Summary

Throughout this chapter, we have discussed five different formulations with two different numerical schemes that can be used to numerically approximate the equations governing sediment transport. For both test problems, we have seen that the classic Lax-Wendroff scheme produced poor numerical results with spurious oscillations present. The flux-limited version of Roe's scheme did not produce

spurious oscillations for Formulations B and C, but did with Formulation A-SF. Formulation A-CV with the flux-limited version of Roe's scheme also produced poor numerical results for test problems with $A = 1$ and $Q = 50$ but produced accurate numerical results for small values of A and Q. Formulation A-SF was extremely inaccurate due to the numerical results suffering from spurious oscillations if either scheme was used. This is due to the formulation having a singular Jacobian matrix. If a small value of A is used, Formulations B and C with both schemes suffered more from diffusion than Formulation A-CV. This is due to Formulation A-CV discretising the water flow and bed update separately resulting in considerably less time steps required to reach the final computational run time. Formulation A-CV has an overall morphological time step, which is calculated by using

$$\Delta t = \frac{\nu \Delta x}{\max_i(|\lambda|)}, \quad \text{where} \quad \lambda = \frac{3\xi A u^3}{h}.$$

Now,

$$\max_i(|\lambda|) = \frac{3\xi A \max_i(|u^3|)}{\min_i(|h|)}$$

and from the numerical results of Channel Test Problem A with $Q = 10$, $\hat{B} = 1$ and $D = 10$, $\max_i(|u|) \approx 1.1$ and $\min_i(|h|) \approx 9$ thus, we obtain

$$\max_i(|\lambda|) \approx 0.759795A,$$

and by using, $\Delta x = 10$ and $\nu = 0.8$,

$$\Delta t \approx \frac{\nu \Delta x}{0.759795A} = 10.52915589A^{-1} \quad \text{seconds} \quad .$$

For small values of A, the morphological time step is large, i.e. if $A = 0.001$ then $\Delta t \approx 10529$ seconds, and as $A \to 1$, $\Delta t \to 10$ seconds. This implies that for small values of A, Formulation A-CV takes a small amount of time steps to reach the final computational run time but as A tends to one, the formulation takes longer due to the formulation iterating the water flow to an equilibrium state each time the bed is updated. For the other formulations, with $A = 0.001$ the eigenvalues are

$$\lambda_1 \approx -8.28, \quad \lambda_2 \approx 0.000772 \quad \text{and} \quad \lambda_3 \approx 10.51$$

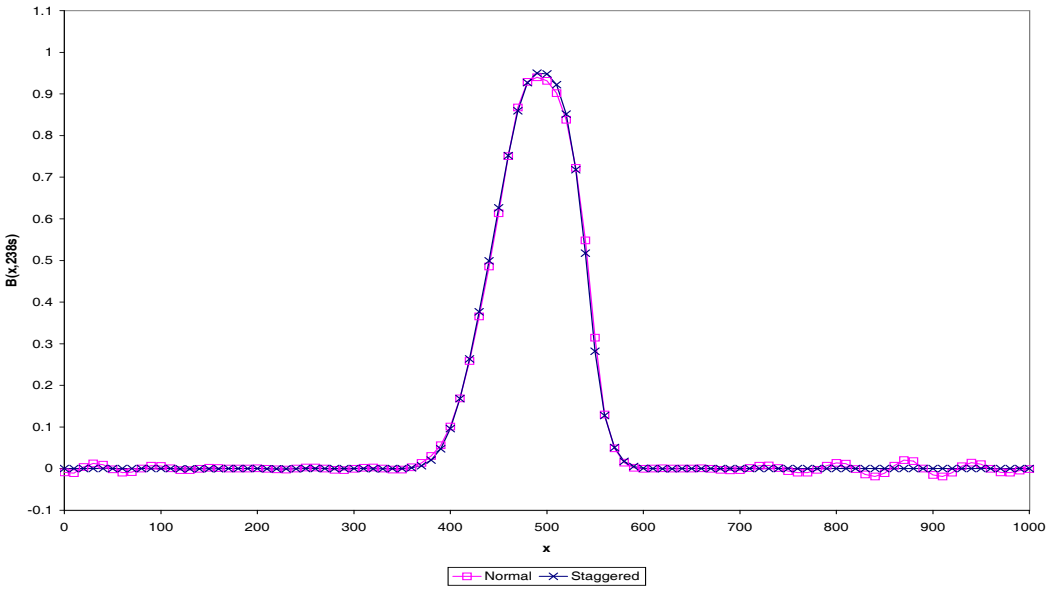

Figure 3.25: Comparison of the different schemes with Formulation A-NC for Channel Test Problem A using $A = 1$, $\hat{B} = 1$ and $Q = 10$ at $t = 238s$ (B).

and the eigenvalues associated with the water flow, λ_1 and λ_3, are the dominant eigenvalues and determine the overall time step of the scheme, which is approximately $\Delta t \approx 0.7$. As A becomes large, the eigenvalue associated with the bed-updating equation becomes the dominant eigenvalue but for realistic test problems, the value of A is usually small. Thus a numerical scheme that can be used with a large time step is required for all unsteady formulations, such as an implicit scheme.

Formulation A-NC with the flux-limited version of Roe's scheme produced accurate numerical results for test problems where A is small but as $A \to 1$, spurious oscillation started to appear in the numerical results. We can minimise these oscillations by using a smaller Courant number, but this can be impractical due to long computational run times. As an alternative, we could use the flux-limited version of Roe's Scheme to numerically approximate the shallow water equations with

$$B_i^{n+1} = B_i^n - s\xi(q^*_{i+\frac{1}{2}} - q^*_{i-\frac{1}{2}}), \tag{3.17}$$

where

$$q^*_{i+\frac{1}{2}} = \begin{cases} q^n_i + \frac{1}{2}(1-\nu^n_{i+\frac{1}{2}})(q^n_{i+1}-q^n_i)\Phi^n_i & \text{if } \nu^n_{i+\frac{1}{2}} > 0 \\ q^n_{i+1} - \frac{1}{2}(1+\nu^n_{i+\frac{1}{2}})(q^n_{i+1}-q^n_i)\Phi^n_i & \text{if } \nu^n_{i+\frac{1}{2}} < 0 \end{cases},$$

to numerically approximate the bed-updating equation for Formulation A-NC. Unfortunately, the numerical scheme becomes unstable resulting in the scheme being considerably worse than the normal approach (3.12). However, by using a staggered approach,

$$q^*_{i+\frac{1}{2}} = \begin{cases} q^{n+1}_i + \frac{1}{2}(1-\nu^{n+1}_{i+\frac{1}{2}})(q^{n+1}_{i+1}-q^{n+1}_i)\Phi^n_i & \text{if } \nu^{n+1}_{i+\frac{1}{2}} > 0 \\ q^{n+1}_{i+1} - \frac{1}{2}(1+\nu^{n+1}_{i+\frac{1}{2}})(q^{n+1}_{i+1}-q^{n+1}_i)\Phi^n_i & \text{if } \nu^{n+1}_{i+\frac{1}{2}} < 0 \end{cases}, \tag{3.18}$$

we can minimise these spurious oscillations without having to reduce the Courant number, see Figure 3.25. Here, we can see that all oscillations have been eliminated resulting in a smooth numerical solution, that is considerably more accurate than the normal approach.

Formulations B and C with the flux-limited version of Roe's scheme started to produce different numerical results than Formulation A-CV as $A \to 1$ due to the formulation assuming that the discharge and total height of the river are constant throughout the domain. Thus, Formulation A-CV should only be used for test problems where the riverbed is interacting slowly with the water flow.

Hence, the flux-limited version of Roe's scheme was considerably more accurate for all formulations. Formulation A-NC produced accurate numerical results for test problems where the riverbed interacts slowly with the water flow but became unstable when the riverbed interacts quickly with the water flow, unless the staggered scheme was used. Formulation A-SF was the worst formulation and both schemes with Formulation A-CV became unstable when the riverbed interacts quickly with the water flow or the velocity is large. Formulation A-CV produced different numerical results to Formulations A-NC, B and C when the riverbed is interacting quickly with the water flow and both schemes become unstable when the velocity is large. Thus, Formulation A-CV should only be used for test problems where Q and A are small whereas Formulations B and C can be used for any test problem

with any value of A and Q. In the next chapter, we extend the numerical schemes discussed in this chapter and the previous chapter to two dimensions.

Chapter 4

Numerical Schemes for Systems of Conservation Laws in Two Dimensions

So far, we have only discussed sediment transport in one dimension. In this chapter we discuss a variety of numerical techniques that can be used to approximate the equations governing sediment transport in two dimensions. The classic Lax-Wendroff scheme in 2D with either a pointwise or second order accurate source term approximation, a flux-limited 2D Lax-Wendroff scheme, a flux-limited 2D version of Roe's scheme and dimensional splitting will be discussed and the numerical results compared using a 2D wave propagation test problem. The source terms will be constructed to satisfy a 2D version of the C-property of Bermúdez & Vázquez [1]. All numerical schemes will be derived so that they can be used to approximate systems of conservation laws with source term in 2D,

$$\frac{\partial \mathbf{w}}{\partial t} + \frac{\partial \mathbf{F}(\mathbf{w})}{\partial x} + \frac{\partial \mathbf{G}(\mathbf{w})}{\partial y} = \mathbf{R}, \tag{4.1}$$

where $\mathbf{F}(\mathbf{w})$ and $\mathbf{G}(\mathbf{w})$ are the flux-functions and $\mathbf{R}$ is the source term, which can be re-written as

$$\mathbf{R} = \mathbf{f} + \mathbf{g}, \tag{4.2}$$

where $\mathbf{f}$ and $\mathbf{g}$ contains the x or y derivative terms only of the source term respectively. To help illustrate the numerical techniques, we use the 2D shallow water equations,

$$\begin{bmatrix} h \\ uh \\ vh \end{bmatrix}_t + \begin{bmatrix} uh \\ hu^2 + \frac{1}{2}gh^2 \\ huv \end{bmatrix}_x + \begin{bmatrix} vh \\ huv \\ hv^2 + \frac{1}{2}gh^2 \end{bmatrix}_y = \begin{bmatrix} 0 \\ -ghB_x \\ -ghB_y \end{bmatrix}, \tag{4.3}$$

where $h(x, y, t)$ is the height of the water above the bottom of the channel (m), $B(x, y, t)$ is the height of the riverbed (m) and $u(x, y, t)$ and $v(x, y, t)$ are the velocities in the x and y direction, respectively (m/s). Some of the numerical schemes discussed in this chapter require the Jacobian matrices of the fluxes, which for the 2D shallow water equations are

$$\mathbf{A} = \frac{\partial \mathbf{F}}{\partial \mathbf{w}} = \begin{bmatrix} 0 & 1 & 0 \\ c^2 - u^2 & 2u & 0 \\ -uv & v & u \end{bmatrix} \quad \text{and} \quad \mathbf{B} = \frac{\partial \mathbf{G}}{\partial \mathbf{w}} = \begin{bmatrix} 0 & 0 & 1 \\ -uv & v & u \\ c^2 - v^2 & 0 & 2v \end{bmatrix},$$

where $c = \sqrt{gh}$, whose corresponding eigenvalues for $\mathbf{A}$ are

$$\lambda_1^F = u - c, \quad \lambda_2^F = u \quad \text{and} \quad \lambda_3^F = u + c,$$

and for $\mathbf{B}$ are

$$\lambda_1^G = v - c, \quad \lambda_2^G = v \quad \text{and} \quad \lambda_3^G = v + c.$$

The eigenvectors are, for $\mathbf{A}$

$$\mathbf{e}_1^F = \begin{bmatrix} 1 \\ u - c \\ v \end{bmatrix}, \quad \mathbf{e}_2^F = \begin{bmatrix} 0 \\ 0 \\ c \end{bmatrix} \quad \text{and} \quad \mathbf{e}_3^F = \begin{bmatrix} 1 \\ u + c \\ v \end{bmatrix},$$

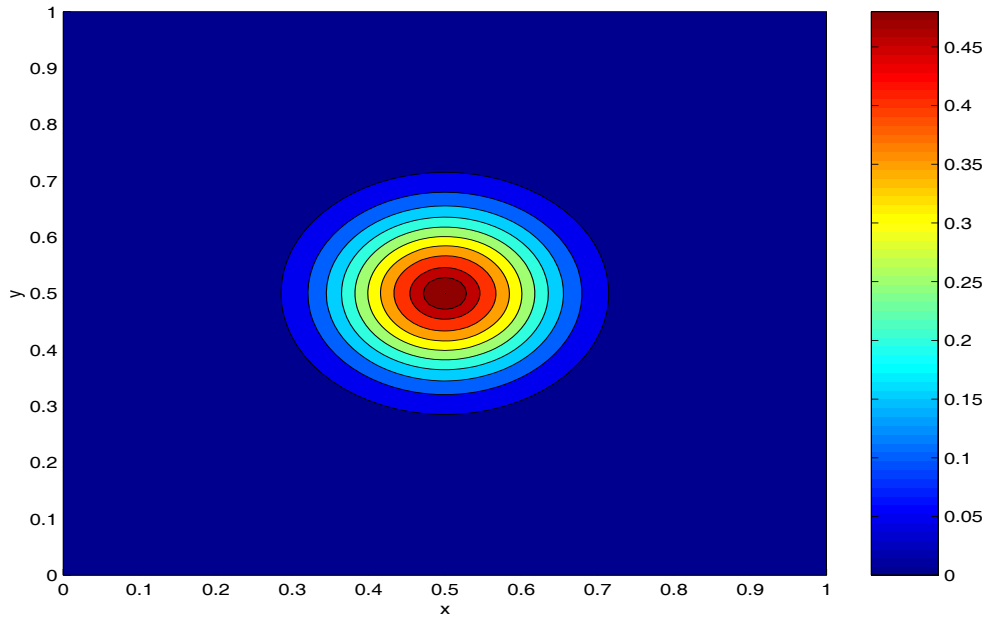

Figure 4.1: Illustration of the initial bathymetry for 2D Test Problem B (B).

and for $\mathbf{B}$

$$\mathbf{e}_1^G = \begin{bmatrix} 1 \\ u \\ v-c \end{bmatrix}, \quad \mathbf{e}_2^G = \begin{bmatrix} 0 \\ -c \\ 0 \end{bmatrix} \quad \text{and} \quad \mathbf{e}_3^G = \begin{bmatrix} 1 \\ u \\ v+c \end{bmatrix}.$$

4.1 2D Test Problem: Wave Propagation Test Problem

We use a two dimensional wave propagation test problem, which was discussed by LeVeque [26] and Hubbard & Garcia-Navarro [18], for the 2D shallow water equations to illustrate the accuracy of the numerical schemes discussed in this chapter. For this test problem, the riverbed is fixed. The initial conditions consist

of

$$h(x,y,0) = \begin{cases} 1.01 - B(x,y) & \text{if } 0.1 < x < 0.2,\ 0 \leq y \leq 1 \\ 1 - B(x,y) & \text{otherwise} \end{cases},$$
$$u(x,y,0) = 0, \quad v(x,y,0) = 0$$

with bathymetry

$$B(x,y) = 0.5\exp\left(-50\left((x-0.5)^2 + (y-0.5)^2\right)\right),$$

which is illustrated in Figure 4.1. We use a gravitational constant of $g = 1$, which was used by LeVeque [26]. For this test problem, the small disturbance in the river splits into two waves which propagate in opposite directions. One of the waves propagates over the hemisphere that is present in the riverbed. This can cause difficulties in obtaining an accurate numerical approximation, depending on how the source term is approximated.

4.2 Conservative Numerical Schemes in 2D

For 2D systems, there are numerous techniques that can be used to approximate the system (4.1). In this thesis, we consider two techniques: a basic finite difference scheme and dimensional splitting. Both approaches are discretised on a cartesian mesh, see Figure 4.2, where Δx and Δy are the spatial step sizes in the x and y direction respectively and $\mathbf{F}^*_{i+\frac{1}{2},j}$ and $\mathbf{G}^*_{i,j+\frac{1}{2}}$ are the numerical flux-function in the x and y direction respectively. As with the 1D case, we non-dimensionalise the variables,

$$x^* = \frac{x}{L}, \quad y^* = \frac{y}{L}, \quad t^* = \frac{t}{T}, \quad h^* = \frac{h}{L}, \quad B^* = \frac{B}{L},$$
$$g^* = \frac{gT^2}{L}, \quad v^* = \frac{vT}{L} \quad \text{and} \quad u^* = \frac{uT}{L},$$

where

$$L = \max_{i,j}(|x_{I,j} - x_{0,j}|, |y_{i,J} - y_{i,0}|) \quad \text{and} \quad T = \sqrt{\frac{L}{g}}$$

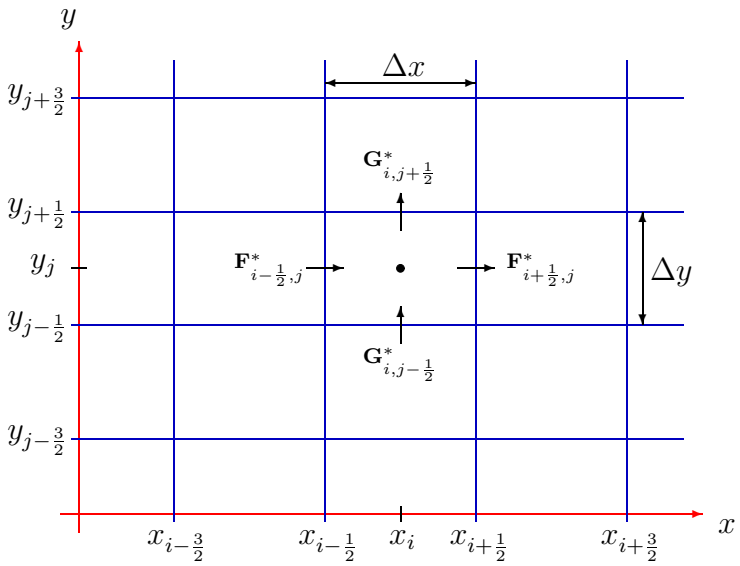

Figure 4.2: The two dimensional mesh.

denote the non-dimensional coefficients and L is the maximum length of the domain. Non-dimensionalising the variables in this way results in the spatial and time step-sizes being less than one, i.e. $\Delta x, \Delta y < 1$ and $\Delta t < 1$, which ensures the error of a numerical scheme does not grow. For all schemes, we use the basic free flow boundary conditions,

$$\mathbf{w}^{n+1}_{-i,j} = \mathbf{w}^n_{0,j}, \quad \mathbf{w}^{n+1}_{I+i,j} = \mathbf{w}^n_{I,j}, \quad \mathbf{w}^{n+1}_{i,-j} = \mathbf{w}^n_{i,0} \quad \text{and} \quad \mathbf{w}^{n+1}_{i,J+j} = \mathbf{w}^n_{i,J},$$

where $i, j = 1$ to 5.

4.2.1 Basic Finite Difference Scheme

The most basic approach for approximating (4.1) is to construct a finite difference scheme of the form

$$\mathbf{w}^{n+1}_{i,j} = \mathbf{w}^n_{i,j} - s_x \left(\mathbf{F}^*_{i+\frac{1}{2},j} - \mathbf{F}^*_{i-\frac{1}{2},j} \right) - s_y \left(\mathbf{G}^*_{i,j+\frac{1}{2}} - \mathbf{G}^*_{i,j-\frac{1}{2}} \right) + \Delta t \mathbf{R}^*_{i,j}, \tag{4.4}$$

where

$$s_x = \frac{\Delta t}{\Delta x}, \quad s_y = \frac{\Delta t}{\Delta y}.$$

The numerical flux-functions $\mathbf{F}^*_{i+\frac{1}{2},j}$ and $\mathbf{G}^*_{i,j+\frac{1}{2}}$ and source term approximation $\mathbf{R}^*_{i,j}$ can be obtained by either discretising the whole system (4.1) or by discretising the system separately in the two coordinate directions. If the system is discretised separately in the two coordinate directions, then any of the one dimensional numerical fluxes discussed in Chapter 2 can be used and the source term approximation is re-written as

$$\Delta t \mathbf{R}^*_{i,j} = s_x \mathbf{f}^*_{i,j} + s_y \mathbf{g}^*_{i,j}, \tag{4.5}$$

where $\mathbf{f}^*_{i,j}$ and $\mathbf{g}^*_{i,j}$ are the source term approximations that contain the x and y direction components only. To ensure the basic finite difference scheme remains stable, we use a variable time step

$$\Delta t = \frac{\nu \min(\Delta x, \Delta y)}{\max_{i,j}(|\lambda^F|, |\lambda^G|)},$$

where λ^F and λ^G are the eigenvalues of the Jacobian matrices $\mathbf{A}$ and $\mathbf{B}$ respectively and ν is the required Courant number. Unless stated, all versions of the basic finite difference scheme discussed in this chapter are stable for $\nu \leq \frac{1}{2}$.

4.2.2 Dimensional Splitting Scheme

Strang [39] derived a dimensional splitting approach that can be used to approximate two dimensional systems of conservation laws (4.1). The approach discretises the system in parts, effectively solving

$$\frac{1}{2}\frac{\partial \mathbf{w}}{\partial t} + \frac{\partial \mathbf{F}(\mathbf{w})}{\partial x} = \mathbf{f} \tag{4.6}$$

and

$$\frac{1}{2}\frac{\partial \mathbf{w}}{\partial t} + \frac{\partial \mathbf{G}(\mathbf{w})}{\partial y} = \mathbf{g} \tag{4.7}$$

by re-writing the source term as (4.2). The most basic form of dimensional splitting is to discretise in two steps, where an approximation of (4.6) is obtained using a half a time step, $\frac{\Delta t}{2}$. The results are then used as the initial conditions for (4.7), which is then approximated using a half a time step to obtain results at the next time level t^{n+1}. Hence, we obtain the first order dimensional splitting scheme,

$$\mathbf{w}_{i,j}^{(1)} = \mathbf{w}_{i,j}^{n} - s_x \left(\mathbf{F}^*_{i+\frac{1}{2},j} - \mathbf{F}^*_{i-\frac{1}{2},j} \right) + s_x \mathbf{f}^*_{i,j} \tag{4.8a}$$

and

$$\mathbf{w}_{i,j}^{n+1} = \mathbf{w}_{i,j}^{(1)} - s_y \left(\mathbf{G}^{(1)}_{i,j+\frac{1}{2}} - \mathbf{G}^{(1)}_{i,j-\frac{1}{2}} \right) + s_y \mathbf{g}^{(1)}_{i,j}, \tag{4.8b}$$

where $\mathbf{F}^*_{i+\frac{1}{2},j}$ and $\mathbf{G}^*_{i,j+\frac{1}{2}}$ can be any of the numerical flux functions discussed in Chapter 2. Unfortunately, the scheme is only first order accurate in time. However, Strang [39] extended the approach to be second order accurate in time by discretising in three steps, where an approximation of (4.6) is obtained using a quarter a time step, $\frac{\Delta t}{4}$. The results are then used as the initial conditions for (4.7), which is then approximated using a half a time step, $\frac{\Delta t}{2}$. These results are then used as the initial conditions for (4.6) using a quarter a time step to obtain results at the next time level t^{n+1}. Hence we obtain a second order accurate dimensional splitting scheme,

$$\mathbf{w}_{i,j}^{(1)} = \mathbf{w}_{i,j}^{n} - \frac{s_x}{2} \left(\mathbf{F}^*_{i+\frac{1}{2},j} - \mathbf{F}^*_{i-\frac{1}{2},j} \right) + \frac{s_x}{2} \mathbf{f}^*_{i,j}, \tag{4.9a}$$

$$\mathbf{w}_{i,j}^{(2)} = \mathbf{w}_{i,j}^{(1)} - s_y \left(\mathbf{G}^{(1)}_{i,j+\frac{1}{2}} - \mathbf{G}^{(1)}_{i,j-\frac{1}{2}} \right) + s_y \mathbf{g}^{(1)}_{i,j} \tag{4.9b}$$

and

$$\mathbf{w}_{i,j}^{n+1} = \mathbf{w}_{i,j}^{(2)} - \frac{s_x}{2} \left(\mathbf{F}^{(2)}_{i+\frac{1}{2},j} - \mathbf{F}^{(2)}_{i-\frac{1}{2},j} \right) + \frac{s_x}{2} \mathbf{f}^{(2)}_{i,j}. \tag{4.9c}$$

One advantage of using dimensional splitting is that the CFL condition of the scheme is less restrictive than the basic finite difference scheme. However, both versions of the dimensional splitting schemes require considerably more computations than the basic finite difference scheme. The first and second order versions of the dimensional splitting scheme require two and three times as many calculations than the basic finite difference approach respectively. To ensure the dimensional splitting scheme

remains stable, we use a variable time step

$$\Delta t = \frac{\nu \min(\Delta x, \Delta y)}{\max_{i,j}(|\lambda^F|, |\lambda^G|)}.$$

Unless stated, all versions of the dimensional splitting scheme discussed in this chapter are stable for $\nu \leq 1$.

4.2.3 2D C-Property

The C-property discussed in Section 2.2.2 can be extended to two dimensions. Consider the 2D shallow water equations for the quiescent flow case,

$$u(x, y, t) \equiv 0, \quad v(x, y, t) \equiv 0 \quad \text{and} \quad h(x, y, t) \equiv D - B \quad \forall (x, y, t).$$

For this stationary case, $\mathbf{w}_t = 0$ thus, the flux functions and source terms balance

$$\mathbf{F}(\mathbf{w})_x + \mathbf{G}(\mathbf{w})_y = \mathbf{R}.$$

In the 1D case, we only needed to balance two terms but here, there are now three terms that need to balance, which can be considerably harder to obtain numerically. However, by re-writing the source term as (4.2) and splitting the equation in two, we obtain

$$\mathbf{F}(\mathbf{w})_x = \mathbf{f} \quad \text{and} \quad \mathbf{G}(\mathbf{w})_y = \mathbf{g}.$$

Here, the fluxes must balance with the source term approximations. To obtain this condition numerically, a scheme must balance the numerical fluxes with the source term approximations,

$$\mathbf{F}^*_{i+\frac{1}{2},j} - \mathbf{F}^*_{i-\frac{1}{2},j} = \mathbf{f}^*_{i,j} \quad \text{and} \quad \mathbf{G}^*_{i,j+\frac{1}{2}} - \mathbf{G}^*_{i,j-\frac{1}{2}} = \mathbf{g}^*_{i,j}.$$

If the source term approximations balance with the numerical fluxes, then the numerical scheme satisfies:

- the approximate C-property, if the numerical scheme is accurate to the order $O(\Delta x^2)$, when applied to the quiescent flow case;
- the exact C-property, if the numerical scheme is exact when applied to the quiescent flow case.

If a numerical scheme does not satisfy the C-property (exact or approximate) then spurious waves may occur in the numerical results, as illustrated in one dimension.

4.3 Lax-Wendroff Scheme in 2D

The classic 2D Lax-Wendroff scheme is a basic finite difference scheme (4.4), where the whole system is discretised, and is derived by using the Taylor's series expansion,

$$\mathbf{w}_{i,j}^{n+1} \approx \mathbf{w}_{i,j}^{n} + \Delta t(\mathbf{w}_t)_{i,j}^{n} + \frac{\Delta t^2}{2}(\mathbf{w}_{tt})_{i,j}^{n} + O(\Delta t^3)$$

to obtain the numerical flux-functions

$$\begin{aligned}\mathbf{F}^{*}_{i+\frac{1}{2},j} = \frac{1}{2}\left(\mathbf{F}^{n}_{i+1,j} + \mathbf{F}^{n}_{i,j}\right) - \frac{s_x}{2}\mathbf{A}^{n}_{i+\frac{1}{2},j}\left(\mathbf{F}^{n}_{i+1,j} - \mathbf{F}^{n}_{i,j}\right) \\ - \frac{s_y}{8}\left(\mathbf{A}^{n}_{i+1,j}\left(\mathbf{G}^{n}_{i+1,j+1} - \mathbf{G}^{n}_{i+1,j-1}\right) + \mathbf{A}^{n}_{i,j}\left(\mathbf{G}^{n}_{i,j+1} - \mathbf{G}^{n}_{i,j-1}\right)\right) \quad (4.10a)\end{aligned}$$

and

$$\begin{aligned}\mathbf{G}^{*}_{i,j+\frac{1}{2}} = \frac{1}{2}\left(\mathbf{G}^{n}_{i,j+1} + \mathbf{G}^{n}_{i,j}\right) - \frac{s_y}{2}\mathbf{B}^{n}_{i,j+\frac{1}{2}}\left(\mathbf{G}^{n}_{i,j+1} - \mathbf{G}^{n}_{i,j}\right) \\ - \frac{s_x}{8}\left(\mathbf{B}^{n}_{i,j+1}\left(\mathbf{F}^{n}_{i+1,j+1} - \mathbf{F}^{n}_{i-1,j+1}\right) + \mathbf{B}^{n}_{i,j}\left(\mathbf{F}^{n}_{i+1,j} - \mathbf{F}^{n}_{i-1,j}\right)\right). \quad (4.10b)\end{aligned}$$

The scheme requires an approximation of the Jacobian matrices, which can be approximated by averaging the neighbouring cells,

$$\mathbf{A}^{n}_{i+\frac{1}{2},j} = \mathbf{A}\left(\frac{\mathbf{w}^{n}_{i+1,j} + \mathbf{w}^{n}_{i,j}}{2}\right) \quad \text{and} \quad \mathbf{B}^{n}_{i,j+\frac{1}{2}} = \mathbf{B}\left(\frac{\mathbf{w}^{n}_{i,j+1} + \mathbf{w}^{n}_{i,j}}{2}\right).$$

For the source term approximation, we use a pointwise approach

$$\mathbf{R}^*_{i,j} = \begin{bmatrix} 0 \\ -\frac{g}{4\Delta x}\left(h^n_{i+1,j} + h^n_{i-1,j}\right)\left(B^n_{i+1,j} - B^n_{i-1,j}\right) \\ -\frac{g}{4\Delta y}\left(h^n_{i,j+1} + h^n_{i,j-1}\right)\left(B^n_{i,j+1} - B^n_{i,j-1}\right) \end{bmatrix} \tag{4.11}$$

but as with the 1D case, this is a crude approximation of the source term since it does not make the scheme satisfy the C-property. The classic 2D Lax-Wendroff is stable for $\nu \leq \frac{1}{\sqrt{2}}$.

Figure 4.3 and Figure 4.4 show the numerical results obtained using the classic 2D Lax-Wendroff scheme (4.10) with the pointwise source term approximation (4.11) at $t = 0.1$ for the 2D Test Problem. The scheme was used with $\Delta x = \Delta y = 0.001$ and $\nu = 0.4$. Here, we can see that even though the test problem has not been run for very long, the scheme has produced very poor numerical results with spurious oscillations present. Even though the water surface is supposed to be smooth away from the disturbances, a hemisphere has appeared on the water surface just above the hemisphere in the riverbed. The poor results obtained are due to the pointwise source term approximation which results in the scheme not satisfying the C-property.

In 1D, we derived a second order accurate source term approximation for the classic 2D Lax-Wendroff scheme, which made the scheme satisfy the C-property. A 2D version of this scheme can be obtained by including the source term in the Taylor series expansion when deriving the classic 2D Lax-Wendroff scheme to obtain

$$\mathbf{R}^* = \Delta t \mathbf{R} + \frac{\Delta t^2}{2}\left(\mathbf{R}_t - (\mathbf{AR})_x - (\mathbf{BR})_y\right).$$

Now, by re-writing the source term using (4.2), we obtain

$$\mathbf{R}^* = \Delta t\left(\mathbf{f} + \mathbf{g}\right) - \frac{\Delta t^2}{2}\left((\mathbf{Af})_x + (\mathbf{Bg})_y\right) - \frac{\Delta t^2}{2}\left((\mathbf{Ag})_x + (\mathbf{Bf})_y\right),$$

where the term $\frac{\Delta t^2}{2}\mathbf{R}_t$ has been omitted for convenience and is discretised separately. Even though this term has been omitted, the source term approximation still ensures the scheme satisfy the C-property. Hence, we obtain a second order accurate source

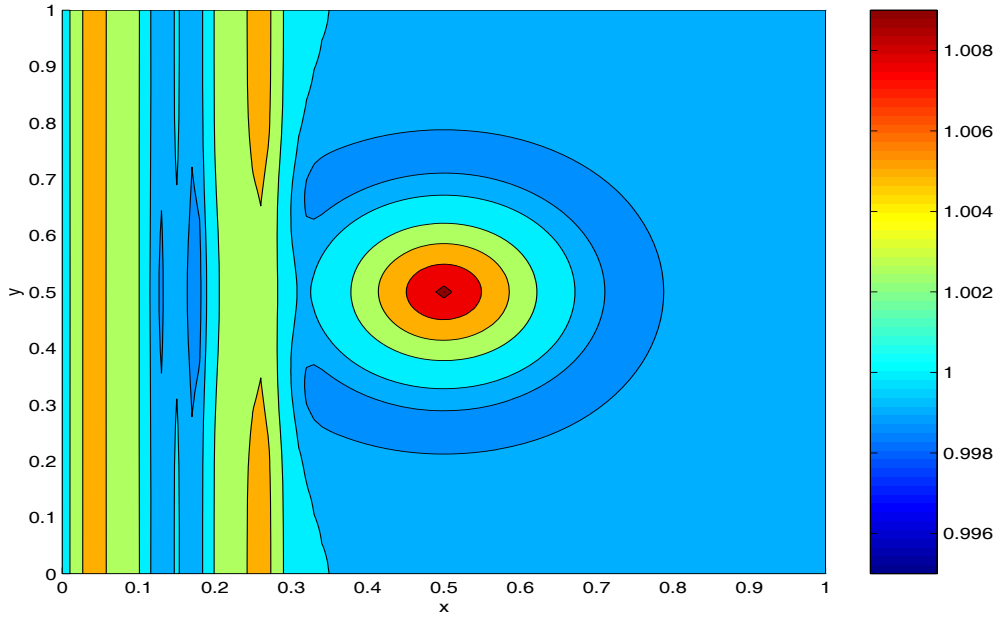

Figure 4.3: Numerical results of the classic 2D Lax-Wendroff scheme at $t = 0.1$ $(h + B)$.

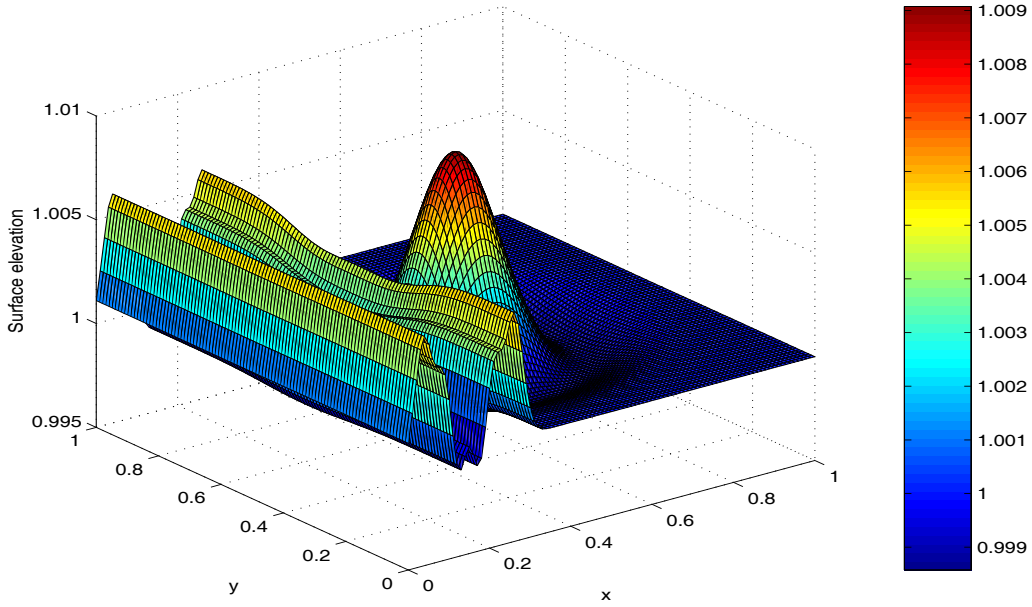

Figure 4.4: Numerical results of the classic 2D Lax-Wendroff scheme at $t = 0.1$ $(h + B)$.

term approximation,

$$\begin{aligned}\mathbf{R}^*_{i,j} = \frac{1}{2\Delta x}\left(\left(\mathbf{I} - s_x\mathbf{A}^n_{i+\frac{1}{2},j}\right)\mathbf{f}^n_{i+\frac{1}{2},j} + \left(\mathbf{I} + s_x\mathbf{A}^n_{i-\frac{1}{2},j}\right)\mathbf{f}^n_{i-\frac{1}{2},j}\right)\\ + \frac{1}{2\Delta y}\left(\left(\mathbf{I} - s_y\mathbf{B}^n_{i,j+\frac{1}{2}}\right)\mathbf{g}^n_{i,j+\frac{1}{2}} + \left(\mathbf{I} + s_y\mathbf{B}^n_{i,j-\frac{1}{2}}\right)\mathbf{g}^n_{i,j-\frac{1}{2}}\right)\\ - \frac{s_x}{2\Delta y}\left((\mathbf{Ag})^n_{i+1,j} - (\mathbf{Ag})^n_{i-1,j}\right) - \frac{s_y}{2\Delta x}\left((\mathbf{Bf})^n_{i,j+1} - (\mathbf{Bf})^n_{i,j-1}\right),\end{aligned}$$

which can be re-written in a more convenient way as

$$\Delta t\mathbf{R}^*_{i,j} = s_x\left(\mathbf{f}^-_{i+\frac{1}{2},j} + \mathbf{f}^+_{i-\frac{1}{2},j}\right) + s_y\left(\mathbf{g}^-_{i,j+\frac{1}{2}} + \mathbf{g}^+_{i,j-\frac{1}{2}}\right), \tag{4.12}$$

where

$$\mathbf{f}^\pm_{i+\frac{1}{2},j} = \frac{1}{2}\left(\mathbf{I} \pm s_x\mathbf{A}^n_{i+\frac{1}{2},j}\right)\mathbf{f}^n_{i+\frac{1}{2},j} \mp \frac{s_y}{2}\left((\mathbf{Ag})^n_{i+1,j} + (\mathbf{Ag})^n_{i,j}\right)$$

and

$$\mathbf{g}^\pm_{i,j+\frac{1}{2}} = \frac{1}{2}\left(\mathbf{I} \pm s_y\mathbf{B}^n_{i,j+\frac{1}{2}}\right)\mathbf{g}^n_{i,j+\frac{1}{2}} \mp \frac{s_x}{2}\left((\mathbf{Bf})^n_{i,j+1} + (\mathbf{Bf})^n_{i,j}\right).$$

For the 2D shallow water equations, we obtain

$$\mathbf{f}^n_{i+\frac{1}{2},j} = \begin{bmatrix} 0 \\ -\frac{g}{2}\left(h^n_{i+1,j} + h^n_{i,j}\right)\left(B^n_{i+1,j} - B^n_{i,j}\right) \\ 0 \end{bmatrix},$$

$$\mathbf{f}^n_{i,j} = \begin{bmatrix} 0 \\ -\frac{g}{2}h^n_{i,j}\left(B^n_{i+1,j} - B^n_{i-1,j}\right) \\ 0 \end{bmatrix},$$

$$\mathbf{g}^n_{i,j+\frac{1}{2}} = \begin{bmatrix} 0 \\ 0 \\ -\frac{g}{2}\left(h^n_{i,j+1} + h^n_{i,j}\right)\left(B^n_{i,j+1} - B^n_{i,j}\right) \end{bmatrix}$$

and

$$\mathbf{g}^n_{i,j} = \begin{bmatrix} 0 \\ 0 \\ -\frac{g}{2}h^n_{i,j}\left(B^n_{i,j+1} - B^n_{i,j-1}\right) \end{bmatrix}.$$

The $\frac{\Delta t^2}{2}\mathbf{R}_t$ term, which was omitted earlier, can be included by using the chain rule $\mathbf{R}_t = \mathbf{R}_{\mathbf{w}}\mathbf{w}_t$. Thus, we obtain a semi-implicit version of the 2D Lax-Wendroff scheme

$$\begin{aligned}\mathbf{w}_{i,j}^{n+1} = \mathbf{w}_{i,j}^{n} &- s_x\left[\mathbf{I} - \frac{\Delta t}{2}\left(\mathbf{R}_{\mathbf{w}}\right)_{i,j}^{n}\right]^{-1}\left(\mathbf{F}^{*}_{i+\frac{1}{2},j} - \mathbf{F}^{*}_{i-\frac{1}{2},j}\right)\\ &- s_y\left[\mathbf{I} - \frac{\Delta t}{2}\left(\mathbf{R}_{\mathbf{w}}\right)_{i,j}^{n}\right]^{-1}\left(\mathbf{G}^{*}_{i,j+\frac{1}{2}} - \mathbf{G}^{*}_{i,j-\frac{1}{2}}\right) + \Delta t\left[\mathbf{I} - \frac{\Delta t}{2}\left(\mathbf{R}_{\mathbf{w}}\right)_{i,j}^{n}\right]^{-1}\mathbf{R}^{*}_{i,j},\end{aligned}$$

where for the 2D shallow water equations

$$\left(\mathbf{R}_{\mathbf{w}}\right)_{i,j}^{n} = \begin{bmatrix} 0 & 0 & 0 \\ -\frac{g}{2\Delta x}\left(B^{n}_{i+1,j} - B^{n}_{i-1,j}\right) & 0 & 0 \\ -\frac{g}{2\Delta y}\left(B^{n}_{i,j+1} - B^{n}_{i,j-1}\right) & 0 & 0 \end{bmatrix}.$$

To illustrate the accuracy of the second order accurate source term approximation, we use the 2D Test Problem. Figure 4.5 and Figure 4.6 show the numerical results obtained using the classic 2D Lax-Wendroff scheme (4.10) with the second order accurate source term approximation (4.12) at $t = 0.7$ for the 2D Test Problem. The scheme was used with $\Delta x = \Delta y = 0.001$ and $\nu = 0.4$. Here, we can see that even though the numerical results are considerably more accurate than using the pointwise source term approximation (4.11), spurious oscillations have started to appear in the numerical results.

4.4 Flux-Limited Lax-Wendroff Scheme in 2D

The Lax-Wendroff scheme suffers from spurious oscillations, which can be minimised by adapting the scheme so that it satisfies the TVD property. Flux-limiter methods are used to obtain a high resolution scheme by constructing numerical flux functions of the form

$$\mathbf{F}^{TVD}_{i+\frac{1}{2},j} = \mathbf{F}^{FO}_{i+\frac{1}{2},j} + \mathbf{\Phi}\left(\mathbf{F}^{SO}_{i+\frac{1}{2},j} - \mathbf{F}^{FO}_{i+\frac{1}{2},j}\right) \quad \text{and} \quad \mathbf{G}^{TVD}_{i,j+\frac{1}{2}} = \mathbf{G}^{FO}_{i,j+\frac{1}{2}} + \mathbf{\Phi}\left(\mathbf{G}^{SO}_{i,j+\frac{1}{2}} - \mathbf{G}^{FO}_{i,j+\frac{1}{2}}\right)$$

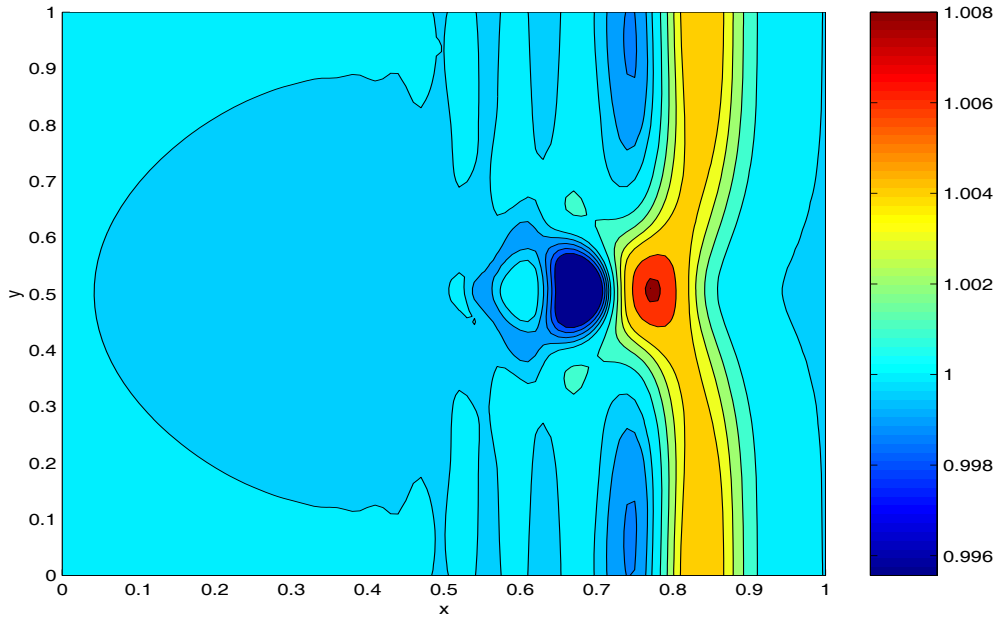

Figure 4.5: Numerical results of the classic 2D Lax-Wendroff scheme with the second order accurate source term approximation at $t = 0.7$ $(h + B)$.

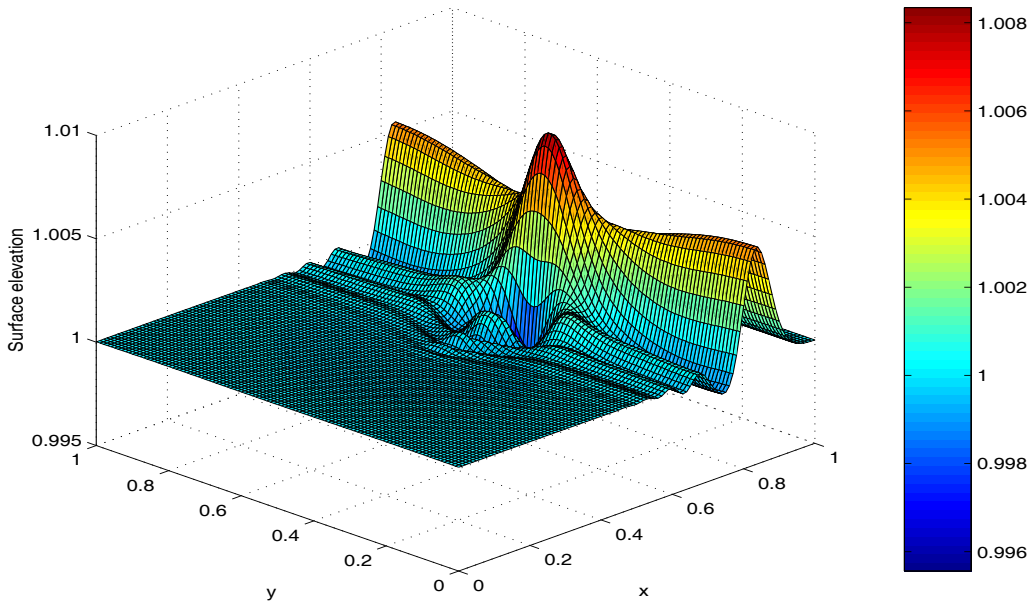

Figure 4.6: Numerical results of the classic 2D Lax-Wendroff scheme with the second order accurate source term approximation at $t = 0.7$ $(h + B)$.

where $\mathbf{F}^{SO}_{i+\frac{1}{2},j}$ and $\mathbf{G}^{SO}_{i,j+\frac{1}{2}}$ are second order numerical fluxes, $\mathbf{F}^{FO}_{i+\frac{1}{2},j}$ and $\mathbf{G}^{FO}_{i,j+\frac{1}{2}}$ are first order numerical fluxes, $\mathbf{\Phi} = \text{diag}(\Phi_k)$ and Φ_k is a flux-limiter. By using the classic Lax-Wendroff numerical flux (4.10) with the first order upwind numerical flux,

$$\mathbf{F}^{*}_{i+\frac{1}{2},j} = \frac{1}{2}\left(\mathbf{F}^{n}_{i+1,j} + \mathbf{F}^{n}_{i,j}\right) - \frac{1}{2}|\mathbf{A}^{n}_{i+\frac{1}{2},j}|\left(\mathbf{w}^{n}_{i+1,j} - \mathbf{w}^{n}_{i,j}\right),$$

we obtain the flux-limited Lax-Wendroff numerical flux

$$\begin{aligned}\mathbf{F}^{*}_{i+\frac{1}{2},j} = {} & \frac{1}{2}\left(\mathbf{F}^{n}_{i+1,j} + \mathbf{F}^{n}_{i,j}\right) - \frac{1}{2}\left(\mathbf{X}|\mathbf{\Lambda}^{F}|\mathbf{L}\mathbf{X}^{-1}\right)^{n}_{i+\frac{1}{2},j}\left(\mathbf{w}^{n}_{i+1,j} - \mathbf{w}^{n}_{i,j}\right) \\ & - \frac{s_y}{8}\mathbf{\Phi}^{n}_{i+\frac{1}{2},j}\left(\mathbf{A}^{n}_{i+1,j}\left(\mathbf{G}^{n}_{i+1,j+1} - \mathbf{G}^{n}_{i+1,j-1}\right) - \mathbf{A}^{n}_{i,j}\left(\mathbf{G}^{n}_{i,j+1} - \mathbf{G}^{n}_{i,j-1}\right)\right), \quad (4.13a)\end{aligned}$$

where $\mathbf{X}$ is a matrix containing the right eigenvectors, $\mathbf{e}^{F}_{k}$, of the Jacobian matrix associated with $\mathbf{F}$, $\mathbf{\Lambda}^{F} = \text{diag}(\lambda^{F}_{k})$ is the diagonal matrix of eigenvalues, λ^{F}_{k}, and

$$\mathbf{L} = \text{diag}\left(1 - \Phi(\theta_k)(1 - s|\lambda^{F}_{k}|)\right).$$

Similarly, for $\mathbf{G}$ we obtain

$$\begin{aligned}\mathbf{G}^{*}_{i,j+\frac{1}{2}} = {} & \frac{1}{2}\left(\mathbf{G}^{n}_{i,j+1} + \mathbf{G}^{n}_{i,j}\right) - \frac{1}{2}\left(\mathbf{Y}|\mathbf{\Lambda}^{G}|\mathbf{L}\mathbf{Y}^{-1}\right)^{n}_{i,j+\frac{1}{2}}\left(\mathbf{w}^{n}_{i,j+1} - \mathbf{w}^{n}_{i,j}\right) \\ & - \frac{s_x}{8}\mathbf{\Phi}^{n}_{i,j+\frac{1}{2}}\left(\mathbf{B}^{n}_{i,j+1}\left(\mathbf{F}^{n}_{i+1,j+1} - \mathbf{F}^{n}_{i-1,j+1}\right) - \mathbf{B}^{n}_{i,j}\left(\mathbf{F}^{n}_{i+1,j} - \mathbf{F}^{n}_{i-1,j}\right)\right), \quad (4.13b)\end{aligned}$$

where $\mathbf{Y}$ is a matrix containing the right eigenvectors, $\mathbf{e}^{G}_{k}$, of the Jacobian matrix associated with $\mathbf{G}$, $\mathbf{\Lambda}^{G} = \text{diag}(\lambda^{G}_{k})$ is the diagonal matrix of eigenvalues, λ^{G}_{k}, and

$$\mathbf{L} = \text{diag}\left(1 - \Phi(\theta_k)(1 - s|\lambda^{G}_{k}|)\right).$$

We require a source term approximation for the numerical scheme that makes the scheme satisfy the C-property and adopt an approach discussed by Hubbard & Garcia-Navarro [18, 19], where the flux functions and source term approximations are balanced so that the numerical scheme satisfies the C-property. As with the 1D case, we construct source term approximations of the form (4.5) where

$$\mathbf{f}^{*}_{i,j} = \mathbf{f}^{TVD}_{i+\frac{1}{2},j} + \mathbf{f}^{TVD}_{i-\frac{1}{2},j}, \quad \mathbf{f}^{TVD}_{i+\frac{1}{2},j} = \mathbf{f}^{FO}_{i+\frac{1}{2},j} + \mathbf{\Phi}^{n}_{i+\frac{1}{2},j}\left(\mathbf{f}^{SO}_{i+\frac{1}{2},j} - \mathbf{f}^{FO}_{i+\frac{1}{2},j}\right),$$

$$\mathbf{g}^*_{i,j} = \mathbf{g}^{TVD}_{i,j+\frac{1}{2}} + \mathbf{g}^{TVD}_{i,j-\frac{1}{2}} \quad \text{and} \quad \mathbf{g}^{TVD}_{i,j+\frac{1}{2}} = \mathbf{g}^{FO}_{i,j+\frac{1}{2}} + \mathbf{\Phi}^n_{i,j+\frac{1}{2}} \left(\mathbf{g}^{SO}_{i,j+\frac{1}{2}} - \mathbf{g}^{FO}_{i,j+\frac{1}{2}} \right),$$

where the superscripts FO and SO denote first and second order accurate source term approximations respectively. In the previous section, we derived a second order accurate source term approximation (4.12) that makes the scheme satisfy the C-property. We use this approximation with the first order approximation of Bermúdez & Vázquez [1] where

$$\mathbf{f}^{FO}_{i\pm\frac{1}{2}} = \frac{1}{2} \left(\left(\mathbf{I} \mp |\mathbf{A}| \mathbf{A}^{-1} \right) \mathbf{f} \right)^n_{i\pm\frac{1}{2},j}$$

to obtain a flux-limited second order approximation of the source term

$$\mathbf{f}^*_{i,j} = \mathbf{f}^-_{i+\frac{1}{2},j} + \mathbf{f}^+_{i-\frac{1}{2},j},$$

where

$$\mathbf{f}^\pm_{i+\frac{1}{2},j} = \frac{1}{2} \left(\mathbf{X} \left(\mathbf{I} \pm \left(\mathbf{\Lambda}^F \right)^{-1} |\mathbf{\Lambda}^F| \mathbf{L} \right) \mathbf{X}^{-1} \mathbf{f} \right)^n_{i+\frac{1}{2},j} \mp \frac{s_y}{2} \mathbf{\Phi}^n_{i+\frac{1}{2},j} \left((\mathbf{Ag})^n_{i+1,j} + (\mathbf{Ag})^n_{i,j} \right).$$

Similarly, for $\mathbf{g}$ we obtain

$$\mathbf{g}^*_{i,j} = \mathbf{g}^-_{i,j+\frac{1}{2}} + \mathbf{g}^+_{i,j-\frac{1}{2}},$$

where

$$\mathbf{g}^\pm_{i,j+\frac{1}{2}} = \frac{1}{2} \left(\mathbf{Y} \left(\mathbf{I} \pm \left(\mathbf{\Lambda}^G \right)^{-1} |\mathbf{\Lambda}^G| \mathbf{L} \right) \mathbf{Y}^{-1} \mathbf{g} \right)^n_{i,j+\frac{1}{2}} \mp \frac{s_x}{2} \mathbf{\Phi}^n_{i,j+\frac{1}{2}} \left((\mathbf{Bf})^n_{i,j+1} + (\mathbf{Bf})^n_{i,j} \right).$$

To illustrate the accuracy of the flux-limited 2D Lax-Wendroff scheme, we use the 2D Test Problem. Figure 4.7 and Figure 4.8 show the numerical results obtained using the flux-limited 2D Lax-Wendroff scheme at $t = 0.7$ for the 2D Test Problem. The scheme is used with spatial step-sizes $\Delta x, \Delta y = 0.01$, $\nu = 0.4$ and the minmod flux-limiter. Here, we can see that the scheme has produced very smooth numerical results, which are in agreement with the results found in Hubbard & Garcia-Navarro [18]. The scheme is considerably more accurate than the classic Lax-Wendroff scheme with either source term approximation.

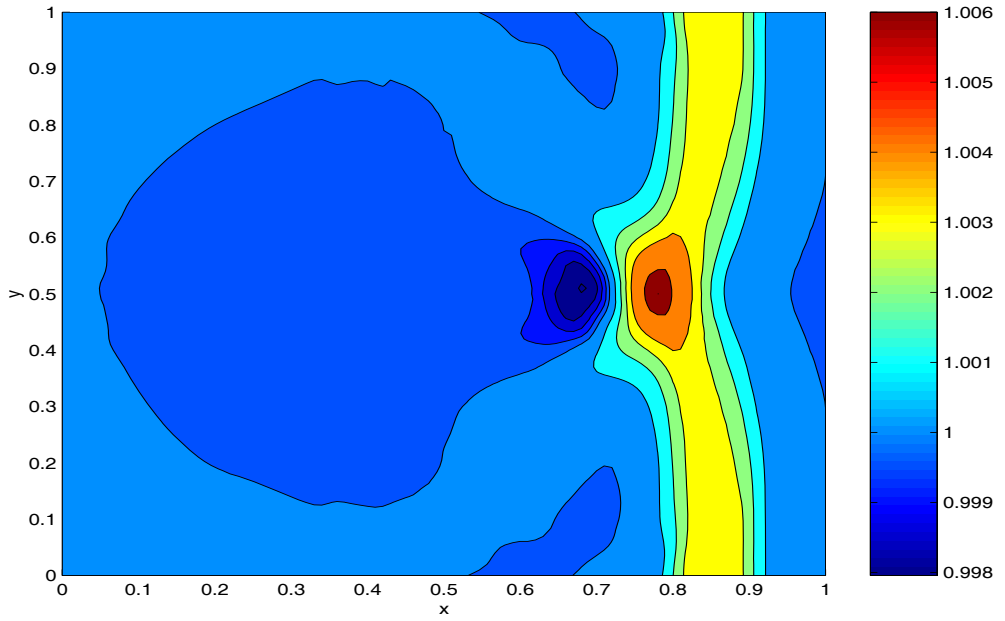

Figure 4.7: Numerical results of the flux-limited 2D Lax-Wendroff scheme at $t = 0.7$ $(h + B)$.

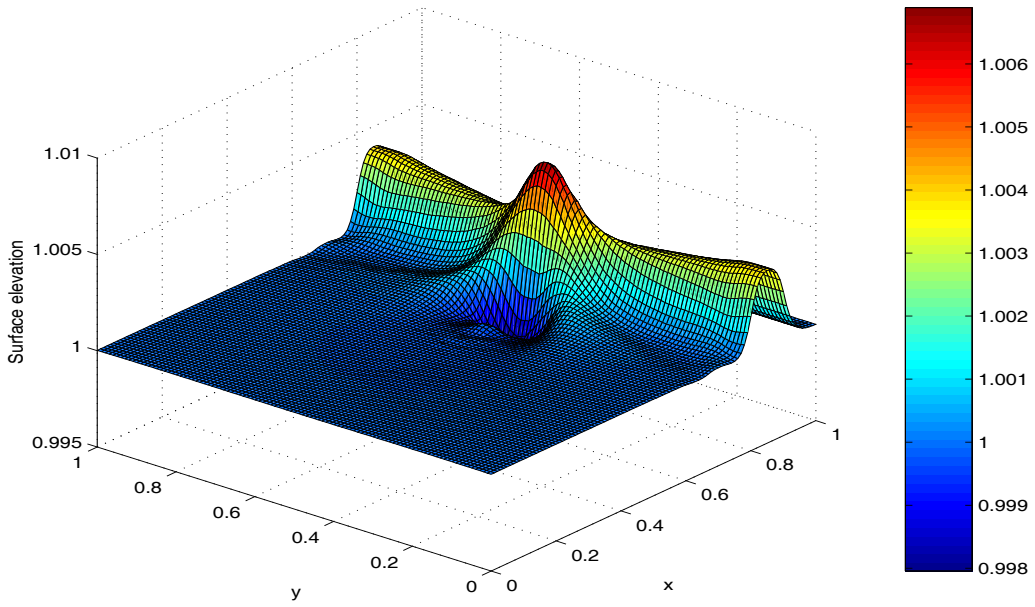

Figure 4.8: Numerical results of the flux-limited 2D Lax-Wendroff scheme at $t = 0.7$ $(h + B)$.

4.5 Roe's Scheme in 2D

In two dimensions, the flux-limited 2D version of Roe's scheme is obtained by discretising the system separately in the two coordinate directions. Hence, we obtain the flux-limited version of Roe's 2D numerical fluxes

$$\mathbf{F}^*_{i+\frac{1}{2},j} = \frac{1}{2}(\mathbf{F}^n_{i+1,j} + \mathbf{F}^n_{i,j}) - \frac{1}{2}\sum_{k=1}^{p}\left[\tilde{\alpha}^F_k|\tilde{\lambda}^F_k|(1-\Phi(\theta^F_k)(1-|\nu^F_k|))\tilde{\mathbf{e}}^F_k\right]_{i+\frac{1}{2},j}, \quad (4.14a)$$

and

$$\mathbf{G}^*_{i,j+\frac{1}{2}} = \frac{1}{2}(\mathbf{G}^n_{i,j+1} + \mathbf{G}^n_{i,j}) - \frac{1}{2}\sum_{k=1}^{p}\left[\tilde{\alpha}^G_k|\tilde{\lambda}^G_k|(1-\Phi(\theta^G_k)(1-|\nu^G_k|))\tilde{\mathbf{e}}^G_k\right]_{i,j+\frac{1}{2}}, \quad (4.14b)$$

where

$$\nu_k = s\tilde{\lambda}_k, \quad \theta^F_k = \frac{(\tilde{\alpha}^F_k)_{I+\frac{1}{2},j}}{(\tilde{\alpha}^F_k)_{i+\frac{1}{2},j}}, \quad I = i - \mathrm{sgn}(\nu^F_k)_{i+\frac{1}{2},j},$$

$$\theta^G_k = \frac{(\tilde{\alpha}^G_k)_{i,J+\frac{1}{2}}}{(\tilde{\alpha}^G_k)_{i,j+\frac{1}{2}}}, \quad J = j - \mathrm{sgn}(\nu^G_k)_{i,j+\frac{1}{2}},$$

and Φ_k can be any of the flux-limiters listed in Table 2.1. The values of $\tilde{\lambda}_k$ and $\tilde{\mathbf{e}}_k$ are the eigenvalues and eigenvectors of the Roe averaged Jacobian matrix, $\tilde{\mathbf{A}}$ or $\tilde{\mathbf{B}}$, and $\tilde{\alpha}_k$ are the wave strengths, which are determined from the decomposition, see Section 2.7 for more details. The superscripts F and G denote if the terms are for Jacobian matrix $\tilde{\mathbf{A}}$ or $\tilde{\mathbf{B}}$, respectively. Glaister [11] determined the following Roe averaged Jacobian matrices for the 2D shallow water equations,

$$\tilde{\mathbf{A}} = \begin{bmatrix} 0 & 1 & 0 \\ \tilde{c}^2 - \tilde{u}^2 & 2\tilde{u} & 0 \\ -\tilde{u}\tilde{v} & \tilde{v} & \tilde{u} \end{bmatrix} \quad \text{and} \quad \tilde{\mathbf{B}} = \begin{bmatrix} 0 & 0 & 1 \\ -\tilde{u}\tilde{v} & \tilde{v} & \tilde{u} \\ \tilde{c}^2 - \tilde{v}^2 & 0 & 2\tilde{v} \end{bmatrix}$$

where $\tilde{c} = \sqrt{g\tilde{h}}$, whose corresponding eigenvalues for $\tilde{\mathbf{A}}$ are

$$\tilde{\lambda}^F_1 = \tilde{u} - \tilde{c}, \quad \tilde{\lambda}^F_2 = \tilde{u} \quad \text{and} \quad \tilde{\lambda}^F_3 = \tilde{u} + \tilde{c},$$

and for $\tilde{\mathbf{B}}$ are

$$\tilde{\lambda}_1^G = \tilde{v} - \tilde{c}, \quad \tilde{\lambda}_2^G = \tilde{v} \quad \text{and} \quad \tilde{\lambda}_3^G = \tilde{v} + \tilde{c}.$$

The eigenvectors are, for $\tilde{\mathbf{A}}$

$$\tilde{\mathbf{e}}_1^F = \begin{bmatrix} 1 \\ \tilde{u} - \tilde{c} \\ \tilde{v} \end{bmatrix}, \quad \tilde{\mathbf{e}}_2^F = \begin{bmatrix} 0 \\ 0 \\ \tilde{c} \end{bmatrix} \quad \text{and} \quad \tilde{\mathbf{e}}_3^F = \begin{bmatrix} 1 \\ \tilde{u} + \tilde{c} \\ \tilde{v} \end{bmatrix},$$

and for $\tilde{\mathbf{B}}$

$$\tilde{\mathbf{e}}_1^G = \begin{bmatrix} 1 \\ \tilde{u} \\ \tilde{v} - \tilde{c} \end{bmatrix}, \quad \tilde{\mathbf{e}}_2^G = \begin{bmatrix} 0 \\ -\tilde{c} \\ 0 \end{bmatrix} \quad \text{and} \quad \tilde{\mathbf{e}}_3^G = \begin{bmatrix} 1 \\ \tilde{u} \\ \tilde{v} + \tilde{c} \end{bmatrix}.$$

The wave strengths are for $\tilde{\mathbf{A}}$

$$\tilde{\alpha}_{1,3}^F = \frac{1}{2}\Delta h \pm \frac{1}{2\tilde{c}}\left(\tilde{u}\Delta h - \Delta(uh)\right) \quad \text{and} \quad \tilde{\alpha}_2^F = \frac{1}{\tilde{c}}\left(\Delta(vh) - \tilde{v}\Delta h\right),$$

where $\Delta\mathbf{w} = \mathbf{w}_{R,j} - \mathbf{w}_{L,j}$, and for $\tilde{\mathbf{B}}$

$$\tilde{\alpha}_{1,3}^G = \frac{1}{2}\Delta h \pm \frac{1}{2\tilde{c}}\left(\tilde{v}\Delta h - \Delta(vh)\right) \quad \text{and} \quad \tilde{\alpha}_2^G = \frac{1}{\tilde{c}}\left(\Delta(uh) - \tilde{u}\Delta h\right),$$

where $\Delta\mathbf{w} = \mathbf{w}_{i,R} - \mathbf{w}_{i,L}$. The Roe averages are

$$\tilde{u} = \frac{\sqrt{h_R}u_R + \sqrt{h_L}u_L}{\sqrt{h_R} + \sqrt{h_L}}, \quad \tilde{v} = \frac{\sqrt{h_R}v_R + \sqrt{h_L}v_L}{\sqrt{h_R} + \sqrt{h_L}} \quad \text{and} \quad \tilde{h} = \frac{1}{2}\left(h_R + h_L\right),$$

where R and L denote the right and left components in either the direction x or y.

For the source term approximation, we also discretise separately (4.2) to obtain

$$\mathbf{f}_{i,j}^* = \mathbf{f}_{i+\frac{1}{2},j}^- + \mathbf{f}_{i-\frac{1}{2},j}^+ \quad \text{and} \quad \mathbf{g}_{i,j}^* = \mathbf{g}_{i,j+\frac{1}{2}}^- + \mathbf{g}_{i,j-\frac{1}{2}}^+, \tag{4.15}$$

where

$$\mathbf{f}_{i+\frac{1}{2},j}^{\pm} = \frac{1}{2}\sum_{k=1}^{p}\left[\tilde{\beta}_k^F\tilde{\mathbf{e}}_k^F(1 \pm \operatorname{sgn}(\tilde{\lambda}_k^F)(1 - \Phi_k(1 - |\nu_k^F|)))\right]_{i+\frac{1}{2},j},$$

$$\mathbf{g}^{\pm}_{i,j+\frac{1}{2}} = \frac{1}{2}\sum_{k=1}^{p}\left[\tilde{\beta}^G_k \tilde{\mathbf{e}}^G_k (1 \pm \text{sgn}(\tilde{\lambda}^G_k)(1 - \Phi_k(1 - |\nu^G_k|)))\right]_{i,j+\frac{1}{2}}$$

and the values of $\tilde{\beta}_k$ are the coefficients of the decomposition of the source terms onto the eigenvectors of the characteristic decomposition, see Section 2.7 for more details. For the 2D shallow water equations we obtain

$$\tilde{\beta}_1 = \frac{\tilde{c}\Delta B}{2}, \quad \tilde{\beta}_2 = 0 \quad \text{and} \quad \tilde{\beta}_3 = -\frac{\tilde{c}\Delta B}{2}$$

for both $\mathbf{F}$ and $\mathbf{G}$. By using this source term approximation, the scheme satisfies the C-property. The flux-limited version of Roe's 2D numerical fluxes (4.14) with source term approximations (4.15) can be used with the basic finite difference scheme (4.4) and the first and second order accurate in time dimensional splitting schemes (4.8) and (4.9) respectively. In this thesis, we denote the flux-limited version of Roe's 2D numerical fluxes with the basic scheme as the B-FLR scheme and the second order dimensional splitting schemes as the DS2-FLR scheme.

To illustrate the accuracy of the basic scheme (B-FLR) and dimensional splitting scheme (DS2-FLR) we use the 2D Test Problem. The schemes are used with $\Delta x, \Delta y = 0.01$, $\nu = 0.4$ and the minmod flux-limiter. Figure 4.9 and Figure 4.10 show the numerical results obtained using the basic scheme (B-FLR) at $t = 0.7$. Here, we can see that the B-FLR scheme has produced numerical results similar to the flux-limited 2D Lax-Wendroff scheme, see Figure 4.7 and Figure 4.8, but the numerical results are slightly more accurate. The results are also similar to those obtained in Hubbard & Garcia-Navarro [18].

Figure 4.11 and Figure 4.12 show the numerical results obtained using the dimensional splitting (DS2-FLR) scheme at $t = 0.7$. Here, we can see that the scheme has produced slightly better numerical results than using the basic finite difference scheme. The results are also similar to those obtained in Hubbard & Garcia-Navarro [18].

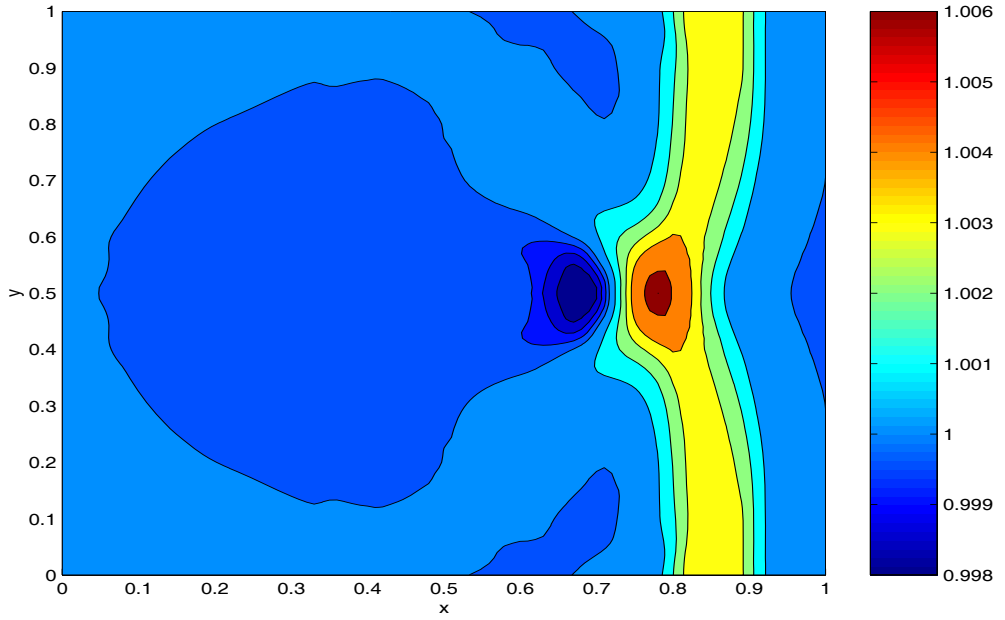

Figure 4.9: Numerical results of the basic scheme (B-FLR) at $t = 0.7$ $(h + B)$.

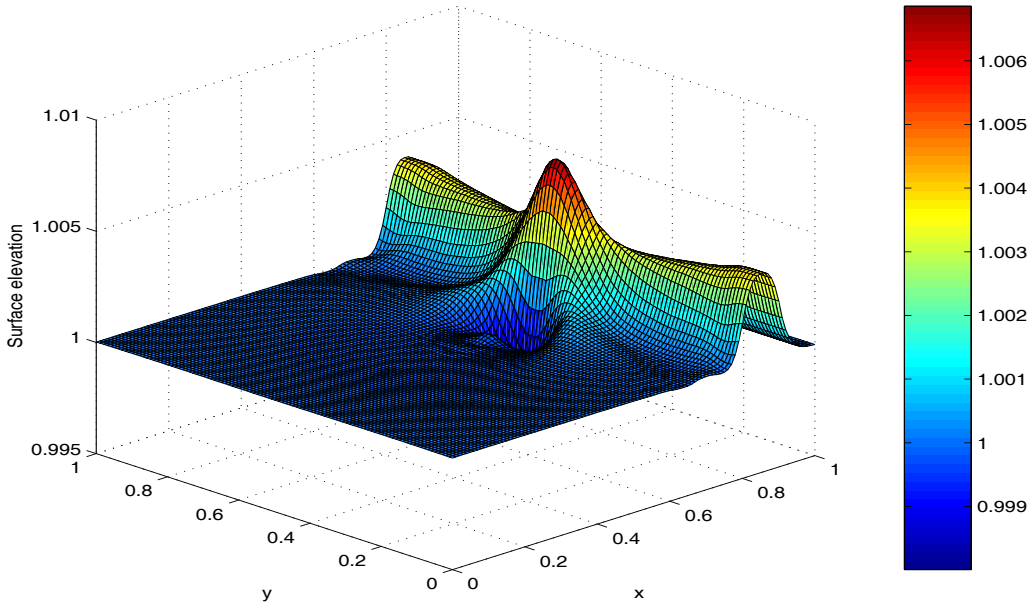

Figure 4.10: Numerical results of the basic scheme (B-FLR) at $t = 0.7$ $(h + B)$.

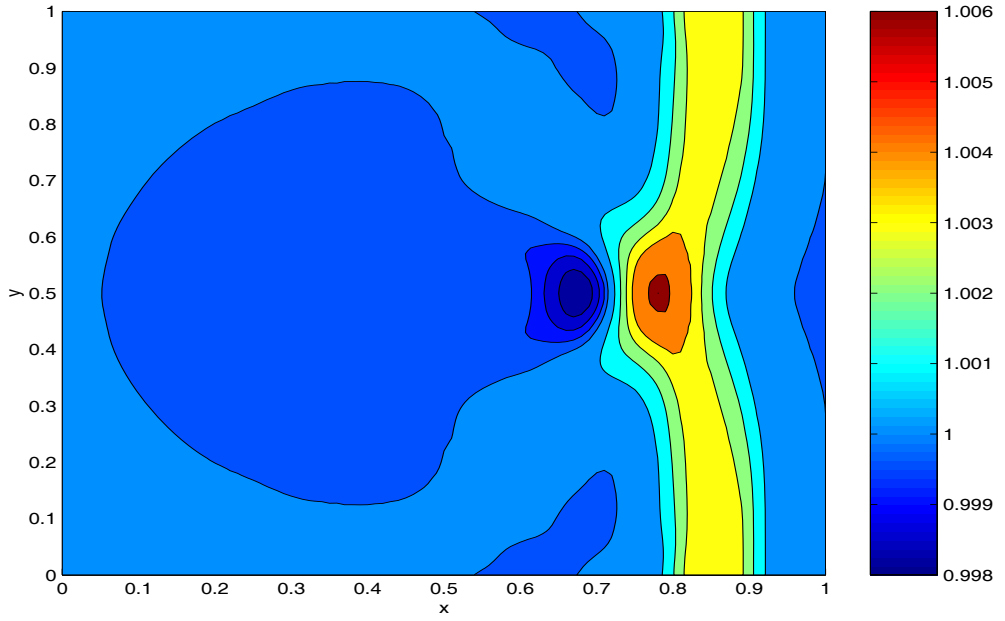

Figure 4.11: Numerical results of the dimensional splitting scheme (DS2-FLR) at $t = 0.7$ $(h + B)$.

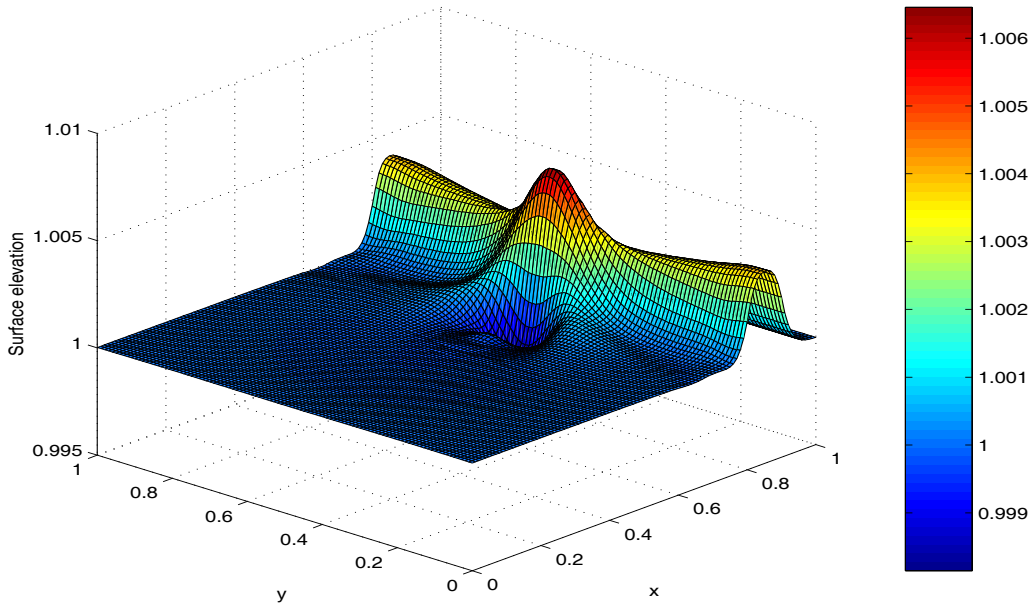

Figure 4.12: Numerical results of the dimensional splitting scheme (DS2-FLR) at $t = 0.7$ $(h + B)$.

4.6 Summary

Throughout this chapter, we have discussed a variety of numerical techniques that can be used to approximate the equations governing sediment transport. We used the 2D shallow water equations to help derive and illustrate the accuracy of the numerical schemes. We showed that the classic 2D Lax-Wendroff scheme suffered badly from spurious oscillations, which were considerably worse when a pointwise source term approximation was used. The second order accurate source term approximation eliminated some of the spurious oscillations and greatly improved the accuracy of the scheme, but spurious oscillations were still present. A flux-limited 2D Lax-Wendroff scheme was derived that was very accurate with no spurious oscillations present in the numerical results. The flux-limited version of Roe's scheme was adapted to two dimensions and the basic finite difference scheme and dimensional splitting schemes were discussed. The numerical results obtained using the flux-limited 2D version of Roe's numerical fluxes were the most accurate with the second order accurate dimensional scheme producing the best set of numerical results.

In the next chapter, we adapt the different formulations discussed in Chapter 3 to two dimensions and use the basic scheme (B-FLR), the second order accurate dimensional splitting scheme (DS2-FLR) and the 2D Lax-Wendroff scheme with pointwise source term approximation to obtain a numerical approximation.

Chapter 5

Numerical Formulations for Approximating the Equations Governing Sediment Transport in Two Dimensions

In the previous chapter we discussed a variety of schemes that can be used to approximate systems of conservation laws in two dimensions. In this chapter, we discuss how to approximate accurately the equations governing sediment transport in two dimensions, which comprise of the equation for conservation of mass,

$$\frac{\partial h}{\partial t} + \frac{\partial (uh)}{\partial x} + \frac{\partial (vh)}{\partial y} = 0, \tag{5.1}$$

the equation for conservation of momentum in the x-direction,

$$\frac{\partial (uh)}{\partial t} + \frac{\partial \left(hu^2 + \frac{1}{2}gh^2\right)}{\partial x} + \frac{\partial (huv)}{\partial y} = -ghB_x, \tag{5.2}$$

the equation for conservation of momentum in the y-direction,

$$\frac{\partial(vh)}{\partial t} + \frac{\partial\left(huv\right)}{\partial x} + \frac{\partial\left(hv^2 + \frac{1}{2}gh^2\right)}{\partial y} = -ghB_y \tag{5.3}$$

and the bed-updating equation,

$$\frac{\partial B}{\partial t} + \xi\frac{\partial(q_1)}{\partial x} + \xi\frac{\partial(q_2)}{\partial y} = 0, \tag{5.4}$$

where $\xi = \frac{1}{1-\epsilon}$ and ϵ is the porosity of the riverbed. Here $h(x, y, t)$ denotes the height of the water above the bottom of the channel, $B(x, y, t)$ denotes the height of the riverbed, $u(x, y, t)$ and $v(x, y, t)$ are the velocities in the x and y direction respectively and $q_1(u, v, h)$ and $q_2(u, v, h)$ are the total (suspended and bedload) volumetric sediment transport rates in the x and y direction respectively. The sediment transport fluxes are not direct functions of B and are more complex in two dimensions.

In Chapter 3, the steady and unsteady approaches were discussed and used to derived five different formulations. Here, we extend the two most accurate formulations to two dimensions. To obtain an approximation of the different formulations some of the different schemes discussed in Chapter 4 are adapted. In this chapter, the classic 2D Lax-Wendroff scheme (4.10) and the basic (B-FLR) and dimensional splitting (DS2-FLR) schemes, which both use the flux-limited 2D version of Roe's numerical flux (4.14), are adapted. A 2D Channel Test Problem is then used to illustrate the accuracy of the two formulations and the different numerical schemes.

5.1 Different Formulations

In Chapter 3, we derived five different formulations that can be used to approximate the equations governing sediment transport in one dimension. In this section, we extend some of the formulations to two dimensions:

- Formulation A-CV will be extended to 2D even though the numerical results sometimes differed from the other formulations in 1D. This is the formulation currently used in industry and is based on the steady approach, where the bed is assumed to have a negligible effect on the water flow.

- Formulation A-NC produced poor numerical results for some of the test problems in 1D and therefore will not be extended to 2D.

- Formulation A-SF produced poor numerical results with spurious oscillations present for all schemes in 1D and will not be extended to 2D.

- Formulation B cannot be extended to 2D since the equation for conservation of momentum in the x direction (5.2) can be re-written in non-conservative variable form as
$$u_t + \left[\frac{1}{2}u^2 + g(h+B)\right]_x + vu_y = 0,$$
but cannot be written in conservative form due to the vu_y term. This is also the case with the equation for conservation of momentum in the y direction.

- Formulation C will be extended to 2D and was one of the most accurate formulations in 1D. This formulation is based on the unsteady approach, where the water flow and bed update are discretised simultaneously.

Thus, Formulation A-CV, which is a steady approach, and Formulation C, which is an unsteady approach, will be extended to two dimensions. The two dimensional sediment transport fluxes must first be derived for the formulations.

5.1.1 Sediment Transport in 2D

In two dimensions, the sediment transport flux is treated as a vector, it's components being given by
$$q_1(u,v,h) = \frac{u|\mathbf{q}|}{|\mathbf{U}|} \quad \text{and} \quad q_2(u,v,h) = \frac{v|\mathbf{q}|}{|\mathbf{U}|},$$

where the magnitude of the velocity is

$$|\mathbf{U}| = \sqrt{u^2 + v^2}$$

and $|\mathbf{q}|$ is the magnitude of the sediment transport flux, which is determined from any of the one dimensional sediment transport fluxes discussed in Section 1.4. For example, if the sediment transport flux (3.3) is used in two dimensions then

$$|\mathbf{q}| = A|\mathbf{U}|^m = A\left(u^2 + v^2\right)^{\frac{m}{2}}. \tag{5.5}$$

Hence, we obtain the sediment transport fluxes in the x and y direction

$$q_1(u,v) = Au\left(u^2 + v^2\right)^{\frac{1}{2}(m-1)} \quad \text{and} \quad q_2(u,v) = Av\left(u^2 + v^2\right)^{\frac{1}{2}(m-1)} \tag{5.6}$$

respectively. Notice that in 2D, the sediment transport fluxes have become more complicated, which leads to even more difficulties in obtaining an accurate numerical approximation. In this thesis, all formulations discussed in 2D will be based on the sediment transport fluxes (5.6) with $m = 3$,

$$q_1(u,v) = Au(u^2 + v^2) \quad \text{and} \quad q_2(u,v) = Av(u^2 + v^2). \tag{5.7}$$

5.1.2 Formulation A

Even though the numerical results obtained from Formulation A-CV differed from the other formulations for certain test problems in 1D, we extend the formulation to 2D as this is the approach currently used in industry. Formulation A is based on the steady approach, which assumes that the bed has a negligible effect on the water flow and decouples the system. This formulation was pioneered by Cunge *et al.* [3] and consists of

- a "fixed-bottom step", where the 2D shallow water equations,

$$\begin{bmatrix} h \\ uh \\ vh \end{bmatrix}_t + \begin{bmatrix} uh \\ hu^2 + \frac{1}{2}gh^2 \\ huv \end{bmatrix}_x + \begin{bmatrix} vh \\ huv \\ hv^2 + \frac{1}{2}gh^2 \end{bmatrix}_y = \begin{bmatrix} 0 \\ -ghB_x \\ -ghB_y \end{bmatrix},$$

  are iterated to an equilibrium state whilst keeping the riverbed fixed.

- a "changing bottom step", where the riverbed is updated whilst keeping all other variables fixes.

The 2D shallow water equations are iterated to an equilibrium state each time the bed is updated and the overall time step is the morphological time step of the bed-updating equation. Numerically, an equilibrium state in two dimensions is obtained when

$$|\mathbf{w}_{i,j}^{n+1} - \mathbf{w}_{i,j}^{n}| \leq \text{tol} \quad \forall (i,j).$$

In two dimensions, this condition is hard to obtain, especially for low tolerance levels as there are a considerable amount of points to satisfy. Thus, the numerical schemes have a cut off time, where if the tolerance level hasn't been obtained but the water surface is calm, the water flow is assumed to have reached an equilibrium state. This cut off time varies considerably depending on which test problem is used.

For Formulation A, the Jacobian matrices of the 2D shallow water equations will be required and are discussed in Chapter 4. An approximation of the wave speeds of the bed-updating equation are required,

$$\lambda^F = \xi \left[\frac{\partial(q_1)}{\partial B} \right] \quad \text{and} \quad \lambda^G = \xi \left[\frac{\partial(q_2)}{\partial B} \right],$$

which can be difficult to obtain. In this thesis, we extend the analytical approach, which was discussed in Section 3.4, to two dimensions. The analytical approach assumes that the discharge and the surface elevation are constant, i.e.

$$h(x,y,t) = D - B(x,y,t), \quad u(x,y,t) = \frac{Q_u}{h(x,y,t)} \quad \text{and} \quad v(x,y,t) = \frac{Q_v}{h(x,y,t)},$$

and then re-writes the velocities in terms of B,

$$u(x,y,t) = Q_u(D-B)^{-1} \quad \text{and} \quad v(x,y,t) = Q_v(D-B)^{-1},$$

so that the sediment transport fluxes can be re-written in terms of B. For example, consider the sediment transport fluxes (5.6) which can now be re-written in terms of B,

$$q_1(u,v) = Au(u^2+v^2)^{\frac{1}{2}(m-1)} = AQ_u\left(Q_u^2+Q_v^2\right)^{\frac{1}{2}(m-1)}(D-B)^{-m}$$

and

$$q_2(u,v) = Av(u^2+v^2)^{\frac{1}{2}(m-1)} = AQ_v\left(Q_u^2+Q_v^2\right)^{\frac{1}{2}(m-1)}(D-B)^{-m},$$

and by differentiating with respect to B, we obtain analytical approximations of the wave speeds,

$$\lambda^F = \frac{A\xi mu}{h}\left(u^2+v^2\right)^{\frac{1}{2}(m-1)} \quad \text{and} \quad \lambda^G = \frac{A\xi mv}{h}\left(u^2+v^2\right)^{\frac{1}{2}(m-1)}. \tag{5.8}$$

5.1.3 Formulation C

A two dimensional version of Formulation C, which is an unsteady approach, can be obtained by re-writing the equations for conservation of momentum in the x and y directions as

$$(uh)_t + \left[hu^2 + \frac{1}{2}gh^2 + ghB\right]_x + (huv)_y = gBh_x \tag{5.9}$$

and

$$(vh)_t + (huv)_x + \left[hv^2 + \frac{1}{2}gh^2 + ghB\right]_y = gBh_y \tag{5.10}$$

respectively by using the chain rule. Now, combining (5.1), (5.9), (5.10) and (5.4) into system form, we obtain

$$\begin{bmatrix} h \\ uh \\ vh \\ B \end{bmatrix}_t + \begin{bmatrix} uh \\ hu^2 + \frac{1}{2}gh^2 + ghB \\ huv \\ \xi q_1 \end{bmatrix}_x + \begin{bmatrix} vh \\ huv \\ hv^2 + \frac{1}{2}gh^2 + ghB \\ \xi q_2 \end{bmatrix}_y = \begin{bmatrix} 0 \\ gBh_x \\ gBh_y \\ 0 \end{bmatrix}. \tag{5.11}$$

If the sediment transport fluxes (5.7) are used with Formulation C, then the Jacobian matrix of $\mathbf{F}$ is

$$\mathbf{A} = \frac{\partial \mathbf{F}}{\partial \mathbf{w}} = \begin{bmatrix} 0 & 1 & 0 & 0 \\ g(h+B) - u^2 & 2u & 0 & gh \\ -uv & v & u & 0 \\ -ud - ve & d & e & 0 \end{bmatrix},$$

where $d = \frac{A\xi}{h}\left(3u^2 + v^2\right)$ and $e = \frac{2A\xi uv}{h}$. One of the eigenvalues of the Jacobian is $\lambda_4^F = u$ and the other three are obtained by solving the cubic

$$P(\lambda, \mathbf{w}) = \lambda^3 - 2u\lambda^2 + \left[u^2 - g(h + B + hd)\right]\lambda + ghud = 0.$$

In Section 3.1.3, we proved that the roots of this polynomial are always real and unequal and deduced that we can use (3.7) to determine the values of the roots. Once the roots of $P(\lambda, \mathbf{w})$ have been obtained, they are used to determine the eigenvectors,

$$\mathbf{e}_k^F = \begin{bmatrix} 1 \\ \lambda_k \\ v \\ \dfrac{u^2 - g(h+B) + (\lambda_k - 2u)\lambda_k}{gh} \end{bmatrix},$$

for $k = 1, 2, 3$ where $a \neq k \neq b$ and if $e \neq 0$ then

$$\mathbf{e}_4^F = \begin{bmatrix} 1 \\ u \\ v - \dfrac{u}{he}(h+B) \\ -\dfrac{1}{h}(h+B) \end{bmatrix} \quad \text{otherwise} \quad \mathbf{e}_4^F = \begin{bmatrix} 0 \\ 0 \\ 1 \\ 0 \end{bmatrix}.$$

Similarly, for $\mathbf{G}$ the Jacobian matrix is

$$\mathbf{B} = \frac{\partial \mathbf{G}}{\partial \mathbf{w}} = \begin{bmatrix} 0 & 0 & 1 & 0 \\ -uv & v & u & 0 \\ g(h+B) - v^2 & 0 & 2v & gh \\ -vd - ue & e & d & 0 \end{bmatrix},$$

where $d = \frac{A\xi}{h}\left(3v^2 + u^2\right)$ and $e = \frac{2A\xi uv}{h}$. One of the eigenvalues of the Jacobian is $\lambda_4^G = v$ and the other three are obtained by solving the cubic

$$P(\lambda, \mathbf{w}) = \lambda^3 - 2v\lambda^2 + \left[v^2 - g(h + B + hd)\right]\lambda + ghud = 0.$$

Once the roots of $P(\lambda, \mathbf{w})$ have been obtained, they are used to determine the eigenvectors,

$$\mathbf{e}_k^G = \begin{bmatrix} 1 \\ u \\ \lambda_k \\ \dfrac{v^2 - g(h+B) + (\lambda_k - 2v)\lambda_k}{gh} \end{bmatrix},$$

for $k = 1, 2, 3$ where $a \neq k \neq b$ and if $e \neq 0$ then

$$\mathbf{e}_4^G = \begin{bmatrix} 1 \\ u - \dfrac{v}{he}(h+B) \\ v \\ -\dfrac{1}{h}(h+B) \end{bmatrix} \quad \text{otherwise} \quad \mathbf{e}_4^G = \begin{bmatrix} 0 \\ 1 \\ 0 \\ 0 \end{bmatrix}.$$

Now that we have discussed Formulations A and C, in the next section we adapt the classic 2D Lax-Wendroff scheme and the 2D variations of the flux-limited version of Roe's scheme.

5.2 Adaptation of the Classic 2D Lax-Wendroff Scheme

The classic 2D Lax-Wendroff scheme has numerical flux functions (4.10) and the source term is approximated using a pointwise approach,

$$\mathbf{R}^*_{i,j} = \mathbf{R}(\mathbf{w}^n_{i,j}),$$

and is commonly used in industry to approximate the equations governing sediment transport in two dimensions. As with the 1D case, the classic 2D Lax-Wendroff scheme suffers badly from spurious oscillations occurring in the numerical results. The pointwise source term approximation results in the scheme not satisfying the C-property.

5.2.1 Formulation A

Formulation A is a steady approach, where the system is decoupled into a water flow approximation followed by a bed update. The classic 2D Lax-Wendroff scheme can be adapted for this formulation. In the previous chapter, the 2D shallow water equations were approximated using the classic 2D Lax-Wendroff scheme, see Section 4.3 for details. However, the scheme needs to be adapted to approximate the bed-updating equation (5.4), which is easily obtained

$$B^{n+1}_{i,j} = B^n_{i,j} - \xi s_x \left((q_1)^*_{i+\frac{1}{2},j} - (q_1)^*_{i-\frac{1}{2},j} \right) - \xi s_y \left((q_2)^*_{i,j+\frac{1}{2}} - (q_2)^*_{i,j-\frac{1}{2}} \right), \qquad (5.12)$$

where the numerical fluxes are

$$(q_1)^*_{i+\frac{1}{2},j} = \frac{1}{2}\left((q_1)^n_{i+1,j} + (q_1)^n_{i,j}\right) - \frac{s_x}{2}\lambda^F_{i+\frac{1}{2},j}\left((q_1)^n_{i+1,j} - (q_1)^n_{i,j}\right) - \frac{s_y}{8}\left(\lambda^F_{i+1,j}\left((q_2)^n_{i+1,j+1} - (q_2)^n_{i+1,j-1}\right) + \lambda^F_{i,j}\left((q_2)^n_{i,j+1} - (q_2)^n_{i,j-1}\right)\right)$$

and

$$(q_2)^*_{i,j+\frac{1}{2}} = \frac{1}{2}\left((q_2)^n_{i,j+1} + (q_2)^n_{i,j}\right) - \frac{s_y}{2}\lambda^G_{i,j+\frac{1}{2}}\left((q_2)^n_{i,j+1} - (q_2)^n_{i,j}\right) - \frac{s_x}{8}\left(\lambda^G_{i,j+1}\left((q_1)^n_{i+1,j+1} - (q_1)^n_{i-1,j+1}\right) + \lambda^G_{i,j}\left((q_1)^n_{i+1,j} - (q_1)^n_{i-1,j}\right)\right)$$

and where λ^F and λ^G are the analytical approximations of the wave speeds of the bed-updating equation (5.8).

5.2.2 Formulation C

The classic 2D Lax-Wendroff scheme (4.10) can be used as written to approximate Formulation C. The Jacobian matrices of the formulation are given in Section 5.1.3 and the source term is approximated with a pointwise approach,

$$\mathbf{R}^*_{i,j} = \begin{bmatrix} 0 \\ \frac{g}{4\Delta x}\left(B^n_{i+1,j} + B^n_{i-1,j}\right)\left(h^n_{i+1,j} - h^n_{i-1,j}\right) \\ \frac{g}{4\Delta y}\left(B^n_{i,j+1} + B^n_{i,j-1}\right)\left(h^n_{i,j+1} - h^n_{i,j-1}\right) \\ 0 \end{bmatrix}.$$

5.3 Adaptation of the Basic and Dimensional Splitting Schemes

Both the basic scheme (B-FLR) and the second order accurate dimensional splitting scheme (DS2-FLR), which both used the flux-limited 2D version of Roe's numerical

fluxes (4.14), produced very accurate numerical results in the previous chapter. This is mainly due to both schemes using the source term approximation (4.15), which results in both schemes satisfying the C-property. Thus, in this section, we adapt both numerical schemes to approximate Formulations A and C.

5.3.1 Formulation A

Formulation A is a steady approach, where the system is decoupled into a water flow approximation followed by a bed update. The flux-limited 2D version of Roe's scheme can be adapted for this formulation. In the previous chapter, the 2D shallow water equations were approximated using both the basic scheme (B-FLR) and dimensional splitting scheme (DS2-FLR), see Section 4.5 for details. However, the schemes needs to be adapted to approximate the bed-updating equation (5.4). Thus, we obtain the following numerical fluxes for the bed-updating equation,

$$(q_1)^*_{i+\frac{1}{2},j} = \frac{\xi}{2}\left((q_1)^n_{i+1,j} + (q_1)^n_{i,j}\right) - \frac{1}{2}\left|\lambda^F_{i+\frac{1}{2},j}\right|\left(1 - \Phi\left(\theta^F_{i+\frac{1}{2},j}\right)\left(1 - \left|\nu^F_{i+\frac{1}{2},j}\right|\right)\right)\left(B^n_{i+1,j} - B^n_{i,j}\right) \quad (5.13a)$$

and

$$(q_2)^*_{i,j+\frac{1}{2}} = \frac{\xi}{2}\left((q_2)^n_{i,j+1} + (q_2)^n_{i,j}\right) - \frac{1}{2}\left|\lambda^G_{i,j+\frac{1}{2}}\right|\left(1 - \Phi\left(\theta^G_{i,j+\frac{1}{2}}\right)\left(1 - \left|\nu^G_{i,j+\frac{1}{2}}\right|\right)\right)\left(B^n_{i,j+1} - B^n_{i,j}\right), \quad (5.13b)$$

where

$$\nu^F_{i+\frac{1}{2},j} = s_x\lambda^F_{i+\frac{1}{2},j}, \quad \nu^G_{i,j+\frac{1}{2}} = s_y\lambda^G_{i,j+\frac{1}{2}}, \quad \theta^F_{i+\frac{1}{2},j} = \frac{B^n_{I+1,j} - B^n_{I,j}}{B^n_{i+1,j} - B^n_{i,j}},$$

$$\theta^G_{i,j+\frac{1}{2}} = \frac{B^n_{i,J+1} - B^n_{i,J}}{B^n_{i,j+1} - B^n_{i,j}}, \quad I = i - \operatorname{sgn}\left(\nu^F_{i+\frac{1}{2},j}\right), \quad J = j - \operatorname{sgn}\left(\nu^G_{i,j+\frac{1}{2}}\right)$$

and Φ can be any of the flux-limiters listed in Table 2.1. Here, λ^F and λ^G are the analytical approximations of the wave speeds of the bed-updating equation (5.8). The numerical fluxes of the bed-updated equation (5.13) can be used with both

the basic finite difference scheme (4.4) and the dimensional splitting schemes (4.8) and (4.9). In this thesis, if the basic scheme (B-FLR) or the dimensional splitting scheme (DS2-FLR) are used then the numerical fluxes (5.13) are used with (4.4) or (4.9) respectively.

5.3.2 Formulation C

Formulation C can be used as written with both the basic scheme (B-FLR) and the dimensional splitting scheme (DS2-FLR). Both versions require the Roe averages of the system. For the sediment transport fluxes (5.7), the Roe averaged Jacobian matrix for $\mathbf{F}$ is

$$\tilde{\mathbf{A}} = \begin{bmatrix} 0 & 1 & 0 & 0 \\ g(\tilde{h}+\tilde{B}) - \tilde{u}^2 & 2\tilde{u} & 0 & g\tilde{h} \\ -\tilde{u}\tilde{v} & \tilde{v} & \tilde{u} & 0 \\ -\tilde{u}\tilde{d} - \tilde{v}\tilde{e} & \tilde{d} & \tilde{e} & 0 \end{bmatrix}.$$

One of the eigenvalues of the Jacobian is $\tilde{\lambda}_4^F = \tilde{u}$ and the other three are obtained by solving the cubic

$$\tilde{P}(\tilde{\lambda}) = \tilde{\lambda}^3 - 2\tilde{u}\tilde{\lambda}^2 + \left[\tilde{u}^2 - g(\tilde{h}+\tilde{B}+\tilde{h}\tilde{d})\right]\tilde{\lambda} + g\tilde{h}\tilde{u}\tilde{d} = 0.$$

The roots of $\tilde{P}(\tilde{\lambda})$ are determined by using the approach discussed in Section 3.1.3. Once the Roe averaged eigenvalues have been obtained, they are used to determine the eigenvectors,

$$\tilde{\mathbf{e}}_k^F = \begin{bmatrix} 1 \\ \tilde{\lambda}_k \\ \tilde{v} \\ \dfrac{\tilde{u}^2 - g(\tilde{h}+\tilde{B}) + (\tilde{\lambda}_k - 2\tilde{u})\tilde{\lambda}_k}{g\tilde{h}} \end{bmatrix},$$

for $k = 1, 2, 3$ where $a \neq k \neq b$ and if $e \neq 0$ then

$$\tilde{\mathbf{e}}_4^F = \begin{bmatrix} 1 \\ \tilde{u} \\ \tilde{f} \\ -\frac{1}{\tilde{h}}(\tilde{h} + \tilde{B}) \end{bmatrix} \quad \text{otherwise} \quad \tilde{\mathbf{e}}_4^F = \begin{bmatrix} 0 \\ 0 \\ 1 \\ 0 \end{bmatrix},$$

where $\tilde{f} = \tilde{v} - \dfrac{\tilde{u}}{\tilde{h}\tilde{e}}\left(\tilde{h} + \tilde{B}\right)$. The wave strengths are

- if $\tilde{e} \neq 0$ then

$$\tilde{\alpha}_k = \frac{\psi_k}{(\tilde{f} - \tilde{v})(\tilde{\lambda}_k - \tilde{\lambda}_a)(\tilde{\lambda}_k - \tilde{\lambda}_b)},$$

  where

$$\begin{aligned} \psi_k = &\left[(2\tilde{u} - \tilde{\lambda}_a - \tilde{\lambda}_b)\tilde{u}\tilde{v} - (\tilde{h} + \tilde{B})g\tilde{v} + (\tilde{\lambda}_a\tilde{\lambda}_b + g(\tilde{h} + \tilde{B}) - \tilde{u}^2)\tilde{f}\right]\Delta h \\ &+ (\tilde{f} - \tilde{v})\left[g\tilde{h}\Delta B + (2\tilde{u} - \tilde{\lambda}_a - \tilde{\lambda}_b)\Delta(uh)\right] - (\tilde{u} - \tilde{\lambda}_a)(\tilde{u} - \tilde{\lambda}_b)\Delta(vh) \end{aligned}$$

  for $k = 1, 2, 3$, where $a \neq k \neq b$ and

$$\tilde{\alpha}_4 = \frac{\Delta(vh) - \tilde{v}\Delta h}{\tilde{f} - \tilde{v}}$$

- if $\tilde{e} = 0$ then

$$\tilde{\alpha}_k = \frac{(\tilde{\lambda}_a\tilde{\lambda}_b + g(\tilde{h} + \tilde{B}) - \tilde{u}^2)\Delta h + (2\tilde{u} - \tilde{\lambda}_a - \tilde{\lambda}_b)\Delta(uh) + g\tilde{h}\Delta B}{(\tilde{\lambda}_k - \tilde{\lambda}_a)(\tilde{\lambda}_k - \tilde{\lambda}_b)}$$

  for $k = 1, 2, 3$, where $a \neq k \neq b$ and

$$\tilde{\alpha}_4 = \Delta(vh) - \tilde{v}\Delta h.$$

For the source term,

$$\tilde{\beta}_k = \frac{(2\tilde{u} - \tilde{\lambda}_a - \tilde{\lambda}_b)g\tilde{B}\Delta h}{(\tilde{\lambda}_k - \tilde{\lambda}_a)(\tilde{\lambda}_k - \tilde{\lambda}_b)} \quad \text{and} \quad \tilde{\beta}_4 = 0,$$

where $k = 1, 2, 3$ and $a \neq k \neq b$.

Similarly for $\mathbf{G}$, the Roe averaged Jacobian matrix is

$$\tilde{\mathbf{B}} = \begin{bmatrix} 0 & 0 & 1 & 0 \\ -\tilde{u}\tilde{v} & \tilde{v} & \tilde{u} & 0 \\ g(\tilde{h} + \tilde{B}) - \tilde{v}^2 & 0 & 2\tilde{v} & g\tilde{h} \\ -\tilde{v}\tilde{d} - \tilde{u}\tilde{e} & \tilde{e} & \tilde{d} & 0 \end{bmatrix},$$

One of the eigenvalues of the Roe averaged Jacobian is $\tilde{\lambda}_4^G = \tilde{v}$ and the other three are obtained by solving the cubic

$$\tilde{P}(\tilde{\lambda}) = \tilde{\lambda}^3 - 2\tilde{v}\tilde{\lambda}^2 + \left[\tilde{v}^2 - g(\tilde{h} + \tilde{B} + \tilde{h}\tilde{d})\right]\tilde{\lambda} + g\tilde{h}\tilde{v}\tilde{d} = 0.$$

The roots of $\tilde{P}(\tilde{\lambda})$ are determined by using the approach discussed in Section 3.1.3. Once the Roe averaged eigenvalues have been obtained, they are used to determine the eigenvectors,

$$\tilde{\mathbf{e}}_k^G = \begin{bmatrix} 1 \\ \tilde{u} \\ \tilde{\lambda}_k \\ \dfrac{\tilde{v}^2 - g(\tilde{h} + \tilde{B}) + (\tilde{\lambda}_k - 2\tilde{v})\tilde{\lambda}_k}{g\tilde{h}} \end{bmatrix},$$

for $k = 1, 2, 3$ where $a \neq k \neq b$ and if $e \neq 0$ then

$$\tilde{\mathbf{e}}_4^G = \begin{bmatrix} 1 \\ \tilde{f} \\ \tilde{v} \\ -\dfrac{1}{\tilde{h}}(\tilde{h} + \tilde{B}) \end{bmatrix} \quad \text{otherwise} \quad \tilde{\mathbf{e}}_4^G = \begin{bmatrix} 0 \\ 1 \\ 0 \\ 0 \end{bmatrix},$$

where $\tilde{f} = \tilde{u} - \dfrac{\tilde{v}}{\tilde{h}\tilde{e}}\left(\tilde{h} + \tilde{B}\right)$. The wave strengths are

- if $\tilde{e} \neq 0$ then

$$\tilde{\alpha}_k = \frac{\psi_k}{(\tilde{f} - \tilde{u})(\tilde{\lambda}_k - \tilde{\lambda}_a)(\tilde{\lambda}_k - \tilde{\lambda}_b)},$$

where

$$\psi_k = (\tilde{f} - \tilde{u}) \left[g\tilde{h}\Delta B + (2\tilde{v} - \tilde{\lambda}_a - \tilde{\lambda}_b)\Delta(vh) \right] - (\tilde{v} - \tilde{\lambda}_a)(\tilde{v} - \tilde{\lambda}_b)\Delta(uh) + \left[(2\tilde{v} - \tilde{\lambda}_a - \tilde{\lambda}_b)\tilde{v}\tilde{u} - (\tilde{h} + \tilde{B})g\tilde{u} + (\tilde{\lambda}_a\tilde{\lambda}_b + g(\tilde{h} + \tilde{B}) - \tilde{v}^2)\tilde{f} \right] \Delta h$$

for $k = 1, 2, 3$, where $a \neq k \neq b$ and

$$\tilde{\alpha}_4 = \frac{\Delta(uh) - \tilde{u}\Delta h}{\tilde{f} - \tilde{u}}.$$

- if $\tilde{e} = 0$ then

$$\tilde{\alpha}_k = \frac{(\tilde{\lambda}_a\tilde{\lambda}_b + g(\tilde{h} + \tilde{B}) - \tilde{v}^2)\Delta h + (2\tilde{v} - \tilde{\lambda}_a - \tilde{\lambda}_b)\Delta(vh) + g\tilde{h}\Delta B}{(\tilde{\lambda}_k - \tilde{\lambda}_a)(\tilde{\lambda}_k - \tilde{\lambda}_b)}$$

for $k = 1, 2, 3$, where $a \neq k \neq b$ and

$$\tilde{\alpha}_4 = \Delta(uh) - \tilde{u}\Delta h.$$

For the source term,

$$\tilde{\beta}_k = \frac{(2\tilde{v} - \tilde{\lambda}_a - \tilde{\lambda}_b)g\tilde{B}\Delta h}{(\tilde{\lambda}_k - \tilde{\lambda}_a)(\tilde{\lambda}_k - \tilde{\lambda}_b)} \quad \text{and} \quad \tilde{\beta}_4 = 0,$$

where $k = 1, 2, 3$ and $a \neq k \neq b$.

The Roe averaged values are

$$\tilde{v} = \frac{\sqrt{h_R}v_R + \sqrt{h_L}v_L}{\sqrt{h_R} + \sqrt{h_L}}, \quad \tilde{u} = \frac{\sqrt{h_R}u_R + \sqrt{h_L}u_L}{\sqrt{h_R} + \sqrt{h_L}}, \quad \tilde{h} = \frac{1}{2}\left(h_R + h_L\right),$$

$$\tilde{B} = \frac{1}{2}\left(B_R + B_L\right), \quad \tilde{d}^F = \frac{A\xi\left(\sqrt{h_R} + \sqrt{h_L}\right)}{\sqrt{h_L}h_R + \sqrt{h_R}h_L}\left(u_R^2 + u_Ru_L + u_L^2 + \tilde{v}^2\right),$$

$$\tilde{d}^G = \frac{A\xi\left(\sqrt{h_R} + \sqrt{h_L}\right)}{\sqrt{h_L}h_R + \sqrt{h_R}h_L}\left(v_R^2 + v_Rv_L + v_L^2 + \tilde{u}^2\right),$$

$$\tilde{e}^F = \frac{\xi\left[2\sqrt{h_R}\sqrt{h_L}(u_R v_R + u_L v_L) + (h_L u_R + h_R u_L)(v_R + v_L)\right]}{(\sqrt{h_R}h_L + \sqrt{h_L}h_R)(\sqrt{h_R} + \sqrt{h_L})}$$

and

$$\tilde{e}^G = \frac{\xi\left[2\sqrt{h_R}\sqrt{h_L}(v_R u_R + v_L u_L) + (h_L v_R + h_R v_L)(u_R + u_L)\right]}{(\sqrt{h_R}h_L + \sqrt{h_L}h_R)(\sqrt{h_R} + \sqrt{h_L})}.$$

5.4 2D Channel Test Problem: Conical Sand Dune Test Problem

To determine which formulation and scheme is the most accurate, we use a conical sand dune test problem as discussed by Chesher *et al.* [2] and De Vriend [6]. The test problem consists of a channel of length $1000m \times 1000m$ with dummy initial conditions

$$h^*(x, y, 0) = 10 - B(x, y, 0), \quad u^*(x, y, 0) = \frac{Q}{h^*(x, y, 0)}, \quad v^*(x, y, 0) = 0$$

and the initial bathymetry consists of a conical sand dune,

$$B(x, y, 0) = \begin{cases} \sin^2\left(\frac{\pi(x-300)}{200}\right)\sin^2\left(\frac{\pi(y-400)}{200}\right) & \text{if } 300 \leq x \leq 500,\ 400 \leq y \leq 600, \\ 0 & \text{otherwise} \end{cases}$$

and is illustrated in Figure 5.1. The upstream boundary has constant discharge,

$$h^{n+1}_{-i,j} = h^n_{0,j}, \quad (uh)^{n+1}_{-i,j} = Q, \quad (vh)^{n+1}_{-i,j} = (vh)^n_{0,j} \quad \text{and} \quad B^{n+1}_{-i,j} = B^n_{0,j},$$

where Q is a constant and the downstream boundary conditions are

$$\mathbf{w}^{n+1}_{I+i,j} = \mathbf{w}^n_{I,j}, \quad \mathbf{w}^{n+1}_{i,-j} = \mathbf{w}^n_{i,0} \quad \text{and} \quad \mathbf{w}^{n+1}_{i,J+j} = \mathbf{w}^n_{i,J},$$

where $i, j = 1$ to 5. To obtain the initial conditions, the water flow with the dummy initial conditions and boundary conditions are iterated to an equilibrium state whilst

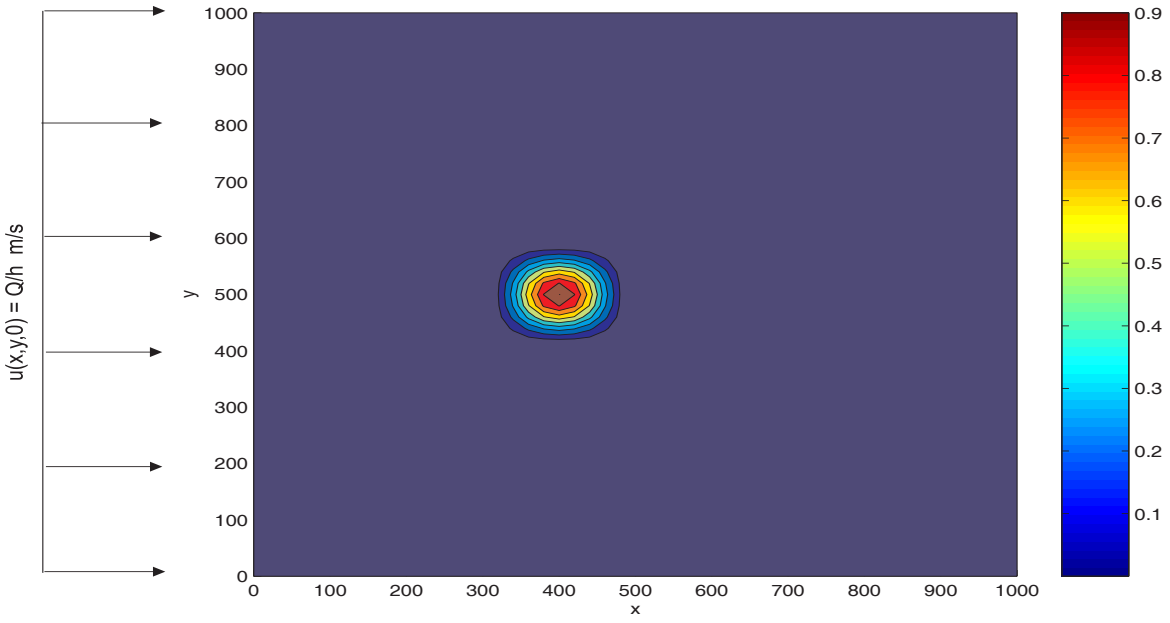

Figure 5.1: Initial conditions for 2D Channel Test Problem A (B).

keeping the bed fixed, where

$$|\mathbf{w}_{i,j}^{n+1} - \mathbf{w}_{i,j}^{n}| \leq \text{tol}$$

and tol is the desired tolerance level. The sediment transport fluxes (5.7) are used and the porosity is taken as $\epsilon = 0.4$. To ensure the error of the numerical schemes do not grow, the variables are non-dimensionalised,

$$x^* = \frac{x}{L}, \quad y^* = \frac{y}{L}, \quad t^* = \frac{t}{T}, \quad h^* = \frac{h}{L}, \quad B^* = \frac{B}{L},$$

$$g^* = \frac{gT^2}{L}, \quad v^* = \frac{vT}{L}, \quad A^* = \frac{AL}{T^2}, \quad \text{tol}^* = \frac{\text{tol}}{L} \quad \text{and} \quad u^* = \frac{uT}{L},$$

where

$$L = \max_{i,j}(|x_{I,j} - x_{0,j}|, |y_{i,J} - y_{i,0}|) \quad \text{and} \quad T = \sqrt{\frac{L}{g}}$$

denote the non-dimensional coefficients. In this thesis, we take $Q = 10$ from which the initial conditions illustrated in Figure 5.2 may be obtained. Notice that small

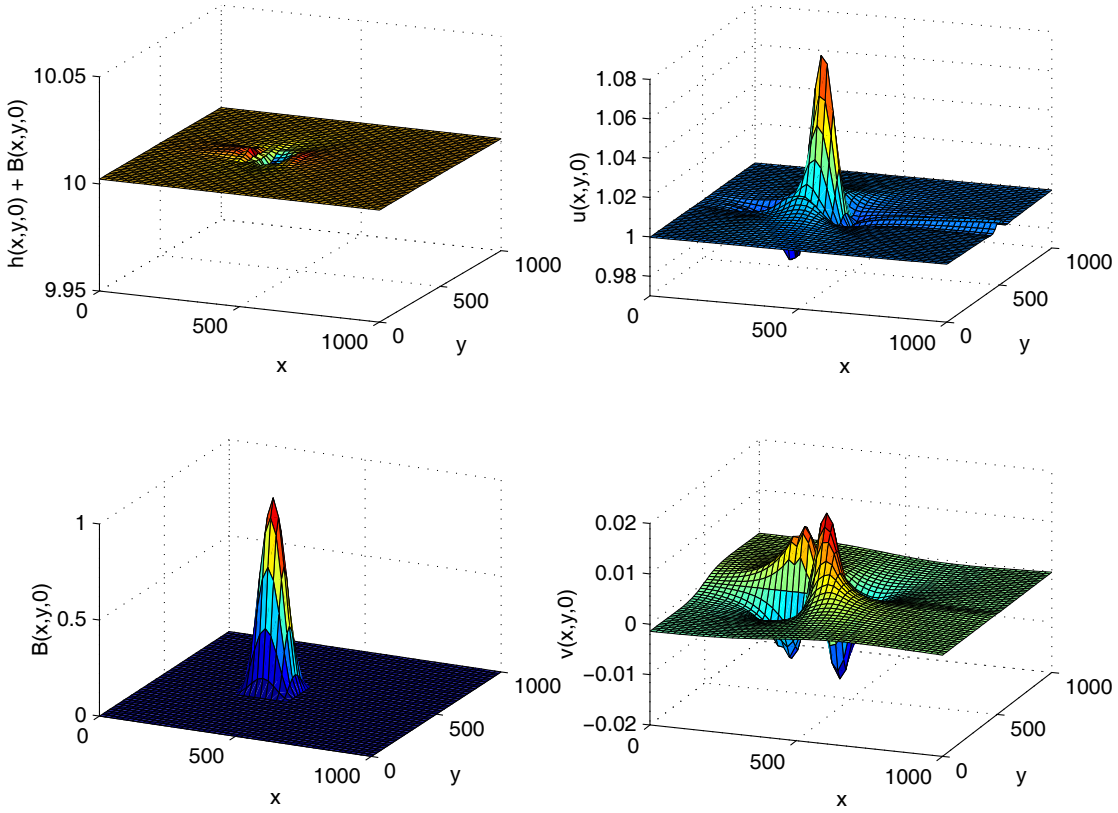

Figure 5.2: Initial conditions for 2D Channel Test Problem with $Q = 10$.

kinks are present in the initial conditions, which do not grow over time. Unless stated, the initial conditions illustrated are used for the 2D Channel Test Problem.

5.4.1 Approximate Solution for Angle of Spread

De Vriend [6] derived an approximate solution for the angle of spread of the pulse in the riverbed. For the conical sand dune test case, the pulse in the riverbed gradually changes into a star shaped pattern, which spreads out over time. An approximate solution for the angle of spread of the star shaped pattern can be obtained by

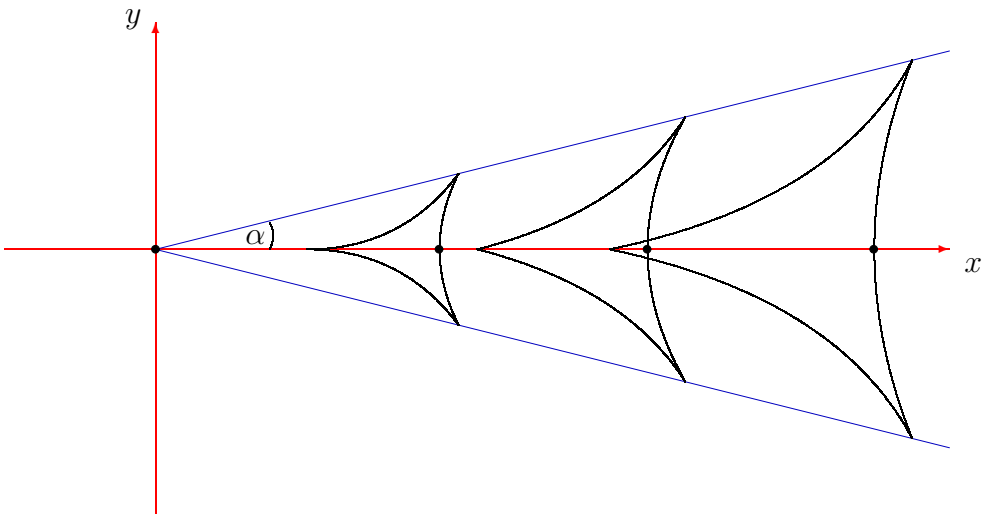

Figure 5.3: Approximate solution for angle of spread.

assuming that the riverbed is interacting slowly with the water flow, i.e. $A < 0.01$, and the water flow is in an equilibrium state. This allows the equations of water flow, i.e. (5.1), (5.2) and (5.3), to be simplified,

$$(uh)_x + (vh)_y = 0, \quad \left[\frac{1}{2}u^2 + g(h+B)\right]_x + (huv)_y = 0$$

and

$$(huv)_x + \left[\frac{1}{2}v^2 + g(h+B)\right]_y = 0.$$

Thus, De Vriend determined an approximate solution for the angle of spread for the star shaped pattern,

$$\tan\alpha = \frac{3T_u\sqrt{3}}{9T_u - 8T_h},$$

where

$$T_u = \frac{\hat{\mathrm{U}}}{\hat{q}}\left[\frac{\partial\hat{q}}{\partial\hat{\mathrm{U}}}\right] - 1 \quad \text{and} \quad T_h = \frac{h}{\hat{q}}\left[\frac{\partial\hat{q}}{\partial h}\right] - 1,$$

which is illustrated in Figure 5.3. Here, $\hat{q}$ denotes the streamwise sediment transport flux and $\hat{\mathrm{U}} = \sqrt{u^2+v^2}$ the streamwise velocity. For example, if the sediment transport flux (3.3) is used in two dimensions, then the streamwise sediment transport

flux is

$$\hat{q} = A\hat{\mathrm{U}}^m = A\left(u^2 + v^2\right)^{\frac{m}{2}}$$

from which we obtain

$$T_u = \frac{\hat{\mathrm{U}}}{A\hat{\mathrm{U}}^m}\left[Am\hat{\mathrm{U}}^{m-1}\right] - 1 = m - 1$$

and

$$T_h = \frac{h}{A\hat{\mathrm{U}}^m}\left[\frac{\partial\left(A\hat{\mathrm{U}}^m\right)}{\partial h}\right] - 1 = -1.$$

Hence, the analytical approximation of the angle of spread for the star shaped pattern is

$$\tan\alpha = \frac{3\sqrt{3}(m-1)}{9m-1},$$

and if $m = 3$ then the angle of spread is

$$\alpha = \tan^{-1}\left(\frac{3\sqrt{3}}{13}\right) = 21.7867893^o.$$

5.5 Numerical Results

In the next few sections, we use the classic 2D Lax-Wendroff scheme, the basic scheme (B-FLR) and dimensional splitting scheme (DS2-FLR) with Formulations A and C to obtain an approximation for the 2D Channel Test Problem. The 2D Channel Test Problem is used with a riverbed that is interacting slowly and quickly with the water flow so that Formulations A and C can be compared. Both the basic and dimensional splitting schemes use the flux-limited 2D version of Roe's numerical flux (4.14). All numerical schemes in this section are used with $\Delta x = \Delta y = 20m$ and the minmod flux-limiter. The basic scheme is used with $\nu = 0.4$ and the dimensional splitting scheme is used with $\nu = 0.8$. Formulation A is used with a tolerance level of tol = 0.00001 and a cut off time of 15 minutes is used to determine if the water flow has reached an equilibrium state.

5.5.1 Formulation A: Numerical Results for a Bed which is Interacting Slowly with the Water Flow

We first consider the 2D Channel Test Problem with a riverbed that is interacting slowly with the water flow, i.e. $A = 0.001$. The classic 2D Lax-Wendroff scheme, the basic scheme (B-FLR) and the dimensional splitting scheme (DS2-FLR) are used with Formulation A to obtain an approximation of the conical sand dune test problem at $t = 100$ hours. The numerical results of the classic 2D Lax-Wendroff scheme with Formulation A are not illustrated due to the scheme producing spurious oscillations in the results almost immediately, which rendered the scheme unstable. From Figure 5.4 and Figure 5.5 we can see that the B-FLR scheme has produced smooth numerical results that do not suffer from spurious oscillations. Also, from Figure 5.6 and Figure 5.7 we can see that the DS2-FLR scheme has produced smooth numerical results that are similar to the B-FLR scheme. However, both schemes produced kinks in the numerical results and DS2-FLR scheme has produced a slightly different star shaped pattern than the B-FLR scheme. Figure 5.8 and Figure 5.9 illustrate the approximate angle of spread compared to the numerical results for the B-FLR scheme and DS2-FLR scheme respectively. Here we can see that the DS2-FLR scheme produced an angle of spread for the star shaped pattern that was closer to the approximate angle of spread than the B-FLR scheme. Also, notice that from Figure 5.10 we can see that both schemes produced small kinks in the numerical results and have increased the total height of the river by a small amount. However, the DS2-FLR scheme produced numerical results with fewer kinks present and with an angle of spread that was closer to the approximate value. Thus, the DS2-FLR scheme is the most accurate scheme. The numerical results of the B-FLR scheme and the DS2-FLR scheme are devoid of the spurious oscillations present in the numerical results obtained with PISCES, see Chesher *et al.* [2], in some simulations and therefore represent a notable improvement.

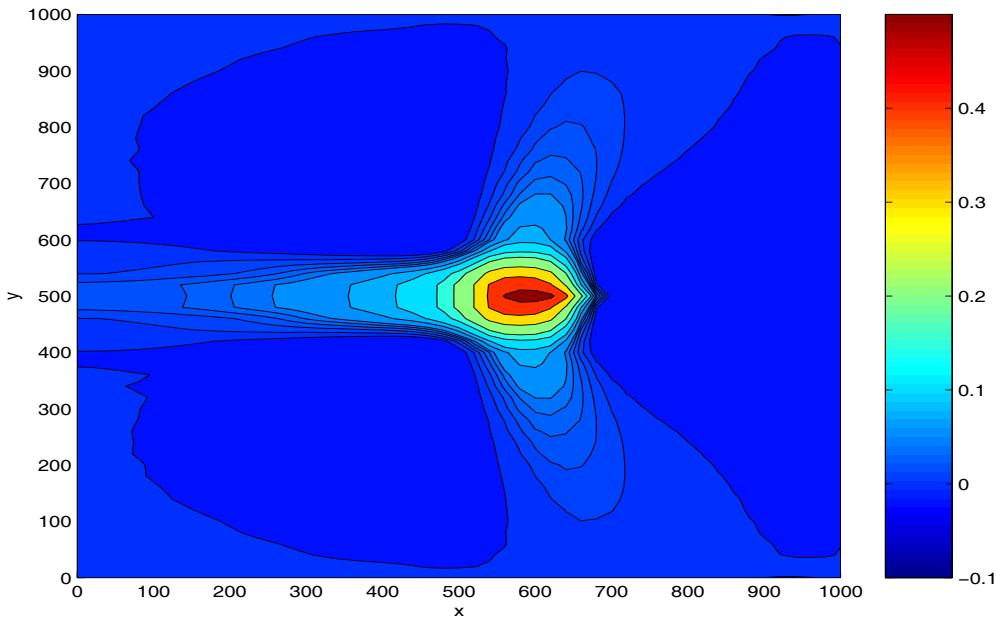

Figure 5.4: Numerical results for Formulation A using the basic scheme (B-FLR) with $A = 0.001$ and at $t = 100h$ (B).

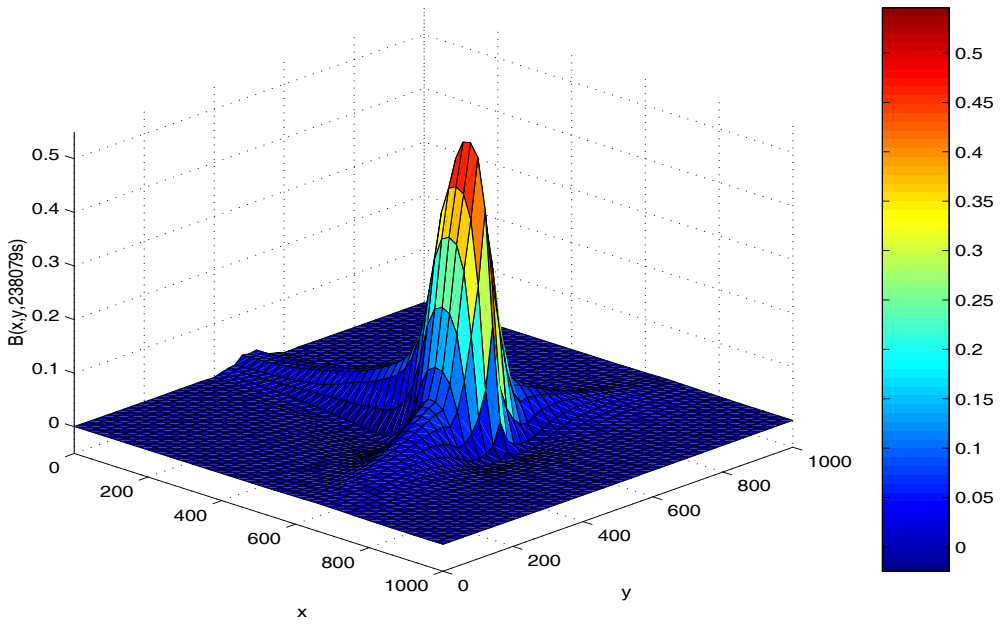

Figure 5.5: Numerical results for Formulation A using the basic scheme (B-FLR) with $A = 0.001$ and at $t = 100h$ (B).

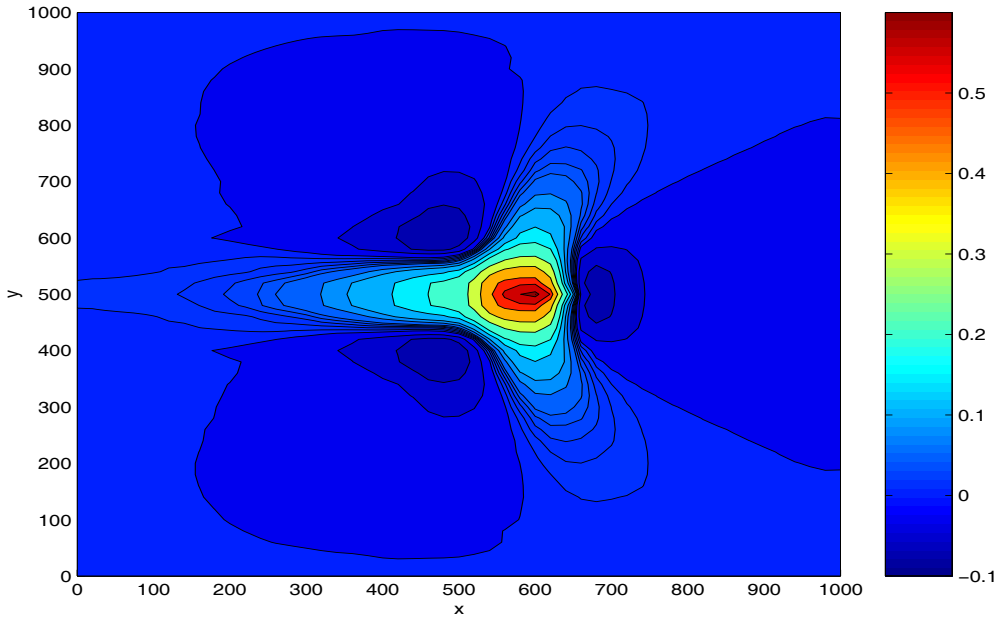

Figure 5.6: Numerical results for Formulation A using the dimensional splitting scheme (DS2-FLR) with $A = 0.001$ and at $t = 100h$ (B).

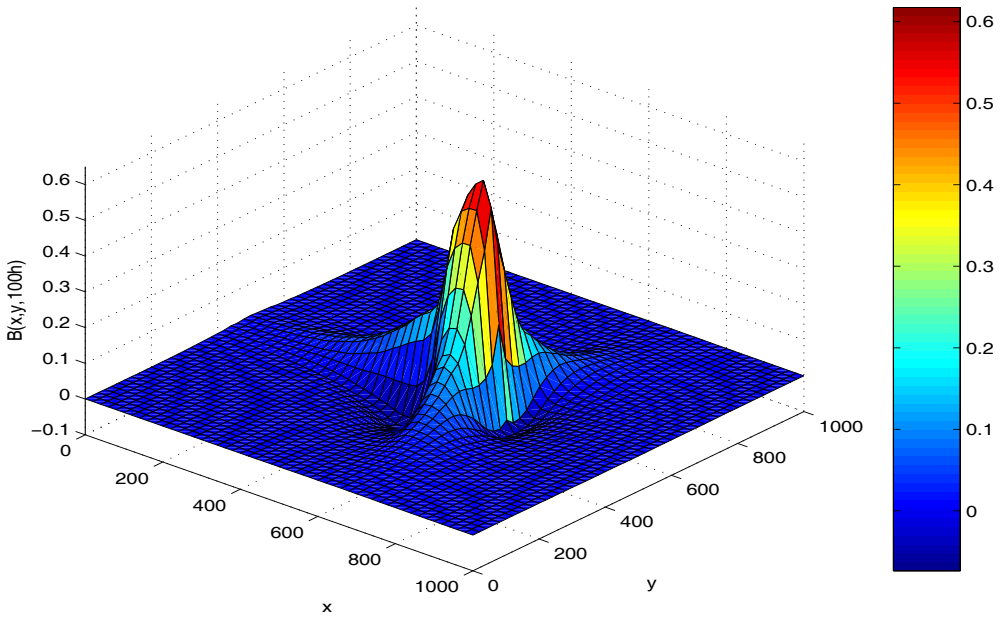

Figure 5.7: Numerical results for Formulation A using the dimensional splitting scheme (DS2-FLR) with $A = 0.001$ and at $t = 100h$ (B).

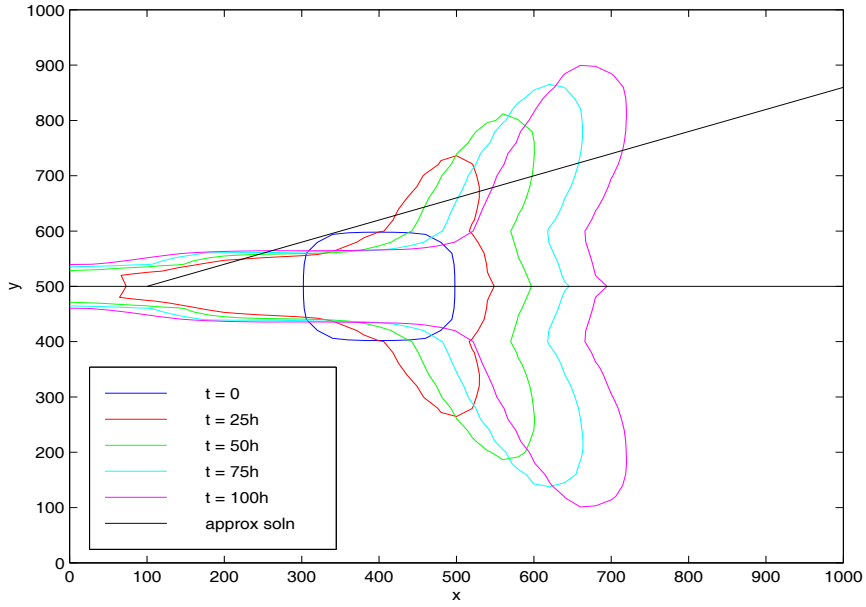

Figure 5.8: Illustration of the angle of spread for Formulation A using the basic scheme (B-FLR) with $A = 0.001$ (B).

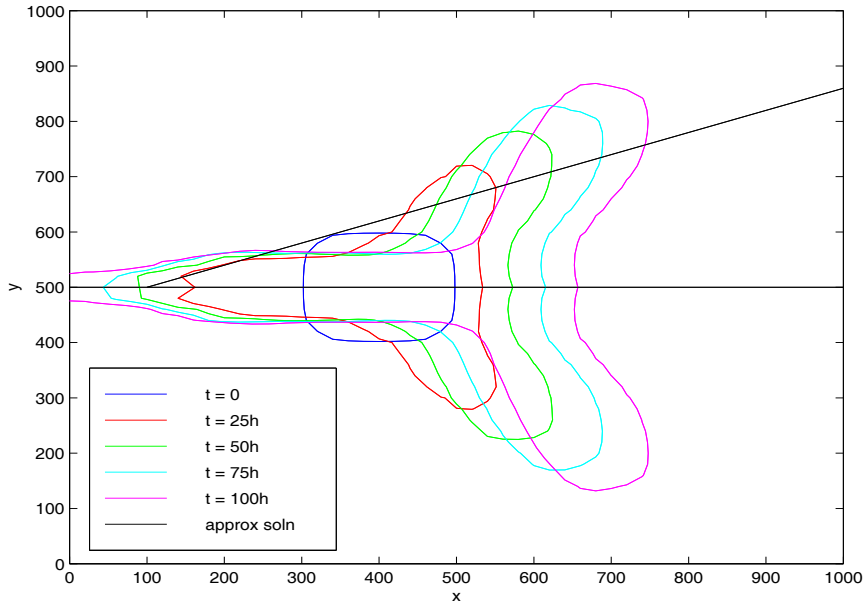

Figure 5.9: Illustration of the angle of spread for Formulation A using the dimensional splitting scheme (DS2-FLR) with $A = 0.001$ (B).

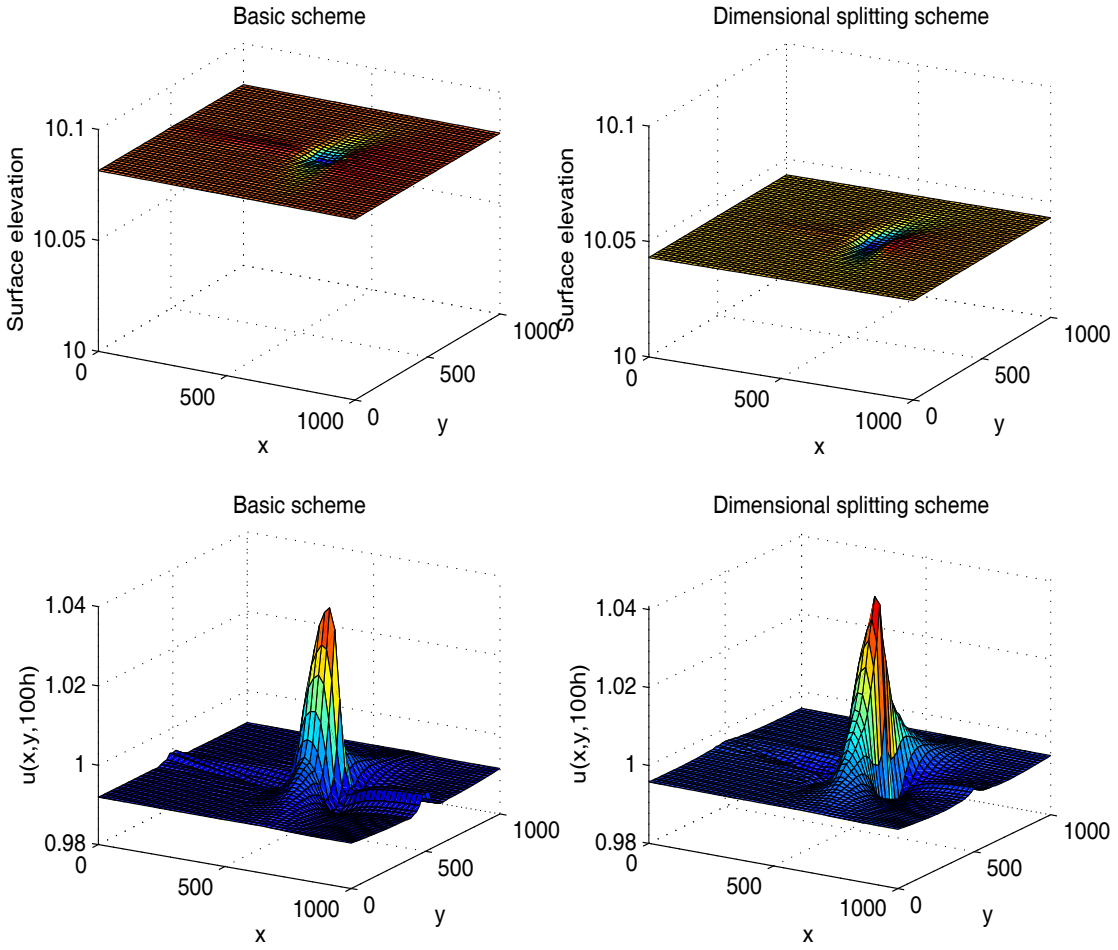

Figure 5.10: Numerical results for Formulation A using the basic scheme (B-FLR) and the dimensional splitting scheme (DS2-FLR) with $A = 0.001$ and at $t = 100h$.

5.5.2 Formulation C: Numerical Results for a Bed which is Interacting Slowly with the Water Flow

Formulation C is now used with the classic 2D Lax-Wendroff scheme, the basic scheme (B-FLR) and the dimensional splitting scheme (DS2-FLR) to obtain a numerical approximation of the 2D Channel Test Problem for a riverbed that is interacting slowly with the water flow, i.e. $A = 0.001$, at $t = 100$ hours. From Figure 5.11 and Figure 5.12 we can see that the classic 2D Lax-Wendroff scheme has produced spurious oscillations in the numerical results. However, from Figure 5.13 and Figure 5.14 we can see that the B-FLR scheme has produced smooth numerical results that do not suffer from spurious oscillations. Also, from Figure 5.15 and Figure 5.16 we can see that the DS2-FLR scheme has produced smooth numerical results that are similar to the B-FLR scheme. Notice that no kinks are present in the numerical results obtained with Formulation C, but kinks were present in the results obtained with Formulation A. Figure 5.17 and Figure 5.18 illustrate the approximate angle of spread compared to the numerical results for the B-FLR scheme and DS2-FLR scheme respectively. As with the numerical results obtained with Formulation A, here we can see that the DS2-FLR scheme produced an angle of spread for the star shaped pattern that was closer to the approximate angle of spread than the B-FLR scheme. The angle of spread obtained from using Formulation C with the B-FLR scheme and the DS2-FLR scheme are also closer to the approximate value than the angle of spread obtained from using Formulation A. However, from Figure 5.19 we can see that the numerical results obtained with Formulation C have significantly increased the total height of the river and velocity from their original values. This is due to all schemes requiring a considerable amount of time steps to reach the final computation time of 100 hours and the upstream boundary also having constant discharge imposed. Thus, a numerical scheme that can be used with large time steps such as an implicit scheme is required to obtain an approximation of Formulation C. Also, notice that a few small kinks are present in the total height of the river and velocity for the numerical results of Formulation C but they do not appear in the riverbed and are not as prominent as with Formulation A. As with the numerical results obtained with Formulation A, the numerical results

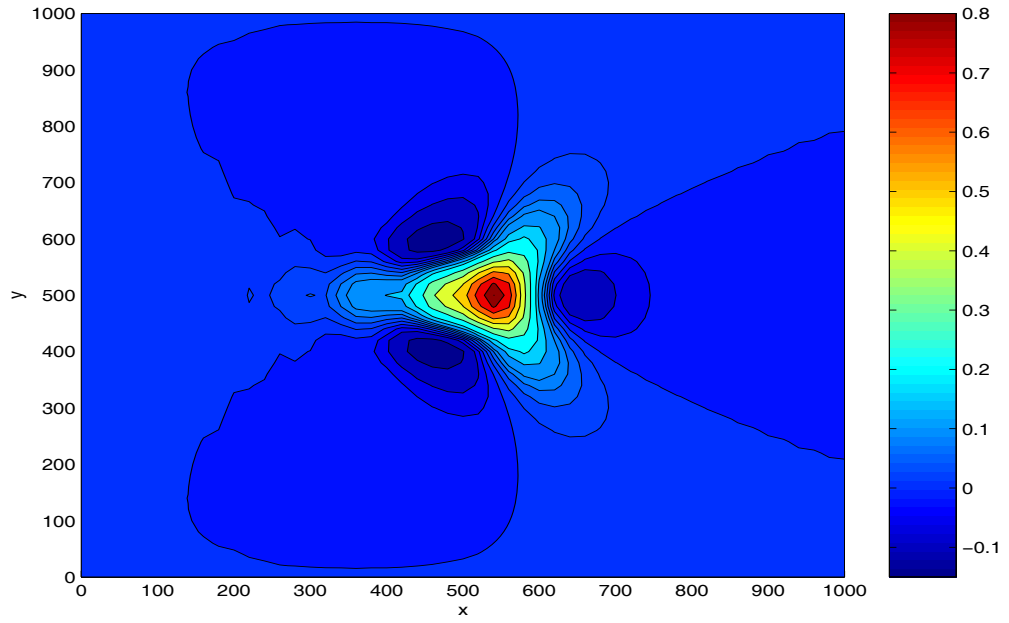

Figure 5.11: Numerical results for Formulation C using the classic 2D Lax-Wendroff scheme with $A = 0.001$ and at $t = 100h$ (B).

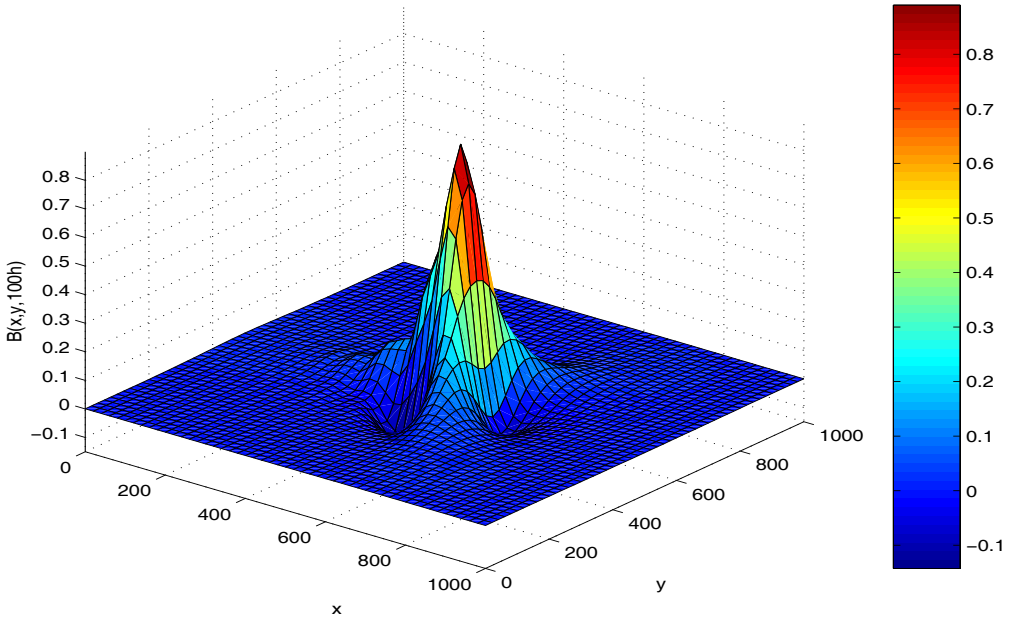

Figure 5.12: Numerical results for Formulation C using the classic 2D Lax-Wendroff scheme with $A = 0.001$ and at $t = 100h$ (B).

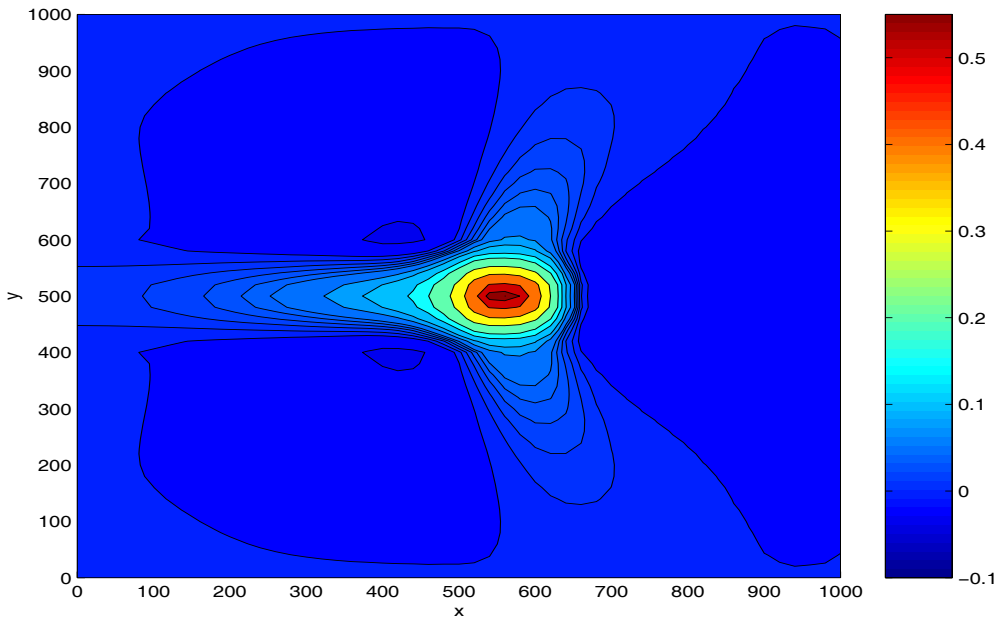

Figure 5.13: Numerical results for Formulation C using the basic scheme (B-FLR) with $A = 0.001$ and at $t = 100h$ (B).

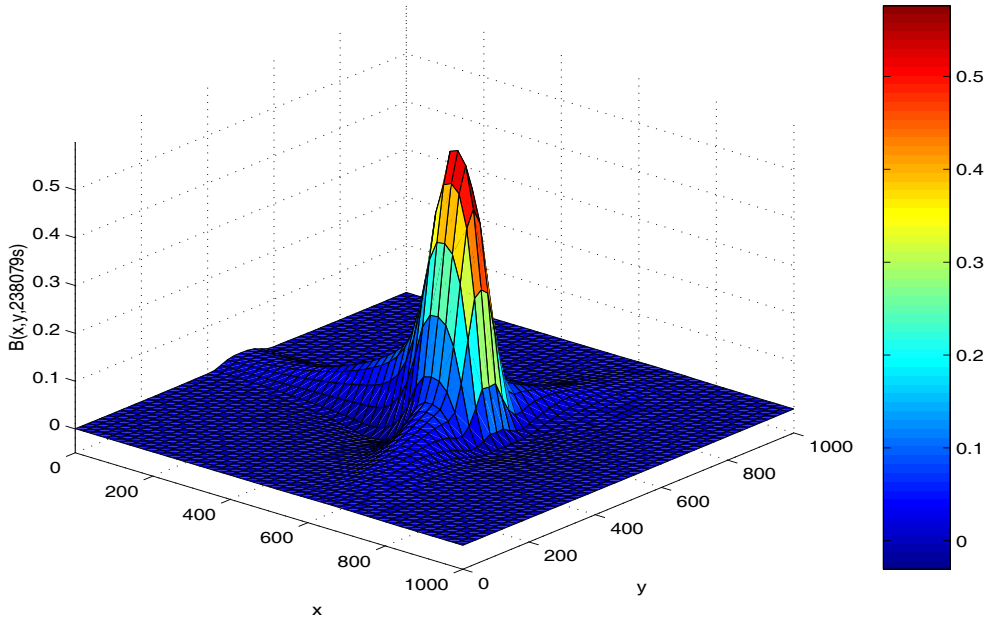

Figure 5.14: Numerical results for Formulation C using the basic scheme (B-FLR) with $A = 0.001$ and at $t = 100h$ (B).

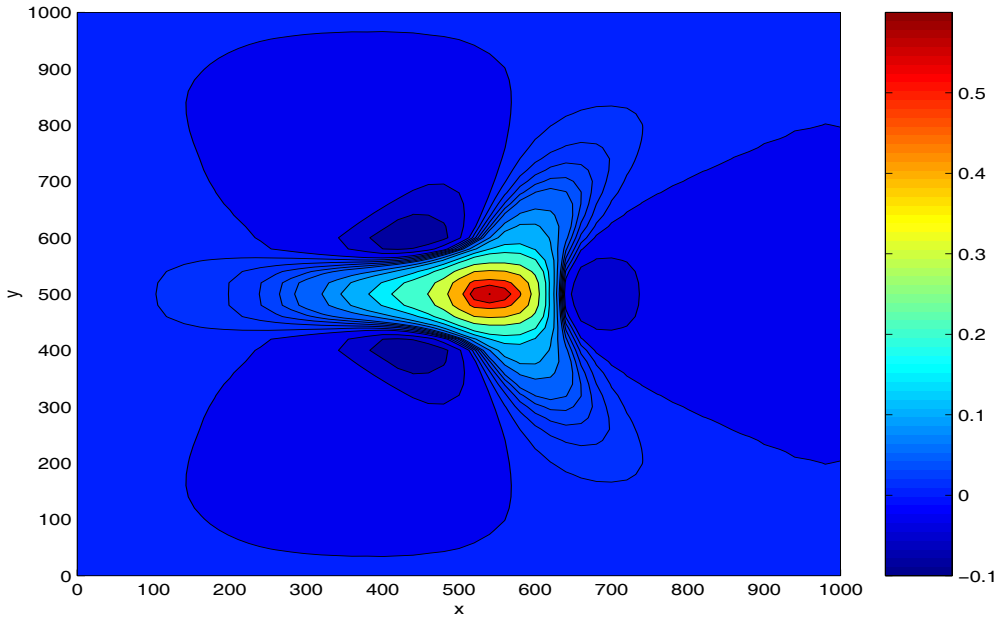

Figure 5.15: Numerical results for Formulation C using the dimensional splitting scheme (DS2-FLR) with $A = 0.001$ and at $t = 100h$ (B).

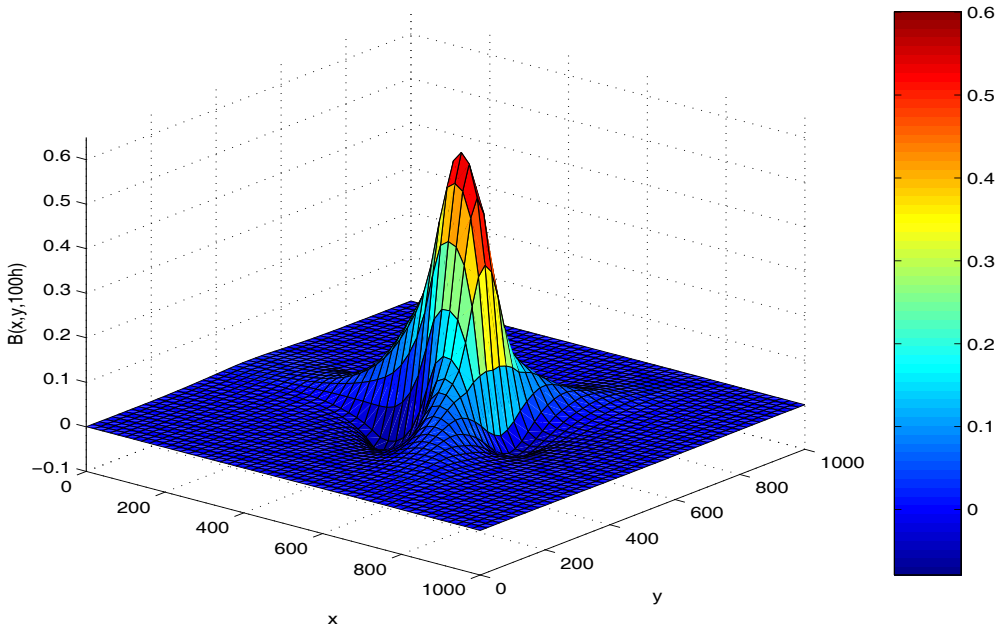

Figure 5.16: Numerical results for Formulation C using the dimensional splitting scheme (DS2-FLR) with $A = 0.001$ and at $t = 100h$ (B).

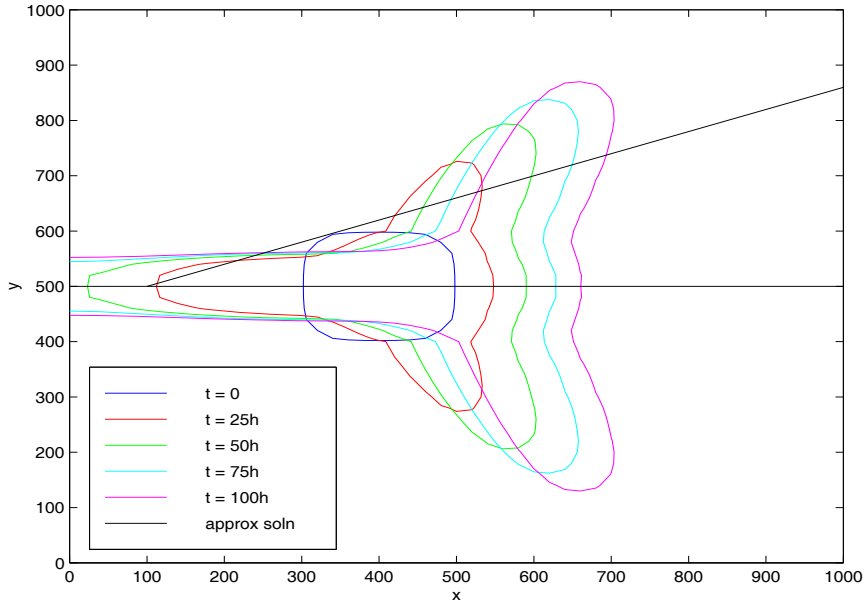

Figure 5.17: Illustration of the angle of spread for Formulation C using the basic scheme (B-FLR) with $A = 0.001$ (B).

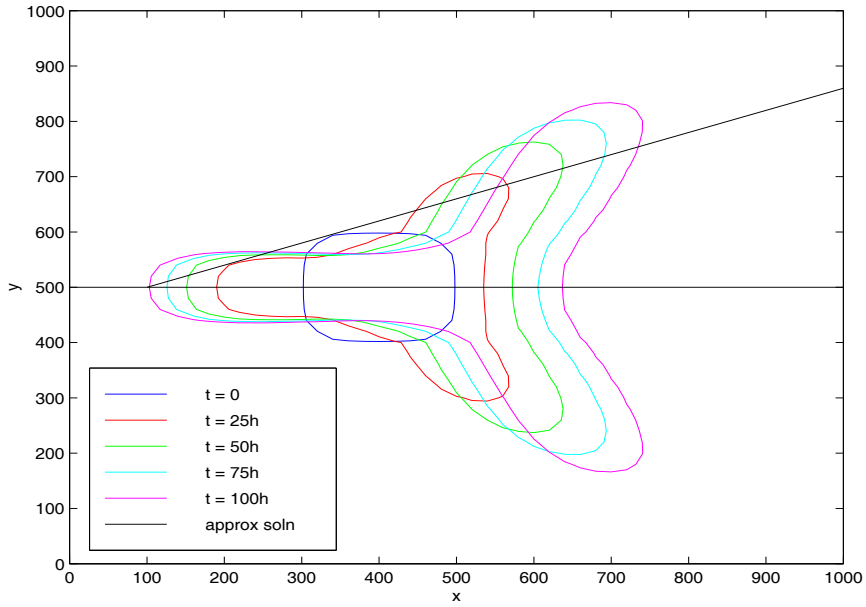

Figure 5.18: Illustration of the angle of spread for Formulation C using the dimensional splitting scheme (DS2-FLR) with $A = 0.001$ (B).

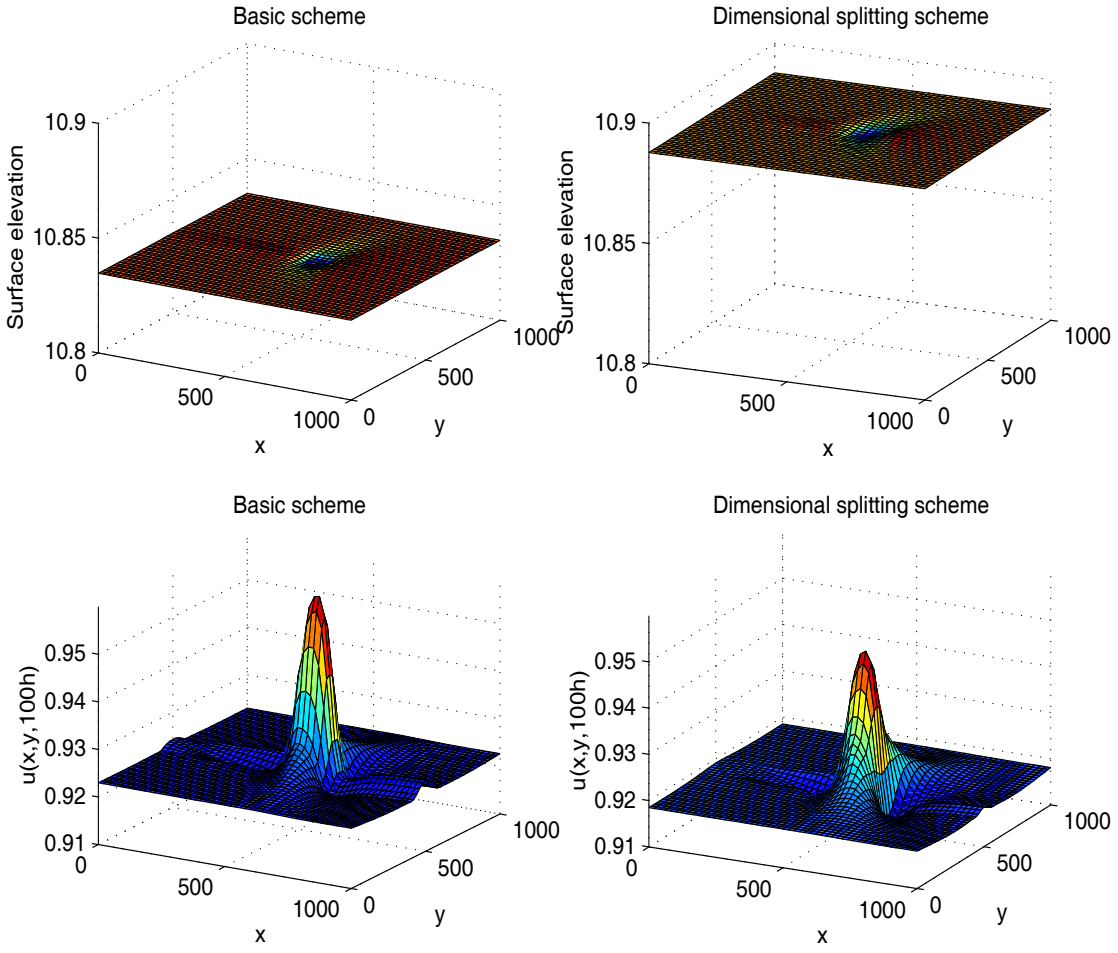

Figure 5.19: Numerical results for Formulation C using the basic scheme (B-FLR) and the dimensional splitting scheme (DS2-FLR) with $A = 0.001$ and at $t = 100h$.

of the B-FLR scheme and the DS2-FLR scheme are devoid of the spurious oscillations present in the numerical results obtained with PISCES, see Chesher *et al.* [2], in some simulations and therefore represent a notable improvement.

5.5.3 Formulation A: Numerical Results for a Bed which is Interacting Quickly with the Water Flow

For the second test problem, we use the 2D Channel Test Problem with a riverbed that is now interacting quickly with the water flow, i.e. $A = 1$. The classic 2D Lax-Wendroff scheme, the basic scheme (B-FLR) and the dimensional splitting scheme (DS2-FLR) are used with Formulation A to obtain an approximation of the conical sand dune test problem at $t = 500$ seconds. The numerical results of the classic 2D Lax-Wendroff scheme with Formulation A are not illustrated due to the scheme producing spurious oscillations in the results almost immediately, which rendered the scheme unstable. From Figure 5.20 and Figure 5.21 we can see that the B-FLR scheme produced numerical results with no spurious oscillations present. By using the DS2-FLR scheme, we obtain the numerical results illustrated in Figure 5.22 and Figure 5.23. Here, we can see that the DS2-FLR scheme has produced numerical results that differ to the B-FLR scheme. This is due both schemes producing completely different star shaped patterns. The DS2-FLR scheme has produced a step in the ramp behind the star-shaped pattern whereas the B-FLR scheme produced a smooth ramp without a step present. The step present in the numerical results of the DS2-FLR scheme was also present when $A = 0.001$ was used, but the step is now larger. The angle of spread of the star shaped patterns also differs. Also, notice that both schemes have produced kinks in the numerical results. Figure 5.24 shows the total height of the river and velocity for the B-FLR scheme and DS2-FLR scheme. Notice that both schemes have produced slightly different numerical results where the height of the river and velocity has changed from the original values. This is due to the formulation imposing a constant discharge on the upstream boundary and requiring a considerable amount of time steps to reach the final computation time of 500 seconds.

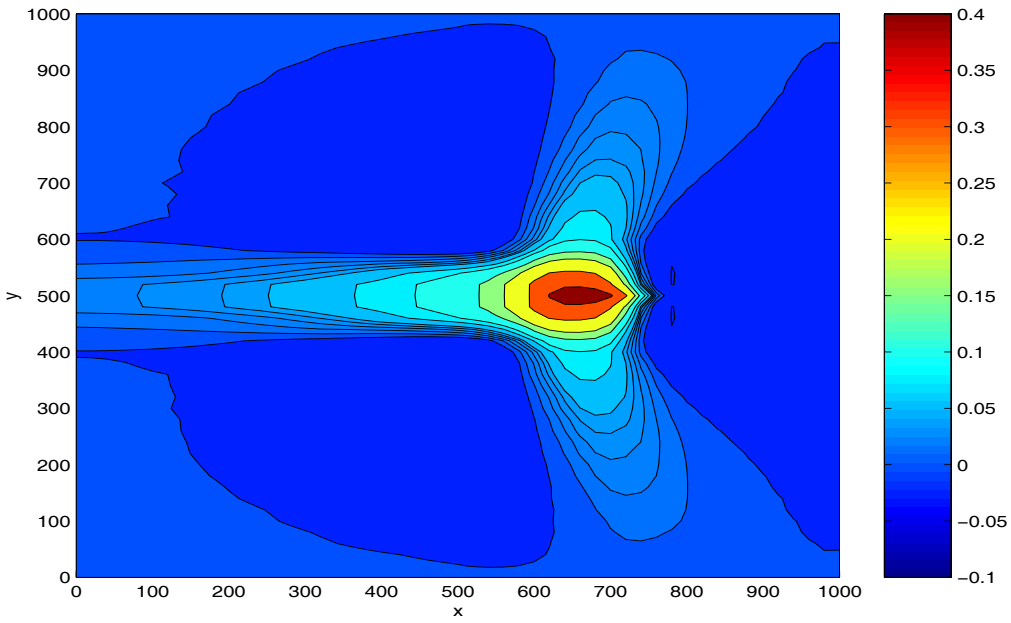

Figure 5.20: Numerical results for Formulation A using the basic scheme (B-FLR) with $A = 1$ and at $t = 500s$ (B).

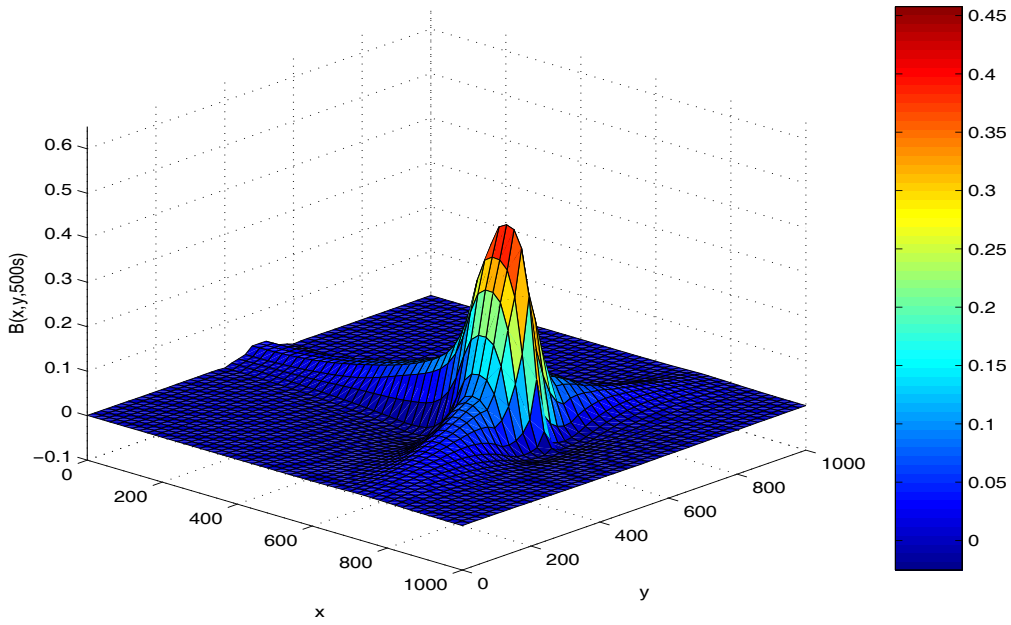

Figure 5.21: Numerical results for Formulation A using the basic scheme (B-FLR) with $A = 1$ and at $t = 500s$ (B).

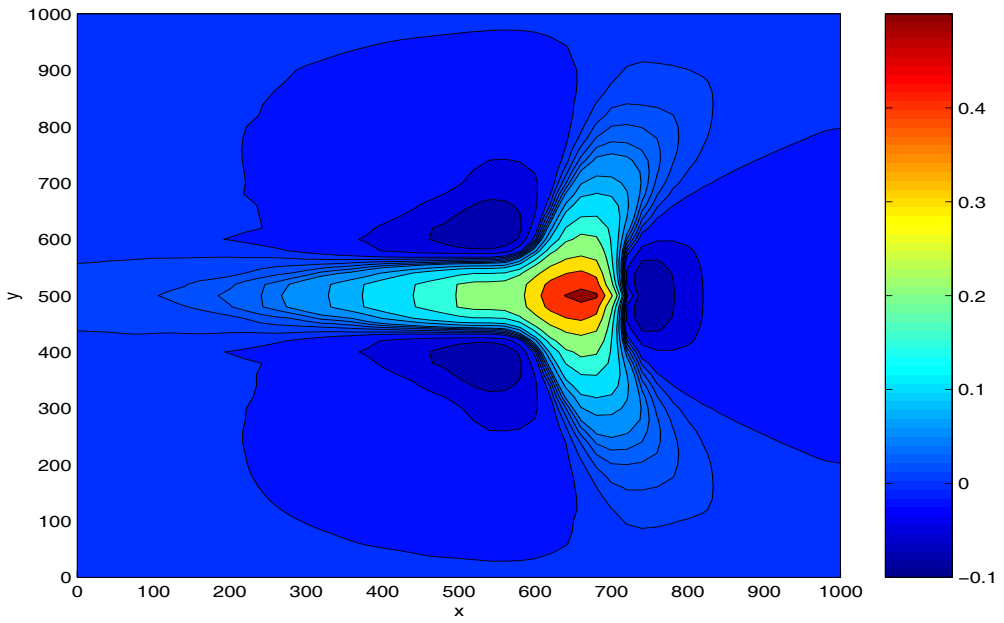

Figure 5.22: Numerical results for Formulation A using the dimensional splitting scheme (DS2-FLR) with $A = 1$ and at $t = 500s$ (B).

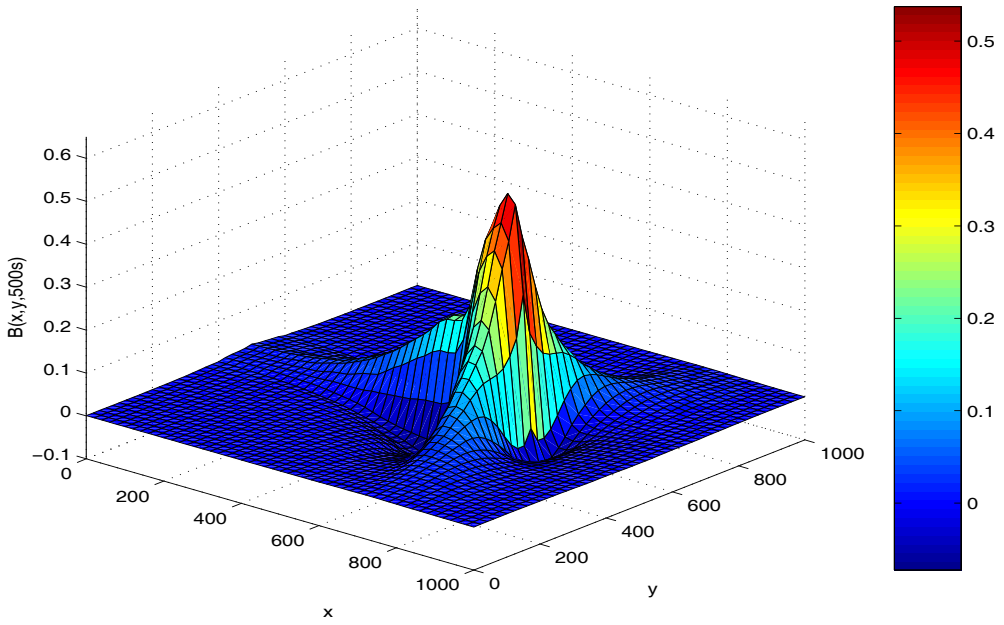

Figure 5.23: Numerical results for Formulation A using the dimensional splitting scheme (DS2-FLR) with $A = 1$ and at $t = 500s$ (B).

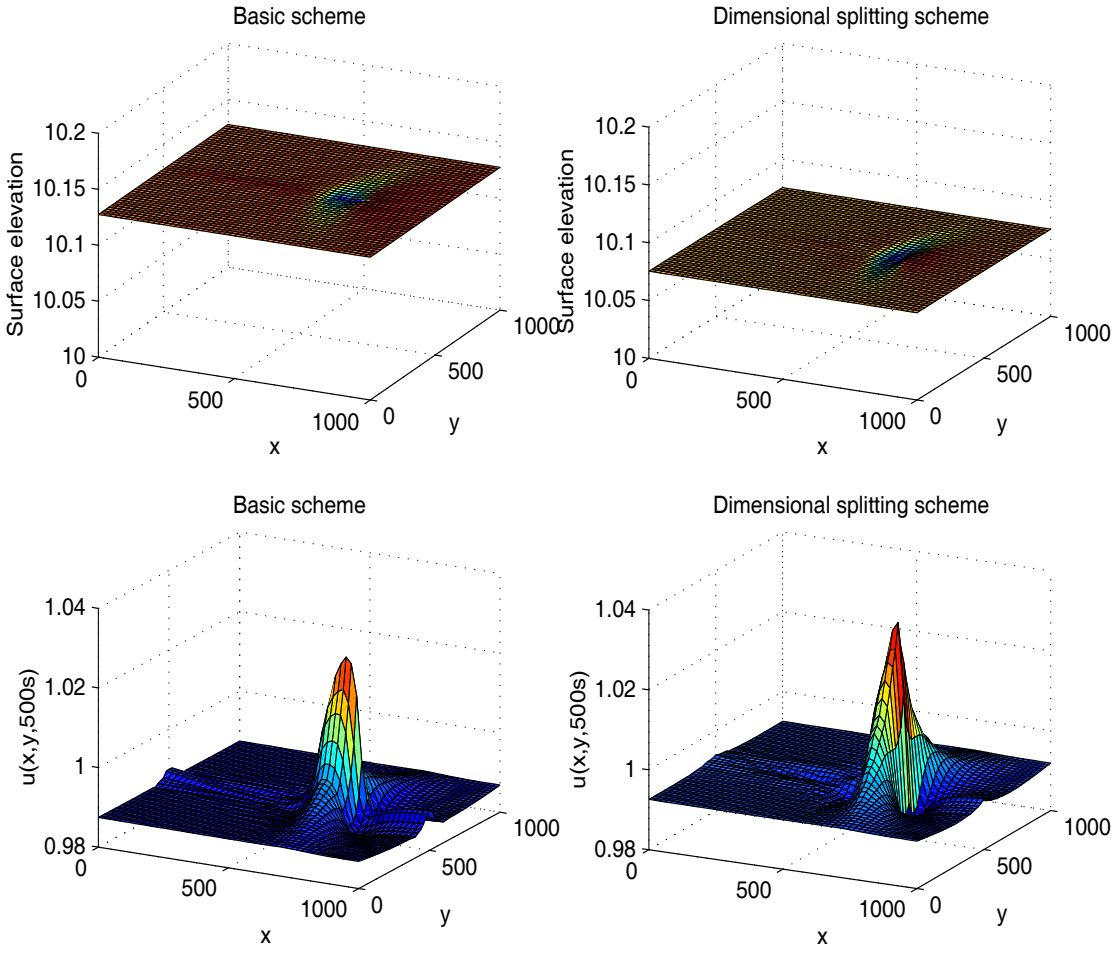

Figure 5.24: Numerical results for Formulation A using the basic scheme (B-FLR) and the dimensional splitting scheme (DS2-FLR) with $A = 1$ and at $t = 500s$.

5.5.4 Formulation C: Numerical Results for a Bed which is Interacting Quickly with the Water Flow

Formulation A is now used with the classic 2D Lax-Wendroff scheme, the basic scheme (B-FLR) and the dimensional splitting scheme (DS2-FLR) to obtain a numerical approximation of the 2D Channel Test Problem for a riverbed that is interacting quickly with the water flow, i.e. $A = 1$, at $t = 500$ seconds. Figure 5.25 and Figure 5.26 illustrate the numerical results of the classic 2D Lax-Wendroff scheme. Here, as with $A = 0.001$, we can see that the classic 2D Lax-Wendroff scheme has produced very poor numerical results due to spurious oscillations occurring in the numerical results. From Figure 5.27 and Figure 5.28 we can see that the B-FLR scheme produced smooth numerical results with no spurious oscillations or kinks present. By using the DS2-FLR scheme, we obtain the numerical results illustrated in Figure 5.22 and Figure 5.23. Here, we can see that as with Formulation A, the DS2-FLR scheme has produced numerical results that differ to the B-FLR scheme due to the star shaped pattern differing. The DS2-FLR scheme has also produced a smoother ramp behind the star shaped pattern than the B-FLR scheme. The angle of spread of the star shaped pattern also differs for the B-FLR scheme and the DS2-FLR scheme. Also, from Figure 5.31 we can see that the total height of the river and velocity have remained close to the initial values and the results are also smooth with very few kinks present. As with $A = 0.001$, the numerical results obtained with Formulations A and C differed, but considerably more with $A = 1$ due to the sand dune being moved slightly faster with Formulation A than Formulation C. This significant difference also occurred in one dimension, see Chapter 3, when a large value of A was used and was due to Formulation A-CV assuming the water flow is in an equilibrium state, which resulted in a constant discharge being imposed.

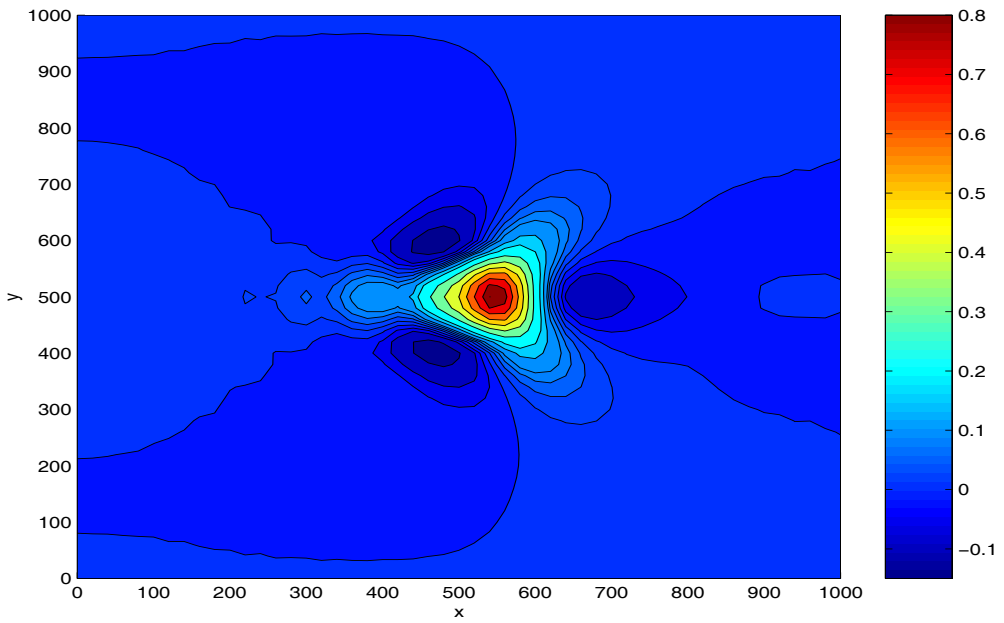

Figure 5.25: Numerical results for Formulation C using the classic 2D Lax-Wendroff scheme with $A = 1$ and at $t = 500s$ (B).

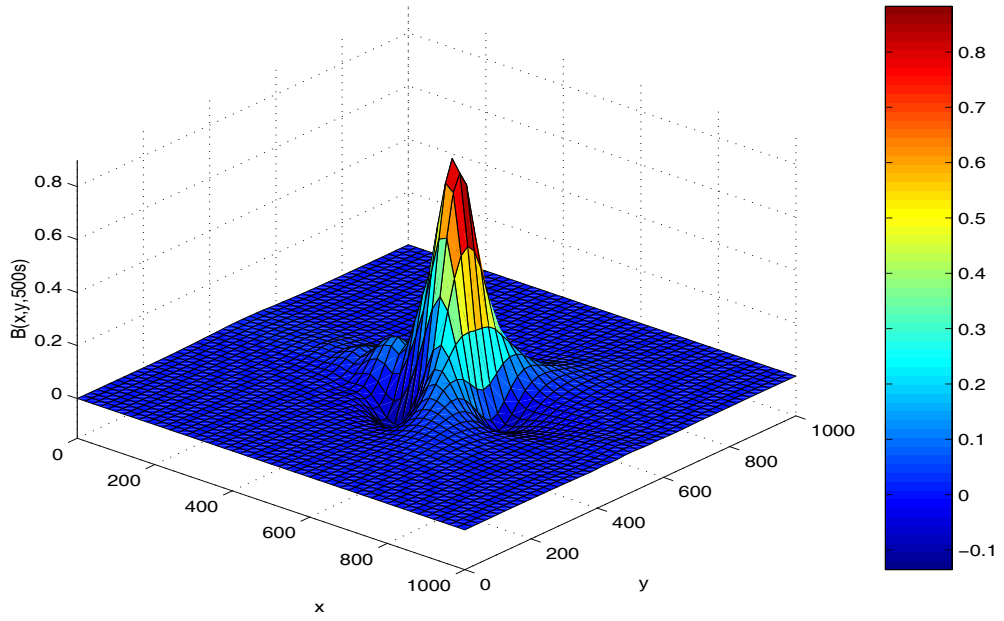

Figure 5.26: Numerical results for Formulation C using the classic 2D Lax-Wendroff scheme with $A = 1$ and at $t = 500s$ (B).

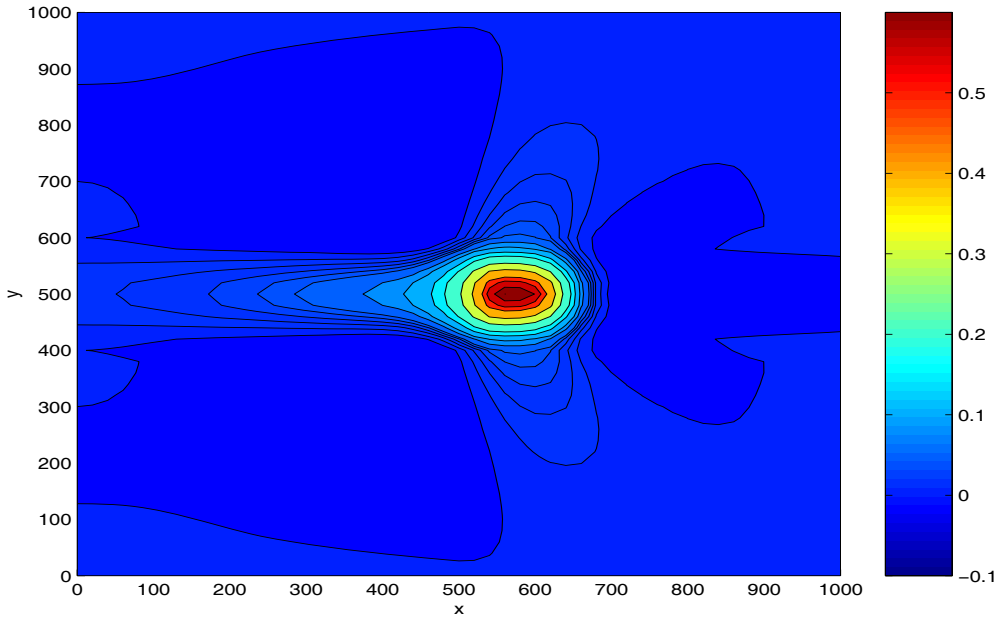

Figure 5.27: Numerical results for Formulation C using the basic scheme (B-FLR) with $A = 1$ and at $t = 500s$ (B).

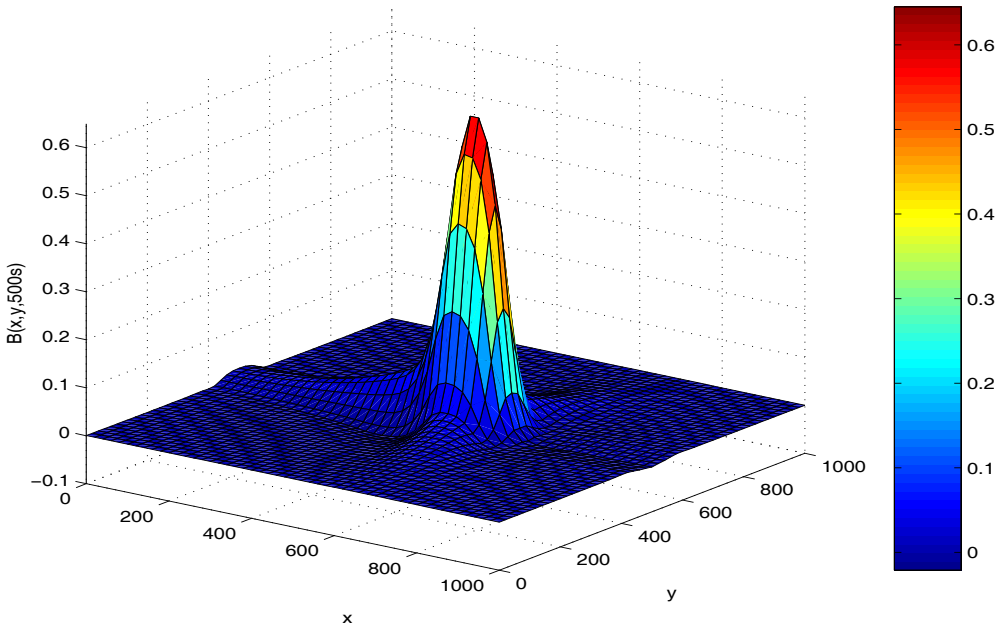

Figure 5.28: Numerical results for Formulation C using the basic scheme (B-FLR) with $A = 1$ and at $t = 500s$ (B).

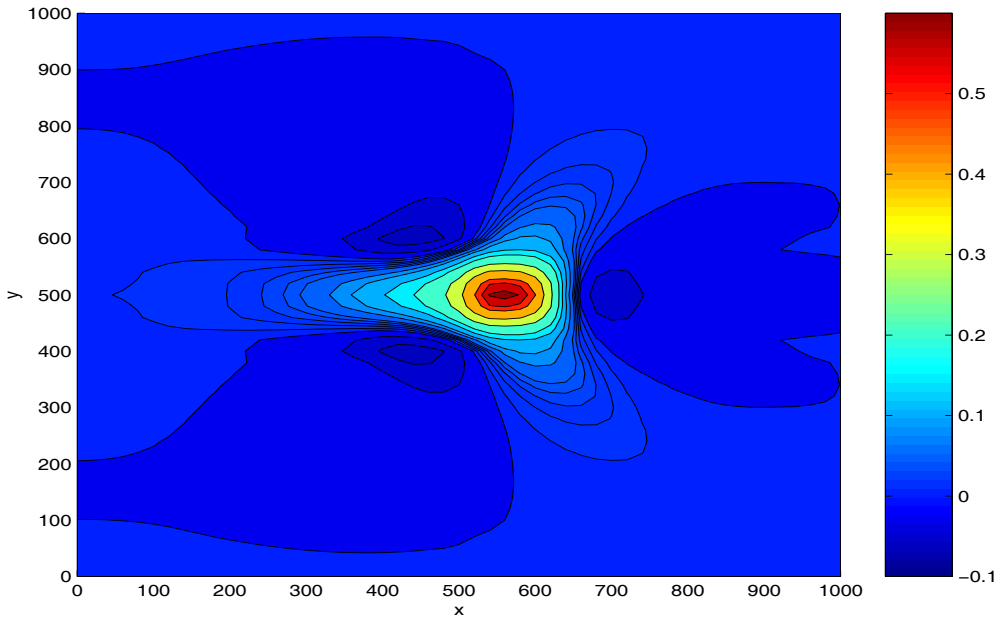

Figure 5.29: Numerical results for Formulation C using the dimensional splitting scheme (DS2-FLR) with $A = 1$ and at $t = 500s$ (B).

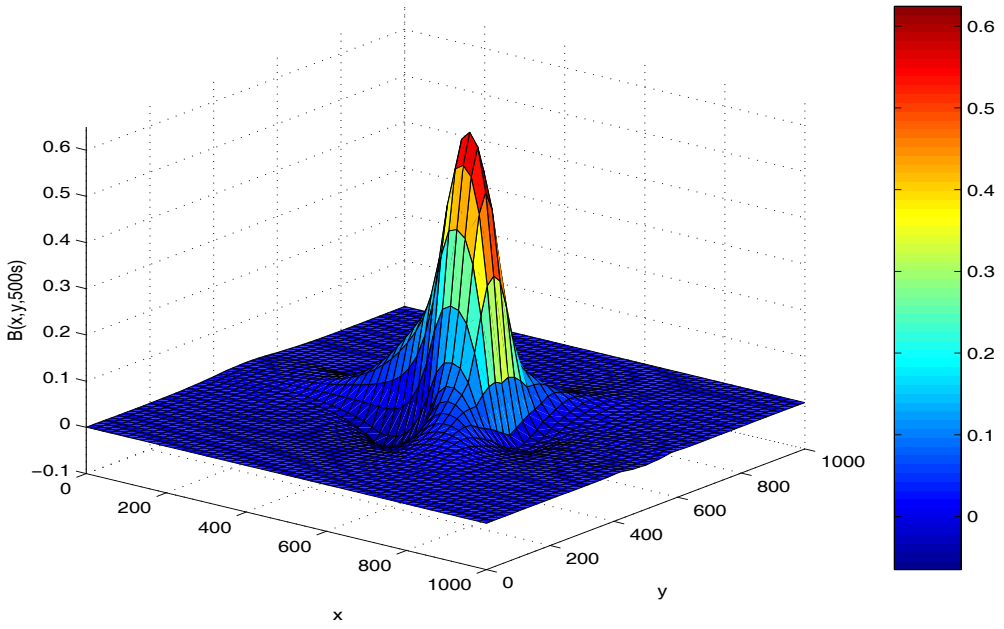

Figure 5.30: Numerical results for Formulation C using the dimensional splitting scheme (DS2-FLR) with $A = 1$ and at $t = 500s$ (B).

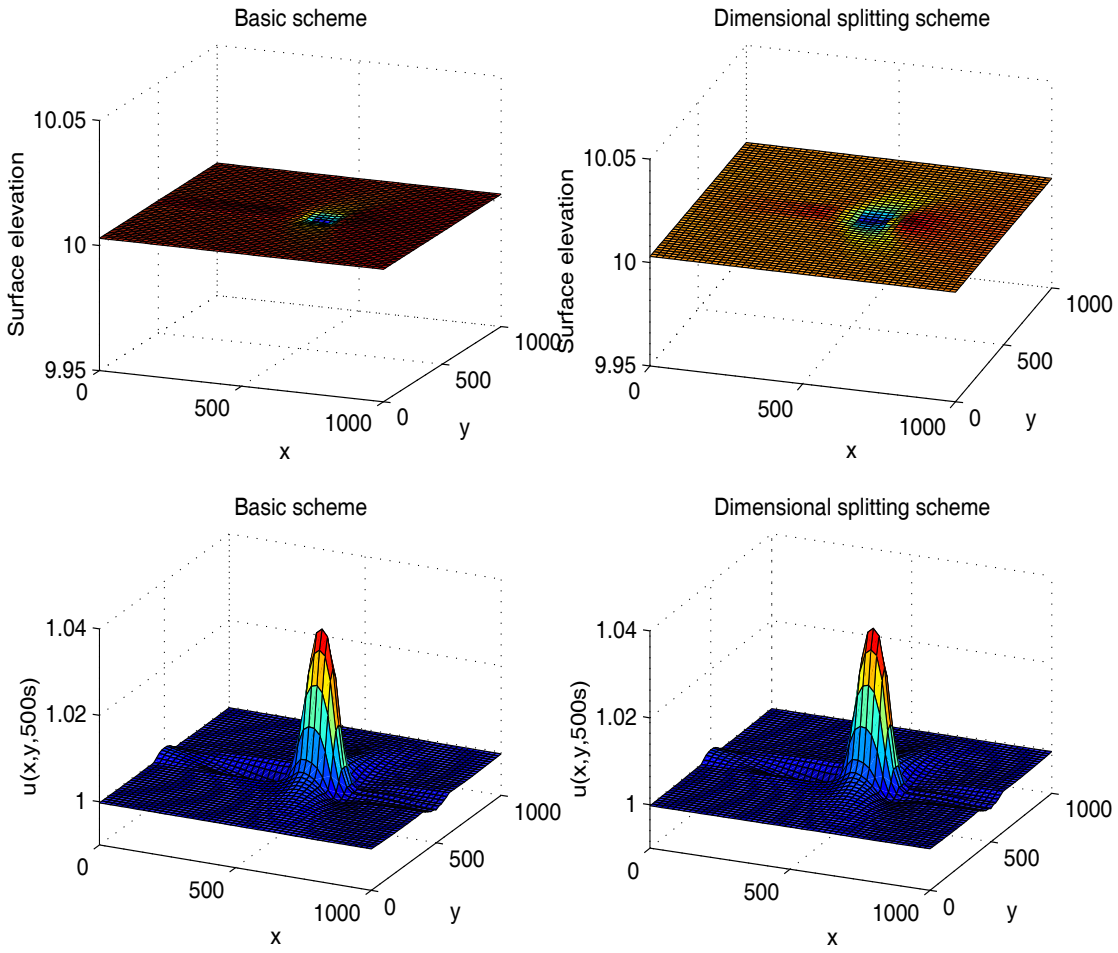

Figure 5.31: Numerical Results for Formulation C using the basic scheme (B-FLR) and the dimensional splitting scheme (DS2-FLR) with $A = 1$ and at $t = 500s$.

5.6 Summary

In this chapter, we extended Formulations A-CV and C to two dimensions and adapted the classic 2D Lax-Wendroff scheme, the basic scheme (B-FLR) and the dimensional splitting scheme (DS2-FLR) to approximate each formulation. A two dimensional conical sand dune test problem was used to determine which scheme was the most accurate. The 2D Channel Test Problem was used with a riverbed that interacts either quickly, $A = 1$, or slowly, $A = 0.001$, with the water flow so that the different formulations and numerical schemes could be thoroughly tested. For both formulations, the classic 2D Lax-Wendroff scheme produced poor numerical results for all values of A and with Formulation A, the scheme became unstable almost immediately due to spurious oscillations overpowering the numerical results. Formulation A with either the B-FLR scheme or the DS2-FLR scheme produced numerical results with no spurious oscillations present, but kinks appeared in the numerical results for all values of A. The numerical results obtained with Formulation C and either the B-FLR scheme or the DS2-FLR scheme were very smooth and did not suffer from spurious oscillations or kinks, which were present when Formulation A was used. Notice that the numerical results obtained with the B-FLR scheme and the DS2-FLR scheme differ for both formulations. When Formulation A is used with the DS2-FLR scheme, a step appears in the ramp behind the star shaped pattern, which is more prominent when $A = 1$, and does not appear when Formulation C or the B-FLR scheme is used. Also, the angle of spread obtained produced by the DS2-FLR scheme is closer to the approximate value than the B-FLR scheme. The numerical results of the riverbed for both formulations were similar when $A = 0.001$ but when $A = 1$ was used, Formulation A moved the sand dune at a faster wave speed than Formulation C. When $A = 0.001$ was used, the schemes with Formulation C dramatically changed the surface elevation and velocity whereas Formulation A only changed the values slightly. However, when $A = 1$ was used, the different schemes with Formulation A changed the surface elevation and velocity significantly from the initial values whereas Formulation C with the schemes produced values very close. This is due to Formulation C with the different schemes requiring a considerable amount of time steps to reach the final computation time

of $t = 100$ hours when $A = 0.001$ but requiring very few time steps when $A = 1$ due to the final computation time now being $t = 500$ seconds. Formulation C with the B-FLR scheme uses an average time step of $\Delta t \approx 0.72$ seconds for all values of $A \leq 1$ due to the eigenvalues of the water flow being the dominant values. Thus, for $A = 0.001$, the B-FLR scheme requires approximately 500,000 time steps to reach the final computation time whereas with $A = 1$, the scheme only requires approximately 695 time steps. A constant discharge is imposed at the upstream boundary at each time step thus, when a small value of A is used, a large amount of time steps are required, which results in the boundary condition changing the surface elevation and velocity. Formulation A also produces a different surface elevation and velocity from the initial values, but for a large value of A. This is due to the formulation assuming the water flow is in an equilibrium state so that the water flow can be approximated separately from the water flow and a large morphological time step can then be used. For the B-FLR scheme, Formulation A has an overall morphological time step that is computed using

$$\Delta t = \frac{\nu \min\left(\Delta x, \Delta y\right)}{2\max_{i,j}\left(|\lambda^F|, |\lambda^G|\right)},$$

where

$$\lambda^F = \frac{3A\xi u}{h}\left(u^2 + v^2\right) \quad \text{and} \quad \lambda^G = \frac{3A\xi v}{h}\left(u^2 + v^2\right).$$

Now, from the initial values we obtain

$$\min_{i,j}(|h|) \approx 9, \quad \max_{i,j}(|u|) \approx 1.08 \quad \text{and} \quad \max_{i,j}(|v|) \approx 0.01,$$

which implies that

$$\max_{i,j}(|\lambda^F|) \approx 0.6999A \quad \text{and} \quad \max_{i,j}(|\lambda^G|) \approx 0.0064805556A.$$

Thus,

$$\Delta t \approx \frac{\nu \min(\Delta x, \Delta y)}{1.3998A}$$

and since values of $\nu = 0.8$ and $\Delta x = \Delta y = 20$ were also used, we obtain

$$\Delta t \approx 11.4302A^{-1} \quad \text{seconds} \quad .$$

Hence, when a small value of A is used, the morphological time step is large, i.e. $A = 0.001$ implies that $\Delta t \approx 11,430$ seconds, but as $A \to 1$, $\Delta t \to 11$ seconds. Also, Formulation A iterates the water flow to an equilibrium state each time the bed is updated, which has a cut off time of $t = 15$ minutes and results in Formulation A requiring a considerable amount of computations when a large value of A is used. Thus, a numerical scheme that can be used with large time steps, such as implicit schemes, or more accurate boundary conditions are required to obtain a better approximation of the different formulations. Hence, Formulation A can only be used for small values of A. The DS2-FLR scheme produced considerably more accurate numerical results for all formulations than any of the other schemes due to the angle of spread of the star shaped pattern and the numerical results obtained were very smooth.

Chapter 6

Conclusions and Further Work

6.1 Conclusion

Throughout this thesis, we have discussed a variety of numerical techniques for approximating the equations governing sediment transport in one and two dimensions. In Chapter 1, the equations governing sediment transport were derived and two different sediment transport fluxes were discussed.

Chapter 2 discussed how to obtain an accurate approximation of one dimensional systems of conservation laws with source terms. The shallow water equations were used to illustrate the different numerical techniques and the accuracy of the schemes. The Lax-Friedrichs scheme, classic Lax-Wendroff scheme, MacCormack scheme and Roe's scheme were all adapted to approximate systems of conservation laws with source terms. High resolution schemes were also constructed so that the numerical scheme satisfies the Total Variational Diminishing property, which ensures no spurious oscillations occur in the numerical results. Three test problems were used to determine which numerical scheme was the most accurate in one dimension. The flux-limited version of Roe's scheme was the most accurate scheme in one dimension.

In Chapter 3, five different formulations based on either a steady or unsteady approach were derived to obtain an approximation of the equations governing sediment transport. The flux-limited version of Roe's scheme and the classic Lax-Wendroff scheme were used to obtain a numerical approximation of the different formulations. Two test problems were considered and the numerical results compared to determine which formulation and scheme was the most accurate. We illustrated that the flux-limited version of Roe's scheme was considerably more accurate than the classic Lax-Wendroff scheme, which produced poor numerical results for all formulations and became unstable for all variations of Formulation A. Formulation A-SF with all schemes produced poor numerical results due to spurious oscillations being present. We also showed that Formulation A-NC can only be used for small values of A unless the staggered scheme (3.18) was used. We also illustrated that Formulation A-CV, which is a steady approach, can only be used for small values of A and Q whereas Formulations B and C, which are unsteady approaches, can be used for all values of A and Q. Unfortunately, the numerical schemes of Formulations A-NC, B and C suffered badly from diffusion due to the schemes requiring a considerable amount of time steps to reach the final computation time when a small value of A was used.

Chapter 4 discussed how to obtain an accurate approximation of a system of conservation laws with source term in two dimension. The 2D shallow water equations were used to illustrate the numerical techniques and the accuracy of the different schemes. The classic 2D Lax-Wendroff scheme, the flux-limited 2D Lax-Wendroff scheme and the flux-limited version of Roe's scheme were extended to two dimensions. A basic scheme and a dimensional splitting scheme was also discussed. A 2D test problem was used to determine which scheme produced the most accurate numerical results. The numerical schemes were compared for a 2D test problem and the DS2-FLR scheme produced the most accurate numerical results.

In Chapter 5, the equations governing sediment transport in two dimensions were approximated. Formulations A-CV and C were extended from one dimension to approximate the equations in two dimensions. The classic 2D Lax-Wendroff scheme, the basic scheme (B-FLR) and the dimensional splitting scheme (DS2-FLR) were

adapted to approximate Formulations A and C. We illustrated that as with the one dimensional case, the classic 2D Lax-Wendroff scheme produced poor numerical results for all formulations and became unstable almost immediately with Formulation A. Both the B-FLR scheme and the DS2-FLR scheme produced kinks in the numerical results with Formulation A but did not with Formulation C, where the numerical results were very smooth. The DS2-FLR scheme produced more accurate numerical results than the B-FLR scheme due to the angle of spread for the star shaped pattern being closer to the approximate value. We also illustrated that Formulation A can only be used for small values of A due to the formulation being a steady approach whereas Formulation C can be used for all values of A.

Therefore, in this thesis we have illustrated that formulations based on the steady approach can only be used for small values of A and Q whereas formulations based on the unsteady approach, with the exception of Formulation A-SF, can be used for all values of A and Q. If a large value of A was used, the numerical results of the steady approached differed significantly to the unsteady approach. The classic Lax-Wendroff scheme produced poor numerical results for all formulations in one and two dimensions whereas the adaptations of the flux-limited version of Roe's scheme produced very accurate numerical results.

6.2 Further Work

There is a considerable amount of further work that requires investigation. For example, Formulations A-CV and A-NC require a more robust and accurate approximation of the wave speed of the bed-updating equation. This can be considerably difficult to obtain, especially if the sediment transport flux is determined by a "black box" approach. In this thesis, all the formulations and numerical schemes discussed in one and two dimensions are based on the sediment transport flux discussed by Grass [14] and need to be adapted to approximate a general sediment transport flux, including the "black box" approach. Numerical schemes that can use large time steps, such as implicit schemes need to be investigated with

the unsteady approaches so that the numerical results of the unsteady approach are less diffusive. Friction, wind resistance and other factors can be included in the shallow water equations and the different formulations and numerical schemes adapted. For Formulation A-CV, instead of iterating the equations to an equilibrium state and then updating the bed, an approximation of the two simplified equations (1.3) and (3.2), which were discussed by Cunge *et al.* [3], can be obtained instead. In two dimensions, finite volume schemes and genuinely multidimensional upwinding schemes, see Hubbard & Baines [17] and Garcia-Navarro *et al.* [10] for more details, need to be investigated and used to numerically approximate the different formulations. With these scheme, instead of the basic cartesian mesh being used, different grids can also be used such as triangles and even adaptive unstructured grids, where the mesh is determined to conform with the geometry. This enables a more accurate numerical approximation to be obtained.

References

[1] A. Bermúdez & M. E. Vázquez, Upwind Methods for Hyperbolic Conservation Laws with Source Terms, *Computers and Fluids* **Vol. 23 No. 8**, 1049 - 1071 (1994).

[2] T.J Chesher, H.M Wallace, I.C. Meadowcroft & H.N. Southgate, PISCES: A Morphodynamic Coastal Area Model First Annual Report, *HR Wallingford*, **Report SR 337**, April 1993.

[3] J.A. Cunge, F.M. Holly & A. Verway, Practical Aspects of Computational River Hydraulics, *Pitman* (1980).

[4] J.S. Damgaard, Numerical Schemes for Morphodynamic Simulations, *HR Wallingford*, **Report IT 459**, March 1998.

[5] J.S. Damgaard & T.J. Chesher, Morphodynamic Simulations of Helwick Bank, *HR Wallingford*, **Report TR 31**, 1997.

[6] H.J. De Vriend, 2DH Mathematical Modelling of Morphological Evolutions in Shallow Water, *Coastal Engineering* **11** (1987), 1 - 27.

[7] M. De Vries, River-bed Variations - Aggradation and Degradation, *I.H.A.R. International Seminar on Hydraulics of Alluvial Streams*, New Dehli (1973).

[8] H.A. Einstein, The Bed-Load Function for Sediment Transportation in Open Channel Flows, *US Dept. of Agriculture*, Techn. Bulletin **1026** (1950).

[9] P. Garcia-Navarro, A. Fras & I. Villanueva, Dam-Break Flow Simulation: Some Results for One-Dimensional Models of Real Cases, *J. of Hydrology* **216**, 227 - 247 (1999).

[10] P. Garcia-Navarro, M.E. Hubbard & A. Priestly, Genuinely Multidimensional Upwinding for the 2D Shallow Water Equations, *J. Comput. Phys.* **121**, 79 (1995).

[11] P. Glaister, Difference Schemes for the Shallow Water Equations, *Numerical Analysis Report* **9/97**, *University of Reading* (1987).

[12] P. Glaister, Approximate Riemann Solutions of the Shallow Water Equations, *J. Hydraul. Research* **Vol 26**, 293 - 306 (1988).

[13] E. Godlewski & P-A. Raviart, Numerical Approximation of Hyperbolic Systems of Conservation Laws, Applied Mathematical Sciences 118, Springer-Verlag, ISBN 0-387-94529-6 (1991).

[14] A.J. Grass, Sediment Transport by Waves and Currents, *SERC London Cent. Mar. Technol*, Report No: **FL29** (1981).

[15] A. Harten, High Resolution Schemes for Conservation Laws, *J. Comput. Phys.* **49** (1983).

[16] A. Harten & S. Oscher, Uniformly High Order Accurate Non-Oscillatory Scheme I, *SIAM J. Num. Anal.* **24**, 229 - 309 (1982).

[17] M.E. Hubbard & M.J. Baines, Conservative Multidimensional Upwinding for the Steady Two Dimensional Shallow Water Equations, *J. Comput. Phys.* **138**, 419 - 448 (1997).

[18] M.E. Hubbard & P. Garcia-Navarro, Flux Difference Splitting and the Balancing of Source Terms and Flux Gradients, *Numerical Analysis Report* **3/99**, *University of Reading* (1999).

[19] M.E. Hubbard & P. Garcia-Navarro, Flux Difference Splitting and the Balancing of Source Terms and Flux Gradients, *J. Comput. Phys.* **165**, 89 - 125 (2000).

[20] J. Hudson, Numerical Techniques for the Shallow Water Equations, *Numerical Analysis Report* **2/99**, *University of Reading* (1999). A colour postscript version of this report can be obtained at http://www.rdg.ac.uk/AcaDepts/sm/home.html.

[21] J. Hudson & P.K. Sweby, Numerical Formulations for Approximating the Equations Governing Bed-Load Sediment Transport in Channels and Rivers, *Numerical Analysis Report* **2/2000**, *University of Reading* (2000). A colour postscript version of this report can be obtained at http://www.rdg.ac.uk/AcaDepts/sm/home.html.

[22] G.-S. Jiang, D. Levy, C.-T. Lin, S. Osher & E. Tadmor, High-Resolution Non-Oscillatory Central Schemes with Non-Staggered Grids for Hyperbolic Conservation laws, *SIAM J. Num. Anal.* **35**, 2147 - 2168 (1998).

[23] P.D. Lax, Hyperbolic Systems of Conservation Laws and the Mathematical Theory of Shock Waves, volume 11 of *Regional Conference Series in Applied Mathematics*, ISBN 0-89871-177-0.

[24] P.D. Lax & B. Wendroff, Systems of Conservation Laws, *Comm. Pure and Appl. Math.* **13**, 217 - 237 (1960).

[25] R.J. LeVeque, Numerical Methods for Conservation Laws, Birkhäuser Verlag, ISBN 3-7643-2723-5 (1992).

[26] R.J. LeVeque, Balancing Source Terms and Flux Gradients in High-Resolution Godunov Methods: The Quasi-Steady Wave Propagation Algorithm, *J. Comput. Phys.* **146** (1998).

[27] R.J. LeVeque & H.C. Yee, A Study of Numerical Methods for Hyperbolic Conservation Laws with Stiff Source Terms, *J. Comput. Phys.* **86**, 187 - 210 (1990).

[28] R.W. MacCormack, The Effects of Viscosity in Hybervelocity Impact Cratering, *AIAA Paper*, 69 - 354 (1969).

[29] D.J. Needham & R.D. Hey, On Nonlinear Simple Waves in Alluvial River FLows: A Theory for Sediment Bores, *Phil. Trans. R. Soc. Lond. A* **334**, 25 - 53 (1991).

[30] Haim Nessyahu & Eitan Tadmor, Non-Oscillatory Central Differencing for Hyperbolic Conservation Laws, *J. Comput. Phys.* **87**, 408 - 463 (1990).

[31] N. Perdreau and J.A. Cunge, Sedimentation dans les estuaries et les embouchures bouchon marin et bouchon fluvial, *I.A.H.R. International Seminar on Hydraulics of Alluvial Streams*, Paris (1971).

[32] Niels Ramsing & Jens Gundersen, Seawater and Gases: Tabulated Physical Parameters of Interest to People Working with Microsensors in Marine Systems, Unisense. Obtained via the web at www.unisense.com.

[33] P.L. Roe, Approximate Riemann Solvers, Parameter Vectors and Difference Schemes, *J. Comput. Phys.* **43**, 357 - 372 (1981).

[34] P.L. Roe, Numerical Algorithms for the Linear Wave Equation, *Royal Aircraft Establishment Technical Report* **81047** (1981).

[35] P.L. Roe, Upwind Diferencing Schemes for Hyperbolic Conservation Laws with Source Terms. In *Proc. First International Conference on Hyperbolic Problems, Carasso, Raviart and Serre (Editors)*, 41-51. Springer (1986).

[36] R.L. Soulsby, Dynamics of Marine Sands, A Manual for Practical Applications, *HR Wallingford*, **Report SR 466**, February 1997.

[37] M.R. Spiegel & J. Liu, Mathematical Handbook of Formulas and Tables, Second Edition, *Schaum's Outline Series*, McGraw-Hill, ISBN 0-07-038203-4 (1999).

[38] J.J. Stoker, Water Waves, Wiley Interscience (1957).

[39] G. Strang, On the Construction and Comparison of Difference Schemes, *SIAM J. Num. Anal.* **5**, 506 - 517 (1968).

[40] P.K. Sweby, High Resolution Schemes Using Flux Limiters for Hyperbolic Conservation Laws, *SIAM J. Num. Anal.* **21**, 995 (1984).

[41] B. van Leer, Towards the Ultimate Conservative Difference Scheme II: Monotonicity and Conservation Combined in a Second Order Scheme, *J. Comput. Phys.* **14**, 361 - 370 (1974).

[42] L.C. van Rijn, Sediment Transport: Part I: Bed Load Transport; Part II: Suspended Load Transport; Part III: Bed Forms and Alluvial Roughness, *Proc. ASCE Journal of Hydraulics Division*, **Vol 110**, HY10, 1431-1456; HY11, 1613 - 1641; HY12, 1733 - 1754 (1984).

[43] L.C. van Rijn, Principles of Sediment Transport in Rivers, Estuaries and Coastal Seas, Aqua Publications, ISBN 90-800356-2-9 (1993).

[44] M.E. Vázquez-Cendón, Improved Treatment of Source Terms in Upwind Schemes for the Shallow Water Equations in Channels with Irregular Geometry, *J. Comput. Phys.* **148**, 497 - 526 (1999).

[45] H.C. Yee, Upwind and Symmetric Shock-Capturing Schemes, *NASA Ames Research Center Technical Memoranda* **89464** (1987).

[46] D.D.L. Zanré & D.J. Needham, On the Hyberbolic Nature of the Equations of Alluvial River Hydraulics and the Equivalence of Stable and Energy Dissipating Shocks, *Geophys. Astrophys. Fluid Dynamics* **76**, 193 - 222 (1994).